

FINAL

**SHEPLEY'S HILL
BEDROCK INVESTIGATION**



**PREPARED BY
GANNETT FLEMING, INC.
AND
US EPA REGION 1**

ROC CONTRACT NO. EP-W-05-020

JULY 2012

EXECUTIVE SUMMARY	1
1.0 PURPOSE	7
2.0 OBJECTIVES.....	10
3.0 ORGANIZATION OF THE REPORT	11
4.0 SITE SETTING	12
4.1 PHYSICAL SETTING.....	12
4.2 GEOLOGICAL SETTING	12
4.3 METEOROLOGICAL SETTING	14
5.0 FIELD ACTIVITIES AND RESULTS.....	15
5.1 SURFACE EXPRESSION OF BEDROCK FRACTURES	16
5.1.1 <i>LiDAR survey</i>	16
5.1.2 <i>Linear trace analysis</i>	16
5.1.3 <i>Fracture mapping at bedrock outcrops</i>	17
5.1.4 <i>Radiation survey</i>	19
5.2 SURFACE GEOPHYSICS	20
5.3 SHALLOW BEDROCK BORINGS	22
5.3.1 <i>Phase 1a and 1b borehole objectives, rationale and locations</i>	22
5.3.2 <i>Percussion drilling</i>	23
5.4 GEOPROBE OVERBURDEN DRILLING.....	24
5.5 BOREHOLE GEOPHYSICS.....	25
5.6 WATER LEVELS	26
5.6.1 <i>Manual gauging and interpreted potential surfaces</i>	26
5.6.2 <i>Continuous gauging by transducer</i>	27
5.6.3 <i>Apparent vertical gradients within shallow bedrock</i>	28
5.6.4 <i>Head differences between overburden and shallow bedrock</i>	30
5.6.5 <i>Bedrock water-level response to precipitation events</i>	31
5.6.6 <i>Water level data from the N5 piezometer pair</i>	33
5.7 SLUG TESTS ON OPEN BEDROCK BOREHOLES.....	38
5.8 FIELD ANALYSIS FOR ARSENIC	39
5.9 SHALLOW WELL INSTALLATION	41
5.10 DEEP BOREHOLE	42
5.10.1 <i>Deep borehole objectives</i>	42
5.10.2 <i>Rationale for location</i>	43
5.10.3 <i>Drilling methodology and observations during coring</i>	44
5.10.4 <i>Summary of observations on the core</i>	44
5.10.5 <i>Well installation</i>	46
5.11 WATER LEVELS IN SCREENED WELLS	46
5.12 LOCATION SURVEY	48
6.0 BEDROCK MINERALOGY.....	49
6.1 PHASE I: ANALYSIS OF EXISTING SHL CORES	49
6.1.1 <i>Objectives</i>	49
6.1.2 <i>Methods</i>	49
6.1.3 <i>Phase I results</i>	52
6.2 PHASE II: ANALYSIS OF DEEP CORE.....	54
6.2.1 <i>Motivation</i>	54
6.2.2 <i>Deep core mineralogical analysis</i>	55
6.2.3 <i>Phase II results</i>	56
6.3 PRELIMINARY X-RAY DIFFRACTION RESULTS	59
6.4 CONCLUSIONS FROM MINERALOGICAL ANALYSIS	60

7.0 FRACTURE NETWORK.....	63
7.1 SUB-REGIONAL FRACTURE NETWORK	65
7.2 SHEPLEY’S HILL SCALE FRACTURE NETWORK.....	66
7.3 SITE-SCALE FRACTURE NETWORK	70
8.0 IMPLICATIONS FOR GROUNDWATER HYDROLOGY	76
8.1 SITE SCALE.....	76
8.2 SHEPLEY’S HILL SCALE.....	78
8.3 SUB-REGIONAL SCALE	82
9.0 BOREHOLE WATER CHEMISTRY	83
9.1 METHODS	83
9.2 RESULTS	83
9.3 DISCUSSION	85
9.4 WATER CHEMISTRY CONCLUSIONS	87
10.0 DISCUSSION: UNIFIED CONCEPTUAL MODEL.....	88
11.0 RECOMMENDATIONS	92
12.0 REFERENCES	95

List of Figures

Figure 1.0-1(a). Sub-regional scale topographic map of Shepley's hill and environs.

Figure 1.0-1(b). Sub-regional aerial photograph of Shepley's hill and environs.

Figure 1.0-2(a). Topographic map showing site area at Shepley's hill scale and relevant monitoring wells of interest on adjacent landfill.

Figure 1.0-2(b). Aerial photograph showing site area at Shepley's hill scale and relevant monitoring wells of interest on adjacent landfill.

Figure 1.0-3. Site-scale topographic map showing study area, monitoring wells and boring locations.

Figure 4.2-1. Sub-regional scale bedrock geologic map of Shepley's hill and environs.

Figure 5.1-1. Photograph of outcrop showing exposed joint surface on sheeting fracture.

Figure 5.1.2-1(a). Linear trace analysis, Shepley's hill scale.

Figure 5.1.2-1(b). Linear trace analysis and major fracture zones, Shepley's hill scale.

Figure 5.1.3-1. Map showing locations of bedrock outcrops and monitoring well locations in study area.

Figure 5.1.3-2. Lower-hemisphere stereoplot of site-scale foliation orientations.

Figure 5.1.3-3. Lower-hemisphere stereoplot of site-scale fracture and joint orientations.

Figure 5.1.3-4. Plan view compilation of outcrop mapping in central area at site scale.

Figure 5.2-1. Surface geophysical survey profiles and outcrop mapping.

Figure 5.3.1-1. Schematic diagram showing general fracture relationships

Figure 5.3.1-2. Phase 1a and 1b bedrock boring locations superposed on fracture map.

Figure 5.4-1. Contour map of overburden thickness at site-scale.

Figure 5.6.1-1. Interpreted piezometric surface, April 24, 2009.

Figure 5.6.1-2. Interpreted piezometric surface, August 5, 2009.

Figure 5.6.1-3. Interpreted piezometric surface, September 9, 2009.

Figure 5.6.1-4. Interpreted piezometric surface, March 17, 2010.

Figure 5.6.5-1(a)-(d). Change in water level in response to precipitation events, Spring 2009; (a) boring 20-1; (b) boring Q4-2; (c) boring 3-1; (d) boring CAP-3.

Figure 5.6.6-1. Head difference at the N5 piezometer pair (deep minus shallow); (a) 2007; (b) 2008; (c) 2009; (d) 2010.

Figure 5.7-1. Histogram of $\log_{10}(K)$; K in ft/d.

Figure 5.10.3-1. Large open fracture at approximately 39 ft bgs. Note wide bands (several cm thick) of iron oxidation adjacent to fracture surface.

Figure 5.10.3-2. Close-up of fracture in Figure 5.10.3-1 showing bleached zone surrounding iron-oxidation band; bleaching is inferred to be relict hydrothermal alteration.

Figure 5.10.3-3(a). Vertically oriented calcite-filled vein with sulfide minerals (tentatively identified as pyrite and arsenopyrite). Depth interval = 108.25-108.4 ft.

Figure 5.10.3-3(b). Quartz vein with silver-colored sulfide mineral (possibly arsenopyrite). Depth interval ~133 ft.

Figure 5.10.3-3(c). Large quartz vein with pyrite at approximately 98 ft bgs.

Figure 5.11-1. Water levels in screened wells, 5 February 2010 to 24 September 2010.

Figure 6.0-1. Locations of bedrock core samples examined.

Figure 6.1.2-1. Core from N5 showing alteration (Fe oxidation) along a fracture surface.

Figure 6.1.2-2. Thin section of sample from SHP-99-29X. Rectangles mark target areas for quantitative analysis by EM.

Figure 6.1.2-3(a). Backscattered electron image of arsenopyrite crystal in silicate matrix, from SHP-99-29X core.

Figure 6.1.2-3(b). Arsenic (red) and sulfur (blue) single-element maps of crystal shown in Figure 6.1.2-3(a).

Figure 6.1.2-4(a). SEM image of an arsenopyrite crystal from SHP-99-29X core.

Figure 6.1.2-4(b). Element scan at point marked in Figure 4a. Most prominent peaks (left to right) correspond to Fe, As, and S.

Figure 6.1.2-5. EM image of a sulfide crystal in a sample from SHP-99-29X; quantitative analysis (data presented in text, from Map Label F in Fig. 6-2) was performed at the points indicated. Results are consistent with an identification of arsenopyrite.

Figure 6.1.2-6(a). Vein filling (backscattered electron image) from SHP-99-29X.

Figure 6.1.2-6(b). As element map of area outlined in Figure 6a.

Figure 6.1.2-6(c). S element map of area outlined in Figure 6a.

Figure 6.1.2-6(d). Na element map of area outlined in Figure 6a.

Figure 6.1.3-1(a). Element map of Fe for the area shown in Figure 6-5 (arsenopyrite from SHP-99-29X). Note Fe in microcrack below the arsenopyrite crystal.

Figure 6.1.3-1(b). Element map of As for the area shown in Figure 6-5 (arsenopyrite from SHP-99-29X). Note As, in association with Fe, in microcrack below the arsenopyrite crystal.

Figure 6.2.3-1. Deep corehole sample from 24.8-25.1 ft depth; bright area composed primarily of Fe-oxide with As (EDS scan at point marked by yellow star in photomicrograph).

Figure 6.2.3-2. Deep corehole 88.9 ft depth sample: As-bearing “rubbly” coating on fracture surface (EDS scan at point in photomicrograph). Coating contains Fe, As, Al, Si, and Ca.

Figure 6.2.3-3(a). 97.9 ft depth: Arsenopyrite fracture mapping area BSE

Figure 6.2.3-3(b). 97.9 ft depth: Arsenopyrite fracture mapping area; As (blue), S (red)

Figure 6.2.3-4. 97.9 ft depth: Arsenopyrite (EDS scan at point in photomicrograph); identification is based on presence of Fe, As, and S.

Figure 6.2.3-5. Deep corehole 97.9 ft depth: coating adjacent to arsenopyrite (EDS scan at point in photomicrograph), inferred to be As-bearing Fe-oxide based on absence of S.

Figure 6.2.3-6. Deep corehole 97.9 ft depth: Arsenopyrite grain (bright area) with corroded margins (EDS scan at point in photomicrograph).

Figure 6.2.3-7(a). Deep corehole 125.7 ft depth: BSE image of mapping area

Figure 6.2.3-7(b). Deep corehole 125.7 ft depth: mapping area; Al (blue); As (green); Fe (orange). These images suggest that As is present with Fe-oxide and aluminosilicate minerals (possibly biotite?).

Figure 7.1-1. Sub-regional geology and fracture features

Figure 7.3-1. North-south interpretive geologic cross sections at site scale

Figure 7.3-2. East-west interpretive geologic cross section at site scale

Figure 7.3-3. Photograph of northwest-striking subvertical fracture intersected by CH-1, 87.3-89.6 ft bgs.

Figure 8.0-1. Modeled particle tracks under ambient conditions and with groundwater extraction at 44 and 49 gpm (combined) at EW-01 and EW-04. From ECC (2009).

Figure 8.2-1. Delineation of the recharge area on Shepley's Hill that contributes to bedrock groundwater flow toward the overburden aquifer beneath Shepley's Hill Landfill.

Figure 9.3-1. Sodium and chloride in groundwater from the new bedrock wells. Sodium values in bedrock groundwater are comparable to those reported from the Long-Term Monitoring Program, while chloride is at the low end of the range.

Figure 9.3-2(a). Specific conductivity in bedrock groundwater as a function of screen elevation. Note that bedrock well 20-1 is anomalously high, with an average specific conductivity comparable to the deepest screen (CH-1D).

Figure 9.3-2(b). pH in bedrock groundwater as a function of screen elevation. Note that the average pH in bedrock well 20-1 is somewhat elevated in comparison to groundwater from other wells of similar depth.

Figure 9.3-3. Calcium and magnesium in bedrock wells. Both Ca and Mg are low in comparison to results from the Long-Term Monitoring Program and may reflect different geochemical controls on solubility in the new bedrock wells in comparison to reactions involving Ca and Mg in overburden groundwater.

List of Tables

- Table 5.3.2-1. Shallow bedrock borehole characteristics.
- Table 5.5-1. Summary of borehole geophysical logging program.
- Table 5.6.2-1. Periods of continuous water-level monitoring in open bedrock borings.
- Table 5.6.3-1. Water elevations at bedrock borehole pairs based on manual measurements.
- Table 5.6.4-1. Water levels in bedrock borings and nearby overburden wells based on manual measurements.
- Table 5.6.5-1. Correlation of water-level changes and precipitation, Spring 2009.
- Table 5.6.6-1. Annual characteristics of the head difference at the N5 piezometer pair.
- Table 5.6.6-2. Head difference, arsenic, iron, potassium, and calcium concentrations at bedrock piezometer screen N5-P1.
- Table 5.7-1. Hydraulic conductivity inferred from slug tests in open bedrock borings.
- Table 5.8-1. Field and laboratory test results for arsenic in bedrock groundwater.
- Table 5.9-1. Screen intervals for shallow bedrock monitoring wells.
- Table 5.9-2. Development of shallow bedrock wells.
- Table 6.1.2-1. Cores sampled for Phase I petrographic analysis.
- Table 6.2.3-1. Samples for petrographic analysis of deep cores.
- Table 7.2-1. Summary of steeply dipping fracture sets at Shepley's Hill scale.
- Table 7.3-1. Site-scale fracture network summary.
- Table 8.1-1. Horizontal hydraulic gradient estimated from water elevations at select well pairs.
- Table 9.2-1. Analytical results from all sampling rounds.

List of Appendices

Appendix A: LiDAR survey

Appendix B: Meteorological data

Appendix C: Surface fracture mapping

Appendix D: BaSIS survey

Appendix E: Surface geophysics

Appendix F: Percussion drilling logs

Appendix G: Overburden Geoprobe borings and well installation

Appendix H: Borehole geophysics

Appendix I: Pressure transducer data

Appendix J: Slug tests

Appendix K: Well construction

Appendix L: Deep corehole log

Appendix M: Location survey

Appendix N: Petrography (University of Massachusetts)

Appendix O: Groundwater analytical data

EXECUTIVE SUMMARY

The Shepley's Hill Bedrock Investigation (SHBI) was carried out to examine the hydrology of the fractured rock system west of Shepley's Hill Landfill, to characterize the mineralogy of selected bedrock core specimens, and to analyze the geochemistry of groundwater within the bedrock aquifer upgradient of the landfill. The bedrock ridge of Shepley's Hill, which rises immediately to the west of the landfill, is a primary recharge area for groundwater in the overburden aquifer that lies beneath the landfill. Conditions allowing for direct recharge of the overburden beneath the landfill were eliminated by construction of a low-permeability capping system in the mid-1990s

The hydrology of the bedrock aquifer is controlled by the network of intersecting fractures that cut across the rock mass. The fracture network was characterized by numerous, complementary methods that reveal information at different scales and levels of detail. At the ground surface, certain fracture sets are manifested through their influence on the topography of the hill. High-resolution aerial photography and a Light Detection and Ranging (LiDAR) survey were carried out in order to develop detailed imagery of the surface morphology. Prominent lineaments are represented by a series of massive step-like features trending from south to north, as well as features trending from south-southwest to north-northeast, most notably represented by the steep slope of Shepley's Hill where it rises from the landfill to the east. Perhaps the most conspicuous surface manifestation of bedrock fracturing is a northwest-southeast striking valley feature which cross cuts the Shepley's Hill outcrop area, extending for hundreds of feet as a linear region generally devoid of outcrops, in an area where exposures are otherwise unusually plentiful. This major bedrock valley is believed to coincide with a hydraulically significant fracture zone designated herein as the Nona-Shep Fracture Zone (NSFZ). In the region where the Shepley's Hill fracture zone disappears beneath the landfilled area to the east, fracture orientations were measured in detail on outcrops across an approximately 300 by 500 feet area designated as the *study area*. Prominent joint sets include one oriented roughly southeast to northwest, dipping steeply to the southwest; one oriented roughly south to north, dipping steeply to the east; and one oriented approximately west to east, dipping steeply to the south. The first two of these sets (SE-NW and S-N) correspond to the predominant lineaments observed on the scale of the aerial photography and LiDAR survey. Also readily visible in outcrop are shallow- to moderately-dipping "sheeting" fractures, typically striking south-southwest to north-northeast, and dipping to the east-southeast. These fractures roughly mimic the overall topography of the hill, but dip toward the landfill at a somewhat steeper angle than the surface slope.

A surface geophysical survey was conducted using both two-dimensional resistivity and low-frequency ground-penetrating radar (GPR) methods, in order to obtain information regarding the fracture network in the third (vertical) dimension. The resistivity survey detected features consistent with the steeply dipping, SE-NW joint set that corresponds to the major topographic expression (i.e., NSFZ) as noted in the foregoing discussion. The GPR survey proved to be most sensitive to the subhorizontal and shallow- to moderately-

dipping sheeting fractures, and suggests that these fractures are present at higher density in the uppermost ~40 ft below ground surface.

Eighteen shallow bedrock borings were installed within an area approximately 300 ft square, encompassed by the surface-mapped study area, and extending to the margin of the overburden aquifer on the west edge of the landfill. Percussion drilling was selected for its ability to orient the borings relative to the target fracture sets, as well as for its relatively high speed and low cost. Maximum boring depth achieved is approximately 70 ft bgs. Descriptive logs of the drill cuttings show sporadic intervals high in iron oxides, interpreted to be indications of water-bearing fractures. All eighteen open borings were characterized using a suite of geophysical tools, including caliper, acoustic televiewer (ATV), heat-pulse flow meter (HPFM), natural gamma, fluid resistivity, and fluid temperature logs. ATV logs were completed in seven holes and HPFM logs were completed in nine holes, due to resource limitations and/or the quality of the borings. The geophysical logs indicate predominant fracture dip orientations to the southeast (presumably the sheeting fractures), as well as to the south, northwest, and northeast. However, the ATV spatial coverage included few wells located within the NSFZ, so NW-SE striking fractures, with dips to the southwest may be under-represented by these data. The HPFM generally detected the highest groundwater flow rates in fractures within the uppermost 50 ft. High HPFM flow rates were also observed in some boreholes which intersect the trace of the prominent NW-SE striking Shepley's Hill fracture zone.

Water levels in fifteen of the open bedrock borings were gauged continuously with recording pressure transducers for various periods of time. All locations show very rapid and large-amplitude responses to recharge events, particularly in late winter and early spring when the shallow subsurface thaws and evapotranspiration is minimal. Water level changes of the order of 10 ft are observed in association with discrete recharge events, rising and falling within a few days. Longer-term, seasonal changes are of the order of several tens of feet as water levels rise in late winter and spring, and decline through the summer when evapotranspiration is maximal and, consequently, recharge is minimal. The qualitative response of the water levels within the fractured-rock aquifer of the hill indicates a well-interconnected fracture network of relatively high hydraulic diffusivity (i.e., characteristic response time is small) and low porosity (i.e., a modest volume of recharge results in a large increase in water level). The interpreted potential surface indicates that flow in the fractured-rock aquifer of the hill is generally parallel to the surface topographic gradient, resulting in overall flow toward the overburden aquifer to the east-southeast. Falling- and rising-head slug tests were performed in 15 of the open borings; inferred effective hydraulic conductivities ranged from 0.06 to 120 ft/d, with a geometric mean of 2.0 ft/d.

The eighteen open shallow bedrock boreholes were sampled and the groundwater was analyzed in the field for arsenic. Results ranged from 5 µg/L to 300 µg/L. The results appear to be strongly influenced by turbidity, with the maximum result obtained on a sample that was opaque with suspended silt derived from the drilling. A later analysis by the same method, following a period of sediment settling from the same water sample, yielded 70 µg/L As.

Eight boreholes were selected for installation of permanent monitoring wells in order to provide for both water-level measurements and groundwater sampling targeted at specific fracture intervals.

In order to interrogate the NSFZ directly, a deep corehole was drilled on the eastern margin of the study area, where the sandy overburden beneath Shepley's Hill Landfill pinches out against the rising bedrock of the hill. Continuous core was recovered from 18 to 151 ft bgs. The core exhibits abundant well-developed fractures, many of which show evidence of active flow of water in the form of iron oxide staining, with reaction zones penetrating as much as several inches into the adjacent matrix. These zones result from the weathering of iron minerals such as amphiboles, pyroxenes, and sulfides in the bedrock. A well pair was installed to target a very large subhorizontal sheeting fracture encountered in the interval 36 to 41 ft bgs and a zone of intersection of steeply dipping and subhorizontal fractures in the interval 85 to 95 ft bgs, including subvertical fracturing associated with the NSFZ

Selected intervals of the bedrock from archived core acquired through historical drilling beneath and adjacent to Shepley's Hill Landfill, as well as from the new core obtained in the SHBI, were examined using optical microscopy, scanning electron microscopy (SEM) with energy-dispersive spectrometry (EDS), and electron microprobe analysis. Abundant sulfide minerals were observed, including pyrite (FeS_2) and arsenopyrite (FeAsS), as well as As-bearing weathering products. The latter were not identified definitively due to their small volume as fracture coatings; however, scorodite ($\text{Fe}^{3+}\text{AsO}_4 \cdot 2\text{H}_2\text{O}$) was tentatively identified. A variety of secondary phases are present, including oxides and carbonates.

The conceptual model for the bedrock fractures to emerge from this study holds that there is a transmissive network that conducts groundwater from a recharge area on Shepley's Hill, flowing to the east-southeast toward the landfill. The fracture network is composed of subhorizontal to moderately dipping, laterally extensive sheeting fractures that are related to glacial erosion and subsequent stress relief due to post-glacial unloading, as well as a number of steeply dipping joint sets. The latter are the result of the tectonic history of the area, including deformation in the Clinton-Newbury Fault zone, in which the site lies. The most conductive fracture set for shallow groundwater is likely the sheeting fractures. However, fracturing appears to be further enhanced within the NSFZ, particularly where steeply dipping structures intersect with sheeting fractures. Available boring pairs on Shepley's Hill exhibit higher water levels in the deeper holes in every case examined, regardless of the season. This is in contrast to typical observations in a recharge area in a classical porous aquifer (e.g., unconsolidated overburden), where vertical gradients drive downward flow. In the fractured rock of Shepley's Hill, the higher water levels at greater depth suggest that vertical connectivity between the subhorizontal sheeting fractures is limited. The same observation holds for the well pair installed in the deep corehole where the bedrock surface descends beneath the sandy overburden aquifer to the east. Continuously recording pressure transducers showed that the head at the deeper screen (85 – 95 ft bgs) was always greater than the head at the

shallower screen (36 – 41 ft bgs) from February through September 2010, even as heads fell overall by 20 to 25 feet during this period.

The average hydraulic gradient estimated from water levels gauged in the array of shallow bedrock borings on the hill as groundwater approaches the intersection of the bedrock upland with the sandy overburden aquifer to the east is approximately 0.15. Along with the geometric mean effective hydraulic conductivity of 2.0 ft/d inferred from slug tests, this implies a groundwater flux across the study area of approximately 0.3 ft/d. If most groundwater flow occurs in the uppermost 50 ft of the bedrock, where the fracture density and apertures are expected to be greatest, and 30 ft of that interval is typically saturated, then this inferred flux corresponds to a total discharge of approximately 9.0 ft³/d per linear foot parallel to the ridge. An independent upper bound on the expected volume flow rate can be estimated from annual precipitation. Data for 2005 – 2009 show average annual precipitation of 48 in (4.0 ft). The distance from the Shepley's Hill ridge crest to the eastern margin of the study area is approximately 340 ft. Therefore, the average total precipitation to fall on this area of the hill is approximately 3.7 ft³/d per linear foot parallel to the ridge. The discharge rate estimated from the observed hydraulics is greater than the upper bound imposed by available precipitation, possibly because the study site straddles a fracture zone that localizes flow, such that the site is not representative of the entire ridge. In addition, uncertainty in the bulk hydraulic properties of the fractured rock may contribute to the discrepancy.

The total area of the catchment on Shepley's Hill that contributes to groundwater flow toward Shepley's Hill Landfill is approximately 5.4×10^5 ft². The average total precipitation that falls on this recharge area is approximately 2.2×10^6 ft³/yr, or 31 gpm. Net recharge is expected to be some fraction of this value due to evapotranspiration losses and surface runoff.

Past discussions of hydrological processes affecting Shepley's Hill Landfill have raised questions concerning "run-under," whereby precipitation or meltwater from the elevated bedrock of Shepley's Hill flows as surface runoff to the toe of the eastern slope, where it enhances recharge of the overburden aquifer at the western margin of the landfill. The results of the bedrock investigation suggest that this scenario is not significant in the hydrology of the system. Recharge of the fractured rock aquifer of Shepley's Hill occurs readily, as seen in the rapid and large-amplitude response of water levels in borings on the hill, and the fractured rock exhibits ample transmissivity to carry this groundwater toward the landfill in the subsurface. Given that heads in the bedrock aquifer of the hill are significantly higher than heads observed in the overburden aquifer to the east, it is expected that some fraction of the bedrock groundwater discharges upward to the overburden. This inference is supported by water-level data collected in a piezometer pair in the center of the landfill, approximately 400 ft downgradient of the toe of the slope in the study area. The data show that the head difference between the shallow bedrock screen and the water-table screen at this location, when averaged over each year of monitoring, is positive, i.e., there is a potential gradient to drive net upward flow from bedrock to overburden. The "run-under" scenario is not necessary to bring water from recharge on Shepley's Hill to the overburden aquifer beneath the landfill.

The eight new shallow bedrock wells, as well as the two wells installed in the deep corehole were sampled in November 2009 and March 2010 for laboratory analysis; one shallow well and the deep screen in the corehole were sampled in a third round conducted in June 2010. Arsenic was detected in only one of the shallow wells on the hill, at a maximum concentration of 91 µg/L. Arsenic was detected in the shallow corehole well at a maximum concentration of 27 µg/L, but the results are believed to be strongly influenced by the high turbidity associated with the loss of drilling water and cuttings to the large fracture in the screen interval. The deep corehole well yielded arsenic at a maximum concentration of 400 µg/L. The shallow groundwater on the hill exhibits chemistry indicative of recent recharge, including low pH, high DO, high ORP, and low alkalinity. The groundwater at the deep corehole screen shows the chemical signatures of more extensive water-rock interactions, as expected for a location where water has traveled a longer path from its recharge area, with a correspondingly longer residence time, including higher pH and alkalinity and lower DO and ORP. In contrast to groundwater elsewhere in the Shepley's Hill Landfill system, the water at the deep corehole well, although showing hundreds of µg/L arsenic, is relatively low in dissolved iron. A possible interpretation is that the arsenic is present in bedrock groundwater due to oxidation of arsenopyrite to intermediate phases, such as scorodite. The scorodite, in turn, may undergo incongruent dissolution, forming hydrous ferric oxide (HFO; a solid precipitate) and aqueous arsenate anion.

The report concludes with an attempt to integrate the data accumulated in this investigation, and to tie it to what is known from previous work on the landfill system to the east, with its complementary focus on the hydrology and geochemistry of the overburden aquifer. It is hypothesized that arsenic was transported from the Berwick Formation metasediments into the Ayer and Chelmsford granites by hydrothermal fluids associated with the intrusion and later metamorphism, resulting in formation of arsenic-containing sulfide minerals in certain local subdomains. Later uplift, erosion, and weathering exposed those sulfides to meteoric water, which oxidized the sulfides, and transported dissolved arsenic toward the overburden and bedrock aquifers east of the hill. In the overburden, post-glacial oxidation of comminuted sulfides and other iron-bearing minerals also yielded HFO, onto which arsenic is known to sorb. Limited soil data from SHL show generally increasing arsenic concentrations with depth in the overburden and a strong correlation with iron. The specific hydrologic processes responsible for this distribution are not known, but may be related to the observed upwardly discharging bedrock groundwater under present-day conditions. Conditions allowing for direct recharge of the overburden beneath the landfill were eliminated by construction of a low-permeability capping system in the mid-1990s. However, the area beneath the landfill was open to the atmosphere and direct recharge for most of its history, and the hydraulic and geochemical regime operating prior to the present capped condition is not known.

In the shallow overburden, post-glacial wetlands developed on the surficial sediment, forming peat deposits that were subsequently buried by further accumulation of sand and gravel and land-filled waste. The development of a landfill in the 20th century may have impacted groundwater redox conditions, and the presence of local peat deposits may also

have played a role. Perturbations to the redox environment remobilized arsenic through reductive dissolution of the HFO and release of sorbed arsenic, contributing to the high dissolved arsenic detections found in the overburden aquifer today.

In summary, the goals of the investigation were: to characterize the bedrock fracture network in the study area; to assess the role of fractured bedrock in transport of groundwater from the point of recharge on the hill to discharge into the overburden and bedrock beneath the landfill; to characterize bedrock groundwater chemistry; and to perform a limited petrographic analysis of bedrock mineralogy. These goals have been satisfied by the data collected under this investigation, and support the unified conceptual model presented.

1.0 PURPOSE

The purpose of the Shepley's Hill Bedrock Investigation (SHBI) is to address data gaps identified with respect to the role of the bedrock in the hydrology and geochemistry of the Shepley's Hill groundwater system. In particular, previous work has suggested that the elevated bedrock ridge of Shepley's Hill, which lies immediately to the west of Shepley's Hill Landfill (SHL), is a primary recharge area for groundwater in the overburden aquifer underlying the landfill (e.g., Harding ESE, 2003; AMEC, 2008). A groundwater divide is assumed to coincide roughly with the SSW-NNE crest of the hill, with groundwater flowing generally toward the landfill to the southeast (Figure 1.0-1(a) and (b)). The contribution of this flow to the overall water budget for the aquifer underlying the landfill is significant, because the landfill is capped with an impermeable, PVC geomembrane, which essentially eliminates direct recharge over approximately 84 acres of the sandy overburden to the east of the hill (Figure 1.0-2(a) and (b)). Therefore, groundwater beneath the landfill is supplied from areas upgradient of the cap to the south and west, including Shepley's Hill.

A working assumption of this study was that a significant portion of recharge to the landfill area and the thick overburden aquifer beneath it must come from the bedrock-dominated uplands of Shepley's Hill. In this context, it must be noted that, if precipitation on the hill is to recharge the overburden aquifer to the east, water must flow eastward as surface runoff; travel via groundwater flow through thin and discontinuous overburden deposits; move through the fractured bedrock; or be transported by some complex interaction of these multiple processes. Since the overburden to the east is quite thick (of the order of 100 ft in the central portion of the landfill), and tapers essentially to zero thickness as the underlying bedrock rises to the west to outcrop on Shepley's Hill, the nature of bedrock-overburden interactions along the interface between the western boundary of the landfill and the Shepley's Hill upland represented a key data objective. While much of the hill is bare outcrop, some fraction of it has thin soil cover, and, locally, thicker patches of overburden occur. Thicker overburden deposits (i.e., greater than 10 ft.) were identified in the valley feature that cuts from SE to NW in the vicinity of the study area. Immediately adjacent to the landfill cap, overburden deposits approximately 18 feet in thickness were encountered at a corehole location drilled for this investigation (CH-1), suggesting a rather abrupt and complex transition from bedrock uplands to the deep valley feature filled with glacial deposits which underlies the landfill.

One scenario by which precipitation falling on Shepley's Hill can reach the overburden aquifer to the east would entail recharge to the fractured rock aquifer of the hill, groundwater flow within the bedrock toward the east, and discharge upward into the sandy overburden beneath the landfill cap. Another scenario entails surface runoff from the hill, with direct recharge to the overburden where it pinches out and the landfill cap terminates against the rising bedrock of the hill. The latter scenario was considered at the time of development of the numerical groundwater flow model for Shepley's Hill Landfill to evaluate remedial alternatives (Harding ESE, 2003), as well as during subsequent modifications and applications (e.g., CH2MHill, 2004a; AMEC, 2009). The phenomenon has at times been referred to as "run-under." It was represented in the

model by applying supplemental recharge to grid cells along the western edge of the overburden aquifer.

The potential pathways for water to make its way from Shepley's Hill to the overburden aquifer beneath the landfill had not been characterized prior to the present study. The SHBI was designed to apply a broad array of complementary approaches to examination of the hydrology and geochemistry of the fractured rock aquifer of the hill. A limited subdomain of the hill was selected for detailed characterization (Figure 1.0-3). This particular area was chosen because it is upgradient of one existing monitoring well (SHP-99-29X) and an existing piezometer pair (N5-P1/P2), which are among the few groundwater sampling points that penetrate the landfill cap. In addition, the study area encompasses a portion of a southeast-to-northwest trending valley feature that cuts across Shepley's Hill (see LiDAR topographic map, Appendix A). This geomorphological lineament is suggestive of a potentially significant fracture set with roughly the same orientation. Such a fracture set is expressed in the topography because it is a zone of mechanical weakness that was eroded more than the surrounding rock by glacial and post-glacial processes. This zone may provide an important conduit of hydraulically conductive rock that channels groundwater from the hill toward the landfill to the southeast. The study area was characterized by surface mapping of fractures on outcrops, surface geophysical surveys, shallow percussion drilling, borehole geophysics, slug tests, and continuous monitoring of water levels in borings by recording pressure transducers.

The mineralogy of the bedrock and the geochemistry of the bedrock groundwater had received little attention in previous investigations performed at Shepley's Hill Landfill. The bedrock mineralogy is of great significance in understanding the ultimate source of naturally occurring arsenic in the Shepley's Hill system. Devens lies in a regional geological domain, informally referred to as the New England arsenic belt, in which arsenic-bearing minerals are present, and associated groundwater exhibits elevated concentrations of dissolved arsenic (e.g., Ayotte, et al., 1999). Although groundwater in the vicinity of SHL has been shown to be very high in arsenic (e.g., maximum As in the profile boring for extraction well EW-04 of 7.6 mg/L (CH2MHill, 2004b)), only limited visual inspection of the lithology in the vicinity of the landfill had been performed previously. Rock core collected in conjunction with installation of monitoring wells, as well as hand specimens collected from outcrops on Shepley's Hill, were described as exhibiting sulfide minerals and evidence of their dissolution (Harding ESE, 2003). However, no petrographic analysis had been carried out to identify specific arsenic-bearing minerals, if present, or any indications of the processes by which they formed and subsequently were altered. Toward this end, both existing bedrock core from previous drilling at Shepley's Hill Landfill and new core collected from a deep bedrock boring installed in the present investigation were examined by transmitted-light and scanning electron microscopy (SEM), as well as by electron microprobe.

The chemistry of groundwater in the bedrock has been analyzed for a few scattered locations in the course of characterization and monitoring of the landfill. The SHBI affords an opportunity to sample and analyze bedrock groundwater upgradient of the landfill in a number of shallow borings (up to about 80 ft bgs), as well as in a pair of

deeper wells (screened at 36 – 41 and 85 – 95 ft bgs) located at the base of the slope and at the western margin of the landfill cap.

2.0 OBJECTIVES

The Work Plan (Gannett Fleming, 2007) set forth the following objectives:

1. To locate fractures in shallow bedrock and to characterize the fracture network with respect to frequency and orientation, in order to develop better insight into the nature and extent of communication between bedrock and overburden groundwater, and possible “underflow” at the edge of the landfill cover;
2. To sample bedrock groundwater from these holes, with particular focus on geochemical parameters that may contribute to arsenic mobilization and transport;
3. To characterize bedrock lithology along the western edge of the landfill, with attention to fracture zones that are mineralized. This will be supplemented with limited petrographic analysis on core material that is already available and on samples obtained during this study from a deep borehole on the eastern edge of the study area.

To address these objectives, and to support the overall purpose of the project as described in Section 1.0, numerous activities were conducted. These activities are described in the following sections. Data, observations, and results are summarized throughout the report and attached as appendices, and are used to develop an internally consistent, unified conceptual model.

3.0 ORGANIZATION OF THE REPORT

This report is intended primarily as a compilation of data acquired in the course of the Shepley's Hill Bedrock Investigation for archival purposes, with a minimum of interpretation. To this end, much of the supporting material is relegated to appendices, which are attached in electronic formats. The sections describing elements of the investigation are arranged in a rough chronological sequence, although many activities overlapped or entailed two or more mobilizations, interspersed with other portions of the study. The chronological ordering of the report is chosen to emphasize the rationale behind each step, as information accumulated from prior activities. For example, the fracture mapping on surface outcrops supported the location of the surface geophysical lines; the surface geophysical data supported the locations and orientation of the shallow bedrock borings; the drilling logs supported the selection of borings for further characterization by borehole geophysics; the cumulative information from all of these activities supported the choice of borings for continuous water-level monitoring; cumulative information again supported the choice of borings for installation of monitoring wells and of the location for the deep corehole.

The first section of this report explains the motivation for this work. Section 2 details the report objectives and includes the goals outlined in the Shepley's Hill Landfill Bedrock Investigation Work Plan. Section 4 describes key aspects of the geology of the SHL area and provides a general lithologic and tectonic framework for this study. Of particular relevance are the bedrock formations, comprising the Berwick metasedimentary unit, the Ayer Granodiorite, and the Chelmsford Granite. In addition, the tectonic setting is also outlined. Field activities are listed and discussed in Section 5, and results are described. These activities include: surface fracture mapping, surface geophysics, Light Detection and Ranging (LiDAR) and Backpack Sodium Iodide Spectroscopy (BaSIS) surveys, percussion drilling, borehole geophysics, installation of pressure transducers and monitoring of water levels, slug testing of open bedrock boreholes, field sampling and analysis for arsenic, and installation of monitoring wells. The last phase of field activities included drilling and coring one deep hole, in which a monitoring well pair was installed. Section 6 contains results and discussion of analyses of SHL bedrock mineralogy. Results of the fracture mapping and a discussion of the fracture network are provided in Section 7 at the sub-regional scale, Shepley's Hill scale, and at the study site scale. Section 8 contains a discussion of the hydrology, both at the local scale of the study site and with respect to the scale of the landfill. Inferences relevant to the SHL scale, such as groundwater flux through shallow bedrock fractures, and a comparison to assumptions and results from the updated groundwater model for SHL, are presented. Results of two rounds of groundwater sampling and analysis from the new bedrock monitoring wells are found in Section 9. All results are interpreted in light of a unified conceptual model, presented in Section 10, which attempts to reconcile the geologic structure, bedrock formations, fracture network, mineralogy, sequence of tectonic events, water chemistry, and hydrology. Section 11 contains a list of recommendations for further investigation, and references are listed in Section 12.

4.0 SITE SETTING

4.1 Physical setting

Shepley's Hill is an elongate bedrock ridge trending approximately south-southwest to north-northeast (Figure 1.0-1(a) and (b)). The feature is roughly 2800 ft long from south to north, and varies in its west-east dimension up to about 1300 ft. It rises from relatively flat topography on all sides, with Shepley's Hill Landfill to the east, the floodplain of Nonacoicus Brook and the Nashua River to the north and west, and an industrial area of former Fort Devens to the south. The hill is wooded and undeveloped, although portions of it have been quarried in the past. The maximum elevation of Shepley's Hill is 366 ft msl (see LiDAR survey, Sec. 5.1.1 and App. A), while West Main Street in the Town of Ayer, to the immediate west of the hill, lies at approximately 235 ft msl. The landfill surface to the east slopes gently from south (maximum altitude 277 ft msl) to north (minimum altitude 225 ft msl). The area chosen for this investigation is adjacent to the north-central portion of the landfill. The highest point on the crest of the hill immediately west of the study area is at 313 ft msl; the landfill surface immediately to the east is in the range 240 to 245 ft msl.

A significant fraction of Shepley's Hill is exposed bedrock outcrop. The rest of the hill has a thin veneer of soil. The study area straddles a valley feature that cuts across the hill in a south-southeast to north-northwest direction. Maximum soil cover encountered within this valley is about 12 ft thick, as determined by GeoProbe refusal (see Sec. 5.4). The ridge crest drops to an elevation of 269 ft msl in this valley. The valley feature is one of several parallel lineaments, with those to the south manifested as a series of steps in the topography. Another prominent lineament forms the east face of the hill, trending south-southwest to north-northeast.

4.2 Geological setting

The following geological description is extracted (with minor edits for consistency with the context of this report) from Koteas, et al., (2010):

The three major rock types in the area of Shepley's Hill are the late Silurian Berwick Formation, the early Devonian Ayer Granodiorite, and the late Devonian Chelmsford Granite (Figure 4.2-1). The Berwick Formation is dominated by metasedimentary rocks that consist of weakly-foliated, interbedded biotite - plagioclase - quartz schists and calc-silicates. The Berwick Formation is locally migmatitic along the tectonized contact with the Chelmsford Granite. The Devens-Long Pond facies of the Ayer Granodiorite, for which the Shepley's Hill area is the type locality, varies between a microcline megacryst-bearing biotite granite to a hornblende-biotite granite-tonalite. Xenoliths of the Berwick Formation are common within the Ayer Granodiorite. The Chelmsford Granite, part of the New Hampshire Plutonic Suite, is a fine-grained muscovite - biotite granite that intrudes the Ayer Granodiorite typically in foliation-parallel, fine-grained, typically <1-

meter-wide dikes. Xenoliths of the Ayer Granodiorite are present occasionally within the Chelmsford Granite.

Shepley's Hill itself is composed entirely of the Ayer Granodiorite and Chelmsford Granite. The majority of the hill is underlain by the Ayer Granodiorite, while the area of the steep eastern slope has been mapped as Chelmsford Granite. A contact between the granitic rocks and the Berwick metasediments is interpreted to lie beneath the landfill to the east (Kopera, 2008). Berwick lithology has been identified in core collected from borings to the east of the landfill near the southern margin of Plow Shop Pond, as well as at piezometer locations N6 and N7 within the landfill. The Berwick Formation has also been mapped to the immediate west of the hill. Contacts between the metasediments and the younger granitic rocks, where exposed, are tectonic. Faulting is associated with the Clinton-Newbury Fault Zone, which is believed to have been most active during the Acadian orogenic event, which culminated in the Late Devonian. The fault system separates the Nashoba-Avalon tectonic terrane (Cambrian to Silurian) to the south and east and the Merrimack terrane (Ordovician to Devonian) to the north and west. The study site lies directly in the fault zone, within sheared rocks of the Merrimack assemblage. The lithologies were subjected to chlorite-grade metamorphism into the Carboniferous Period (~350 to 300 Ma).

An association of the Berwick Formation with elevated arsenic concentrations in groundwater from bedrock wells has been noted previously (e.g., Ayotte, et al., 1999), and similar associations are found in calcareous metasediments throughout a region extending from central Massachusetts to southern Maine known informally as the "New England arsenic belt." Few studies in the region have identified a specific association of arsenic in groundwater with arsenic minerals in crystalline rocks (e.g., Lipfert, et al., 2006; Ryan, et al., 2009). However, in those cases where crystalline rocks appear to be involved, they are in close proximity to metasedimentary lithologies, as at Shepley's Hill.

The present investigation includes petrographic analysis of core samples collected historically at a number of locations to the east of Shepley's Hill and in the current study from a deep (to 151 ft bgs) boring on the eastern margin of the hill. Results are detailed in Section 6.

Shepley's Hill Landfill lies immediately to the east of Shepley's Hill, and at present is a gently sloping plane surface, in part due to cut-and-fill operations associated with the landfill and later grading in the course of closing out and capping the landfill in the 1990s. Historic topographic maps show that the area of the landfill was at one time occupied in part by wetlands. The landfill overlies a glacial outwash deposit, in places of the order of 100 feet thick, composed primarily of sand and gravel, with local basal till. The sands pinch out on the west side of the landfill against the rising bedrock of Shepley's Hill. The outwash is believed to have been deposited during the final retreat of the Wisconsin glaciation, approximately 10,000 years before present.

The geomorphology of Shepley's Hill also presumably reflects Pleistocene glacial and post-glacial processes. The ice sheets likely removed some thickness of the local

bedrock; the hill stands higher than surrounding areas in part because it is composed of granitic rocks that are more resistant to erosion than the nearby metasediments. The often angular, blocky morphology of much of the exposed bedrock likely resulted from “plucking” at the bed of the ice sheet. A thin veneer of soil has developed locally on Shepley’s Hill due to post-glacial weathering and accumulation of organic matter. The soil was found to be as much as 12 ft thick during installation of shallow monitoring wells in the overburden on the hill by GeoProbe (see Sec. 5.4), and greater than 10 ft thick in numerous locations during percussion drilling of the bedrock borings (Sec. 5.3), particularly within the SE-NW valley that cuts across the ridge, around which the study area is focused.

4.3 Meteorological Setting

The Fort Devens climate is typical of the northeastern United States, with long, cold winters and short, hot summers. At the Fitchburg (MA) Municipal Airport, approximately 7.5 miles west of the site, climatic records from January 2005 through December 2009 report an average total annual rainfall of 48.17 inches. The average total monthly rainfall over the same period is relatively uniform, ranging from a low of 2.78 inches in February to a maximum of 5.75 inches in October. Although the data set for 2010 is incomplete, total rainfall was higher than the average for February (5.25 inches) and March (11.28 inches). It is noted that there may be small differences in rainfall between the recording station in Fitchburg and the Shepley’s Hill site, but larger events and general trends are expected to be similar.

During the period of this project (September 2007—September 2010), several rainfall events of 1.0 inch or more occurred. The percussion drilling took place in February 2008, which reported a monthly rainfall total of 6.96 inches. March 2008 was almost as wet, with a monthly total of 5.57 inches. Other months with unusually high rainfall totals occurring during the period spanning this project were: September 2008 (7.41 inches), June 2009 (6.48 inches), July 2009 (8.69 inches), and March 2010 (11.28 inches, of which 5.37 inches fell in one six-day period and 3.86 inches fell in one three-day period).

January is the coldest month, with a mean daily minimum temperature of 17.9 °F (-7.8 °C) and a mean monthly temperature of 26.8 °F (-2.9 °C), respectively. July is the hottest month, with a mean daily maximum temperature of 83 °F (28.3 °C) and a monthly average of 72 °F (22.2 °C). The average annual snowfall is 65 inches. Most of the snowfall occurs between December and March, although snow has been reported for the months of September through May. Wind speed averages 5.9 miles per hour (mph). The highest monthly average is 7.5 mph (March), and the lowest monthly average is 4.8 mph (August and September).

The meteorological data on which this summary is based are included as Appendix B.

5.0 FIELD ACTIVITIES AND RESULTS

The following subsections describe the field activities carried out at the Shepley's Hill site to characterize the bedrock aquifer. The activities are presented in chronological order to emphasize the logical sequence, as each type of data collected was used to support decisions regarding subsequent steps.

Some discussion regarding various *scales of investigation* used for the field effort is warranted. The geologic investigations and other activities were carried out at a variety of scales. The nascent conceptual site model (CSM) was informed by existing and ongoing geologic mapping at regional and sub-regional scales. The project team relied heavily on mapping efforts in progress at the time under the direction of the Office of the Massachusetts State Geologist (OMSG). In particular, information presented in *Preliminary Bedrock Geologic Map of the Ayer Quadrangle*, (Kopera, 2006; reproduced in this report as Figure 4.2-1) was used to provide a *sub-regional* context for more detailed work to follow on this project. The scale of this map is the 1:24,000 scale commonly used for USGS 7.5 minute quadrangle mapping. As such, this scale of investigation is referred to in this report as the “*sub-regional*” or “*quadrangle*” scale, interchangeably. Figures 1.0-1(a) and (b) place the Shepley's Hill area in this *sub-regional* scale context. A somewhat more detailed examination of bedrock structures was carried out at the scale of the approximately 100 acre area comprising the bedrock uplands at Shepley's Hill. This is referred to below as the “*Shepley's hill scale*” of investigation; Figures 1.0-2(a) and (b) highlight the Shepley's Hill upland area. In order to focus the available resources, a subset of the greater Shepley's Hill upland, an area roughly 300 by 300 feet, was designated as ‘the site’. The goal of the project was ultimately to develop a CSM at this scale, referred to hereafter as the “*site scale*”, to a relatively high degree of detail as afforded by the various geological, geophysical, hydrological, and geochemical methodologies directed to the investigation at this scale. Figure 1.0-3 shows the site area within the greater area comprised by the Shepley's Hill upland on the west, and the landfilled area to the east. Topographic contours, outlines of bedrock outcrops, and locations of all borings and monitoring wells installed for this project are included on Figure 1.0-3.¹

¹ Map scales are somewhat counter-intuitive and are typically expressed as a ratio where the first value equates to a unit of distance on the printed map, and the second relates to the equivalent distance in real terms. In other words, as an example, a 1:2000 map scale suggests that one unit of distance on the map equates to 2000 units of distance in real space, i.e., “on the ground”. As such, a one-inch distance on a map of this scale equates to 2000 inches on the ground. In this manner, the map scale ratio is considered a numerical value which is “larger” for more detailed “blown up” maps. Conversely, a map on a regional scale typically has a very “small scale”, i.e., the numerical ratio as expressed as a fractional value is much ‘smaller’. For example, this study examined a number of maps at the ‘sub-regional’ scale, in this case, 1:24,000.

5.1 Surface expression of bedrock fractures

The abundant bedrock exposures at Shepley's Hill provided the initial impetus and starting point for the project. Initial field reconnaissance identified the presence of numerous prominent surface exposures of bedrock exhibiting well-developed joint sets with strike lengths of 50 to 100 feet or more in some cases. Further examination of the fracture system exposed in the outcrops at Shepley's Hill involved a number of related tasks. These included collection of high-resolution aerial photography utilizing Light Detection and Ranging (LiDAR), preparing a linear trace analysis, detailed outcrop mapping, and an experimental surface radiation survey which attempted to detect buried fractures.

5.1.1 *LiDAR survey*

An aerial survey of Shepley's Hill and the adjacent landfill was flown on April 8, 2008, utilizing Light Detection and Ranging (LiDAR). The method results in a high-definition map of the topography, which is contoured in one-foot intervals (Appendix A). High-resolution aerial photographs of the area were also taken as a part of this effort. The LiDAR survey supported several objectives:

- Provide detailed photographic and topographic imagery of Shepley's Hill and Shepley's Hill Landfill as bases for display of spatial data;
- Provide a high-resolution topographic representation of Shepley's Hill as the basis for identification of lineaments that reflect the predominant fracture orientations;
- Provide a precise map of the elevation of the surface of the landfill cover in order to identify areas of settlement for the purpose of regrading and to support a leak-detection survey. (A plan to perform the latter was subsequently abandoned.)

Results of the LiDAR survey are presented in Appendix A.

5.1.2 *Linear trace analysis*

A linear trace analysis (LTA) was prepared using detailed topographic mapping and aerial photography. A LiDAR survey (see Sec. 5.1.1) provided high-resolution photographs and detailed ground surface elevation data which were transformed into a detailed topographic map of the site area with a 1-ft contour interval. Detailed topography of the Shepley's Hill area on a 2-ft. contour interval available from Mass Development was also examined. Linear features believed to correspond to possible bedrock fracture zones were plotted on the maps and checked in the field. Linear features corresponding to anthropogenic features such as roads and stone walls were deleted. Where corroborated by topographic expression and bedrock observations, linear features were retained as potential fracture zones. A map indicating the LTA conducted for the

Shepley's Hill area is shown on Figure 5.1.2-1(a). The LTA information helped to focus subsequent outcrop mapping and contributed to the development of the early-stage CSM. The LTA was also used in conjunction with other information to orient surface geophysical lines and ultimately to select locations for bedrock drilling. It should be noted that the LTA method is most useful in identifying steeply-dipping or near-vertical fractures. As shown on Figure 5.1.2-1(a), the general character of the fracturing at SHL consists of steeply-dipping fractures of several primary strike orientations. North-south striking features, some with strike lengths of hundreds of feet, are visible across the site, and are most prominent in the southern and western portions of Shepley's Hill. East-west striking features are less evident, but are significant in that they occur within the central portion of the study area. Northeast-southwest striking linearity of various outcrops results from the ubiquitous foliation fabric (strikes NE-SW and dips $\sim 50^\circ$ NW). Steeply-dipping fractures of this strike orientation are also present. Lastly, a northwest-to-southeast striking orientation is also observed at the site. A sizable feature of this orientation, with hundreds of feet of strike length can be observed cutting across the northern portion of Shepley's Hill, extending southeastward through the study area before disappearing beneath overburden cover at the western edge of the landfill.

5.1.3 Fracture mapping at bedrock outcrops

Fractures visible on surface outcrops were mapped over an area approximately 300 ft from west to east and 500 ft from south to north, enveloping the somewhat smaller area of the focused bedrock hydrology study (i.e., "site scale"). The first step in fracture mapping consisted of identifying outcrops within the area of interest. Each distinct outcrop was assigned a unique number and the outline of each outcrop was mapped with GPS. Figure 1.0-3 shows the locations of over 30 outcrops examined for this study.

At each outcrop, features of interest were identified and mapped. These features included the following:

- Foliation
- Lineation
- Shear planes
- Mylonitization
- Mineralized veins
- Faults
- Fractures
- Joints

The orientation of each feature was measured by Brunton compass, providing the strike (i.e., the orientation in the map plane of a horizontal line lying in the fracture plane) and dip (i.e., the angle of a line in the fracture plane perpendicular to the strike, measured down from horizontal). Each feature was marked in the field following the measurement, and the locations and elevations were later surveyed. Descriptive information such as strike length, evidence of chemical weathering (e.g., oxidation), joint smoothness or

roughness, planarity, apparent aperture, etc. were recorded in the field notebook. The locations and orientations were entered into a GIS database.

The primary features of interest were open joints. At each outcrop, an effort was made to map all joints with a strike length of five feet or greater, yet features of lesser strike length were also noted in some cases. In many areas, joints with significant strike length, on the order of 25 to 50 feet, were exposed at the surface. Mapping efforts focused on joints sets of greatest interest, which had the following characteristics: long strike length, planar character, smooth surfaces and visible apertures at the surface, and conspicuous evidence of chemical weathering, such as iron or manganese oxides. A key goal of the study was to identify the orientation and spacing of these significant joint sets and to develop an understanding of the interrelationships of the various sets comprising the fracture network at the site.

The primary structural fabric of the bedrock is the foliation. This metamorphic layering is ubiquitous in the study area. Foliation planes were commonly observed to correspond to shear planes and some are associated with small offsets and micro-scale folding. In some areas, a mylonitic texture was observed. Foliation generally strikes northeast with dips on the order of 50 degrees to the northwest. However, local dips may be lower or higher depending on the intensity of localized small-scale shearing. Open joints were locally observed in outcrop and in core coincident with foliation planes.

Several predominant joint sets were identified. Subhorizontal “sheeting” fractures are common in the study area. These significant features typically strike roughly from north-northeast to south-southwest, and typically dip to the east-southeast at 20 to 30 degrees, with a range of dips from near zero to 50 degrees. These fractures approximately mimic the surface topography, but with a somewhat steeper slope toward the landfill, (i.e., the fractures tend to descend to greater depth beneath the bedrock surface in the down-slope direction). It was observed that these fractures are generally perpendicular to the foliation, and therefore may share a genetic relationship with foliation. However, it appears that post-glacial stress relief has been accommodated primarily on these features. The Office of the Massachusetts State Geologist (S. B. Mabee, personal communication, 2008) reports that in areas where pre-existing bedrock fabric exhibits dips of less than 55 degrees, post-glacial stress relief is commonly observed to be coincident with the pre-glacial fabric (i.e., foliation). In areas where bedrock fabric exhibits steeper dips, post-glacial stress relief fractures (“sheeting fractures”) typically cross-cut pre-existing fabric at low to moderate angles, roughly corresponding to surface topography. Shepley’s Hill appears to be consistent with this general rule, yet a number of very flat (sub-horizontal) sheeting fractures, which cross-cut pre-existing rock fabric, were also identified in some core samples despite the predominance of the higher-angle variety.

A spreadsheet which contains all of the bedrock data collected is included in Appendix C. The data set includes the following information for each feature of interest: feature ID number, outcrop number, XYZ coordinates, feature type, strike, dip, azimuth, plunge, strike length, and other descriptive information. Appendix C also contains detailed maps for each outcrop with the locations and orientations of pertinent features plotted. Figure

5.1.3-2 presents a compilation of the outcrop-scale structural data presented at the site-scale. The representation of the mappable fractures and joints enables a two-dimensional visualization of the fracture system as an integrated *network*. In this manner the fracture mapping effort significantly advanced the CSM by presenting a working model for the fracture network at the site including the orientation, strike length, spacing and interrelationships of the various significant joints sets. This information was used in turn to determine locations for surface geophysical surveys and shallow and deep bedrock drilling, all of which ultimately contributed to the overall goal of establishing an understanding of the fracture network in three dimensions at the site scale. The follow-on efforts are discussed in subsequent sections, below.

5.1.4 Radiation survey

In a search for non-invasive methods of identifying bedrock fractures and in an effort to develop a more robust understanding of the fracture network at Shepley's Hill, particularly in those areas where bedrock is not exposed at the surface, it was hypothesized that discrete areas of elevated radiation may correlate with bedrock fracture zones, mapped or unmapped. To further test this concept in the SHL context, EPA collaborated with Idaho National Laboratory (INL) on experimental radiation surveys using a portable Backpack Sodium Iodide Spectroscopy (BaSIS) system with real-time measurement and integrated GIS capabilities. The BaSIS technology was developed at the Idaho National Laboratory for use at radiologically contaminated Cold War era legacy sites. The BaSIS system is comprised of commercial off-the-shelf equipment including a 3 in. × 5 in. sodium iodide (NaI) radiation detector, multichannel analyzer, real-time differential corrected global positioning system, a control computer and wireless display.

It was hypothesized that naturally occurring radioactive radon gas preferentially migrates along bedrock fractures. As such, it is expected that radon concentrations, and subsequently the related radioactive decay products, occur in higher concentrations above these fractures than over adjacent areas which are not fractured. The decay products of radon (^{222}Rn) include several gamma-ray emitting radionuclides. These decay products emit gamma-rays that can be detected with the NaI detector in the BaSIS system. Therefore, the primary objective of the radiation measurements at Shepley's Hill was to determine whether or not the locations of buried bedrock fractures could be identified based on the relative concentrations of radon daughter products. Additionally, measurements of other naturally occurring radionuclides, ^{40}K and ^{232}Th , were performed to evaluate whether or not their concentrations could be correlated to bedrock fracture sets.

The BaSIS report is included in Appendix D. It is not clear that the BaSIS survey was successful with respect to the goal of potentially identifying buried fracture zones, particularly at the detailed site-scale. The most meaningful correlation of the radiation measurements collected appears to coincide with locations of exposed bedrock or subcrop areas with thin cover. Thick soil cover therefore appears to attenuate the

radiation signal. It should also be noted that the BaSIS results do appear to suggest a correlation to larger-scale fractures at the scale of the entire Shepley's Hill area. However, these findings do not rule out the potential for elevated concentrations of radon (specifically ^{222}Rn) to be present in the soils above the subsurface fractures. Further testing with more robust methods would be needed to more definitively establish a positive or negative correlation.

5.2 Surface geophysics

In support of efforts to better understand the nature of the fracture system in the site area, a surface geophysical study was conducted in September of 2007 by Hager GeoScience, Inc., (HGI), under contract to Gannett Fleming. The report completed for this effort, *Geophysical Survey for Fractures, Shepley's Hill Landfill, Former Fort Devens, Ayer, Massachusetts, September 27, 2007*, is included as Appendix E. The following paragraph provides a brief synopsis of the surface geophysical studies, and discusses the contributions of these data toward subsequent phases of the project.

As discussed in Section 5.1, above, surface geologic mapping efforts identified and mapped a number of fracture sets in the site area. Several predominant orientations were observed with the following strike orientations: northwest-southeast, northeast-southwest, north-south, and to a lesser degree, east-west. Surface geophysical surveys were initiated as a means to further assess the subsurface extent of the fractures mapped on the surface, as well as to potentially identify features which were not apparent at the ground surface. Two methods were used: 2-dimensional electrical resistivity (RES) profiling, and ground penetrating radar (GPR) using low-frequency antennae. Plate 1 (App. E) indicates the orientations and surface positions of the geophysical survey lines. RES surveys are often successful in identifying steeply dipping or vertical fractures, particularly if those fractures are extensive and water-filled. Lines RL1 and RL2 (Plate 1, App. E), oriented NNE-SSW and WNW-ESE respectively, transect the study area and intersect one another in the central portion of the site. The orientation of RL1 was favorable to identifying steeply-dipping fractures striking east-west and northwest-southeast. The topographic valley feature in the central part of the site has these general orientations, and the subsurface region beneath this valley was a key investigation target for RL1. RL2 was oriented in a manner favorable to potentially locating northeast-southwest and north-south striking features. At the suggestion of HGI, lines RL1 and RL2 were also surveyed with GPR using low-frequency antennae (400- and 200-MHz). It was hoped that site conditions were favorable for the detection of low-angle features using the GPR in this configuration. In addition to lines RL1/GPR Line 3 and RL2/GPR Line 4, two additional short survey lines (GPR Lines 1 and 2) were also included to the east of lines RL1/GPR Line 3 in an effort to better understand the "valley feature" as it plunges successively deeper approaching the capped landfill area.. Additionally, GPR has the ability to identify shallow-dipping or flat-lying reflectors if there is sufficient electrical contrast along layer boundaries. In this respect, identification of buried "sheeting" fractures, and establishing lateral continuity of such features was a primary goal of the GPR surveys.

Plates 2 through 6 (App. E) present the interpretive resistivity and GPR profiles (i.e., cross sectional diagrams). Figure 5.2-1 presents selected resistivity and GPR profiles in conjunction with fractures and joints mapped at the surface. Several first-order observations are noted from these data. It is significant that RL1 indicates a distinct feature near the center of the study area with a steep southerly dip. The orientation of this feature appears to correspond well with the major topographic valley feature in the study area, and corroborates the presence and potential importance of hydraulically significant features of northwest-southeast strike in this region of the site. The subsurface materials south of this feature appear to be less electrically resistive (i.e., more conductive) than those to the north of it.

GPR survey data were successful in identifying numerous laterally extensive gently-to-moderately-dipping fractures in the shallow subsurface (generally 60 feet or less). These features appear to undulate, perhaps mimicking the irregular nature of the upper bedrock surface topography (Fig. 5.2-1). It is also likely that the undulatory nature results from a composite structure of numerous specific joints with varying strike and dips angles. We interpret these features generally to be “sheeting” fractures resulting from rapid stress relief coincident with the wasting glacial ice sheet. While the continued presence of these features is not clear from GPR below 60 feet bgs, (the effective rate of penetration for this study), drilling data from deeper levels (Section 5.10, below) indicates the sporadic continued presence of these features to depths beyond 100 feet bgs. Shallow- to moderate-depth drilling (Sec. 5.3, below) also corroborates the presence and importance of these shallow- to moderately-dipping features. A key finding of the GPR surveys suggests that the density of shallow- to moderately-dipping features is greatest in the uppermost ~ 40 feet of the subsurface materials (fracture spacing on the order of ~ 5 feet), and fracturing is somewhat less common below 40 feet (spacing on the order of 5 to 10 feet or more). It is relevant to note here that RES profiles also indicate a preponderance of low-resistivity material (higher conductivity) in the uppermost 40 or so feet of the bedrock. Lastly, it should also be noted that the GPR response on the shallow- to moderately dipping features seems to be more intense in the vicinity of significant steeply-dipping fractures. For example, GPR Line 3 shows a region of larger aperture fracturing in the area of the intersection of this alignment with the major northwest-southeast striking valley feature.

The geophysical survey results were useful in helping to refine the understanding of the fracture system, which in turn was useful in determining specific drilling locations and particular targets for confirmation and further characterization. More discussion of the surface geophysical survey results is included in relevant sections below, where appropriate, including Section 5.3, Percussion Drilling, Section 5.10 Deep Borehole, and Section 5.10.1, Rationale for (deep borehole) location.

5.3 Shallow bedrock borings

Bedrock borings were installed in a scattered array across the study site (Fig. 5.1.3-1), from a maximum ground surface elevation of approximately 278 ft msl on the hill to a minimum ground surface elevation of 243 ft msl at the foot of the slope where the overburden aquifer to the east pinches out against the rising bedrock. Section 5.3.1 below summarizes the rationale invoked to site the shallow bedrock borings, and Section 5.3.2 outlines the drilling method employed.

The bedrock borings were installed in two mobilizations, referred to in the following as Phase 1a (February 2008) and Phase 1b (September 2008). See further discussion in Section 5.3.2.

5.3.1 Phase 1a and 1b borehole objectives, rationale and locations

Objectives for Phase 1a and 1b borings included the following:

- Spatial coverage in all areas of the site
- Shallow and deeper bedrock control points
- Well couplets to determine vertical gradients
- Target areas of high fracture density
- Penetrate representative “sheeting” fracture sets
- Target specific subvertical fracture sets
- Interrogate laterally extensive NW-SE striking fracture system

An initial working CSM for the fracture network at the site was developed on the basis of geologic/fracture mapping (Sec. 5.1.3, and App. C) and subsurface geophysical surveys (Sec. 5.2, and App. E). The CSM developed from these data sets suggested a number of general characteristics of the bedrock system including widely-spaced steeply-dipping fracture sets and moderately- to shallowly-dipping fractures with a somewhat greater fracture density in the uppermost 40 feet of bedrock. On this basis, the CSM generally evoked a two-tiered system with a more highly fractured upper bedrock, comprised of intersecting sets of subvertical fractures and sheeting fractures in the uppermost 40 feet of bedrock. The deeper bedrock, in this case defined as greater than 40 feet below the top-of-bedrock, consists predominantly of steeply-dipping fractures. The laterally extensive NW-SE striking fracture system which bisects the site was interpreted to be of particular importance. A generalized diagram which illustrates these relationships is presented on Figure 5.3.1-1. The evolution of the CSM for the fracture system is discussed in detail in Section 7.0, below.

The Phase 1a and 1b boreholes were targeted to specific fracture sets identified through surface mapping and surface geophysics. Figure 5.3.1-2 shows the Phase 1a/1b borehole locations superimposed on a fracture map generated from outcrop data. The array of boreholes sought to provide a reasonable level of spatial coverage within the site area as well as targeting unique fractures of interest. In many locations, couplets with co-located shallow and deep boreholes were installed in an effort to isolate shallow and deeper bedrock zones. Steeply-dipping fracture systems, such as the NW-SE trending system in the central part of the site, were targeted with angled borings to maximize probability of penetration. In such cases, azimuths of the angled boreholes were selected to intersect the fractures of greatest interest at a near perpendicular angle.

5.3.2 Percussion drilling

Eighteen borings were installed in the bedrock of Shepley's Hill by means of percussion drilling. Locations and orientations were selected based on information collected by surface outcrop mapping, surface geophysical surveys, and analysis of topographic lineaments, as outlined in Sections 5.1 and 5.2. Percussion drilling was chosen because of its relatively high speed and low cost, as well as its ability to install oriented borings. Angled borings increase the probability of crossing steeply dipping fracture sets. These advantages were judged to outweigh the disadvantages of the method, which often yields deviated and rough-walled holes.

Drilling of the shallow (up to 73 ft bgs) bedrock borings followed the same sequence at all locations. A socket was drilled approximately 2 to 3 feet into the top of rock. Four-inch Schedule 40 PVC pipe was cemented into the socket as a protective casing to allow each boring to be isolated from surface runoff and debris, and to provide for a cap. At locations with soil cover above the bedrock, the PVC casing was pushed through the soil immediately after the socket was drilled, while the boring through the soil remained open. Locations where the soil cover was found to be greater than about 8 ft thick were abandoned, so that the holes could be cased with a single, 10-ft PVC pipe. When the cement grout had set, each hole was advanced through the PVC surface casing.

The open bedrock borings were drilled in two mobilizations. Seven holes, each approximately 4 inches in diameter, were completed in the first mobilization in February 2008 (Phase 1a). An unusual mid-winter thaw during this field effort created very muddy conditions that proved impassable for the drill rig. Operations were suspended until September 2008 (Phase 1b), when 11 additional borings were completed, each approximately 3.5 inches in diameter. Drill cuttings were caught in a kitchen strainer and visually logged (e.g., color, texture, etc.) for each boring (App. F).

The locations of the 18 borings are shown on Figure 5.1.3-1. Borehole orientations and depths are summarized in Table 5.3.2-1.

5.4 Geoprobe overburden drilling

During the installation of the first phase of bedrock boreholes during the winter of 2008, it was discovered that overburden deposits were more variable and notably thicker than expected in some areas. This discovery caused practical difficulties in installing the bedrock wells, and also forced the project team to consider more carefully the role of overburden within the study area as a potential pathway for groundwater from the hill area to the landfill. In particular, the saturated thickness of overburden materials in the central topographic valley portion of the study area was estimated based on results from casing installation in support of the bedrock drilling. In order to address this data need, a series of small diameter borings were installed by the Office of Environmental Measurement and Evaluation (OEME) unit of USEPA Region 1 using Geoprobe equipment. On June 4 and 5, and July 1, 3, and 28, 2008, a total of 23 shallow borings were advanced to the top-of-bedrock surface; eight of these were finished as small diameter (1.25-inch I.D.) monitoring wells, each with at 2 foot screened interval (0.010-inch-slot screen), sand pack (No. 1 sand), and a two-foot bentonite seal. The borings and wells are located on Figure 5.3-1. Appendix G provides the boring depths and well construction details, bedrock depths, and other pertinent information for all small-diameter overburden wells and borings advanced for the project. Boring logs and well construction diagrams are included in Appendix G. Also included in Appendix G is a memorandum from OEME which documents the small-diameter boring/well installation details and provides GPS coordinate information. It should be noted that the wells were later re-surveyed and tied into the site well network (Sec. 5.12).

Figure 5.4-1 presents an interpretation of the overburden thickness as indicated from small-diameter boring and well data, as well as top-of-rock information obtained from bedrock borehole installations (Secs. 5.3, 5.10), surface bedrock outcroppings (Sec. 5.1.3), and surface geophysical surveys (Sec. 5.2). However, note that the contours presented reflect computer interpolation of the overburden thickness, and do not adequately account for the abrupt thickening of overburden eastward beneath the landfill cover. The small-diameter drilling program identified several areas with relatively thick lenses of overburden deposits on the order of 10 feet or more in thickness. This finding underscored the possibility that significant groundwater flow occurs within the overburden materials, and that the discontinuous patches of overburden may store water temporarily following precipitation or snowmelt events, allowing it to drain slowly to the underlying fracture network. Therefore, these represent elements of the CSM that needed to be clarified. In conjunction with synoptic bedrock water level measurement efforts, water levels were also collected at the small diameter overburden wells in order to better quantify the variability and *saturated thickness* of the overburden deposits. A more detailed discussion of the importance of groundwater flow within the wedge of overburden materials is included in Section 5.6.4.

5.5 Borehole geophysics

Following installation of the 18 bedrock boreholes during Phases 1a and 1b of drilling, a suite of borehole geophysical surveys was completed. The work was conducted in October and November of 2008 by Hager Geoscience, Inc., under subcontract to Gannett Fleming, Inc. The complete report summarizing this effort, entitled, *Borehole Geophysical Logging, Former Devens Landfill, Ayer, MA, Hager Geoscience, Inc., January 2009*, is included as Appendix H. A brief summary follows.

Techniques used included the following:

- Caliper
- Fluid Temperature and Fluid Resistivity
- Natural Gamma
- Acoustic Televiewer (ATV)
- Heat-pulse Flow-meter (HPFM)
- Borehole Deviation

Caliper, fluid temperature, fluid resistivity, and natural gamma logging was completed for all boreholes. Due to resource constraints as well as a number of technical complications, ATV, HPFM, and borehole deviation surveys were not conducted for all borings. Table 5.5-1 presents an overall summary of the borehole logging². As noted in this table, borehole deviation, poor borehole condition (e.g., borehole roughness), diameter variations, and other factors precluded complete coverage with all methods. While not ideal, this outcome was foreseen by the project team as a potential negative to the overall investigation approach. Conversely, the ability to cover a much wider area using a lower cost drilling method for Phase 1a/1b was an offsetting advantage, particularly given the heterogeneous nature of fractured rock. In any case, the borehole geophysical data collected was used in conjunction with other data sets, such as water level measurements, slug test data, etc. to identify a subset of Phase 1a/1b monitoring wells for permanent monitoring well installation as well as to refine the CSM in terms of locating a suitable location for installing a deep core-hole using traditional rock coring methods. Use of the borehole geophysics and other data sets relative to these tasks is discussed further in Sections 5.9 (Shallow bedrock well installation) and 5.10.1 (Rationale for location, deep bedrock borehole), below. The role of the borehole geophysical data with respect to evolution of the overall CSM for the fracture system is discussed in detail in Section 7.0, Fracture Network, below.

² Note that discrepancies in Table 5.5-1 for “BR casing” and “stickup” reflect differences between estimated and measured casing stickup; refer to Appendix H.

Table 5.5-1, Summary of borehole geophysical logging program

Well ID/Group	OB (ft)	BR casing [1] (ft)	stickup [3] (ft)	W.L. [2] (ft below TOC)	TD	Open hole in rock	water-filled hole
A							
27-2	0	2.5	3	24.82	73.00	19.32	48.18
27-1	0	3	2	19.20	80.00	14.20	60.80
Q5-1	0	3	2	10.27	55.21	5.27	44.94
Q5-2	0	2.5	2	10.85	58.51	6.35	47.66
CAP-1B	7	3.5	2	13.28	58.11	0.78	44.83
CAP-2B	8	3.5	2	13.00	58.71	-0.50	45.71
20-1	0	2.5	1	23.61	70.30	20.11	46.69
3-2	0	2.5	1.5	30.75	59.32	26.75	28.57
Q4-1	7.5	2	0.5	12.67	51.11	2.67	38.44
27-30B-1 [4]	0	2.5	3	19.66	59.26	14.16	39.60
				TOTAL	623.53	TOTAL	445.42
B							
27-30B-2	0	2.5	3	21.13	22.21	15.63	1.08
CAP-4	9	1.5	2	10.39	13.81	-2.11	3.42
CAP-3	6	3	2	15.24	40.91	4.24	25.67
Q4-2	8.5	2.5	1.5	14.26	53.41	1.76	39.15
20-2	0	2.5	0.5	18.03	25.31	15.03	7.28
3-1	0	2.5	1.5	30.77	49.18	26.77	18.41
3-2	0	2.5	1.5	30.75	59.32	26.75	28.57
3A-1	0	2.5	1.5	30.37	52.21	26.37	21.84
3A-2 [4]	0	2.5	1.5	27.14	55.01	23.14	27.87

[1] est. 2.5 for most holes; some not recorded

[2] from top of casing; most recent measurement: 10/23/.

[3] approximate

[4] lower priorities

5.6 Water levels

The following sections describe collection of water-level data by means of manual measurements and recording pressure transducers installed in the open bedrock borings on Shepley's Hill, as well as related results from the piezometer pair N5-P1/P2, which lies approximately 550 ft downgradient to the east, within the footprint of the landfill (Fig. 1.0-2(a) and (b)), and serves as a control point to place the site-scale results in the broader context.

5.6.1 Manual gauging and interpreted potential surfaces

Water levels were gauged on occasion at the newly installed open bedrock borings and wells on Shepley's Hill. From these data, it is possible to develop interpretations of the hydraulic potential surface in the fractured rock of the study area. Recall that the borings are of varying depth below ground surface, and that many of them are angled holes. It is emphasized that interpretation of the potential surface implicitly assumes that the predominant fractures at each location are interconnected, and that the system behaves in

some sense as an equivalent porous medium. The assumption generally is borne out by the data; that is, the interpreted hydraulic potential surface tends to mimic the overlying surface topography, as is typically the case for an ideal porous medium. It is also noted that groundwater flow directions can be inferred to be normal to the equipotentials only if the effective hydraulic conductivity of the fractured rock is transversely isotropic. In this case, two of the principal directions of the conductivity tensor are of equal magnitude, while the third is different. This can occur, for example, in a layered system, in which the hydraulic properties parallel to the layers are the same in all directions, but differ normal to the layers. In the system under study here, which exhibits several major fracture sets of different orientation, including both steeply dipping and sub-horizontal (“sheeting”) fractures, it may be reasonable to suppose that the effective conductivity at scales of hundreds of feet is isotropic in the plane of the sheeting fractures.

Manual water levels were gauged at all available borings on April 24, 2009; August 5, 2009; September 9, 2009; and March 17, 2010. Interpretations of the potential surface on each of these dates are shown in Figures 5.6.1-1 to 5.6.1-4. The gauging carried out in spring (April 2009 and March 2010) captures relatively high-groundwater conditions (maximum water elevation measured: 271.26 ft msl at 20-2, March 2010), and that done in summer (August 2009 and September 2009) reflects relatively low-groundwater conditions (minimum water elevation measured at the same point: 261.27 ft msl at 20-2, September 2009). The overall shape of the potential surface does not change significantly seasonally; rather, it appears that water levels fall throughout the system as it progresses from the high-recharge events of late winter and early spring to conditions of minimal or no recharge in late summer. Borings higher on the hill see larger seasonal changes than do the borings at the toe of the slope, where water levels are “buffered” by proximity to the overburden aquifer to the east. For this reason, the hydraulic gradient in the fractured-rock aquifer of the hill is steepest at times of high water levels in the late winter and early spring, and declines in magnitude into late summer and fall. (See further discussion in Section 8.1.)

The interpreted potential surface (Figures 5.6.1-1 to 5.6.1-4) roughly mimics the overlying topographic surface. For flow in an isotropic porous medium, this implies groundwater flow on the scale of Shepley’s Hill overall that is directed from the ridge crest toward the landfill to the ESE. On the site scale (i.e., on the scale of the area covered by the shallow bedrock borings installed for this investigation), groundwater flow appears to converge on the valley feature that cuts diagonally across the ridge from SSE to NNW. The interpreted potential surface shows a relatively flat “plateau” in the center of the study area.

5.6.2 Continuous gauging by transducer

Recording pressure transducers were installed in 15 open bedrock borings for various periods of time (Table 5.6.2-1), depending upon availability of the holes (e.g., those drilled in February 2008 or in September 2008) and availability of transducers (acquired in two separate purchases). Boring 27-30B-2 was not gauged by recording transducer

because it is a shallow hole (~20 ft bgs) that is often dry. A transducer was not installed in boring Q5-2 because it is paired closely with another boring (Q5-1) of similar depth, albeit of different orientation. Boring CAP-4 was not gauged because the hole collapsed shortly after drilling. Water levels in all other holes were recorded for various periods. The transducer in boring Q4-1 was downloaded after a brief trial period from 4/18/08 to 4/30/08, but subsequently was lost when the cable from which it was suspended broke, and the instrument could not be recovered. Data from boring 27-1 recorded after 5/21/09 were lost due to failure of the transducer electronics.

Table 5.6.2-1. Periods of continuous water-level monitoring in open bedrock borings

Boring	Transducer period
3-1	4/18/08 – 12/17/09
3-2	4/18/08 – 9/25/09
3A-1	4/18/08 – 2/26/09
3A-2	4/18/08 – 2/26/09
20-1	4/18/08 – 9/24/09
20-2	4/18/08 – 2/5/10
27-1	2/26/09 – 5/21/09
27-2	2/18/09 – 9/22/09
27-30B-1	2/26/09 – 9/23/09
27-30B-2	not instrumented
CAP-1B	2/26/09 – 12/17/09
CAP-2B	2/26/09 – 9/24/09
CAP-3	2/26/09 – 12/17/09
CAP-4	not instrumented
Q4-1	4/18/08 – 4/30/08
Q4-2	2/18/09 – 12/17/09
Q5-1	2/18/09 – 9/23/09
Q5-2	not instrumented

The complete transducer records are included in Appendix I in spreadsheet format.

5.6.3 Apparent vertical gradients within shallow bedrock

The bedrock borings on Shepley’s Hill include two vertical pairs drilled to different depths in close proximity: 20-1 and 20-2, and 27-30B-1 and 27-30B-2. It is of interest to examine water levels at these boring pairs for indications of the vertical hydraulic gradients that prevail in the shallow bedrock of the hill. The data collected in Table 5.6.3-1 represent manual water-level measurements collected at five times. Arrows indicate the sense of the vertical gradient (upward where the head in the deep boring is greater than the head in the shallow boring).

Table 5.6.3-1. Water elevations at bedrock borehole pairs based on manual measurements.

Boring	Depth (ft btoc)	Elevation (ft msl)				
		10/23/08	4/24/09	5/21/09	8/4/09	9/10/09
20-1	68.7	264.79↑	260.70↑	262.68↑	262.94↑	261.27↑
20-2	25.2	263.42	255.93	260.80	260.60	250.19
27-30B-1	59	262.00↑	254.17↑	259.44	259.04↑	248.09
27-30B-2	22.25	261.95	253.74	NM	258.02	NM

In every instance for which data are available, the water level in the deeper boring is higher than that in the shallow boring paired with it. This is somewhat counterintuitive based on experience with overburden aquifers, where the vertical component of the hydraulic gradient in a recharge area is expected to be downward. However, it is emphasized that the present data are from open borings that intersect numerous fractures of varying orientation, aperture, and connectivity. Therefore, the water level in each boring probably reflects primarily the head in the conductive fracture or fractures at the highest head intersected. Vertical connectivity may be limited locally, particularly if the sub-horizontal sheeting fractures predominate in transmitting water. In general, one might expect that, at any given location, deeper fractures are recharged higher on the hill, and shallower fractures are recharged at lower elevations closer to the boring. This may explain the persistently higher water levels observed in the deeper boring in each well pair. Deeper sheeting fractures may be connected to a water-filled network that extends to higher elevations upgradient than shallower sheeting fractures.

It is also interesting to note that, when water levels are relatively low (e.g., 4/24/09 and 9/10/09), the head difference at the well pair is larger; when water levels are relatively high, the head differences are smaller. This suggests that the shallower fracture network drains more readily (i.e., the shallow boring sees much greater changes), while the deeper network sustains more constant head conditions.

Manual water-level data are also available for the deep corehole well pair, located at the eastern “toe” of the hill and the western edge of the landfill. These wells were gauged prior to development on 10/13/09. The water elevation in the deep well, CH-1D, was 234.80 ft msl, while that in the shallow well, CH-1S, was 233.12 ft msl. That is, the head at the deeper screen (85 to 95 ft bgs) was 1.68 ft higher than at the shallower screen (36 to 41 ft bgs). The corehole wells were gauged again in conjunction with sampling events November 2 – 4, 2009, and March 16 – 17, 2010. In November 2009, the water elevations in CH-1D and CH-1S were 233.09 ft msl and 232.96 ft msl, respectively, showing a head at the deeper screen 0.13 ft greater than that at the shallow screen. In March 2010, the water elevations at CH-1S and CH-1D were 247.02 ft msl and 246.79 ft msl, respectively, indicating a head at depth 0.23 ft greater than that in the shallower bedrock.

As discussed in the foregoing, a possible explanation for the head differences observed at the deep corehole well couplet is that the deeper fractures are plumbed to a recharge area higher on the hill, while the shallower fractures are plumbed to a recharge area lower on the hill. Therefore, the deeper heads tend to be higher than the shallower heads, particularly if the vertical interconnection of the fractures is not well developed. Again, this is consistent with the inference that the sub-horizontal sheeting fractures tend to dominate the fracture conductivity.

Continuous gauging of the corehole well pair by transducers from February 2010 to September 2010 (see Sec. 5.11) verified that the water level at the deep screen was consistently higher than that at the shallow screen. The head difference increased in magnitude throughout the monitoring period from a few tenths of a foot in February to over seven feet in September, as water levels overall decreased from their late winter – early spring maximum to their fall minimum.

5.6.4 Head differences between overburden and shallow bedrock

One comprehensive round of water-level measurements in both the overburden piezometers and the open bedrock borings was collected on April 24, 2009. There are no locations where a bedrock boring is immediately adjacent to an overburden piezometer, but there are a few locations where the distances are relatively small, and the ground surface elevations are similar. These include MW-22, which is in a relatively flat area a short distance downgradient of borings 27-1 and 27-2; MW-7 in close proximity to CAP-1B; MW-16 in close proximity to Q4-1; MW-4-1 close to CAP-2B; and MW-1 close to CAP-4. Table 5.6.4-1 shows water elevations observed on April 24, 2009; arrows accompanying the bedrock groundwater elevations indicate the direction of the apparent vertical gradient relative to the nearby overburden well (upward where the bedrock water level is greater than the overburden level, downward where the overburden water level is higher).

These water levels indicate that the heads in the overburden and bedrock higher on the hill (MW-22, 27-1, 27-2) are roughly equilibrated, exhibiting small differences. At the foot of the hillslope, the head in the overburden at MW-7 is 6.21 ft higher than that in the bedrock at nearby CAP-1B, and the head at MW-4-1 is 2.31 ft higher than at CAP-2B. A comparison between MW-1 and CAP-4 is perhaps not as meaningful, because CAP-4 collapsed shortly after it was drilled. From these limited data, it is difficult to generalize about the connectivity between overburden soil and underlying bedrock. In the three locations noted, the overburden and shallow bedrock appear to be well connected (MW-22, 27-1, 27-2) or the overburden groundwater is “perched” relative to the underlying bedrock (MW-7, CAP-1B; MW-4-1, CAP-2B), suggesting locally poor vertical connectivity.

Table 5.6.4-1. Water levels in bedrock borings and nearby overburden wells based on manual measurements.

OB well	BR boring	Water elevation (ft msl)
MW-22		263.54
	27-1	263.90↑
	27-2	262.40↓
MW-7		244.88
	CAP-1B	238.67↓
MW-16		dry
	Q4-1	262.23
MW-4-1		245.55
	CAP-2B	243.24↓
MW-1		245.01
	CAP-4	245.57↑

5.6.5 Bedrock water-level response to precipitation events

Recording pressure transducers were deployed in a number of borings for varying periods of time (see Table 5.6.2-1). It is of interest to examine the data for the response to measurable rain events. Recharge is expected to exhibit strong seasonality because of the effects of freezing and evapotranspiration. In particular, recharge can be erratic in the winter, when surface soil is frozen and much of the precipitation occurs as snow. Occasional winter thaws can release water to recharge. Recharge is typically at a maximum in early spring, when evapotranspiration is low due to mild temperatures and low plant activity. As summer progresses, a smaller fraction of precipitation goes into recharge, while a larger fraction is lost back to the atmosphere via evapotranspiration. In the fall, recharge often increases again, as temperatures drop and plant activity subsides.

For present purposes, rainfall and water-level data have been isolated for two periods, March – April 2009, and August – September 2009. The former is expected to encompass what is typically the period of greatest recharge; the latter is typically characterized by falling groundwater levels. These generalizations, of course, neglect anomalous events of extraordinary rainfall or drought. In 2009, ten precipitation events were recorded at the Fitchburg airport (about 8 miles west of the site) in March and April, ranging in magnitude from 0.10 to 1.67 inches. (Daily records have been summed where rainfall was recorded for consecutive days.) In August and September, five events were recorded, ranging from 0.17 to 1.71 inches. Borings 20-1, Q4-2, 3-1, and CAP-3 were selected for examination because they each had a transducer during the period of interest, and they represent locations successively lower on the hill, from 20-1 (closest to the ridge crest and presumed groundwater divide) to CAP-3 (at the break in slope between the bedrock hill and the adjacent alluvium of the landfill area).

Figure 5.6.5-1 exhibits a plot of the change in water level versus precipitation for boring 20-1 in March and April 2009. The plot and linear regression omit one datum for March 8 – 10, when 0.69 in (0.0575 ft) precipitation was recorded, and the water level at this location rose 3.45 ft. This apparently anomalous event (relative to the other events shown on this plot) likely represents rain that fell while there was still snow on the hill, so that the large rise in water level includes water derived from snowmelt, and is not closely correlated with the magnitude of the rainfall. For the nine events shown on the plot, water-level changes correlate with rainfall. The linear regression indicates that the water level change is approximately 10 times the rainfall. In a local (i.e., with no coupling to adjacent areas at different elevations) and static (i.e., with no groundwater flow) system, the water level would rise by a factor scaling with the inverse of the porosity and with the fraction of the precipitation that goes to recharge:

$$\Delta h = \frac{\beta P}{n}$$

where Δh is the change in water level, β is the fraction of precipitation that goes to groundwater recharge, P is the magnitude of the precipitation event, and n is the fracture porosity. The regression analysis for 20-1 in March and April shows that $\Delta h/P = 9.8$. If one assumes a typical fracture porosity of $n = 0.02$, this implies that the fraction of precipitation going to recharge is approximately $\beta = 0.2$. This value is comparable to those typically estimated for overburden aquifers regionally, suggesting that recharge to the fractured bedrock occurs readily. It is noted that downgradient flow within the fracture network is able to carry off some of the recharge on the time scale of a typical precipitation event, so that the measured water-level response likely underestimates the true recharge.

Five rainfall events were recorded at Fitchburg Airport in August and September. Water-level changes were monitored at 20-1 for three of these events; one occurred while the transducer was above the water surface due to the drop in water levels throughout the system in late summer and early fall; one occurred after the transducer was removed for well installation (September 24). Of the three remaining events, two (rainfall of 0.17 and 0.81 inches) were accompanied by water-level declines, and one (rainfall of 1.71 inches, or 0.1425 ft) was accompanied by a rise of 0.93 feet. The two events that were accompanied by declines in the water level are interpreted to be too small in magnitude to overcome the longer-term decline in water levels that was observed during this season. The large rainfall event of 1.71 inches was detectable as a recharge event that temporarily raised the groundwater level at 20-1, with a response about 6.5 times the input. This response is comparable in magnitude to that observed in the spring events, which exhibited a multiplier of 9.8 based on the linear regression shown in Figure 5.6.5-1.

Results for borings Q4-2, 3-1, and CAP-3 are presented in Figures 5.6.5-2, 5.6.5-3, and 5.6.5-4, respectively, again for March and April, 2009, precipitation events, omitting one that occurred over March 8 to 10. Correlations of water-level changes and rainfall are summarized in Table 5.6.5-1. The response of water levels at Q4-2 is similar to that at 20-1, as discussed in more detail in the foregoing, with the ratio $\Delta h/P$ being slightly

lower at 8.2. Near the eastern margin of the hill, both 3-1 and CAP-3 show a notably smaller response to the same precipitation events, both exhibiting a ratio of $\Delta h/P$ of approximately 1.9. The reasons for this apparent difference in the response at borings high on the hill (20-1, Q4-2) and those near the toe of the slope (3-1, CAP-3) are not known from this limited data analysis. A possible factor is that water levels in the fractured bedrock near the toe of the slope on the eastern margin of the hill are “buffered” by water levels in the adjacent overburden aquifer, which exhibits notably smaller changes due to its much greater porosity. Rapid excursions in groundwater levels in the fractured rock at the eastern margin of the hill are expected to relax relatively quickly by flow toward and discharge to the overburden to the east, a process that may proceed on the time scale of a typical rain event. It is noted that not only does the ratio $\Delta h/P$ appear to decrease at locations lower on the hill, but the correlation coefficient, r^2 , also decreases systematically.

Table 5.6.5-1. Correlation of water-level changes and precipitation, Spring 2009.

Boring	$\Delta h/P$	r^2
20-1	9.8	0.63
Q4-2	8.2	0.53
3-1	1.9	0.38
CAP-3	1.9	0.42

The general lack of response to precipitation in August and September, as discussed in the foregoing for 20-1, is also seen in the data for the three borings lower on the hill. As noted, water levels were falling throughout this period, and this overall trend appears to have overwhelmed any short-term response to precipitation. These results serve to emphasize the seasonality of recharge in this system.

5.6.6 Water level data from the N5 piezometer pair

Recording pressure transducers have been deployed in the N5-P1/P2 piezometer pair, located approximately 800 ft ENE of corehole CH-1, since April 2007 (Fig. 1.0-2(a) and (b)). This affords an opportunity to examine the relationship between bedrock and overburden water levels at a location in the north-central portion of the landfill, and, in turn, the relationship of water levels within the landfill footprint to those in the elevated recharge area to the west on Shepley’s Hill. The deep piezometer, N5-P1, is screened 7 ft below the top of the bedrock (88.5 ft bgs), in the interval 95.5-97.5 ft bgs. The shallow piezometer, N5-P2, is screened in the overburden, in the interval 23-28 ft bgs, such that the top of the screen is typically 1 to 4 ft below the water table. Although these two piezometer screens are separated vertically by 67.5 ft, and the hydraulic head varies spatially in some unknown fashion between them, the head difference between the two elevations is assumed to provide some measure of the direction of exchange of water

between the bedrock fracture network and the sandy overburden at this location. Because boring logs for the overburden aquifer in the vicinity of the landfill typically show relatively homogeneous, conductive, sandy material throughout its depth, it is reasonable to assume that the head variation between the shallow screen, N5-P2, and the underlying bedrock interface remains small at all times. Therefore, it is likely that a large fraction of the head difference observed between the deep and shallow piezometer screens actually occurs over the seven-foot layer of rock between the bedrock screen, N5-P1, and the overlying bedrock / overburden interface. When the head in the bedrock fractures just below the interface is greater than that in the overburden just above the interface, bedrock groundwater will discharge upward to the overburden wherever interconnected fractures intersect the interface. Conversely, when the head in the bedrock is lower than that in the overburden, the overburden groundwater will recharge the fracture network from above.

Figure 5.6.6-1 displays the head difference between the two N5 piezometer screens, calculated as the head at the bedrock screen, P1, minus the head at the overburden screen, P2. Therefore, positive values indicate a tendency toward upward flow from bedrock to overburden, and negative values indicate a tendency for downward flow from overburden to bedrock. Groundwater elevations were calculated by adjusting the measured head for each piezometer to agree with the manual measurements taken when the transducers were installed and/or reinstalled. The head difference was then calculated from the two records.

The data were not compensated for barometric pressure variations, because the standard compensation step simply subtracts the measured barometric pressure head from the total heads recorded by the transducers. Therefore, the barometric pressure corrections cancel one another when the head difference between the two piezometers is calculated. It is recognized that the barometric corrections for a water-table screen and for a bedrock screen are often handled differently, because the atmospheric loading to the bedrock groundwater is transmitted in part via elastic deformation of the rock (Jacob, 1940). The “noise” evident in the plot of head difference between the two piezometers, reflects short-term variation (i.e., of the order of a few days) in atmospheric pressure and the difference in the response to these fluctuations between the water-table and bedrock wells. It is noted that the magnitude of the fluctuations in the calculated head difference is of the order of ± 0.1 ft, while the standard deviation of the barometric pressure head measured at the site over a one-year period is about 0.3 ft, suggesting that the “noise” displayed in the plot of the head difference represents the difference in the magnitude of the response of overburden and bedrock groundwater to the same atmospheric loading. The annual range of head difference is of the order of 1 ft, an order of magnitude greater than the scale of the short-term fluctuations, suggesting that the longer-term variations seen in the data are genuine trends.

Figures 5.6.6-1(a) to 5.6.6-1(d) show the water-level difference for the N5 piezometer pair for 2007 – 2010, by calendar year. Only a partial record is available for 2007, because the data logging in both piezometers began on April 26, and a partial record is available for 2010, because the data loggers were last downloaded on September 24. In 2008, data are absent for a period from January 1 until January 17 because the memory in

the N5-P1 data logger was full. Daily rainfall data from the Fitchburg, MA, airport meteorological station are displayed in Figures 5.6.6-1(a) to 5.6.6-1(d) for comparison.

Inspection of the records for the head difference at the N5 piezometer pair (Figs. 5.6.6-1(a) to 5.6.6-1(d)) reveals variability from year to year, but some patterns appear to be repeatable. The head difference reaches a (positive) maximum in mid-winter to early spring, and tends to fall to negative values in summer and fall. The highest positive head difference recorded in 2008 was reached on February 29; the highest value attained in 2009 occurred on January 10. (Note that these extreme values may be exaggerated by barometric pressure effects at the time, but they are nonetheless local peaks superimposed on a broader peak in the longer-term trend.) The lowest (most negative) head difference in 2007 occurred on September 11; that in 2008 was observed on May 31, with comparable lows persisting into July; that in 2009 was recorded on September 27.

It appears that positive head differences, i.e., a tendency to drive flow upward from bedrock into overburden, generally occur during periods of high recharge and, correspondingly, higher water levels overall. In New England, monthly precipitation averaged over many years is fairly uniform; it does not exhibit large seasonal variation. For any particular month in any particular year, of course, precipitation can depart significantly from long-term averages. Groundwater recharge tends to be greatest in late winter and early spring, when snow melts, surface soil thaws, and evapotranspiration is low (i.e., temperatures are low and plant activity is minimal). This is reflected in relatively high water levels throughout the Shepley's Hill system, and maxima in the magnitude of the head difference at N5-P1/P2. Negative head differences at N5 tend to occur in summer and early fall, when groundwater recharge is at a minimum (evapotranspiration is at a maximum), and water levels are falling overall. Under these conditions, overburden groundwater tends to flow downward to recharge the underlying bedrock aquifer at this location.

The seasonal reversal in the sign of the head difference between N5-P1 and N5-P2 is believed to be due to the difference in the "storage" mechanisms for the semi-confined, fractured-bedrock aquifer and the unconfined, overburden aquifer. For a confined aquifer, storage of water mass associated with transient changes in head is accommodated by compression of the water and dilation of the porous skeleton. Because water and rock are relatively incompressible, the storativity of a bedrock aquifer is relatively small. For an unconfined aquifer, storage is accommodated by saturation of void space above the water table, and the capacitance of the aquifer is characterized by the specific yield, which can approach the porosity in magnitude. Because the storativity of the fractured rock aquifer is much smaller than the specific yield of the overburden aquifer, water levels in the overburden respond more slowly to seasonal variation of recharge than do water levels in the underlying bedrock. During summer and early fall, the water level at the bedrock piezometer screen, N5-P1, drops more rapidly than that at the overburden piezometer screen, N5-P2, until the former is lower than the latter, and there is a tendency for the overburden to recharge the underlying bedrock.

The long-term average head difference at the N5 piezometer pair appears to be positive, indicating a net upward discharge of bedrock groundwater to the overburden. Table 5.6.6-1 summarizes characteristic parameters for each year covered by the gauging. Several observations are consistent from year to year. The minimum head differences fall in a fairly narrow range (-0.30 to -0.53 ft), as do the maxima (+0.66 to +0.87 ft), and the maximum is in each case greater than the magnitude of the minimum. The head difference averaged over the year is positive for the two years (2008 and 2009) for which the records cover the full year (2009) or nearly the full year (2008; data are missing for January 1 through January 17). The head differences averaged over the available data for 2007 and 2010 are negative. However, it is noted that the portions of those years for which data are not available (January to April, 2007; September to December 2010) are periods typically characterized by positive head differences. Therefore, it is likely that the averages shown in Table 5.6.6-1 are biased low due to the partial-year data coverage. It is inferred that the long-term average head difference at the N5 location is positive, representing net upward discharge from bedrock to overburden. The average over all available data, disregarding the observation that the data coverage is not balanced across all seasons, is +0.08 ft.

Table 5.6.6-1. Annual characteristics of the head difference at the N5 piezometer pair.

Year	Minimum Δh (ft)	Maximum Δh (ft)	Average Δh (ft)	No. of data
2007*	-0.49	+0.66	-0.10	5701
2008	-0.30	+0.99	+0.28	8369
2009	-0.40	+0.73	+0.09	8756
2010*	-0.53	+0.87	-0.06	6394

*partial year

It is noted that groundwater elevations in the fractured rock of Shepley's Hill are higher than those in the overburden aquifer to the east throughout the year. Therefore, it is likely that groundwater discharges upward from bedrock to the overburden throughout the year at locations close to the eastern margin of the hill, where the overburden pinches out against the rising bedrock. It is inferred from the data presented here from the N5 piezometer pair that, at the N5 location, approximately 400 ft east of the margin of the hill, the vertical head difference is seasonal, driving upward discharge in periods of high water levels on the hill, and downward flow in periods of lower water levels in the recharge area. It is inferred that a line separating a domain of upward discharge (bedrock to overburden) from downward recharge (overburden to bedrock) shifts seasonally, typically moving east of the N5 piezometer pair during late winter and early spring, and lying to the west of this location during the summer.

In view of the apparent reversal of the vertical hydraulic gradient at the N5 piezometer pair, it is of interest to seek a possible correlation with available arsenic analyses. A brief review of historical sampling of the N5-P1 piezometer yields eight events for which the

water levels at the P1 and P2 screens were recorded, and groundwater samples were analyzed for arsenic³ (CH2MHill, 2007; ECC, 2008, 2009, 2010). The results are summarized in Table 5.6.6-2. Six of the sampling events were carried out when the shallow head was greater than the deep head, implying downward flow from the overburden into shallow bedrock. For these events, the arsenic concentrations fell in the range 4429 to 5970 µg/L. Two sampling events were executed when the deep head was greater than the shallow head, implying upward flow from bedrock to overburden. Under these conditions, the arsenic concentrations were 1930 and 1748 µg/L. Within this limited data set, the results are consistent, and suggest that arsenic concentrations in the deep overburden at this location may be approximately 5000 µg/L or higher, and arsenic is advected downward to the shallow bedrock fracture network when the shallow head is greater. Bedrock groundwater at this location appears to be at concentrations less than 2000 µg/L as it approaches the bedrock – overburden interface when the deep head is higher. Unlike the bedrock groundwater [observed at CH-1D (see Sec. 9.0)], arsenic in N5-P1 is highly correlated with dissolved iron. The lowest arsenic concentrations in N5-P1 correspond to the lowest levels of iron (9100 and 11000 µg/L) and potassium (4900 and 3500 µg/L) but elevated calcium (96000 and 79000 µg/L). Some caution should be exercised in interpretation of these results, as the data obtained from N5-P1 to date also suggest some correlation of arsenic with turbidity. Only continued monitoring can confirm a relationship between dissolved arsenic concentrations and up-flow versus down-flow at this location.

Table 5.6.6-2. Head difference, arsenic, iron, potassium, and calcium concentrations at bedrock piezometer screen N5-P1.

Date	Δh (P1 – P2) (ft)	As (µg/L)	Fe (µg/L)	K (µg/L)	Ca (µg/L)
8/5/2005	-0.2	4450	23000	5200	85000
4/13/2006	-0.18	4940	30000	5900	72000
6/6/2006	-0.01	5970	41000	6600	70000
9/25/2006	-0.14	4560	30000	6000	73000
12/12/2006	+0.51	1930	9100	4900	96000
10/18/2007	-0.13	4856	33000	5900	69000
10/3/2008	+0.4	1748	11000	3500	79000
10/22/2009	-0.16	4429	34000	5200	70000

³ Baseline geochemical data (August 2005) were communicated directly to the BCT by CH2MHill.

5.7 Slug tests on open bedrock boreholes

Slug tests were conducted in all of the shallow bedrock borings where sufficient water was present (Table 5.7-1). Fifteen locations were characterized in this fashion. Two shallow holes, 20-2 and 27-30B-2 (paired with deeper holes 20-1 and 27-30B-1, respectively) contained only a few feet of water at the time of the testing (July – September 2009), and would not accommodate both the transducer and the slug. Boring CAP-4 collapsed shortly after drilling, and also contained only a few feet of water in the remaining portion of the hole. These three holes were not characterized by slug tests.

The slug tests followed conventional procedures. Each boring was first gauged manually for total depth and depth to water. A transducer was programmed to record water levels at one-second intervals, and was lowered to about 15 ft below the static water level. The slug consisted of PVC pipe filled with sand, 5 ft long and 1.5 inches in outside diameter, which displaced about 0.06 ft³. In the 4-inch borings, this slug displaces the water level by about 0.7 ft; in the 3.5-inch borings, the water is displaced by about 0.9 ft. The slug was lowered on a rope to just above the static water surface, and then allowed to free-fall to a depth just below the initial static water surface. This causes a rapid rise in the water level in the boring due to the displaced volume, followed by a transient recovery as the excess head drives water out into the fractured rock, and the head in the boring equilibrates with the surrounding groundwater. This is known as a “falling head” test. Fifteen minutes were allowed to pass in order to provide ample time for the equilibration. The slug was then pulled out as quickly as possible, resulting in a rapid drop in the water level within the boring, again followed by a time-dependent recovery. This phase is known as a “rising head” test. Data logging was continued for 15 minutes after the withdrawal. Post-test data analysis verified that the 15 minute recording interval was, in most cases, adequate to capture the transient recovery of the water level in the boring. For a few relatively “tight” holes, the recovery time was longer than 15 minutes, but the data were sufficient to support interpretation.

The data were interpreted using the Hvorslev model. It is emphasized that standard slug-test models of any type may not apply to a fractured-rock setting. Therefore, results from this exercise should be regarded as qualitative, yielding a reasonable estimate of the order of magnitude of the “effective” hydraulic conductivity of the bulk rock on the scale of the saturated borehole length, but not a precise measure. The simplest form of the Hvorslev model assumes a homogeneous porous medium extending radially without bound, and assumes that the screen length for the well is much greater than the well radius. In fractured rock, of course, it is possible that the transient water-level recovery is controlled by flow into or out of a small number of predominant fractures of larger aperture and greater interconnectivity. For present purposes, the “screen length” in the Hvorslev model is taken to be the saturated borehole length under static conditions, i.e., the difference between the total depth and the depth to water prior to the slug tests. The Hvorslev model is based on an analytical approximation to the flow that takes the form of an exponential decline in the magnitude of the initial head perturbation. The rate constant is inferred from the time required for the water level change to reach e^{-1} ($\cong 0.37$) times its initial value (i.e., the maximum excursion recorded). It is noted that most of the

data collected in the boreholes in the study area are “well-behaved,” in the sense that they typically exhibit a smooth, transient recovery, asymptotically approaching the undisturbed, equilibrium water level. However, many do not show the exponential decline predicted by the Hvorslev analysis; i.e., they do not plot as a straight line on a semi-logarithmic plot ($\log(\Delta h)$ vs t). Nonetheless, all data were reduced following the standard Hvorslev protocol, identifying the time at which the disturbance has dropped to 37% of its initial magnitude. In cases in which the recovery was very slow, and the head perturbation had not reached 37% of its maximum magnitude within the period of data recording, such as at boring 20-1, the exponential function was fitted to the available (“early-time”) data. Spreadsheets containing the full recorded data for each boring are included in Appendix J.

Results of the slug tests are summarized in Table 5.7-1. Most show good agreement between the falling- and rising-head tests, with estimated conductivities within a factor of two. Exceptions are Q5-1, CAP-2B, and 3A-1, each of which shows a wider disparity between the falling- and rising-head results; estimates are, nonetheless, within an order of magnitude. One hole, 3A-2, was tested on two occasions, separated by approximately eleven months, over which time the static water level at this boring rose over 4 feet. Results from this repeat testing were highly reproducible.

Many descriptive parameters characterizing natural systems are found to be log-normally distributed, and this is often the case for random samples of the hydraulic conductivity of a given aquifer. For this reason, the appropriate central tendency for the hydraulic conductivity, K , is typically taken to be the geometric mean. In the present case, estimates of K vary widely, from a minimum of 0.06 ft/d (2.3×10^{-5} cm/s) at 20-1 to a maximum of 120 ft/d (4.2×10^{-2} cm/s) at 3A-2. A histogram of $\log(K)$ is shown in Figure 5.7-1, and indicates that the distribution is reasonably approximated as normal, or, equivalently, the distribution of K is log-normal. The histogram and descriptive statistics were constructed by treating the falling- and rising-head results for each boring as independent data. The geometric mean of the 30 values assembled in this fashion is 2.0 ft/d (7.1×10^{-4} cm/s), and values one standard deviation of the log-transformed values below and above the mean are 0.28 ft/d (9.8×10^{-5} cm/s) and 15 ft/d (5.1×10^{-3} cm/s), respectively.

For comparison, the effective conductivities for the shallow fractured bedrock inferred from the slug tests are comparable to conductivities typically found in silty sands (of the order of 10^{-5} to 10^{-1} cm/s) to clean sands (of the order of 10^{-4} to 10^0 cm/s) (Freeze and Cherry, 1979, Table 2.2). The hydraulic conductivity of the sandy overburden aquifer beneath Shepley’s Hill Landfill estimated by various methods (slug tests, pumping tests, calibration of a landfill-scale numerical flow model) is 45 ft/d (1.6×10^{-2} cm/s).

5.8 Field analysis for arsenic

From September 8 to 10, 2009, samples were collected from the open boreholes and field-tested for arsenic using a Hach™ kit. The field test procedure is based on the

Gutzeit method, developed in 1879 for arsenic determination (van Geen et al., 2004). In this method, aqueous inorganic arsenic is reduced to arsine gas, AsH_3 , which then reacts with a silver or mercury salt to produce a colored compound. The intensity of color produced by this reaction corresponds to the arsenic concentration in the original sample. Although it was known at the outset that this method does not yield accurate As concentrations, particularly when As is present in only trace amounts, the information obtained from field-screening of groundwater in the open boreholes was considered in selecting locations for installation of permanent well screens.

Using the pre-packaged Hach kit reagents and a 50-ml water sample, the first step in the field procedure oxidizes any sulfide to sulfate, to prevent false-positive results, and the oxidation is subsequently neutralized. Zinc powder and sulfamic acid are added to produce AsH_3 , which reacts with a test strip impregnated with mercuric bromide. The color of the As-Hg salt that forms due to this reaction ranges from pale yellow to orange-brown, and visual comparison of the test result to the chart supplied with the kit enables estimates of As concentrations from 0 to 500 $\mu\text{g/L}$.

The Hach kit is relatively inexpensive, simple, and straightforward to use. No external standards are required, minimizing opportunity for operator error. Drawbacks include the lack of accuracy, and length of time required for the field screening. On average, approximately 40 minutes were required for each analysis. However, the kit provides a pair of bottles so that two samples can be run simultaneously. In this exercise, results were apparently biased by sample turbidity. One borehole (3-2) yielded an extremely silty sample; field notes indicate that water pumped from this borehole was “tan/beige” at the time the arsenic sample was taken. The Hach result from this sample was approximately 300 $\mu\text{g/L}$. This borehole was re-sampled at the end of the day, when it was noted that the water appeared to be very clear. The arsenic test result at that time was 70 $\mu\text{g/L}$.

Results of the field arsenic screening are provided in Table 5.8-1. No results are reported from the deep corehole, which was not drilled until 9/28/2009. Field As values ranged from a minimum of 5 $\mu\text{g/L}$ to 70 $\mu\text{g/L}$, with one extreme value of 300 $\mu\text{g/L}$ for the turbid sample from borehole 3-2.

For comparison, the lab results from the eight boreholes completed as monitoring wells are provided here. With the exception of the result from borehole 3-2, the comparison between field and lab analyses is not good. The test kit correctly returned values consistent with the lab’s non-detect results for 3 out of 8 samples analyzed by both methods, but apparently overestimated As concentrations in 50% of the samples. It is possible that the overestimated values are due to turbidity in the open-borehole samples.

Table 5.8-1. Field and laboratory test results for arsenic in bedrock groundwater

BOREHOLE	FIELD ARSENIC RESULT (UG /L)	LAB ARSENIC RESULT (UG/L)
CAP-2B	70	10 U
27-30B-1	5	10 U
27-2	5	10 U
27-1	30	10 U
20-1	60	10 U
Q5-1	30	10 U
Q4-1	10	10 U
3-2	300/70*	63

*sampled twice; first sample was extremely turbid, second sample was clear.

5.9 Shallow well installation

Permanent small-diameter monitoring wells were installed in a sub-set of the shallow and moderately-deep bedrock boreholes installed during the first phases of drilling. In order to maximize budget and long-term viability of the borehole network for water level and water quality monitoring, preference in selecting those locations for permanent well emplacement was given to the deeper borings and angled borings, with some exceptions. In most cases, where a shallow and deeper set of paired boreholes was drilled, the deeper borehole was selected for permanent monitoring well installation. In this respect, a number of couplets were created across the site for determination of vertical hydraulic gradients between shallow open-hole bedrock borings and screened monitoring wells installed in deeper bedrock. Another goal of the well installation program was to place priority on those locations within the influence of the Shepley's Hill Fault Zone. Permanent monitoring well locations are shown on Figure 5.3-1, a map showing locations of all data collected for the project. Permanent monitoring well locations are also presented on Figures 5.6.1-1 to 5.6.1-4, which show potentiometric maps for various dates.

With regard to vertical well placement within the borehole, efforts were made to target specific fractures of interest based on an examination of drilling/chip logs (App. F) and borehole geophysical logs (App. H). Priority was given to hydraulically significant fractures as interpreted from the geophysical logs. Screened lengths varied from 5 to 15 feet, depending on the number and character of available fractures. Well diameters varied from 1.25" (I.D.) to 1.5" (I.D.) and were constructed using standard well construction techniques. A sand-pack of Number 2 sand was installed in the annular space surrounding the well screen and extended approximately 2 feet above the top of the screen. Above this, a four-foot bentonite seal using coarse bentonite chips (e.g., 'hole plug') was installed. Generally, above the bentonite seal, the boreholes were backfilled with sand and/or a mixture of cement-bentonite grout and finished with expansion plugs. However, poor borehole condition (e.g., borehole collapse) resulted in numerous exceptions. Angled boreholes required additional efforts. Centralizers were installed with the angled borehole screens, and sand pack and bentonite were installed using a

tremie pipe. Detailed well construction diagrams are included as Appendix K. Table 5.9-1 lists the screened interval and other pertinent data for all on-site monitoring wells, including a summary of specific fractures of interest. The well couplet installed in the deep bedrock core hole (CH-1) is discussed in detail below in Section 5.10 (Deep Borehole).

The eight shallow bedrock wells were developed shortly after installation (Table 5.9-2). A period of 12 to 20 months passed between drilling the borings and construction of the wells. Development was performed with a variety of devices. A footvalve (inertial) pump was used initially, because the wells are of small diameter, and the depth to water is typically around 30 ft below the top of the casing. However, because some of the wells were installed without grout in order that the upper portion of the open boring would be accessible for sampling, it was found that the stress imposed by oscillation of the tubing caused vertical motion of the wells. Well 3-2 settled approximately 0.75 ft, and well 27-1 settled about 1.5 ft. For this reason, much of the subsequent development was performed with a slender submersible pump. The water level at CAP-2B was sufficiently shallow that it was developed with a peristaltic pump. Field parameters were not measured during development. In general, each well was purged aggressively until the water ran clear. Between 3 and 9 static well volumes were removed from each well, with the exception of 3-1, from which only 1.5 volumes were removed due to very slow recharge.

5.10 Deep borehole

5.10.1 Deep borehole objectives

In addition to the shallow bedrock holes that were drilled as part of the SHL Bedrock Investigation, a deep borehole was scoped primarily for the purpose of retrieving bedrock core. The objectives of the deep corehole were:

- to obtain additional information about fracture density, aperture, and orientation to greater depth;
- to install a bedrock well couplet for hydrologic and chemical characterization;
- to seek visual evidence of water-rock interaction (alteration, staining, etc.); and
- to characterize the arsenic mineralogy of selected samples.

A detailed description of this core is attached as Appendix L. Total depth of the borehole is 151 feet below ground surface. The overburden is 18 ft thick at the boring location. Total length of borehole that was cored is 133 feet, and core recovery was generally excellent (from 82.5 % to 100 %). The dominant rock type appears to be Chelmsford Granite, with occasional inclusions of Ayer Granodiorite. This is consistent with the lithologies shown on the most current version of the bedrock map of the area (Kopera, 2008) and with the location of this boring near the contact between these units.

5.10.2 Rationale for location

The location for the deep core hole was chosen based on a review of the data collected in the previous phases of work. Additional synthesis of information from the outcrop mapping, fracture trace analysis, surface geophysics, geologic information and borehole geophysics from the Phase 1a/1b borings, slug test data, and analysis of water level data was used to update the working CSM. This information was used to determine the deep bedrock corehole location CH-1, indicated on Figure 5.3.1-2. It should be noted that the deep bedrock corehole sought primarily to target prominent steeply-dipping structures as the 18 shallow and moderately deep bedrock boreholes drilled during Phase 1a/1b provide a reasonable degree of coverage for the shallow fracture system. Figure 5.3.1-2 indicates the predominant steeply-dipping fracture sets of interest. The prominent NW-SE striking lineament, hereafter designated the Shepley's Hill Fault, is highlighted on this figure. Interim data collected up to that point in the project supported the hypothesis that this feature may play a significant role in groundwater flow at Shepley's Hill. For example, contours of the groundwater head field show pronounced inflections in the area of the Shepley's Hill Fault. Angled borehole 27-2 was drilled to provide preliminary information regarding the nature of fracturing in the vicinity of the Shepley's Hill Fault. Borehole 27-2 was oriented at a 60-degree angle in a southwesterly azimuth in an effort to maximize potential for hitting steep fractures in the NW-SE strike direction. Borehole 27-2 was drilled to 71.6 feet bgs. Near the base of this borehole, a significant fracture was detected which exhibited ambient downward flows in excess of 2 gpm, some of the largest identified in the HPFM program. While the ATV tool was unable to resolve fracture orientations at the base of the borehole, this fracture was interpreted to be associated with the Shepley's Hill Fault, and further supported the presence and hydraulic importance of the feature.

In view of this information, CH-1 was located in the projected down-dip direction of the Shepley's Hill Fault in the area adjacent to the landfill cap in an effort to target deep groundwater potentially associated with the Shepley's Hill Fault in the area immediately up-gradient of the landfill. Based on outcrop mapping and geophysical data, the Shepley's Hill Fault was interpreted to dip between 70 degrees to the southwest to near vertical. It is also significant with respect to siting the location for CH-1 that 2-D resistivity profiling (App. E) suggested that the Shepley's Hill Fault demarcated a zone of more highly conductive rock (e.g., less fractured) to the north of the fault with a region of more conductive rock to the south of the fault, (e.g., more highly fractured). Corehole CH-1 was initially located in these respects near CAP-4. However, poor quality of the upper bedrock in the CAP-4 area necessitated moving the CH-1 location southward to its final location just south of MW-4. In this location, it was anticipated that CH-1 would penetrate a highly fractured interval consisting mainly of moderately-dipping sheeting fractures in the uppermost 50 feet, and the Shepley's Hill Fault would be intersected at approximately 150 feet bgs depending on the dip of the fault at depth. Additional discussion concerning the evolution of the overall CSM for the fracture system is discussed in detail in Section 7.0, Fracture Network, below.

5.10.3 Drilling methodology and observations during coring

Corehole CH-1 was drilled by the wireline method. A temporary outer steel casing was driven to bedrock, which was encountered at approximately 18 ft bgs. Continuous core was recovered from the top of rock to approximately 151 ft bgs. HQ core was recovered, which is characterized by a 63.5 mm (2.5 in) diameter, and leaves a boring 96 mm (3.8 in) in diameter.

Advancement of the corehole proved to be relatively slow, due to the very hard rock. The drillers changed from a #8 to a #10 diamond bit, and replaced the drilling head with one capable of a higher rotation rate. The corehole was advanced over six days.

The core exhibited a very large, sub-horizontal fracture at approximately 40 ft bgs, with extensive iron staining penetrating ~4 cm into the matrix above and below. Drilling water losses increased noticeably below this depth. Water loss at greater depth was typically about 2000 gallons per day. Below approximately 60 ft bgs, no water returned to the surface from the boring during drilling. Total water loss over the six days of active drilling was approximately 10,750 gallons. Most of the water is believed to have been lost to the large fracture encountered at ~40 ft bgs. This inference is further supported by observed water-level spikes during drilling of the deep corehole in nearby borings CAP-3 (approximately 24 ft away) and 3-1 (approximately 90 ft away). CAP-3 recorded water-level increases of approximately 2.5 ft; the bottom of the boring is at approximately 197 ft msl, while the large fracture encountered in CH-1 is at an elevation of about 209 ft msl. Water levels at boring 3-1 increased approximately 2 ft during the wireline coring at CH-1; the bottom of 3-1 is at an elevation of approximately 221 ft msl.

Additional evidence that the fracture at about 40 ft bgs was the principal sink for the drilling water was seen during well development. The screened well spanning this interval (CH-1S) was developed by means of a Waterra footvalve pump over a period of several hours. Approximately 160 gallons, equivalent to about 150 well volumes, were removed from the well. The discharge remained extremely turbid throughout development. Subsequent low-flow sampling of the well for chemical analysis also showed very high turbidity. The turbidity is most likely due to the drill cuttings that were carried into the fracture as it took in drilling water.

5.10.4 Summary of observations on the core

A descriptive core log is provided in Appendix L.

Key observations from the core logs are:

1. Numerous mineralized fractures in the granite were observed. The core is not oriented, but fracture strikes and dips were inferred relative to foliation, which is assumed to be fairly uniform in the study area. Orientations are consistent with dominant fracture sets measured from surface outcrops. These are:

- a. striking northwest-southeast, dipping southwest (note: this orientation corresponds to the 'big' valley feature on Shepley's Hill in the area on which this investigation is focused);
- b. striking northeast-southwest, dipping southeast;
- c. sub-horizontal to moderately dipping (to the southeast), sheeting fractures, particularly prominent in the upper ~50 feet of core;

Less frequent fractures were identified with N-S and E-W strikes.

2. Apparently open fractures are observed frequently in the upper ~50 feet of core. Density of open fractures generally decreases with increasing depth in borehole. However, open fractures were observed as deep as ~120 feet.
3. Open fractures show evidence of water-rock interaction. Alteration around fracture surfaces is well defined by bands of iron oxide varying in width from a few mm to several cm (an example is shown in Fig. 5.10.3-1). Iron oxidation on heavily weathered fracture surfaces ranges in color from deep brown-black to yellow, yellow-orange, and red. An unidentified green phase was also observed on fracture surfaces. Other secondary phases, formed by low-temperature aqueous alteration, may be present.
4. Fractures are often surrounded by a 'bleached' zone, lighter in color than the surrounding matrix, believed to be indicative of hydrothermal alteration (Fig. 5.10.3-2), i.e., interaction with hot fluids. Bleached zones are also observed around filled (mineralized) fractures that are not open. We infer that the hydrothermal alteration was early in the history of these rocks, and that some of those fractures remained open or were reactivated in recent times, such that the modern weathering (most notably, the Fe-oxide staining) is superposed on the bleaching.
5. Some parts of the core contained numerous cross-cutting filled fractures, inferred to represent multiple episodes of mineralization. These features are described on the rock core log (App. L) as 'stockwork.' This term is commonly used to refer to thin, closely spaced, randomly oriented or structurally controlled veins associated with ore deposits.
6. Some fracture surfaces are thinly coated with calcite, and some have a thin layer of dark green chlorite. Some of the mineralized fractures contain calcite, but most appear to be filled with quartz. Calcite was positively identified during core logging by testing with dilute hydrochloric acid.
7. Macroscopic sulfide minerals are observed; both gold- and silver-colored sulfide phases are visible. These phases are found along mineralized veins (Fig. 5.10.3-3) and also disseminated within the granitic matrix as an interstitial filling and as discrete, euhedral crystals visible with a hand lens.

5.10.5 Well installation

A well couplet was installed in corehole CH-1. Screen intervals were targeted at fractured intervals of interest as identified by inspection of the recovered core. A 1.5-inch-diameter PVC well was placed in the deep interval 85 to 95 ft bgs (CH-1D), with a 10-slot screen. This interval was selected for a permanent well because of the observation of both a near-vertical fracture and a sub-horizontal fracture in close proximity, representing a possible key intersection in the fracture network. A deep screen is of particular interest with respect to the groundwater chemistry, because the deep core appears to exhibit a greater prevalence of unaltered sulfide minerals. In addition, water at depth is expected to have a longer residence time from its origin in upgradient recharge, and therefore more time to interact with the bedrock mineralogy, than does shallow groundwater. A 1-inch diameter well was placed in the CH-1 boring across the shallow interval 36 to 41 ft bgs (CH-1S), again with a 10-slot screen. The shallow interval was chosen to span the very large sub-horizontal fracture encountered around 39-40 ft bgs. Well construction diagrams are included in Appendix K.

Both the shallow and deep wells in the corehole were developed approximately one week after well construction. The wells were purged with a footvalve pump, using a powered device attached to the outer protective casing to oscillate the tubing. When the pump inlet was placed at the screen depth in the deep hole (CH-1D, 85 – 95 ft bgs), the valve would jam, and no water could be removed. However, the footvalve functioned properly if placed at a shallower depth, a few feet below the free surface in the riser. Therefore, the well was purged with the pump inlet well above the screen. CH-1D drew down rapidly, and the purge was accomplished by continually lowering the footvalve to follow the falling free surface. Approximately 30 gallons, or about 3 well volumes, were removed in this fashion. The water ran clear at the end of the purge. The shallow well, CH-1S (36 – 41 ft bgs) pumped readily with little drawdown. A total of approximately 160 gallons was removed from this well, or about 150 well volumes. The water continued to be very turbid, even at the end of this aggressive purge, which can be ascribed to the very large volume of drilling water (>10,000 gallons) and associated cuttings believed to have been lost primarily to this interval.

5.11 Water levels in screened wells

Recording transducers were deployed on February 5, 2010, in three of the new monitoring wells installed during this investigation. While transducers placed in open borings (Sec. 5.6.2) record the net effect of all water-bearing fractures that intersect the hole, those placed in monitoring wells are targeted at specific fractures spanned by the screened intervals (Secs. 5.9 and 5.10.5). Transducers were installed in boring Q4-1 and in the deep corehole well pair, CH-1S/D. Q4-1 lies approximately 97 ft upgradient of CH-1S/D. These placements afford an opportunity to compare the water-level response of a shallow boring on the elevated portion of the hill (Q4-1) to those of the shallow and deep screens at the toe of the slope. In addition, transducers deployed in overburden monitoring well SHP-99-29X, located approximately 250 ft ENE of CH-1, and in the

bedrock/overburden piezometer pair N5-P1/P2, located approximately 520 ft ENE of CH-1, were available over the same period.

The transducers were downloaded on September 24, 2010. The complete data are included in Appendix I in spreadsheet format. The period from February to September, 2010, encompassed an unusually wet late winter / early spring and an unusually hot, dry summer. If precipitation were distributed uniformly throughout the year, the long-term monthly average would be about 4 inches per month. Precipitation in February and March, 2010, was 5.25 in and 11.28 in, respectively. Average rainfall from April through September, 2010, was 2.8 inches per month.

Figure 5.11-1 shows the water elevations at Q4-1, CH-1S/D, SHP-99-29X, and N5-P1/P2 for the period February through September, 2010. In addition, the figure shows daily precipitation recorded at Fitchburg, MA, approximately 8 mi west of the site. The records show some of the significant differences between the response of the bedrock aquifer in the recharge area on the hill and the responses at downgradient locations in both bedrock and overburden.

Q4-1 shows sharp responses to the large precipitation events of February and March, with the water level rising as much as 8 ft within a few hours, and subsequently falling to pre-rainfall levels within a few days. The shallow fractured rock near or at the surface on the hill is evidently recharged readily by rapid infiltration. The magnitude of the response is large due to the relatively low fracture porosity, typically assumed to be of the order of 0.02 in fractured crystalline rock. The system drains rapidly due to its relatively high hydraulic diffusivity. The water level at this location declined monotonically from late April through June, when the water level fell below the transducer depth (as shown by the flat response in the latter part of the record). It is interesting to note that numerous smaller precipitation events (<0.5 in) during this period are not discernible in the water level record, suggesting that evapotranspiration was sufficiently high during these warmer months that little, if any, of the precipitation falling on the hill went to recharge. Recharge in 2010 appears to be dominated by contributions in late winter and early spring.

CH-1S and CH-1D exhibit water-level changes that mirror very closely those recorded at Q4-1. Peaks and declines associated with the February and March precipitation events are similar in their timing, but the amplitude of the head changes at the foot of the hillslope is notably smaller. The first jump in water levels shown in the plots is approximately 8 ft at Q4-1, 4 ft at CH-1D, and 3 ft at CH-1S. The total drop in water levels from their peak in April until the water level in Q4-1 fell below the transducer around July 1 was about 21 ft at Q4-1, 12 ft at CH-1D, and 17 ft at CH-1S.

The transducer record for SHP-99-29X is highly erratic, and bears little resemblance to either the response upgradient (e.g., at CH-1) or downgradient (e.g., at N5). The noisy interval of this record persists throughout the period of higher water levels from March through June. It is speculated that the transducer was near or beyond its upper pressure limit when water levels were around 222 ft msl, and that this portion of the record is not

meaningful. The monotonic decline through the remainder of the summer is consistent with the response at other wells in the system.

At N5-P1 and -P2, the water levels over the same period are profoundly different. The individual recharge events that are evident in the records on (Q4-1) and adjacent to (CH-1) to the hill are not manifested in the water levels recorded at N5. This is because the N5 boring penetrates the landfill cap, which eliminates recharge locally. Water levels at N5 change in response to inputs from the margins of the landfill and from leakage from or to the underlying bedrock. Although the recharge in open areas surrounding the landfill is episodic, the transport of head changes and water is a diffusive process, and the “spiky” variations at the margins of the cap are damped out at N5, some 500 ft from the margin. It is interesting to note that the response at the shallow overburden screen, N5-P2, lags that in the deep bedrock screen, N5-P1. Both the minimum water level reached near March 1 and the maximum reached near May 1 were from one to two weeks later at N5-P2 than at N5-P1. The unconfined shallow overburden aquifer responds to the long-term, seasonal changes more slowly than does the semi-confined bedrock aquifer.

5.12 Location survey

Horizontal and vertical positions (X,Y,Z) of features of interest for this investigation were surveyed with a Leica TC 307 total station capable of distance measurement accuracy of 2 mm and an angle measurement accuracy of 7 seconds. Project features were first tied into existing site features, e.g., monitoring wells, on a relative basis. Elevations with respect to mean sea level NAD27 (North American Datum of 1927) were calculated for new features in order to be self-consistent with the pre-existing site well network. The survey efforts took place on several successive dates as the work progressed. Data for all features surveyed for this investigation are included as Appendix M. Features surveyed included stations where bedrock outcrop data was collected, beginning and end-points of geophysical survey lines, borehole and monitoring well locations, and elevations of monitoring well water level measurement points, typically the high-point on inner well riser or well casing. Following surveying, the water-level measuring points particular to each well were marked on the well casings with an indelible marker to insure consistency between measurement events. It should also be noted that in several instances, well casings became damaged and required replacement. This, in turn, required resurveying. The survey tables included in Appendix M include a comment field where such changes are noted.

6.0 BEDROCK MINERALOGY

Under the guidance of Gannett Fleming, two graduate students in the Department of Geological Sciences, University of Massachusetts/Amherst (UMass) performed a limited study of SHL bedrock mineralogy as part of the Bedrock Investigation. This portion of the overall effort was performed in two phases. In the first phase of this work, samples were taken from existing SHL bedrock cores that are currently stored at Devens. The second phase of the study focused exclusively on samples from the deep core that was obtained under this Bedrock Investigation. Locations of the core samples examined are shown on Figure 6.0-1. The following sub-sections describe key results of the petrographic analyses. The full data reports from UMass are included as Appendix N.

6.1 Phase I: Analysis of existing SHL cores

6.1.1 Objectives

Selected samples from archived SHL bedrock cores were analyzed at the UMass/Amherst Department of Geological Sciences under the direction of Gannett Fleming personnel. These cores, currently stored at Devens, have not been analyzed previously, and little quantitative information on mineralogy in bedrock underlying SHL is available. For this initial reconnaissance, samples were examined by scanning electron microscopy with an energy-dispersive spectrometer (SEM/EDS), followed by more quantitative analysis by electron microprobe (EM).

The primary objectives of this work were:

- to identify mineral phases, such as iron or manganese oxides or sulfides, that may play a critical role in determining arsenic behavior in SHL groundwater
- to quantify arsenic concentrations in such phases
- to examine fracture surfaces for evidence of rock-water interaction

6.1.2 Methods

The number of samples analyzed in Phase I of the SHL bedrock mineralogy study was limited. Ideally, it would have been preferable to analyze a larger number of samples, taken from all of the existing cores, in order to capture the mineralogical variability that is likely present in SHL bedrock. However, the limited scope of this study permitted the examination of a relatively small fraction of the available material. Therefore, these results should be interpreted accordingly.

Given the small number of samples scoped in this study, the selection of cores for mineralogical analyses attempted to maximize spatial coverage of sampling locations. In addition, samples were selected to ensure that the key bedrock lithologies beneath SHL were represented. These units are the metasediments of the Berwick Formation (late

Silurian), and the Ayer Granodiorite and the Chelmsford Granite (both Devonian). The cores sampled for this work are listed below.

Table 6.1.2-1. Cores sampled for Phase I petrographic analysis

CORE ID	LOCATION	LITHOLOGIC DESCRIPTION [1]	LITHOLOGIC UNIT [2]
SHM-93-10C	southeast of Red Cove	Dark gray, well-bedded to massive meta-mudstone with boudins / brecciated layers	Berwick / Oakdale Fm
SHP-99-29X	western edge of landfill	Well-foliated, medium to coarse-grained granite gneiss. Lots of compositional variation due to varying amounts of bt and qtz. Secondary muscovite.	Sheared Ayer Granite
SHM-93-22C	toe of landfill	Light-beige medium-coarse grained granite gneiss	Sheared Chelmsford Granite
N2-P1	northwest side of Red Cove	Well foliated, equigranular qtz-fsp-bt gneiss	Sheared (fine-grained?) Ayer Granite
N5-P1	central landfill, approximately halfway between Shepley's Hill and Red Cove	Well-foliated / sheared med-coarse grained qtz-fsp-bt granite with secondary muscovite flakes.	Sheared med-grained Chelmsford Granite
N7-P1	north end of landfill	Well banded mudstone and quartzite with sub-centimeter-scale alternating whitish quartzite and dark gray phyllite / mudstone "beds" / laminations.	Oakdale Formation?

[1] Lithologic descriptions are from field notes provided to EPA and GF by J. Kopera (Office of the Massachusetts State Geologist), 3/23/2007. Mineral abbreviations are: qtz, quartz; fsp, feldspar; bt, biotite.

[2] Identification of lithologic units is tentative and is based on information from J. Kopera (from Kopera, 2006).

The first step in selecting samples for analysis consisted of visual examination of the cores, for macroscopic structure and texture, and for the presence of fractures showing evidence of alteration (e.g., Fe-staining or mineralization). The overall goal of this work was to characterize arsenic-bearing phases, particularly where such phases may indicate low-temperature, water-rock reactions. Macroscopic evidence of alteration along fracture surfaces in the SHL cores occurs as discrete zones of iron staining up to a few centimeters wide on either side of the fracture plane (Fig. 6.1.2-1). Accordingly, areas of interest were marked on the cores and included fractures showing evidence of alteration as well as adjacent, unaltered rock.

Thin sections were cut from these areas and examined optically by transmitted light, for mineral texture, location of fractures and vein fillings, and presence and distribution of opaque sulfide minerals. An example, from the SHP-99-29X core, is shown in Figure 6.1.2-2.

Scanning electron microscopy (SEM) was used to locate areas of interest on the thin sections. These were primarily zones showing arsenic enrichment. The SEM yields qualitative analytical information, in either of two ways:

- Element maps: an image showing areas of the sample surface having a higher concentration of an element of interest than the surrounding matrix. Only one element can be imaged in this manner at a time. An example is shown in Figures 6.1.2-3(a) and 6.1.2-3(b).
- Energy-dispersive spectra: multiple elements are identified in a relatively small area of interest on a sample surface. Peak heights cannot be used to quantify phase compositions, but elemental components may provide insight into mineral identification (Fig. 6.1.2-4(a) and 6.1.2-4(b)).

Neither of these methods is quantitative, but the results were used to pinpoint locations for more detailed analysis by electron microprobe (EM).

The electron microprobe was used for quantitative analysis of key areas of interest, such as discrete arsenic-rich crystals (Fig. 6.1.2-5) or vein-filling material showing arsenic enrichment on the element maps (Figs. 6.1.2-6(a) through 6.1.2-6(d)).

The EM data corresponding to the points shown on Target Area F, Figure 6.1.2-5 are:

Map F	Normalized wt% in sulfide					
	As	Cu	Fe	S	Ni	Total
1	45.6487	0	34.423	19.8968	0.0315	100
4	45.3614	0.0117	34.4416	20.1564	0.0288	100
5	43.3342	0.0292	35.1241	21.5017	0.0107	100
6	44.1268	0.0211	34.8009	21.0176	0.0335	100
7	44.5468	0	34.8517	20.564	0.0375	100

These data are converted to atom percentages, which correspond to the mole fractions:

Map F	Concentration (atom %) in sulfide					
	As	Cu	Fe	S	Ni	Total
1	32.9912	0	33.3754	33.6044	0.0291	100.00
4	32.6997	0.01	33.308	33.9558	0.0265	100.00
5	30.7879	0.0245	33.4781	35.6998	0.0097	100.00
6	31.5196	0.0178	33.3484	35.0837	0.0306	100.00
7	31.9547	0	33.5389	34.4722	0.0343	100.00

The molar ratios of As, Fe, and S are nearly 1:1:1, as expected for the stoichiometry of arsenopyrite, FeAsS. It is noted that trace amounts (< 0.1%) of Cu and Ni are also present. The molar ratios of As, Fe, and S were generally consistent from crystal to crystal within a sample, and between samples. The amounts of Cu and Ni were also consistently low, < 0.1%. These data are consistent with the identification of arsenopyrite.

6.1.3 Phase I results

Key results and observations from the Phase I work are summarized here:

- The occurrence of arsenic in some of the SHL bedrock samples examined in this study was described by the UMass investigators as “pervasive.” However, obtaining a representative, quantitative concentration of arsenic in these lithologies would be difficult, given the heterogeneous distribution of the host phases. Any bulk-rock arsenic concentration will be a function of the scale of sampling. Quantification of the mass of arsenopyrite in the SHL bedrock lithologies would require substantial additional coring, sampling of those cores, and mineralogical analysis. Although the results presented here are from an extremely limited study, it is important to note that arsenic was frequently observed in two of the cores (SHP-99-29X and N5) analyzed at UMass.
- Arsenopyrite (FeAsS) is confirmed and is common in bedrock from SHP-99-29X. Arsenopyrite was also identified in the N5 core. However, all other samples selected for this study (SHM-93-10C, N2, N7, and SHM-93-22C) showed little or no arsenic mineralogy.

- Three primary modes of occurrence are observed:
 1. *In crystalline phases.* Pristine euhedral crystals composed mainly of Fe, As, and S are found in samples from SHP-99-29X core (e.g., Figs. 6.1.2-4(a) and 6.1.2-4(b)). From the molar concentrations of these elements obtained by EM analysis, this phase has been positively identified as arsenopyrite, FeAsS. This mineral was likely formed in the Ayer and Chelmsford granites by metasomatic processes (involving the exchange of fluids at elevated temperature and pressure).
 2. *In vein fillings.* Arsenic is noted in vein fillings, in conjunction with elements found in the granitic matrix (e.g. Na, Ca, K; Figs. 6.1.2-6(a) through 6.1.2-6(d)). This observation suggests that the arsenic precipitated through reactions between minerals in the host rock (primarily alkali and plagioclase feldspars) and late-stage hydrothermal fluids. Also, it appears that multiple episodes of vein-filling mineralization occurred, although the timing of these events is unknown.
 3. *In micro-cracks and along grain boundaries.* Arsenic associated with silicates has been observed along anastomosing grain boundaries between the matrix quartz and feldspars. We speculate that this may be the result of hydrothermal alteration and subsequent metamorphic processes. It is possible that arsenic (as $\text{As}^{+3}/\text{As}^{+5}$) is substituting for silicon (Si^{+4}) and/or aluminum (Al^{+3}) in the silicate minerals.
- The arsenopyrite is likely not primary, i.e., not igneous in origin, because the euhedral shapes (showing well-developed crystal edges and crystal faces; Fig. 6.1.2-4(a)) do not show signs of weathering, as might be expected from later metasomatic reactions, and because they exhibit a preferred orientation that is consistent with metamorphism.
- Iron oxidation is often evident along brittle fractures – for example, between quartz veins and the metamorphosed granite matrix. Iron oxidation is also visible in the granite matrix in the absence of quartz veins.
- Fractures are present at all length scales (from microscopic, as seen in the EM and SEM images, to macroscopic, cross-cutting the cores).
- Some arsenic-substituted pyrite is present.
- Arsenic is present in silicate grains adjacent to arsenopyrite crystals. The arsenic concentration in quartz next to arsenopyrite is lower than the arsenic concentration in adjacent feldspars. The mechanism by which arsenic is incorporated into these silicate crystal structures is unknown at this time but we

speculate that it may involve a coupled substitution of $\text{As}^{3+}/\text{As}^{5+}$ for Si^{4+} and/or Al^{3+} .

- Arsenopyrite crystals in or near fractures tend to be more physically and chemically degraded than arsenopyrite crystals in the granitic matrix.
- Other minerals – e.g., K-feldspar – also show significant chemical alteration near fractures.
- Sulfide phases located on fractures showing evidence of oxidation appear to lose some Fe and As to surrounding mineral grains, while sulfides located away from oxidized fractures are unaffected.
- Fractures often contain a phase or phases composed of As, Fe, and Ca, with no Si or S. Since the electron microprobe results for hydrous or hydrated phases are often unreliable, those phases cannot be identified with any certainty. This material may be a mixture of carbonate and Fe/Mn-oxide or oxyhydroxide phases with sorbed As; alternatively, this mixture may be composed of Fe- and Ca- (and possibly other cations) arsenates.

The possibility that the As-Fe-Ca material represents alteration of arsenopyrite to phases such as scorodite ($\text{Fe}^{3+}\text{AsO}_4\cdot 2\text{H}_2\text{O}$), pharmacolite ($\text{CaHAsO}_4\cdot 2\text{H}_2\text{O}$), and/or other Fe- and Ca-arsenates cannot be ruled out. These phases, if present in the fracture fillings that were observed during the microprobe analysis, may be key indicators of low-temperature, water-rock reactions responsible for mobilizing As from arsenopyrite into more soluble forms, e.g. arsenates. Thin-section examination of the arsenopyrite seen in Figure 6.1.2-5 suggests that this mineral occurs in an area that appears to have been affected by hydrothermal fluids and is adjacent to a quartz vein. Iron and arsenic appear to have been mobilized from the crystal into the adjacent microcrack by fluid interaction, as the vein filling at points 8b and 11 in this photomicrograph report detectable concentrations of both elements (Figs. 6.1.3-1(a) and 6.1.3-1(b)).

6.2 Phase II: Analysis of deep core

6.2.1 Motivation

Although this reconnaissance was limited in scope, the purpose of this work was to examine the new core for As-bearing mineral phases such as primary and secondary oxides and sulfides, and to assess the distribution of these phases with respect to fracture surfaces and vein fillings. Specific questions that this investigation attempted to address were:

1. What discrete arsenic minerals are present? The identification of arsenopyrite in bedrock core samples from SHP-99-29X and N5 (Sec. 6.1) suggested the possible occurrence of As-bearing sulfides at the new core location.

2. What evidence of rock-water interaction is observed on the microscopic scale? In this investigation, the core from location CH-1 shows evidence of significant aqueous alteration, primarily as well-defined bands of iron oxidation, along some of the larger, open fractures (for example, Fig. 5.10.3-1). In addition, microcracks filled with iron oxidation also contain significant concentrations of arsenic. Figures 6.1.3-1(a) and 6.1.3-1(b) show an arsenopyrite crystal adjacent to a microcrack filled with one or more apparent alteration products and containing significant concentrations of Fe and As. Of key interest is the possible presence in this altered material of secondary As phases (e.g., scorodite, $\text{FeAsO}_4 \cdot 2\text{H}_2\text{O}$) formed by dissolution and reprecipitation processes due to groundwater flow through the bedrock fracture network.
3. What elements are associated with As on fracture surfaces, grain boundaries, and in adjacent “bleached” zones surrounding fractures? Although SEM/EDS analysis does not provide unequivocal mineralogical information, the occurrence of As with other elements or suites of elements may be useful for developing and supporting a conceptual geochemical model for this site.
4. What can be concluded about the distribution of arsenic as a function of increasing depth in the core? Despite the limited number of samples, it was hoped that this scoping study might provide some information on large-scale changes in the presence and distribution of arsenic from the top of bedrock to the bottom of the core.
5. Can the information obtained in this study be used to interpret the relative timing of tectonic/hydrothermal events that resulted in fracturing of the granite, mineralization by As-bearing fluids, and subsequent low-temperature, late-stage mobilization of arsenic? A comprehensive geological interpretation was beyond the scope of this investigation. This limited analysis was designed to provide some insight into the relations between episodes of fracturing and mineralization, particularly with respect to arsenic behavior.

6.2.2 Deep core mineralogical analysis

A limited number of samples of the new core were sent to the Geosciences Department at the University of Massachusetts in Amherst for analysis by the same students who performed a similar scoping study of samples from other, existing SHL cores (Sec. 6.1). In consultation with Gannett Fleming personnel, these students selected samples of the deep core for analysis by scanning electron microscopy (SEM) with energy-dispersive x-ray spectroscopy (EDS). This approach was chosen due to the relative efficiency with which samples could be scanned for evidence of minerals containing arsenic and other metals. When the SEM is operated in the backscattered-electron (BSE) imaging mode, phases containing high-atomic-number elements show up as bright areas, allowing the viewer to focus rapidly on portions of the sample containing arsenic, iron, manganese,

and other transition metals. Chemical composition is obtained either by element mapping, in which zones containing a high concentration of an element of interest are visible as bright areas, or by measurement of the energies of the x-rays that are emitted when the sample is exposed to the SEM's electron beam. The SEM is primarily an imaging tool, and detection limits are higher than those that were obtained with the electron microprobe in the previous study of SHL core. Detection limits for this portion of the bedrock mineralogy work are estimated to be in the range of 1000 to 10000 mg/kg (0.1 to 1 wt %).

Neither the element maps nor the energy-dispersive x-ray scans provide structural (i.e., crystallographic) information, so minerals cannot be identified with absolute certainty. Also, minerals with identical compositions but different crystal structures cannot be distinguished solely on the basis of EDS information. Nevertheless, the chemical information collected using the SEM provides valuable insights into the distribution of arsenic in the deep SHL core.

6.2.3 Phase II results

For this study, eight samples representing the three dominant fracture orientations were selected from the deep core.

Table 6.2.3-1. Samples for petrographic analysis of deep core

FOOTAGE IN CORE	FRACTURE DESCRIPTION	SEM/EDS TARGET	OBSERVATIONS
23.6-23.8	oxidized subhorizontal sheeting-fracture-rich zone	orange-red mineralized fracture surfaces with fine-grained metallic xls (possibly pyrite); also, calcite on fracture surface subparallel to the sheeting joint	<ul style="list-style-type: none"> • As-bearing/ REE-phosphates present in limited concentration; may be associated with a relatively old generation of healed veins • Fe + Si precipitates and Fe + Mg oxides dominate the most modern generation of fractures and are associated with reddish-orange staining • Localized As-bearing Fe-oxides in

			some fractures
24.8-25.1	oxidized subhorizontal sheeting fracture	reddish-brown coating with earthy luster on mineralized fracture surface; similar material extends ~1.5 to 2 cm away from fracture surface.	<ul style="list-style-type: none"> • As-bearing Fe-oxides present as anhedral clots and precipitates in open fractures (Fig. 6.2.3-1) • Polymineralic clots of Fe- and Ti-oxides and REE-phosphates present, possibly an earlier generation of mineralization associated with metamorphic foliation • As-bearing Fe-oxides present along some fracture surfaces, not in high concentration as independent phases
~39.3	v. large fracture zone, dip 22° SE, strike parallel to foliation	Reddish-brown Fe-oxide band around fracture surface, bleached zone grading into unaltered matrix	<ul style="list-style-type: none"> • Fe- and Ti-oxides dominate and are largely associated with staining present on surfaces • As-bearing Fe-oxides may be present along some fractures
~87.3-87.5	intersection between near-vertical and NE-striking set of fractures	Dark reddish-brown mineralization on all fracture surfaces; no apparent differences in type of mineralization between the two fracture surfaces.	Same as for ~39.3-ft sample
88.9-89.4	subvertical fracture and horizontal fracture; subvertical fracture follows the trend of the major	heavily mineralized with orange-brown coating; host rock below the fracture surface is unaltered.	<ul style="list-style-type: none"> • As-bearing, “rubbly” fracture coatings present in high concentration, especially on steep

	tectonic fabric in the host meta-granite	Sheeting fracture surface has discontinuous calcite mineralization with orange-brown coating.	fractures (Fig. 6.2.3-2) <ul style="list-style-type: none"> • Preliminary data show As present with Ca, Si, Al, Fe, and Mg as a fine-grained coating
97.9-98.6	2 subhorizontal mineralized fractures	~97.9 ft: calcite precipitates, reddish-orange mineralization, and surface mats of very fine-grained arsenopyrite xls. ~98.6 ft: thin veils of chlorite sheeting; less commonly, calcite. Sections of this surface also have a brighter green mineralization invading subvertical micro-cracks.	<ul style="list-style-type: none"> • As-bearing oxides with Si, Fe, and Ca in healed vein and fracture networks that are very common at these depths • Complex veining structures that include brecciated silicate phases are hosted by As-enriched Ca- and Fe-cements • Arsenopyrite common as anhedral matrix phase. Grains near the margins of open fractures are typically deeply embayed and connected to As-bearing Fe-oxide veins (Figs. 6.2.3-3 through 6.2.3-6).
122.9-123	Slickenside-bearing fracture surface (NE-striking fracture set)	Mineralization on fracture surface has light greenish-brown hue and slightly vitreous luster; Mineralization does not persist in the host rock below the fracture surface.	<ul style="list-style-type: none"> • Subhedral to anhedral Fe, Ti, Cu, Mg oxides present at this sampling depth • As-bearing phases not present despite common Fe-oxides and sulfides; element mapping along 1-3 micrometer-width microfractures suggests that As-

			bearing precipitates are present in some areas
125.5-125.7	dark green chlorite-bearing fracture surface	Chlorite is entirely restricted to this fracture surface though there is some evidence for late mineralization, also chlorite, within subvertical fractures in the same segment of the core.	<ul style="list-style-type: none"> • Fe+Ti-bearing oxides are very common as subhedral to anhedral grains among silicate matrix phases • Element mapping and EDS suggest that As-bearing phases are present along fractures and are associated with Fe-oxides (some in calcite veins) (Fig. 6.2.3-7(a) and (b)).

Note: xls = crystals; REE = rare-earth elements

6.3 Preliminary x-ray diffraction results

In addition to the analyses by SEM/EDS, samples of the deep bedrock core were also examined at UMass by x-ray diffraction (XRD). The XRD results, summarized here, are preliminary and should be interpreted accordingly. These analyses were not part of the Scope of Work for the mineralogical portion of the SHL Bedrock Investigation, but were performed by the UMass students in a further effort to provide unequivocal identification of secondary arsenic-bearing phases, particularly in fracture coatings that appeared to show evidence of aqueous alteration. These secondary phases represent intermediate steps between arsenopyrite in the bedrock and mobilization of arsenic to groundwater in the SHL system.

Many of the XRD patterns confirm the presence of poorly crystalline Fe (oxy)hydroxides and Mn (hydr-)oxides. A broad band with d-spacings between ~2.8 angstroms and 2.5 angstroms and an additional peak at approximately ~1.7 angstroms was not positively identified. However, some coatings that appeared to be slightly more crystalline produced more reliable XRD patterns.

Despite the preliminary nature of this portion of the mineralogical study, three major findings are summarized here. These observations suggest that additional x-ray diffraction analyses of the SHL bedrock core would constrain better the unequivocal identification of secondary alteration phases:

1. Material was sampled from the immediate vicinity of anhedral arsenopyrite crystals that appear to be breaking down. X-ray diffraction patterns from these samples match the mineral scorodite ($\text{Fe}^{3+}\text{AsO}_4 \cdot 2\text{H}_2\text{O}$) very well. This mineral is typically 32.3-32.6 wt% As, and this also matches the EM data from N5 samples. Although estimates for the solubility of this phase vary, order-of-magnitude total arsenic concentration in aqueous solutions in equilibrium with scorodite ranges from approximately 1 mg/L to >10 mg/L (Magalhaes, 2002; Bluteau and Demopoulos, 2007).
2. Fe-rich / Mn-rich \pm Ca coatings that are more crystalline but not directly associated with pyrite or arsenopyrite produced patterns that broadly match three different minerals:
 - arsenoclasite, $\text{Mn}_5(\text{AsO}_4)_2(\text{OH})_4$
 - camgasite, $\text{CaMg}(\text{AsO}_4)(\text{OH}) \cdot 5(\text{H}_2\text{O})$
 - sarmientite, $\text{Fe}_2^{3+}(\text{AsO}_4)(\text{SO}_4)(\text{OH}) \cdot 5(\text{H}_2\text{O})$
3. Where Fe + Mg + Mn + alkali elements (especially Ca, Na, and K) were observed in some of the breccia-like veins in the deep core, the XRD pattern is consistent with the mineral grishunite, $\text{NaCa}_2\text{Mn}_5^{2+}\text{Fe}^{3+}(\text{AsO}_4)_6 \cdot 2(\text{H}_2\text{O})$. A coupled substitution (Na for K and Mn for Mg) that can occur with this mineral may explain some of the compositional variation observed in these coatings, but the XRD data are not definitive. Numerous small clasts of quartz and feldspar in these fracture coatings may be interfering with the interpretation of the XRD patterns of this material.

These results were obtained from an extremely limited reconnaissance study, in an attempt to use XRD for more definitive identification of secondary arsenic minerals, particularly those that might have formed through weathering of arsenopyrite. Nevertheless, the apparent identification of scorodite and, tentatively, numerous other hydrous or hydrated arsenate minerals, is consistent with the aqueous, low-temperature alteration of arsenopyrite and mobilization of arsenic to other, more soluble, phases.

6.4 Conclusions from mineralogical analysis

1. Arsenic is present in the deep core samples in numerous forms. These include:
 - arsenopyrite (identification based on brightness in backscattered-electron images, overall high relief, and high counts for Fe, As, and S in the energy-dispersive spectra)
 - associated with Fe- and Fe-Mg oxides
 - in a tentatively identified, Mg-rich carbonate phase
 - in phosphate grains
 - in association with elements that are typical of silicate minerals (Ca, K, Si, Al), although the nature of this association – i.e., sorbed vs. structurally incorporated – is unclear.

2. Arsenopyrite occurs in samples from the deep core as an anhedral, matrix-filling phase. Euhedral or subhedral crystals (as seen in bedrock from the SHP-99-29X and N5 cores) were not observed in samples from the deep core.
3. As-bearing Fe-oxides are observed in open fractures and are also found immediately adjacent to arsenopyrite grains with embayed or corroded edges. This association is consistent with the aqueous alteration of arsenopyrite to Fe-oxide with sorbed arsenic.
4. Additional SEM and XRD studies would constrain better the trace minerals present in these samples. Unequivocal identification of some of these phases was not possible using the approach adopted for this investigation; however, additional work may yield insights into the nature of the crystal structures hosting the arsenic.
5. Phases containing other metals, including copper, cobalt, tungsten, titanium, and gold, were also observed in samples from the deep core.
6. Given the paucity of data at this time, it is not possible to interpret these results in an accurate chronology of the metamorphic and metasomatic history of the Chelmsford Granite. Any hypothesized processes that mobilized arsenic cannot be associated with specific tectonic or metamorphic events based on the available information. Nevertheless, the observations summarized here clearly indicate that arsenic is associated with calcium- and iron-rich vein fillings and with immediately adjacent silicate minerals.

It is beyond the scope of this portion of the Bedrock Investigation to address all of the questions raised by these results. The pressure-temperature conditions and timing of the metamorphic events to which the SHL bedrock units have been subjected cannot be resolved without significantly more investigation. The origin(s) of the hydrothermal fluid(s) cannot be determined from this limited study. Nevertheless, this work directly addresses some of the issues brought to light by previous investigators.

Previous investigations have qualitatively identified sulfides in the SHL system. Arsenopyrite and As-bearing pyrite were reported from a sample of granite from a gravel pile on Devens (letter report from M. Williams, Dept. of Geosciences, UMass/Amherst to M. Deuger, Army BRAC Office, May 8, 1996). While it may be assumed that this gravel was locally derived, its source is unknown. In a scoping study of three samples from outcrops on Shepley's Hill, EPA/ORD personnel reported finding As associated with metal oxides and As bound to sulfur in phases similar to orpiment and arsenopyrite. This work was reported in an informal memorandum from EPA (T. Luxton et al., 2008) to Gannett Fleming. In the SHL *Supplemental Groundwater Investigation* (SGI; Harding ESE, 2003), pyrite is described in SHL cores but apparently this phase was identified by visual inspection only. It is noted that the pyrite reported in the SGI occurs as discrete inclusions in quartz and feldspar, in thin 'quartz-pyrite veinlets' (presumably mineralized

veins or fractures), and finely disseminated within the bedrock matrix, similar to observations summarized here. The SGI also reported arsenic at 43 mg/kg in a rock chip from the N5 core and noted that this concentration is 'significantly higher' than average values from the literature for crustal or igneous rocks but not unusual for pegmatitic rocks in this part of New England. The specific mineral phase(s) associated with this elevated arsenic was/were not identified.

This investigation yielded the first unequivocal identification of arsenopyrite in bedrock cores from SHL. The presence of arsenic in arsenopyrite and in arsenopyrite alteration products in these bedrock cores clearly has important implications for the elevated groundwater concentrations at SHL.

7.0 FRACTURE NETWORK

This section discusses the evolution of the CSM in terms of the fracture network which emerges through examination of geologic information at the three scales of investigation selected for this study. As it is used here, the term “fracture network” is described principally in terms of properties and characteristics of the bedrock and fractures observed or measured at the site. A central premise for the approach taken in this study is that the inherent properties of the bedrock system at the site - particularly the interconnected fracture network - dictate the resulting groundwater flow regime. Just as detailed piping diagrams are essential to describing water flow in engineered systems, such as household plumbing, it follows then that in order to understand a bedrock flow system at a given scale, at a given level of detail, the fracture system must first be “mapped out” at that scale to the degree possible. Given the limited and relatively expensive tools available to present-day bedrock investigators, a high level of resolution is difficult to achieve, but the level of resolution attained in mapping the fracture network will ultimately determine the level of resolution achievable for other elements and processes of the CSM which are dependent on the fracture network, such as groundwater flow and contaminant transport in the dissolved phase. In other words, the fracture network is integral to everything at a bedrock site. The level of uncertainty in the understanding of the fracture network will be reflected in all other aspects of the CSM. In an effort to highlight the importance of the geologic fracture network with respect to developing a robust overall CSM at a bedrock site, a new term is proposed. Hereafter, we will refer to this distinct element of the CSM as the geologic fracture model (GFM). Depending on the level of resolution afforded by the data set, the GFM may be described in words, conceptual diagrams or a series of two-dimensional representations such as cross-sectional diagrams or fence diagrams. Ideally, if the degree of area coverage and the levels of resolution on the data set are sufficient, a three-dimensional digital representation at the site scale may be able to be constructed.

The sub-regional scale GFM is first discussed, in the context of an area roughly 25 miles square. Next, the GFM is viewed and discussed from the perspective of the “Shepley’s Hill scale” (i.e., approximately 200+ acres). Finally, the GFM is examined at the detailed site-scale, over an area roughly 300 feet by 500 feet.

Some types of geologic data were examined at all three scales of investigation. Other types of data were relied on more extensively for some, but not all scales. These specifics are discussed in the relevant subsections, below. However, several guiding principles are common to all of the scales of interest and warrant some discussion here. Geologic characteristics such as fracture patterns and related features which are revealed at smaller scales (i.e., regional to sub-regional features) are interpreted to be of major significance, and by definition strongly influence geologic characteristics at the larger (more detailed) scales. However, specific features or characteristics may or may not be readily observable at larger scales for a variety of reasons. For example, just as an east-west highway does not trend strictly east-west over its entire length, a regionally extensive geologic feature such as a fracture system or fault may vary significantly from the “average” orientation when viewed at a specific location at a larger scale. As such,

examination of geologic data at larger (more detailed) scales may introduce finer-scale details which appear at first viewing to be at odds with the overarching regional patterns. Some may represent unique features and orientations which are indeed only present at the site-scale, and others may simply reflect site-scale local variation of features which are oriented somewhat differently than the average regional-scale orientations, yet they form a common family of structures. It is important to note here that, while the following and foregoing discussions of the fracture network make several assertions regarding the origin of particular features or classes of fractures, a full assessment of the origin and geologic relationships is beyond the scope of this study. Rather, the goal here was simply to construct an empirical model of the fracture network based mostly on observation, and to vet this “fracture model” against subsequent data sets (e.g., hydrology, geochemistry), in order to ultimately construct a robust internally consistent conceptual site model incorporating all of the data. Since the primary purpose of the study was to examine groundwater flow and arsenic transport in the fractured rock aquifer, it is also important to note that certain characteristics of the bedrock were interpreted to be particularly important with respect to groundwater flow, and were thus assigned a greater level of importance in the overall hierarchy of fractures. Without any particular reference to scale of investigation, such characteristics include the following:

- long linear features indicated on maps or aerial imagery
- linear valley and ridge features
- abrupt or steep topographic escarpments
- fractures or joints with long strike length
- planar and/or smooth fractures or joints
- open fractures visible in core or outcrop
- conspicuous evidence of chemical weathering, such as iron or manganese oxide staining on outcrop, core, or rock chips from drillings.
- relatively large aperture fractures suggested by observations or geophysical data (e.g., ATV logs)
- zones of enhanced electrical conductivity (e.g., from electrical resistivity data)
- zones of increased fluid movement suggested from borehole geophysical logs
- zones of water loss or gain observed during borehole drilling
- shallow gently-dipping reflectors indicated by low-frequency GPR surveys;
- highly sheared or mylonitic zones

- breccia, slickensides or other evidence of displacement
- highly fractured regions where fractures zones of various orientations intersect
- veining and mineralization

7.1 Sub-regional fracture network

In an effort to gain an understanding of the fracture style potentially present at the sub-regional scale, and number of published materials were consulted including the following:

- topographic maps at 1:24,000 or 1:25,000 scale;
- surficial geologic mapping at 1:24,000 scale;
- bedrock geologic mapping at 1:24,000 scale;
- aerial photography at a variety of scales.

Features of significance identified from these sources were inspected in the field. Additional information concerning the geology at the sub-regional scale was communicated to the site team from representatives of the Office of the Massachusetts State Geologist (OMSG), particularly Mr. Joseph Kopera, who was in the process of performing regional geologic mapping for the Ayer quadrangle during the time period data was being collected for the SHL BI. The project team benefitted from numerous informal discussions and examinations of outcrop and core with OMSG during sporadic periods of overlapping work.

An examination of Figure 7.1-1 illustrates the primary geologic and fracture features at the sub-regional scale. On average, a NE-SW regional strike is clearly indicated by this figure which corresponds to the regional trend of the Clinton-Newbury Fault Zone. However, a profound disruption of the average strike pattern occurs in the general area from Mirror Lake on the south to Long Pond to the north. In the area of disruption, which envelopes the site, the massive Ayer and Chelmsford granites and foliated granitoidal gneisses of the Devens gneiss complex (Devonian; Domain 2 of Kopera et. al., 2006) and the adjacent meta-sedimentary rocks of the Merrimack group (Silurian-Ordovician; Domain 1 of Kopera et. al., 2006) strike anomalously north-south before abruptly changing to a region which strikes ENE to WSW in the area near downtown Ayer, MA. Near Lost Pond, in Groton, MA, the “typical” NE-SW regional strike pattern is restored. It is of primary significance, as highlighted on Figure 7.1.-1, to note that Shepley’s Hill itself is in the core of this anomalous sub-regional scale flexure. In fact, the southern portion of the Shepley’s Hill upland is typified by north-south strikes while the northern segment strikes distinctly east-northeast. These trends are mirrored in the profile of the east side of the bedrock upland which exhibits a topographic character typical of glacially plucked uplands. The glacier has plucked the down-ice portions of

the hill, resulting in steep east-facing, north-south striking escarpments on the south portion of the hill; and southeast-facing, northeast-striking escarpments to the north, corresponding to the abrupt shift in the primary fabric of the rock, (i.e., foliation). Another feature of major significance is indicated by topography. There is a deeply incised notch which cuts through the northern portion of Shepley's Hill, striking northwest-southeast. The feature, which is highlighted on figure 7.1-1, corresponds with the change in bedrock strike, and also appears to possibly be associated with an unusually straight section of Nonacoicus Brook which strikes NW-SE for over 2000 feet from the vicinity northwest of Shepley's Hill to near the confluence of Nonacoicus Brook with the Nashua River. It appears that this lineament is an echelon with the similarly oriented structures which bisect Shepley's Hill. The aggregate strike length of this family of features is nearly 4000 feet. On the basis of these observations, the site team has provisionally designated this group of structures the Nona-Shep Fracture Zone. It is likely that these features represent a fault zone with demonstrable displacement. Another significant fracture zone is highlighted on Figure 7.1-1, which has been given the interim designation of the Disc Golf Fracture Zone. This series of fractures appears to be directly related to the north-south strike of the bedrock in the southern and western portions of Shepley's Hill. The feature, while mapped as a stratigraphic contact between the Chelmsford and Ayer granites (Kopera, 2008), is most likely a fault zone given its significant length and character. The fracture zone outcrops as a series of parallel escarpments on the western half of the Shepley's Hill upland. The escarpments are unusually abrupt, and exposures are commonly 10 feet or more in the vertical dimension. Similarly, strike length of the features which make up the zone are hundreds of feet in length; the aggregate strike length of the Disk Golf fracture zone is nearly 1500 feet. It is likely that the Nona-Shep and Disc Golf Fracture Zones are associated with the "hinge" zone in the northern part of Shepley's Hill where strike orientations change abruptly, and have perhaps resulted in order to accommodate stresses in this relatively more deformed region.

7.2 Shepley's Hill scale fracture network

Aerial photography at a variety of scales, data available from a LiDAR survey, and detailed topographic mapping were consulted to examine the fracture network at the scale of the greater Shepley's Hill area. While all of these formats were consulted, the project team relied most extensively on detailed topographic mapping provided by Mass Development Corporation at an approximate scale of 1:1680. This detailed topographic mapping was prepared using a contour interval of 2-feet, which proved to be reliable for identifying linear features mirrored in the site's topography. The site's specific characteristics, particularly the amount of exposed bedrock, and the abrupt angular nature of many of the bedrock exposures, enabled topography to be an effective diagnostic tool for identifying linear features in bedrock which in most cases were confirmed in the field as joint surfaces or fracture sets. In many cases, entire outcrop faces on a scale of 50 feet or more were found to coincide with joint or fracture exposures.

As noted in Section 5.1.2, the linear trace analysis (LTA) method used for this method is most useful in identifying steeply-dipping or near-vertical fractures. As shown on Figure 5.1.2-1(a), the character of the fracturing at SHL consists of near-vertical or steeply-dipping fractures of several primary strike orientations, including the following:

- North-South;
- East-West;
- Northwest-Southeast;
- Northeast-Southwest.

North-south striking features, some with strike lengths of hundreds of feet, are visible across the site, and are most prominent in the southern and western portions of Shepley's hill. East-west striking features are less evident, but are significant in that they are observed within the central portion of the study area. Northeast-southwest striking linearity of various outcrops results from the ubiquitous foliation fabric (strikes NE-SW and dips $\sim 50^{\circ}$ NW). Although they are not as well expressed in topography, field mapping confirmed numerous additional fractures and joints also striking NE-SW, which occur in conjugate relationship to the foliation, and dip to the east at moderate angles. Steeply-dipping fractures of this strike orientation are also present. Lastly, a northwest-to-southeast striking orientation is readily observed at the Shepley's Hill scale, including a major feature of this orientation which separates the northern third of Shepley's Hill from the southern two-thirds, and cuts directly through the heart of the study area. North-south striking fractures are of major significance at the Shepley's Hill scale. The Disc Golf Fracture Zone (Figs. 7.1-1 and 5.1.2-1(b)), is readily distinguishable on a variety of imagery formats and scales, and is expressed in the topography as a region of distinctive linear features, significant in terms of numbers of features, strike length and width of the overall zone normal to linear strike. Since these linear features are readily confirmed in the field, the significance of the group of features led the project team to provide a unique designation (i.e., provisionally, the "Disc Golf Fracture Zone"). These fractures are exposed in the field as steep linear escarpments which were used to advantage by the individuals who selected the layout for the Devens Disc Golf course, which uses the extreme topography to dramatic effect. For example, the Disc Golf Fracture Zone contains individual lineaments which are up to 500 feet or more in strike length. The aggregate length of the zone is on the order of 1500 feet and the overall width of the zone is approximately 250 feet. Fracture spacing within the Disc Golf Fracture Zone is on the order of 25 feet. It should be noted that within the aggregate width of the Disc Golf Fracture Zone, there are numerous second-order features with shorter strike lengths (in the range of 100-300 feet) that exhibit strike orientations which deviate slightly from the overall N-S direction to NNW-SSE strikes and NNE-SSW strikes. It is also significant to note that the eastern boundary of the Disc Golf Fracture Zone occurs near the topographic divide at the ridge crest. As such, the specific Disc Golf Fracture Zone itself does not appear to be hydraulically significant with respect to the groundwater regime within the study area, but rather, it is responsible for the topographic and hydrologic divide which occurs near the ridge crest. However, more

globally, a N-S striking fracture system appears to persist eastward of the Disk Golf Fracture Zone, and is interpreted to be of major importance with respect to the overall area at the Shepley's Hill scale, including the study area. Further examination of Figure 5.1.2-1(b) shows a regular N-S fracture pattern suggested by linear features with strike length on the order of 100-200 feet spaced semi-regularly on the order of 50-150 feet apart. These features appear to cross-cut by NW-SE striking fractures, particularly on the east side of the topographic divide. NW-SE striking fractures are discussed next.

Fractures with NW-SE strike are numerous and appear to be of major significance at the Shepley's Hill scale. A sizable feature of this orientation, with hundreds of feet of strike length, can be observed cutting across the northern portion of Shepley's Hill, extending southeastward through the study area before disappearing beneath overburden cover at the western edge of the landfill. As discussed above, in Section 7.1, the significance of this feature at the sub-regional scale led the investigators to assign a specific name to the feature, i.e., the Nona-Shep Fracture Zone. Similar to the Disc Golf Fracture Zone, the Nona-Shep Fracture Zone is readily observed at a variety of imagery types and scales. At the Shepley's Hill scale, the feature creates a broad irregular valley with an aggregate width on the order of 200 feet, which disrupts the N-S striking ridge crest. As discussed in Section 7.1, the feature appears to be part of an en echelon fracture system which may extend 2000 feet or more to the northwest. To the southeast, within the study area, the feature appears to step southward in an echelon fashion, before striking southeastward beneath the landfill cover system. These relationships will be discussed further in Section 7.3, below. Within the Nona-Shep Fracture Zone, individual fractures indicate strike lengths on the order of 200-400 feet, with lateral spacing on the order of 30 feet are observable on Figure 5.1.2-1(b). However, the density of fracturing within the Nona-Shep zone is believed to be much greater than this, given the presence of the major valley feature. A higher degree of fracturing is interpreted to occur here due to the lack of outcrop and relatively thick soils deposits in an area otherwise consisting of bedrock exposures. Consistent with this interpretation, the higher degree of fracturing in the heart of the Nona-Shep Fracture Zone has allowed enhanced chemical and mechanical weathering which has effectively obfuscated many individual fracture sets at the ground surface.

Southward from the Nona-Shep Fracture Zone, the NW-SE striking system is regularly expressed in the rock mass, spaced at lateral intervals on the order of 200-300 feet apart, with strike lengths on the order of 300-500 feet. It is interesting to note, that while the NW-SE fractures appear to cross-cut N-S striking features on the east side of the ridge crest, the converse appears to be true on the western side of the topographic divide. In this part of Shepley's Hill, the Disc Golf Fracture Zone is the dominant feature, and appears to cross-cut the NW-SE striking sets.

NE-SW striking fracture zones are common at the site, but appear to be less prominent than the NW-SE and N-S sets. Individual linear strike lengths approach 400 feet in some cases, but are more typically in the 50-100 foot range. These features are spaced on the order of 25-75 feet apart, but are mainly evident in the northeastern part of the site, particularly near the eastern margin of the upland where glacial plucking has formed a

steep NE-SW striking outcrop face with an aggregate length of over 1000 feet. Elsewhere in the Shepley’s Hill region, the steeply-dipping NE-SE striking features are not well expressed in the site topography, which suggests that this orientation may be less significant hydraulically. Moderately-dipping features with NE-SW strikes are important, but are not strongly expressed in topography. These features are discussed in detail at the site-scale in Section 7.3, below.

East-west striking linears are also only weakly expressed in the topographic character of Shepley’s Hill. Based on topography, there is some suggestion that E-W features exist, and are spaced on the order of 300 feet or more, with strike lengths also on the order of 300 feet at the Shepley’s Hill scale. It appears that features of this orientation may be more important at the site scale in association with a large-scale en echelon “step” which occurs on the Nona-Shep Fracture Zone in that area. These features are therefore discussed in greater detail at the site-scale in Section 7.3, below.

Figure 5.3.1-1 is a schematic diagram that presents an idealized view of the fracture patterns at the Shepley’s Hill scale. Table 7.2-1 summarizes the spatial relationships of fracture information observable at the Shepley’s Hill scale. Together, this information contributes to a GFM at the Shepley’s Hill scale. Section 7.3, below, will leverage this information in order to develop a GFM at the site scale.

Table 7.2-1 – Summary of steeply dipping fracture sets at Shepley’s Hill scale

Feature	Strike Direction	Strike Length of Individual Fractures(ft)	Lateral Fracture Spacing (ft)	Comment
N-S fractures	N-S	100-200	50-150	Strongly expressed in topography
Disc Golf FZ	NNW; N-S; NNE	100-500	25	Significant N-S fracture zone with 1500+ ft strike length; dominates western half of Shepley’s Hill; aggregate width of zone is 250 ft.
NW-SE Fractures	NW-SE	300-500	200-300	Strongly expressed in topography
Nona-Shep FZ	NW-SE	≥ 200-400	≤ 30	Complex en echelon FZ with 2000+ ft strike length; 200+ feet

				aggregate width of zone
E-W fractures	E-W	≥ 300+	≥ 300+	Weak
NE-SW fractures	NE-SW	50-100	25-75	Expressed only in NE quadrant

7.3 Site-scale fracture network

Figures 7.3-1 and 7.3-2 provide a basis for discussing the GFM at the site scale. Figure 7.3.1 is a series of N-S cross sections coinciding with surface geophysical alignments 1, 2, and 3 (Figure 5.2-1 and Appendix E). Figure 7.3-2 is an E-W cross-section which generally coincides with the geophysical alignment 4, but diverges slightly from this alignment in order to intersect the key CH-1 S/D location. These cross sections have been annotated with the following:

- Borehole and monitoring well locations and depths
- Monitoring well screened interval depths
- Pertinent information from boring logs and chip logs
- Interpreted top-of-rock/overburden contact
- Specific fracture intervals identified from examination of rock core
- Specific fracture intervals interpreted from borehole geophysical data
- Shallowly-dipping GPR reflectors interpreted as fractures or joints
- Offsets to shallowly-dipping GPR reflectors interpreted as steeply dipping fractures

Using this information, “major” fracture sets, such as those which can be correlated from borehole to borehole, have been identified. These include both extensive shallowly-dipping systems as well as steeply dipping sets. An overall interpretation emerges from this combined data set which supports an internally-consistent GFM at the site scale. Figure 7.3-1 presents reflectors identified by HGI from the 100 MHz GPR survey (App. E). The project team correlated the depths of these locations with borehole data as a means of validating the accuracy of these interpretations. Through this process, correlation was observed between GPR reflecting layers and horizons exhibiting direct evidence of fracturing based on borehole data. The overall internal consistency of the data set afforded the project team a relatively high overall level of confidence in the GPR data set. This enabled correlation of GPR reflectors over substantial distances, and led to the identification a number of “major” geologic structures at the site scale, and numerous smaller-scale features. In this case, we have defined “major” features as those having a

strike length of 100 feet or more, with specific geologic characteristics, particularly those of importance to groundwater flow (i.e., open fractures). “Minor” features are thusly defined as those with shorter strike length and less direct evidence supporting open fracturing. Features of interest at the site scale include the following:

- Shallowly-dipping “sheeting fractures” which generally dip to the east or southeast at dip angles varying between 10 degrees and 50 degrees. These features are also referred to as “cross-joints” on boring logs and elsewhere in the report; this class of features is generally conjugate to the foliation, (foliation strikes NE to NNE and dips from 50 to 60 degrees to the west). These features may have strike lengths on the order of 200 feet or more. There is also evidence to suggest that some of these features are traceable in the down-dip direction for 100 feet or more, and are thus “major” geologic structures at the site scale. Minor structures of this type are also common. There is some indication that sheeting fractures, while geologically continuous to greater depths, are more prevalently oxidized in the uppermost 50 feet of bedrock, excepting those areas which are within 50 feet or less from major steeply-dipping structures. In these areas, sheeting fractures appear to be oxidized to depths of over 100 feet into bedrock.
- Evidence of foliation-parallel fracturing is observed in core and from borehole geophysical logging. These features are interpreted to be of minor importance with respect to groundwater flow, and do not appear to have significant lateral extent. Outcrop mapping suggests that strike length of features of this type is on the order of 20 feet or less in both the strike and dip directions. In the subsurface, there is only limited evidence of oxidation staining parallel to foliation, and borehole geophysical logging does not suggest any significant degree of open fracturing in this orientation. However, foliation-parallel features are commonly oxidized where they are associated with intersecting steep fractures. As such, foliation-parallel fracturing may play a limited role in enhancing lateral interconnectivity of the aquifer near major features.
- Steeply-dipping fractures with foliation-parallel strike orientation are also commonly identified. These are minor features which have similar strike, but much steeper dips than foliation. Strike lengths for this class of feature are believed to be on the order of 10’s of feet at most in both the strike and dip directions. Such features are believed to be antithetic to NW-SE striking sub-vertical features and may play a limited role in enhancing lateral interconnectivity of the aquifer near these major features.
- Steeply-dipping to near-vertical features are paramount “major” geologic features at the site scale. These include the NW-SE striking features of the “Nona-Shep” Fracture Zone (NSFZ; dips near vertical to steeply to the SW), N-S striking fracture zones parallel to the Disc Golf Fracture Zone (sub-vertical dips), and E-W striking fracture zones (dips ~ 65⁰ south to near vertical). Individual fractures of the Nona-Shep Fracture Zone have lateral strike lengths of over 100 feet and will be discussed in greater detail below.

- N-S striking fracturing is less prominent within the site area than in other areas of Shepley's Hill. Strike lengths on the order of 50 feet or less are inferred from data at the site scale, and may play a role in enhancing lateral interconnectivity in the central portion of the site area. However, there is some information from previous studies which suggests that a major N-S striking feature exists in the subsurface just east of the site area, e.g., beneath the western portion of the landfill cap area. This will be discussed in greater detail, below.
- E-W striking fractures are most prevalent in the vicinity of the Nona-Shep Fracture Zone, and appear to be related to strain transfer as splays of the Nona-Shep system dissipate and shift southward within the study area in an echelon fashion. In this respect the E-W striking fracturing appears to cross-connect separate splays of the Nona-Shep fracture zone and is therefore important with respect to enhancing interconnectivity in the region of the Nona-Shep Fracture Zone over lateral distances on the order of 50 feet.
- Sub-horizontal fracturing occurs proximal to steeply dipping fractures and appears to provide fracture connection between sheeting fractures and steeply-dipping fractures. These types of features are secondary (i.e., "minor") and extend laterally to distances on the order of 20 to 30 feet .

Figures 7.3-1 and 7.3-2 illustrate the relationships presented above; integrating these N-S and E-W cross-sections creates a working GFM at the site scale. Figure 7.3-1 presents a series of N-S cross sections coinciding with surface geophysical alignments 1, 2, and 3 (east to west). Figure 7.3-2 is an E-W cross-section which generally coincides with the geophysical alignment 4. In discussing pertinent details, the text will refer to these cross section alignments as Lines 1,2, 3, and 4, respectively.

On Figure 7.3-1, the axial trace of the Nona-Shep Fracture Zone (NSFZ) is indicated on lines 1, 2, and 3. Moving from west to east, the axial trace of the NSFZ intersects the land surface near Loc 20, MW-11A, and MW-1. At each location, the bedrock surface is somewhat deeper than the surrounding areas, presumably due to preferential glacial scouring along the fracture zone. Near Loc 20, the core of the NSFZ has an approximate width of 80 feet as evidenced by disruption of gently-dipping radar GPR reflectors and a zone of enhanced conductivity in a vertically-oriented zone approximately 20 feet wide beneath Loc 19 and Loc 20. The northern most fractures associated with the NSFZ intersect line 3 in the vicinity of 500 feet east (horizontal axis, line 3), based on exposures from outcrops 27 and 30B. To the south, the NSFZ appears to dissipate in the vicinity of Q4-3, south of which bedrock becomes sparsely fractured. Significant steep fracturing was not encountered in Q4-1. In this sense, the "core" of the NSFZ is approximately 80-100 feet wide with a fracture density of approximately one steeply-dipping fracture every 10 feet laterally. The "core" zone is enveloped by a less-fractured region which is on the order of 200 feet in total width, with individual fractures spaced 20-30 feet apart. The "core" zone of the NSFZ extends southeastward through Line 2 (~40-130' along the horizontal axis). Still further to the east, the NSFZ core cuts through line 1 from the general vicinity of CAP-3 to CAP-2B; (~50-150 feet along horizontal axis). Another zone of steep NW-SE striking zone of fracturing conjugate to the NSFZ is mapped at the

ground surface in outcrops 3-1 and 3A-1. This related feature appears to strike southeastward beneath the landfill to the south, beyond the southeastern limits of the study area (i.e., upgradient).

A series of gently-dipping GPR reflectors are perhaps the most prominent structures shown on the cross sections. While the structures are locally spaced less than 5 feet apart, in the vertical dimension, correlation of borehole data which penetrate these structures indicates that there are at least two classes of these features. Laterally-extensive features, with strike lengths of 200 feet or more, can be traced across the site subsurface. Such features are highlighted on the cross-sections, where supported by other data sets. In general, the laterally extensive features are dominated by dips to the southeast (apparent dips to south on N-S cross sections), presumably due to “cross joints” observed in outcrops. However, the undulatory nature of the larger structures suggests that they may be composite features made up of intersecting shallowly-dipping features of various orientations. In aggregate, the features generally mimic topography, as would be expected of joints formed from post-glacial stress relief. It is also observed that a broad depression on the parallel and quasi-planar features generally coincides with the location of the NSFZ axial trace, which is also a topographic low. The sharp topographic indentations on the top-of-rock surface near Loc19, Loc11, and MW-1 likely resulted from the enhanced weakness of the rock mass near the “core” of the NSFZ, where vertical fracture density is observed to be greatest. In these areas, the vertical structures combine with the laterally extensive features to form a relatively dense network of fractures. The interpreted “core” of the NSFZ is indicated on lines 1, 2, and 3 (Figure 7.3-3).

Figure 7.3-4 (west to east cross section) provides an examination of the third dimension. Several important observations are facilitated by this cross-section. The intense degree of fracturing to the east at CH-1S/D is in stark contrast with the limited degree of fracturing, even in the shallow subsurface at Q4-1 and 20-1 and 20-2. At these locations, relatively widely-spaced sheeting fractures and/or cross joints are the only fractures which appear important to groundwater flow. In contrast, rocks beneath the CH-1S/D area are densely fractured over the total length of the borehole (from top of bedrock at 18 ft bgs to total depth at 151 ft bgs), and oxidation is observed in core at a depth of 123.3 ft bgs. The presence of “core” of the NSFZ near CH-1S/D, and its absence near Q4-1 and 20-1 and 20-2, is the most likely explanation.

There is some evidence that specific shallow- to moderately-dipping sheeting fractures or cross joints extend from CH1-D/S to upslope boreholes. For instance, a series of important fracture zones were encountered from 39.2 ft bgs to 51.4 ft bgs in CH-1S/D. Dips in this zone are generally to the southeast and vary from 20 to 50 degrees. Up-dip projection of the features places them either near the top of rock in the Q4-1 vicinity or nearby in the generally flat triangular sub-crop area bounded by 20-1, 27-1 and Q4-1. This flat region appears to be an area of relatively greater hydraulic conductivity based on potentiometric maps, presumably due to a higher fracture density. It is also noted that this zone of fractures, particularly the fracture encountered at 39.2 ft bgs in CH-1D/S, is responsible for large volumes of drilling water loss during the installation of these wells. These observations suggest potential structural and hydraulic connectivity along these

features over the approximately 110 feet of lateral distance between Q4-1 and CH-1D/S. Similarly, there appears to be a down-dip connection with a significant sheeting fracture encountered at 37 ft bgs in Q4-1 (dips 45° east) with similarly oriented features identified within the screened interval of CH-1D (screened interval is 85-95 ft bgs). Several sheeting fractures penetrated in the screened interval for CH-1D (85-95 ft bgs) may also project up-dip to the region just beneath the well screen in Q4-1 (SI= 30-40 ft bgs), where a series of fractures are indicated on the caliper and ATV logs at 44.5, 45, 47, and 48 ft bgs. These fractures appear to correspond with the sub-horizontal GPR reflector in this area shown on Line 1 (Fig. 7.3-3).

Monitoring wells 20-1 and 20-2 do not appear to be well connected to other site monitoring wells based on fracture patterns. A gently-dipping sheeting fracture was penetrated at 39 ft bgs, which is within the screened interval at 20-1 (SI=40-50 ft bgs). However, geometry of the system suggests that this fracture, and others intersected by 20-1 and 20-2 project to depths beneath the well network to the east. There is some suggestion that a color change at 14 ft bgs in 20-1 may project to an oxidized zone (120.8 ft bgs) in CH-1D. However, it is likely, given the relatively lower degree of fracturing in the up-gradient areas, that the majority of groundwater flow is focused to the uppermost 50 feet or so of bedrock, even as flow is directed from west to east. An examination of Figure 7.3-4 suggests a potential mechanism for this where water flows eastward, down the dip of shallowly-dipping sheeting fractures and cross joints, but is “short-circuited” upwards, toward the land surface, where sheeting fractures locally intersect moderately-dipping (open) fractures with the opposite dip, such as the foliation-parallel fractures at 47 and 48 ft bgs at Q4-1. In such cases, groundwater flow may resume in the down-gradient flow direction (in this case to the southeast) via sub-parallel open sheeting fractures at higher elevations within the rock column. Conversely, intersection of sheeting fractures with steeply dipping fractures, such as those of the NSFZ, may also redirect groundwater in response to pressure gradients within these features. It should be noted, as shown on Figure 7.3-4, that fracture density appears to be significantly increased in the areas near the intersection of steep structures with sheeting fractures. For example, from 18.5 to 25.3 ft bgs in CH-1D, a series of sub-horizontal fractures appear to cross connect low-angle sheeting fractures and steep fractures. A similar zone also occurs in the vicinity of 92.5 ft bgs in CH-1D, suggesting the phenomenon has more to do with the intersection with steep fractures than to the proximity of the ground surface. Figure 7.3-3 is a photograph of core from CH-1 from the 87.3 to 89.6 interval which shows a highly oxidized sub-vertical fracture cross-cutting the borehole over a significant vertical zone. It is anticipated that numerous other features with similar orientations exist in the subsurface within the NSFZ. With respect to steep fracturing, it must be acknowledged that the limited deep drilling program afforded by this study was not particularly successful in targeting sub-vertical hydraulically significant fractures of the N-S striking group. It is likely that large features, of particular importance to groundwater flow at the Shepley’s Hill scale, underlie the region east of the site, i.e., beneath the landfill cap. For example, cross sections C-C’ and D-D’ of the *Revised Draft Supplemental Ground Water Investigation Report* (Harding ESE, 2003) indicate a deep N-S striking valley beneath the west-central portion of the landfill. A fracture system of this orientation may ultimately be responsible for the N-S trending bedrock valley as well as the north-flowing groundwater regime in this part of the Shepley’s Hill

system. These issues and ideas are discussed further in Section 8, below, *Implications for Groundwater Hydrology*. A fully developed CSM for the site which considers the GFM presented here in conjunction with hydraulic and geochemical data is presented in Section 10, below. Lastly, recommendations for further work are included in Section 11, below.

8.0 IMPLICATIONS FOR GROUNDWATER HYDROLOGY

A primary objective of the Bedrock Investigation is to collect data in support of interpretation of the shallow groundwater hydrology at the junction of the recharge area on Shepley's Hill itself and the adjoining overburden aquifer beneath the landfill to the east. Previous work to characterize the hydrology of the SHL system has indicated that the elevated bedrock hill is a recharge area for groundwater that eventually makes its way eastward to the thick (of the order of 100 ft in some locations) overburden beneath the landfill, ultimately joining a regional flow to the north. This conceptual model generally is consistent with the interpreted hydraulic potential surface for overburden groundwater beneath the landfill, which suggests flow from the direction of Shepley's Hill on the west side of the landfill (see, e.g., CH2MHill, 2006). It should be noted, however, that well control on water levels is sparse in the western portion of the landfill. This picture is also consistent with results of various versions of the numerical model for Shepley's Hill groundwater as it has evolved (e.g., Harding ESE, 2003; CH2MHill, 2006; ECC, 2009), which show (e.g., ECC, 2009, Fig. 5-5; included in the present report as Fig. 8.0-1) groundwater flow paths that originate on Shepley's Hill, travel down a steep gradient to the east, and turn northward beneath the landfill.

As noted in Section 1, if precipitation that falls on Shepley's Hill is to recharge the overburden aquifer to the east beneath the landfill, water must follow one or a combination of several pathways. Surface runoff may carry some rainfall and snowmelt off the hillslope to enter the overburden where it pinches out against the rising bedrock surface. (This process has been referred to in the past as "run-under," because it could, in principle, lead to locally enhanced recharge of the overburden at the western margin of the landfill cap.) Recharge may enter the fractured rock directly in areas of bare outcrop. Precipitation may first be stored and/or transmitted in the patches of soil veneer on the hill, and then move downslope within this thin overburden, or drain to and recharge the underlying fractured rock. Once within the fracture network, groundwater is expected to flow downgradient toward the east-southeast, and eventually to discharge upward into the thick valley-fill deposits underlying Shepley's Hill Landfill. Although these processes are implicit in previous conceptualizations of the SHL hydrologic system, and are represented in a gross, average sense in the numerical groundwater flow model that has evolved in support of various landfill studies, no direct field characterization of the recharge area had been performed prior to this investigation.

8.1 Site scale

The hydraulic gradient in the fractured-rock aquifer on the east flank of the hill, adjacent to the west edge of the landfill cap, is estimated at two times for which manual water-level measurements are available: a period of relatively high groundwater on 4/24/09, and a period of relatively low groundwater on 9/9/09 (Table 8.1-1). The potential surfaces at these times were sketched (Figures 5.6.1-1 and 5.6.1-3, respectively), and show that the hydraulic gradient is generally parallel to the topographic gradient, implying bedrock groundwater flow in the study area to the ESE, directly toward the

landfill. The gradients are steep, and vary significantly as the fracture network on the hill fills during wet periods, and drains during relatively dry periods. The gradients were estimated on four boring pairs that are aligned approximately normal to the equipotentials: from 27-30B-1 to CAP-1B, from 27-1 to CAP-2B, from Q4-1 to CAP-3, and from Q4-2 to 3-1. Under the high water conditions in April, the estimated gradients on the four transects ranged from 0.13 to 0.25, with a mean of 0.18. Under the low water conditions in September, the gradients ranged from 0.088 to 0.17, with a mean of 0.12.

Table 8.1-1. Horizontal hydraulic gradient estimated from water elevations at select well pairs.

Well pair	Distance (ft)	4/24/09		9/9/09	
		Elevation (ft msl)	Gradient (ft/ft)	Elevation (ft msl)	Gradient (ft/ft)
27-30B-1	164	262.00	0.142	248.09	0.103
CAP-1B		238.67		231.12	
27-1	164	263.90	0.126	248.66	0.0877
CAP-2B		243.24		234.25	
Q4-1	86.2	262.23	0.216	250.60	0.166
CAP-3		243.60		236.24	
Q4-2	72.0	263.49	0.254	247.56	0.134
3-1		245.18		237.92	
average			0.184		0.123

It is notable that the boring pair (27-1, CAP-2B) located in the middle of the SE-NW valley feature that cuts across Shepley’s Hill, and on which the study area is centered, yields the lowest estimated gradient, for both high and low groundwater conditions. Steeper gradients are estimated both to the north and to the south of this transect. This observation is consistent with the inference that the valley coincides with a fracture zone of higher effective hydraulic conductivity, and therefore tends to drain more readily than adjacent domains. For this reason, a relatively high flux of groundwater can pass through this zone under a lower potential gradient, and water tends to “funnel” into this feature.

Assuming that the average of the high- and low-water gradients, 0.15, is representative, and adopting the geometric mean hydraulic conductivity indicated by the slug tests of 2.0 ft/d, the groundwater flux through the fractured rock at the margin of the hill is approximately 0.3 ft/d. It is often asserted that the majority of groundwater flow in fractured crystalline rock in New England occurs in the uppermost 50 ft. The prevalence of larger-aperture fractures in the upper 50 ft at the study site was noted in the borehole geophysics data (Sec. 5.5 and App. G). In the present case, water levels in the study area are typically about 20 ft below the surface. Therefore, it is assumed that most of the groundwater flow off the hill in this area occurs within a saturated thickness of 30 ft,

resulting in a total volume flow rate of about 9 ft³/d per linear foot parallel to the eastern margin of the hill and/or western margin of the landfill cap.

Due to the relatively small interconnected porosity of fractured, crystalline rock, the average linear velocity can be high in comparison to typical unconsolidated aquifer materials. The average linear velocity is the rate at which an element of groundwater moves through the local system. In the present case, if a typical fracture porosity of 0.02 is assumed, the estimated flux of 0.3 ft/d results in an average linear velocity of 15 ft/d. (Note that fracture porosity for the Shepley's Hill rock has not been measured directly.)

An upper bound to the groundwater discharge at the eastern margin of the hill can be estimated independent of the observations discussed in the foregoing paragraphs. In particular, the volume flow rate is constrained by the total precipitation that falls on the catchment upgradient of the area of interest. Data for 2005 – 2009 show average annual precipitation of 48 in (4.0 ft) (see Sec. 4.3). It is assumed that the groundwater divide on the upgradient boundary of the recharge area corresponds approximately to the topographic divide on the hill. The distance from the Shepley's Hill ridge crest to the eastern margin of the study area is approximately 340 ft. Therefore, the average total precipitation that falls on this area of the hill is approximately 3.7 ft³/d per linear foot parallel to the ridge. This is an upper bound, because only some fraction of this total is expected to contribute to recharge, with the balance being lost to evapotranspiration and surface runoff. There are several possible reasons for the discrepancy between the estimates of the maximum available recharge based on precipitation records (3.7 ft³/d per linear foot) and the average groundwater discharge based on the observed hydraulics (9.0 ft³/d per linear foot). First, the study area straddles a valley feature that cuts obliquely across the ridge. It is likely that this valley feature localizes recharge that was collected over a longer segment of the ridge in a funnel-like fashion, so that the one-dimensional approximation invoked for the total precipitation falling on this portion of the hill underestimates the available recharge feeding into the study area. Second, the assumptions behind the hydraulic calculation may be in error. In particular, the geometric mean of the slug-test-derived effective conductivities may not be representative, and the estimate of the saturated thickness that carries most of the flow may be incorrect, leading to an overestimate of the total groundwater discharge.

8.2 Shepley's Hill scale

Data were not collected in the present investigation to characterize the groundwater hydrology at the scale of the entirety of Shepley's Hill. However, it is possible to extend the general arguments discussed at the site scale (Sec. 8.1) to the catchment upgradient (and west) of the landfill, as well as to draw upon previous investigations of the landfill system for additional insight.

The flow rate estimated from the observed average hydraulic gradient, the geometric mean hydraulic conductivity from slug tests, and an assumed active saturated thickness for the study site is 9 ft³/d per linear foot parallel to the eastern margin of the hill (Sec.

8.1). It is estimated from the topography that the length of the hill that serves as a recharge area to the landfill area to the east is 1850 ft (Fig. 8.2-1). Therefore, an extrapolation of the site-scale flow estimate to the Shepley's Hill scale indicates that approximately 6.1×10^6 ft³/yr, or, equivalently, 86 gpm, flows from the recharge area on the hill toward the overburden aquifer to the east. As discussed previously, this estimate likely is biased high, based on a comparison to the precipitation available to supply the flow. In addition, the study site was chosen to focus on a geomorphological feature that is believed to reflect a well-developed NW-SE fracture set, and may be more conductive than much of the rest of Shepley's Hill.

The upper-bound estimate for the groundwater discharge from the hill based on total annual precipitation can also be repeated for the Shepley's Hill scale. The catchment for the fractured-rock aquifer upgradient of the landfill is delineated based on the topography (Fig. 8.2-1). It is assumed that the highest elevations along the ridge of Shepley's Hill coincide with the groundwater divide, with water on the east side of this line flowing generally toward the east. To the south and north, secondary ridges roughly perpendicular to the long axis of the hill have been identified that appear to separate the hillslope falling directly toward the landfill from areas that appear to drain to the southeast and northeast, respectively. The area of the resulting recharge area on the steep hillslope upgradient of the landfill is estimated to be 5.4×10^5 ft², or approximately 12 acres. This area is shaded aqua-blue on Figure 8.2-1. For average total annual precipitation of 4.0 ft/yr, this yields a total available water flow of approximately 2.2×10^6 ft³/yr, or 31 gpm. It is noted again that this represents an upper limit to the recharge, because some fraction of the total available water is lost to surface runoff and/or evapotranspiration. The latter is particularly active in the warmer part of the year. As is the case for the site-scale calculations, the total available water is less than the flow estimated based on the hydraulics, in this case by a factor of about 1/3. This suggests that the flow rate based on observations in the study area is biased high, possibly because it is not representative of the average flow moving eastward off the hill, and possibly because the estimates of the hydraulic conductivity and the saturated thickness used in the calculation are in error.

In addition to the direct recharge to the bedrock aquifer on the elevated ridge of Shepley's Hill, there is an area adjacent to the southern end of this domain, used by the Devens Department of Public Works (DPW) for storage of landscaping materials, composting, etc., that also receives recharge for the overburden aquifer beneath the landfill. This area is shaded in blue on Figure 8.2-1, and covers approximately 2.0×10^5 ft², or about 5 acres. Total average annual precipitation over this area is approximately 0.79×10^6 ft³/yr, or 11 gpm. The total of these two domains of groundwater recharge is 7.4×10^5 ft², or about 17 acres. For average total annual precipitation of 4.0 ft/yr, this yields a total available water flow of approximately 3.0×10^6 ft³/yr, or 42 gpm from the catchment on and adjacent to Shepley's Hill, and ultimately feeding into the overburden aquifer beneath the landfill cap. Again, this is an upper bound, because it represents all of the precipitation that falls on these open areas.

A numerical model for the groundwater flow in the overburden aquifer beneath Shepley's Hill Landfill was developed to support remedial design and related decision-making (Harding ESE, 2003; CH2MHill, 2004a; AMEC, 2009)⁴. The Bedrock Investigation affords an opportunity to re-examine some of the assumptions that were made in the model implementation in the absence of extensive characterization of the bedrock hydrology. The model is constructed at a scale that encompasses the recharge area on Shepley's Hill, which plays a key role in the overall water balance for the system. The model specifies 20 in/yr of recharge over the open area between the ridge crest of Shepley's Hill and the western edge of the landfill cap, or about 42% of annual average precipitation. For the area estimated here, $5.4 \times 10^5 \text{ ft}^2$, this amounts to a total input of $0.90 \times 10^6 \text{ ft}^3/\text{yr}$, or 12.8 gpm. The model also applies supplemental recharge to finite difference grid cells along the western edge of the landfill in order to address a concern at the time of the model development for possible "run-under." This additional input to groundwater was intended to represent surface runoff from the elevated bedrock hill that might drain to the foot of the slope, and enter the subsurface adjacent to the edge of the landfill cap. The total supplemental recharge added in this fashion was $1.1 \times 10^6 \text{ ft}^3/\text{yr}$, or 16.2 gpm. The total rate of water input on and immediately adjacent to the hill upgradient of the landfill is then the sum of recharge over the open area of the hill and the supplemental recharge at the foot of the hill, giving $2.0 \times 10^6 \text{ ft}^3/\text{yr}$, or 29.0 gpm. This total is approximately 94% of the annual precipitation that falls over the area of the hill, suggesting that the addition of the supplemental recharge may result in an unrealistically high input of water on the west side of the landfill. It is expected that surface runoff and evapotranspiration remove a significant fraction of the total precipitation, so that it is not available to recharge groundwater.

Further perspective on these estimates of total recharge on the eastern flank of Shepley's Hill is given by the design capacity of the groundwater extraction system situated at the north end of the landfill. A design objective of the extraction and treatment system was to capture as much as possible of the overburden groundwater that passes beneath the landfill. It was estimated that this would require pumping at 50 gpm, and the system has approached this design extraction rate in recent years. It is reassuring that the various estimates of groundwater discharge from Shepley's Hill bedrock are of the same order of magnitude as the estimate of the discharge of the overburden aquifer to the east. Previous interpretations of the hydraulic potential surface in the overburden aquifer beneath Shepley's Hill Landfill, based on field measurements of water levels at available monitoring wells, suggest that the hill is the primary source of recharge, with lesser contributions to the overall water balance from the smaller catchment to the south of the landfill. The flow field simulated by the numerical model further supports this conclusion (see, e.g., Fig. 8.0-1). An upper bound on the recharge rate on the eastern flank of Shepley's Hill based on total precipitation is 31 gpm. An estimate based on the observed hydraulic gradient across the eastern portion of the study area on the hill and estimates of the hydraulic conductivity and active saturated thickness yields 86 gpm. Despite the uncertainty inherent in these estimates, the results of the present investigation

⁴ The following description of the model is based on the references cited. It is the authors' understanding that changes to the manner whereby recharge is applied were made in more recent versions of the model, and are in accord with the general conceptualization of recharge which emerged from this study.

are regarded as generally consistent with past characterization of the groundwater flow in the overburden aquifer to the east. That is, much, if not most, of the input to the overburden aquifer beneath the landfill is derived from recharge on Shepley's Hill. Average total flow rates from recharge on the hill appear to be of the order of tens of gpm, and the extraction system at the north end of the landfill is sized appropriately to capture the flow within the overburden. Of course, these considerations represent only an order-of-magnitude test for consistency between the results of the present investigation of the bedrock aquifer on the hill and previous independent investigations of the overburden aquifer to the east. Details of the exact flow field within the overburden aquifer, including delineation of the capture zone of the extraction system, are not assessed in the present study.

The Supplemental Groundwater Investigation (Harding ESE, 2003) for the overburden aquifer beneath the Shepley's Hill Landfill states:

The effects of potential run-under on groundwater flow under the cap are expected to be small. ... Much of [the] recharge [on Shepley's Hill] is expected to occur as flow in the bedrock. ... During some earlier model construction runs, it was noted that recharge rates [on the hill] up to 30 in/yr did not significantly alter the model calibration or apparent groundwater flow directions. This is because ... the variation in potential recharge from Shepley's Hill is small relative to the aquifer's capacity to conduct groundwater.

The results of the present investigation, representing the first attempt to characterize the bedrock hydrology in detail, support the above statement. It is apparent that significant recharge enters the fractured bedrock on Shepley's Hill, and that groundwater flows within the rock to the east, where some fraction of it discharges upward to the overburden aquifer beneath the landfill. There is little evidence that there is a significant contribution of recharge to the overburden aquifer due to direct infiltration along the western margin of the landfill cap deriving from overland flow from the hill, referred to in the foregoing as "run-under." The investigation team was present in the vicinity of the interface of the bedrock hill and the sandy overburden aquifer to the east on numerous occasions spanning four years, in all seasons of the year, and under wet and dry conditions. No visual evidence of surface runoff arriving or accumulating at the bedrock – overburden interface was seen. A minor exception is a small bedrock "pocket" at the toe of the slope in the study area that holds ponded water for a few days during wet periods. It is notable that the Supplemental Groundwater Investigation model indicated insensitivity to the magnitude of the recharge flux on the hill. Therefore, calibration of the model does not provide a strong constraint on the recharge rate to the fractured rock of Shepley's Hill.

The direct evidence accumulated in the present study offers a more robust indication that Shepley's Hill is a recharge area for the aquifer to the east, and that the pathway from the hill to the overburden aquifer beneath the landfill is primarily through the fractured rock. Observed steep hydraulic gradients (of the order of 10^{-1} ft/ft) and moderate effective hydraulic conductivity (of the order of 10^0 ft/day) for the shallow bedrock indicate a groundwater flux of the order of 10^{-1} ft/day. This flow provides the primary pathway for

water that recharges the bedrock aquifer on the hill, flows toward the east, and discharges upward to the overburden beneath the impermeable landfill cap. The cap prevents direct recharge to a large area of the overburden aquifer, making the bedrock pathway from Shepley's Hill of greater importance to the overall water balance in the overburden.

8.3 Sub-regional scale

Although the sub-regional scale groundwater hydrology was not a subject of this investigation, it is mentioned briefly here in order to acknowledge that recharge on Shepley's Hill contributes to a larger system, beyond the more local phenomena at the study-site scale or the scale of the landfill to the east. A brief description of the role of Shepley's Hill at the sub-regional scale is provided in the following paragraph, based primarily on broad principles of hydrology, rather than on comprehensive data that might be collected to support this interpretation.

Shepley's Hill is an elevated ridge, surrounded on all sides by lower areas with relatively flat topography (sec. 4.1). As such, the hill serves as a recharge area for groundwater that flows radially outward in all directions. In addition to the bedrock flow discussed in the foregoing sections, which flows east-southeast from the ridge crest toward Shepley's Hill Landfill, there is a corresponding flow of recharge accumulated on the west side of the hill, which flows generally toward the west, and ultimately discharges to the Nashua River. Smaller volumes of groundwater originating at the southern and northern ends of Shepley's Hill flow generally to the south and north, respectively, and do not participate in the groundwater system beneath the landfill. It is believed that there is a local groundwater divide in the vicinity of the southern end of Shepley's Hill Landfill, although it has not been located precisely. Groundwater near the large warehouse (former AOCs 32 and 43A) has been shown to flow in a westerly direction, presumably moving around the southern end of the hill and joining the larger-scale flow toward the floodplain of the Nashua River. Recharge to the south end of the ridge likely flows radially off the hill to the southeast, south, and southwest, contributing to the westerly flow toward the river. Similarly, recharge to the north end of the ridge likely contributes to groundwater that flows to the northeast and north, joining the sub-regional flow to the north toward discharge points along Nonacoicus Brook. Some fraction of the groundwater approaching the Nonacoicus Brook drainage is believed to turn to the west and remain in the subsurface, following the general path of the overlying surface water. The brook flows to the Nashua River.

9.0 BOREHOLE WATER CHEMISTRY

9.1 Methods

Between November 2 and 4, 2009, and again between March 16 and 17, 2010, US EPA personnel collected groundwater samples from the new bedrock wells. In late June 2010, wells CH-1D and 3-2 were re-sampled, as these are the only two wells with consistently reportable arsenic concentrations. Samples were obtained using either a bladder pump or a peristaltic pump and were collected according to EPA low-flow protocol. Field water quality parameters, including temperature, specific conductivity, pH, oxidation-reduction potential (ORP), dissolved oxygen (DO), and turbidity, as well as the full laboratory analytical data sheets are provided in Appendix O.

In addition, samples were submitted to the EPA's Office of Environmental Measurement and Evaluation (OEME) in North Chelmsford, MA, where additional analyses were performed. These included:

Anions: bromide, chloride, fluoride, nitrate/nitrite as nitrogen, and sulfate. These analyses were performed using either a Dionex ICS-2000 or DX120 Ion Chromatograph, following the EPA Region 1 SOP, EIASOP-INGDXIC10.

Total Recoverable Metals: aluminum, arsenic, barium, calcium, chromium, cobalt, copper, iron, lead, magnesium, manganese, nickel, potassium, sodium, vanadium, and zinc. EPA Region I SOP, EIASOP-INGDVICP1. Samples were prepared using SOPs based on US EPA Methods 3010A or 3005A and analysis was conducted according to Method 6010B. Samples were analyzed using a Perkin Elmer 4300 Dual View Inductively Coupled Plasma – Optical Emission Spectrometer.

Alkalinity: Sample preparation and analyses for alkalinity were conducted according to the EPA Region 1 SOP, INGALKCARB1.SOP.

Phosphorus: Phosphorus was measured following the EPA Region 1 SOP for total phosphorus in water, EIASOP-INGTP8.

All data were reviewed using the EPA New England OEME Chemistry QA Plan.

9.2 Results

Analytical results from all sampling rounds are presented in Table 9.2-1. For the November 2009 samples, arsenic was reported by the laboratory in only three wells (at values above the reporting limit of 10 ug/L): CH-1S, CH-1D, and 3-2. The maximum As value, 400 ug/L, came from CH1-D, from the June 2010 sampling round. In the March 2010 samples, arsenic was found at levels above the reporting limits (10 to 20 ug/L) in only two wells, CH1-D and 3-2. Concentrations were comparable to values from the previous sampling round (290 ug/L vs. 370 ug/L in CH1-D and 91 ug/L vs. 63 ug/L

in 3-2). Results from these wells stand in contrast to the Hach field test results, obtained from open borings, which may have been compromised by turbidity.

Results from both sampling rounds show pH values ranging from 5.32 (MW27-30B-1) to 7.68 (CH1-D). In general, pH increased with decreasing well screen elevation; lower pHs were observed in wells screened in shallow bedrock, and the highest pH occurs in the deep-bedrock screen.

Alkalinity values from the new bedrock wells range from 4.3 mg/L, as CaCO₃, in 27-30B-1 to 130 mg/L in CH1-D and are strongly correlated with specific conductivity ($R^2 = 0.9554$), calcium, and potassium.

Nitrate was not found above the reporting limits (0.1-0.2 mg/L) in any of the new bedrock wells in the initial sampling round. However, nitrite was reported in four wells, at concentrations ranging from 0.91 to 1.4 mg/L. In contrast, the second round yielded nitrate values ranging from 3.9 mg/L (27-30B-1) to 12 (CH1-D), and no nitrite above the reporting limit (0.1 mg/L). No explanation for these results is apparent at this time.

Sulfate is consistently reported at concentrations around 8 to 10 mg/L. In the initial sampling round, two wells (CH1-S and 20-1) reported elevated sulfate; in the March 2010 round, only 20-1 yielded sulfate at a concentration significantly higher than the other wells (18 mg/L).

Aluminum is present at concentrations ranging from 65 ug/L (Q4-1; 11/5/2009) to 97000 ug/L (CH-1S; 11/5/2009). However, Al is strongly correlated with turbidity ($R^2 = 0.99$, not including non-detects) and the extreme value is likely an artifact. The second sample from CH-1S yielded Al at 5000 ug/L, still higher than Al concentrations in the other wells, and possibly still due to elevated turbidity.

Calcium and magnesium in the bedrock wells range from 4200 to 50000 ug/L and from 420 to 15000 ug/L, respectively. These elements are strongly correlated and are approximately consistent with the trend defined by Ca and Mg values from the SHL long-term monitoring data.

Iron ranges from non-detect at 40 ug/L to a maximum of 31000 ug/L, but is also correlated with turbidity. It is interesting to note that the elevated As concentrations observed in CH-1D and 3-2 are not associated with either Fe or turbidity. In contrast, many of the SHL wells that report significantly elevated arsenic (e.g., SHM-05-40X; SHM-96-5B; SHM-05-42B; SHM-05-41B; N5-P1) show a strong correlation between aqueous As and Fe concentrations.

Elements not detected above the reporting limits in either round (with the exception of the initial sample of CH1-S, which was extremely turbid) are: bromine, chromium, cobalt, copper, nickel, lead, vanadium, and zinc. Sodium and potassium were not analyzed in the second set of samples. In general, concentrations of all other parameters were lower in the March 2010 samples than the November 2009 results. This difference

appears to be due to the decrease in turbidity in most of the wells between the first and second sampling events.

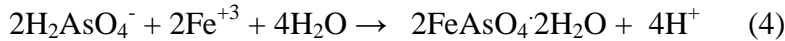
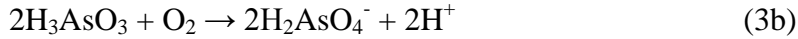
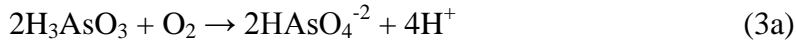
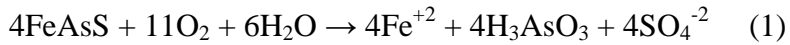
9.3 Discussion

In comparison to data from the SHL Long-Term Monitoring and Maintenance Program, the new bedrock wells are relatively low in alkalinity, specific conductivity, and pH. With only two exceptions (20-1 and CH-1D), ORP values are strongly positive ($> +100$ mV). These observations are consistent with recent infiltration that has had limited time to react with bedrock (i.e., short residence times).

The initial sample from CH-1S was extremely turbid (834.2 NTU). In addition, a large quantity of drilling water apparently went into the open fractures that were encountered in drilling this hole, and attempts to develop this well by removing the estimated volume of added water were unsuccessful. Therefore, analytical results for this well from this initial sampling round must be considered suspect; it is clear from the significant decrease in concentrations reported in the second round that turbidity biased the first set of results. Although the second sampling round from CH-1S is still significantly more turbid than samples from the other wells, the analytical results are consistent with recent infiltration into the shallow bedrock – e.g., elevated DO and ORP, low pH, and low alkalinity. With the exception of Al (5000 ug/L in the second round), all other analytical results from CH-1S are comparable to the ranges measured from the other wells. These observations suggest that turbidity does not compromise the data in this sample, other than for Al.

The maximum arsenic value, 400 ug/L, reported from CH-1D, may be significant. This is the highest arsenic concentration that has been reported within the SHL system from a location that is unequivocally upgradient from the landfill. This result should not be over-interpreted until further data are available, but the November 2009 and March 2010 results, 370 ug/L and 290 ug/L, respectively, are of the same order of magnitude. These arsenic values are not associated with elevated iron concentrations. However, the elevated As in groundwater from this well is nevertheless consistent with the presence of As-bearing minerals in deep-bedrock samples (Sec. 6.0) and the aqueous alteration of those minerals by infiltrating groundwater.

A possible mechanism for the release of arsenic to solution without aqueous iron is the alteration of arsenopyrite to scorodite, followed by the incongruent dissolution of scorodite to a hydrous ferric oxide and arsenate anion (see, e.g., Bluteau and Demopoulos, 2007). Equation (1) produces ferrous iron and arsenite; the oxidation of ferrous iron in Eq. (2) yields hydrous ferric oxide, represented here by FeOOH; Equations (3a) and (3b) are the oxidation of arsenite (from Equation 1) to arsenate species (note that 3b is dominant in the pH range 5-7; Parkhurst and Appelo, 1999); Equation 4 represents the formation of scorodite from ferric iron and arsenate; and Equation (5) is the equilibrium between scorodite and FeOOH and arsenate in solution.



It is of interest to note that the dissolved oxygen (DO) in CH-1D, 0.55 mg/L, associated with As at 370 ug/L is the lowest reported value from the first sampling round for CH-1D, while the ORP measurements are positive and approximately +200 mV. The DO measurement from the second round appears to be in error, although the second ORP value, 163.6 mV, is comparable to the first. ORP continued to decrease and was reported at 99.9 mV in the June 2010 sampling event along with 2.35 mg/L DO.

Groundwater from the bedrock wells reported very low Cl concentrations (minimum of 1.2 mg/L in Q5-1 and 27-1; maximum 2.8 mg/L in CH1-D) relative to Na (minimum 2 mg/L in 27-1, maximum 29 mg/L in CH1-D, excluding the result from the turbid sample from CH-1S). These results are anomalous in comparison to the Na-Cl data from the LTMMP. Chloride results from all of the SHL wells in the long-term monitoring network range from 1 U to 100 mg/L, with a mean value of approximately 20 mg/L. Corresponding Na values from the LTMMP data range from 0.59 mg/L to 83 mg/L, with a mean of 18 mg/L. The average of the Na concentrations from the new bedrock wells, ~14 mg/L, is comparable to values observed elsewhere in SHL groundwater but the Cl levels in the bedrock water are considerably lower (Fig. 9.3-1).

It is of interest to note that the chemistry of water from the deep corehole screen CH1-D appears to be similar to that from 20-1. Both of these wells report higher pH, specific conductivity, and major cation concentrations than the other wells. The high arsenic level found in CH1-D is not associated with comparably elevated iron or manganese, and so cannot be explained by the adsorption-reductive dissolution mechanism believed to be responsible for mobilizing arsenic elsewhere in SHL groundwater.

In addition, the data from the new bedrock wells show that both specific conductivity and pH generally increase with increasing depth in bedrock (Fig. 9.3-2(a), (b)). This observation is consistent with a longer transport pathway and longer residence time in bedrock. It is expected that pH will be higher in deeper bedrock groundwater, as a consequence of buffering due to reaction with bedrock minerals. Similarly, specific conductivity is higher in deeper bedrock groundwater because the solute content is higher due to increased contact with bedrock minerals. Calcium and magnesium in the new bedrock wells are within the range reported from the LTMMP but at the low-concentration end (Fig. 9.3-3). This observation may reflect different mechanisms that

control Ca and Mg solubilities in the SHL system; the bedrock water chemistry may be dominated by reactions involving Ca-, K-, and/or Na feldspars, as alkalinities are relatively low. Alkalinity values in the overburden groundwater are variable but generally higher, and reactions involving Ca-Mg carbonates are likely more significant.

9.4 Water chemistry conclusions

At the time of this report, only two complete sets of analytical data from the new bedrock wells are available. Another sampling event was conducted in June 2010 but only two wells were sampled. Perhaps the most significant observation from the results obtained thus far is the presence of arsenic at several hundred ug/L in the deep-corehole well screen. The observed arsenic at this location is not associated with elevated levels of iron or manganese, suggesting that reductive dissolution of Fe- or Mn-oxide is not the mechanism responsible for arsenic mobilization. This is the first reported occurrence of arsenic at an elevated concentration in groundwater at a location that is unequivocally upgradient from the landfill. In addition, this observation is consistent with the identification of the mineral arsenopyrite in bedrock and other, secondary, arsenic minerals that are formed by aqueous alteration of arsenopyrite (Sec. 6.0). Given the data that are presently available, it is not possible to provide more definite conclusions regarding the mechanism(s) and process(es) that may be responsible for arsenic mobilization.

10.0 DISCUSSION: UNIFIED CONCEPTUAL MODEL

This section attempts to integrate observations from the SHBI, as well as limited previous data collected in conjunction with ongoing Shepley's Hill Landfill characterization, groundwater remediation, and long-term monitoring activities directed by the Army. The emphasis is on the objectives outlined in Section 2.0, which can be grouped under these general categories:

- Establish an understanding of the fracture network which contributes groundwater to the overburden and bedrock beneath the landfill from the upgradient area on its western side;
- Develop better insight into the nature and extent of communication between bedrock and overburden groundwater, and possible "underflow" at the edge of the landfill cover;
- Characterize the chemistry of bedrock groundwater at the western upgradient edge of the landfill;
- Examine the bedrock mineralogy for evidence of arsenic-bearing phases and secondary alteration products formed by rock-water interaction.

The unified conceptual model presented in this section develops links between the geological history of the area, arsenic mobility within the system, and the occurrence of elevated arsenic in modern groundwater. The conceptual model draws upon earlier studies of the geologic and tectonic history and setting of the area (Elements 1 through 4), as well as the results of the Shepley's Hill Bedrock Investigation (Elements 5 through 9), and previous characterization associated with the landfill to the east of the site (Elements 10 and 11). While the findings of the current investigation are described in detail in the foregoing sections of this report, key results are summarized briefly in this section in support of specific elements of the conceptual model.

The unified conceptual model can be outlined as follows:

1. Arsenic occurs in all of the geologic units present in the study area. Arsenic is present in the form of sulfide minerals in the Silurian Berwick Formation, the Early Devonian Ayer Granodiorite, and the Late Devonian Chelmsford Granite at the site and in the surrounding areas (e.g., Robinson, 1981); (Koteas, et al., 2010). A key result of the SHL bedrock investigation is the positive identification of pyrite and arsenopyrite in the Chelmsford Granite. The arsenic mineral cobaltite (CoAsS) was identified in bedrock from core collected adjacent to the Grove Pond well field, approximately three-quarters of a mile east of the SHBI study area (Gannett Fleming, 2002). The lithology at the Grove Pond site has been tentatively identified as the Harvard Conglomerate (a Pennsylvanian

conglomerate containing clasts of Berwick quartzite and chloritoid-hematite phyllite; personal communication, J. Kopera, 2007).

2. Arsenic mineralization occurred very early in the geologic history of the site. The Early Devonian Ayer Granodiorite intruded into the Berwick, with possible exchange of hydrothermal fluids at the margins of the intrusion. The Late Devonian Chelmsford Granite intruded into the Berwick Formation and the Ayer Granodiorite. It is likely that hydrothermal fluids were exchanged between the Berwick and the Chelmsford, bringing arsenic and other elements from the Berwick into veins and cracks in the granite near the margins of the intrusive rocks. Various arsenic-containing minerals formed, including sulfides (e.g., arsenopyrite). Examination of core collected in previous studies of Shepley's Hill Landfill, as well as in the present investigation, shows "bleached" zones surrounding quartz- and calcite-filled veins and cracks. These zones are attributed to hydrothermal alteration. Tectonism and metamorphism continued through the Acadian orogeny (~375-325 Ma); these processes may have driven further transport and alteration of mineral phases.
3. A long period of unknown history followed, including additional episodes of mountain building (e.g., the Alleghenian orogeny during the Permian, 299-251 Ma) and erosion, ultimately bringing these rocks to shallow crustal depth. As burial depth decreased, lithostatic pressure and temperature also decreased. Approximately 350 Ma elapsed between the Early Mississippian epoch (~359 to 345 Ma) and the Quaternary Period (~2.6 Ma to the present).
4. Quaternary glaciation occurred, along with further erosion, bringing the suite of rocks approximately to the present-day configuration. Deglaciation subsequently brought about unloading, which in turn caused dilation of joints and sheeting fractures, allowing increased exposure of bedrock mineralogy to meteoric water. The last phase of Quaternary glaciation culminated approximately 21,000 years before present, with the final retreat occurring about 10,000 years ago. The glacial retreat left behind many of the prominent geomorphologic features seen today in New England, including locally thick deposits of outwash sands, such as that forming the overburden aquifer beneath Shepley's Hill Landfill. Shepley's Hill represents an erosion-resistant "knob" of relatively hard, foliated, granitic rock, surrounded by softer, metamorphic rocks that are also foliated.
5. During the post-glacial Holocene epoch (approximately the last 10,000 years), the present-day hydrologic system began to evolve. The fractured-rock aquifer exposed on Shepley's Hill receives direct recharge by well-oxygenated precipitation and snowmelt. Groundwater flows toward the east in the bedrock, away from the divide along the ridge crest, and discharges upward into the bedrock and overburden aquifers lying at lower elevation to the east. Subhorizontal sheeting fractures appear to dominate the transmission of water through the uppermost 50 feet of crystalline rock, due to their lateral continuity and relatively large apertures. Time-averaged water-level differences (measured

at a piezometer pair N5-P1/P2) several hundred feet downgradient of the study area on the hill indicate periodic upward discharge of groundwater from the fractured-rock aquifer to the sandy overburden.

6. The fracture network is locally influenced by the Nona-Shep Fault Zone (NSFZ), a significant steeply dipping fracture zone which strikes NW to SE through the center of the study area before plunging beneath the capped area. Fractures within the NSFZ are spaced less than 10 feet apart, and dip steeply to the southwest. The zone of intersection of the NSFZ and the shallowly-dipping system in the uppermost 50 feet of bedrock creates a highly-interconnected zone of fracturing which is the primary “drain” for the bedrock uplands within the study area.
7. The direct evidence accumulated in the present study indicates that Shepley’s Hill is a recharge area for the aquifer to the east, and that the pathway from the hill to the overburden aquifer beneath the landfill is primarily through the fractured rock. Observed steep hydraulic gradients (of the order of 10^{-1} ft/ft) and moderate effective hydraulic conductivity (of the order of 10^0 ft/day) for the shallow bedrock indicate a groundwater flux of the order of 10^{-1} ft/day. Water recharges the bedrock aquifer on the hill, flows toward the east, and discharges intermittently upward to the overburden beneath the impermeable landfill cap. The cap prevents direct recharge to a large area of the overburden aquifer, making the bedrock pathway from Shepley’s Hill of greater present importance to the overall water balance in the overburden.
8. Macroscopic sulfide minerals are visible in core collected in this and previous investigations, as are iron-oxide-stained vugs indicative of dissolution of sulfides. Similarly, sulfide phases and various alteration products are also clearly present at smaller scales, as seen using optical and electron microscopy. These observations are consistent with the oxidation of arsenic-bearing sulfide minerals within the bedrock by low-pH, well-oxygenated water infiltrating the interconnected bedrock fractures and formation of a variety of aqueous, low-temperature alteration phases.
9. Continued rock-water interaction subsequently mobilized arsenic from these secondary, alteration phases into groundwater. Dissolved arsenic concentrations from the new bedrock monitoring wells range from non-detected to a maximum of 400 $\mu\text{g/l}$ (in CH-1D). In addition, data from the new bedrock wells show that both specific conductivity and pH generally increase with increasing depth in bedrock. This observation is consistent with a longer transport pathway and longer residence time in deeper bedrock.
10. In the overburden, post-glacial oxidation of comminuted sulfides and other iron-bearing minerals yielded hydrous ferric oxide (HFO), which sorbs arsenic in solution. Limited soil data from SHL show generally increasing arsenic concentrations with depth in the overburden (CH2MHill, 2004c; Harding ESE,

2003) and a strong correlation with iron. The highest soil arsenic detected to date is 81 mg/kg, on a deep sample from the boring for SHP-99-29X, a few feet above the bedrock interface (also, Fe in the same sample was unusually high, reported at 2.22%; Harding ESE, 2003). This location is about 160 ft east (and downgradient) of the eastern edge of Shepley's Hill, where the bedrock surface slopes beneath the overburden. This sample came from 29-30.3 ft bgs or 213.8-212.5 ft MSL, 7-8 ft above bedrock at that location; the soil sample was from below the well screen and below the bottom of the waste.

11. The Shepley's Hill Landfill operated just east of the site since the early 20th century. The landfill was closed and an impermeable cover was constructed in mid-1990s. The highest detections of dissolved arsenic in groundwater in the area are found in the deep overburden aquifer beneath the landfill and are strongly correlated with elevated iron and low (~ 0 to -200 mV) oxidation-reduction potential (ORP). Changes in redox conditions in the deep overburden aquifer beneath the landfill may result in reductive dissolution of hydrous ferric oxide (HFO) coatings on mineral grains in the overburden and mobilization of arsenic to groundwater. This redox shift may be driven by organic carbon transported downward from landfill waste prior to capping. In addition, wetlands and associated peat deposits known to have been present historically in the vicinity of the landfill may also provide organic carbon to the groundwater system. The hydraulic conditions necessary to move shallow groundwater to depth were eliminated by the cap. However, the hydraulic regime following capping continues to evolve, and the pre-cap hydraulic regime is unknown.

11.0 RECOMMENDATIONS

This section presents recommendations for additional investigation of the bedrock aquifer on and adjacent to Shepley's Hill, should the opportunity arise, as well as recommendations for related data gathering. This list is offered primarily as suggestions for future research topics; however, some of the recommendations are more compelling than others, and have been broken out as "highest priority recommendations". Rationales for these additional tasks are provided below. It is the Shepley's Hill Bedrock Investigation project team's assessment that the highest priority recommendations offered below are most critical to better understanding the linkages between the findings of this study and ongoing work related to remediation of the adjacent landfill-impacted system.

The recommendations are grouped roughly in categories, as follows:

Additional characterization of the fracture network:

- Testing should be conducted to verify and quantify the inferred hydraulic connection between the sheeting fractures screened in CH-1S and interpreted sub-crop of these fractures in the generally flat triangular area bounded by 20-1, 27-1 and Q4-1. A tracer test may be useful in this regard;
- In similar fashion, the apparent connection between the sheeting fracture penetrated at 37 ft bgs in Q4-1 and similar fractures intersected by the CH-1D well screen should be further assessed;
- The hydraulic connection, if any, between 20-1 and 20-2 and down-gradient wells Q4-1 and CH-1D/S should be assessed. A tracer test may be useful in this regard;
- Additional shallow and deep well control is needed in more distal areas cross-gradient to the strike of the NSFZ. Given the apparent overall width of the feature (i.e., on the order of 200 feet or more), it may be necessary to go beyond the boundaries of the current study area. This information will be useful in verifying and quantifying the apparent increase in fracture density and hydraulic conductivity proximal to the NSFZ;
- A key data gap relative to the GFM and associated CSM for the site concerns the potential importance of N-S trending fractures in relation to ground water flow. While the current investigation did encounter significant fractures of this orientation, the overall CSM suggests that major N-S striking features may lie to the east of the study area, beneath the landfill cap. In order to more fully evaluate the potential for N-S striking sub-vertical features, an angled drilling program would be needed in order to penetrate such features from the site area. Alternatively, additional vertical drilling could be considered through the capped landfill area;

- Additional deep holes in up-gradient upland areas would be useful toward establishing whether the apparent lack of fracturing in these areas continues at depth, and whether location-with- respect-to-steep-fractures is a determining factor regarding the degree of fracturing in a given borehole. For example, a vertical core-hole could be advanced just south of 20-2, to achieve a total depth similar to that achieved in CH-1D (~ 100 ft amsl). A second core-hole to a similar total depth could be advanced in the valley area between 20-2 and 27-1;
- The effective depth of the NSFZ has not yet been established. Additional deep coring should be considered in an attempt to target the core of the NSFZ at incrementally greater depths. For example, a new borehole could be advanced in the area between CH-1 and CAP-2 A/B to total depth of approximately 240 ft bgs; (i.e., final elevation approximates mean sea level).

Additional characterization of the geochemistry and mineralogy:

- Further characterization of the mineralogy of alteration products of arsenopyrite observed in the petrographic study would improve understanding of the processes that link arsenic-bearing sulfide minerals in the crystalline rock and the appearance of elevated dissolved arsenic in groundwater;
- Additional studies to characterize isotopic composition of groundwater (δD , $\delta^{18}O$) should be conducted to quantify mixing of different groundwater populations;
- Consideration should be given to additional studies to age-date different carbon sources to SHL groundwater (e.g. ^{14}C) in the various carbon pools in the SHL system.

Additional characterization in conjunction with overburden drilling:

- Bedrock core should be recovered at the base of overburden borings advanced to refusal whenever possible in order to identify the rock type, and to support better understanding of the relationships between bedrock lithology, overlying soil composition, and groundwater chemistry;
- Soil samples collected from overburden borings should be characterized to identify relationships of the soil mineralogy and geochemistry to those of the underlying bedrock, as well as the chemistry of co-located porewater.

Highest priority recommendations:

- Tracer tests (e.g., utilizing bromine, fluorescent dye, etc.) would verify interconnectivity and travel times from key points in the system, including standing water in bedrock pockets high on the ridge, wells and borings on and

adjacent to the hill, and monitoring points downgradient within the landfill footprint. Tracer tests are strongly recommended in order to quantify the relationship between monitoring points on the hill and farther downgradient, within the landfill footprint.

- There has been no evaluation to date of hydraulic conductivity in either CH-1S or CH-1D due to the logistical difficulties created by the narrow diameter well casings. A testing approach should be devised, using specialized equipment if necessary, in order to determine the hydraulic conductivity of these important zones.
- Newly installed monitoring wells should be sampled and the groundwater analyzed to test for repeatability and seasonal variability. The EPA OEME has committed to re-sampling the new bedrock wells for at least one and possibly two rounds. Additional sampling should be considered in order to assess seasonal and longer-term variability.
- A synoptic round of water levels on all SHL monitoring points, as well as all available control points to the south (e.g., AOC32/43A) should be executed, in order to define better the catchment, with special attention to locating the groundwater divide near the south end of the landfill. This exercise has not been carried out to date. However, at relatively low cost, this effort would support a regional assessment of groundwater flow in the SHL system.
- The manner in which recharge is applied in the numerical groundwater flow model in the vicinity of Shepley's Hill should be discussed, and revised if appropriate. The current investigation suggests that the supplemental recharge applied along the western edge of the landfill, as implemented in earlier versions of the model, is unrealistic, and that the total water input west of the landfill may have been too large. Again, at relatively low cost, re-running the groundwater model with different input parameters may shed a different light on the overall water balance beneath and downgradient from the landfill.

12.0 REFERENCES

AMEC, 2008, *Draft Supplemental Groundwater and Landfill Cap Assessment for Long-Term Monitoring and Maintenance at Shepley's Hill Landfill*, dated December 2008.

Ayotte, J. D., M. D. Nielsen, G. R. Robinson, R. B. Moore, 1999, *Relation of arsenic, iron, and manganese in ground water to aquifer type, bedrock lithogeochemistry, and land use in the New England coastal basins*, Water Resources Investigations Report, **99-4162**, U. S. Geological Survey, Pembroke, NH.

Bluteau, M.-C. and Demopoulos, G. P., 2007, The incongruent dissolution of scorodite – Solubility, kinetics and mechanism. *Hydrometallurgy* 87:163-177.

CH2MHill, 2006, Start-up extraction test – Shepley's Hill groundwater extraction, treatment, and discharge system, technical memorandum, dated February 28, 2006.

CH2MHill, 2004a, *Remedial Design and Remedial Action Work Plan, Draft Final Sixty Percent (60%) / Draft One-Hundred Percent (100%) Submittal, Groundwater Extraction, Treatment, and Discharge Contingency Remedy*, dated September 2004.

CH2MHill, 2004b, *Shepley's Hill groundwater extraction, treatment, and discharge system, wellfield final design – field data and recommendations*, technical memorandum, dated October 27, 2004.

CH2MHill, 2004c, *Shepley's Hill Landfill Groundwater Extraction, Treatment, and Discharge System: Off Base Direct Push Sampling Work – Well Couplet Recommendations*; technical memorandum to BCT; dated December 17, 2004

CH2MHill, 2007. 2006 Annual Report, Shepley's Hill Landfill, Long Term Monitoring & Maintenance, Devens, Massachusetts. November 2007.

ECC, 2008. 2007 Annual Report, Shepley's Hill Landfill, Devens, Massachusetts. Contract Number W91ZLK-05-D-0009, Task Order 0006, May 2008.

ECC, 2009. 2008 Annual Report, Shepley's Hill Landfill, Devens, Massachusetts. Contract Number W91ZLK-05-D-0009, Task Order 0006, September 2009.

ECC, 2010. 2009 Annual Report, Shepley's Hill Landfill, Devens, Massachusetts. Contract Number W91ZLK-05-D-0009, Task Order 0006, April 2010.

Freeze, R. A., and J. A. Cherry, *Groundwater*, Prentice-Hall, Englewood Cliffs, NH, 1979.

Gannett Fleming, Results from scoping analysis of SHL bedrock. Memorandum to Ginny Lombardo, US EPA Region 1, June 9, 2009.

Gannett Fleming, 2007, Sampling and Analysis Plan, Focused Bedrock Investigation, Former Fort Devens (Devens RFTA), Ayer, Massachusetts, August 2007.

Gannett Fleming, 2002, Grove Pond Arsenic Investigation, technical report prepared for US EPA, March 2002.

Harding ESE, 2003, *Revised Draft Shepley's Hill Landfill Supplemental Groundwater Investigation, Devens Reserve Forces Training Area, Devens, Massachusetts*. US Army Corps of Engineers, New England District, Concord, MA, May 2003

Jacob, C. E., 1940, On the flow of water in an elastic artesian aquifer, *Transactions, American Geophysical Union*, **14**, 446 – 460.

Kopera, J. P., Preliminary Bedrock Geologic Map of the Area Surrounding Shepley's Hill, Towns of Ayer and Devens, Massachusetts. *OMSG Open File Report 06-02*, last modified 10/30/2008.

Koteas, G. C., Keskula, A. J., Stein, C. L., McTigue, D. F., Kopera, J. P., and Brandon, W. C., 2010, Evidence for arsenic mineralization in granitic basement rocks, Ayer Granodiorite, northeastern Massachusetts, Geological Society of America Northeastern Section Annual Meeting, Baltimore, MD, March 16, 2010; http://gsa.confex.com/gsa/2010NE/finalprogram/abstract_169998.htm

Lipfert, G., Reeve, A. S., Sidle, W. C., and Marvinney, R., 2006. Geochemical patterns of arsenic-enriched ground water in fractured, crystalline bedrock, Northport, Maine, USA. *Applied Geochem.* 21(3):528-545.

Luxton, T., 2008. Arsenic Distribution in Exposed Bedrock Outcrops West of Shepley's Hill Landfill near the Red Cove Study Area of Ft. Devens Superfund Site. Memorandum communicated to GF 4/30/2008.

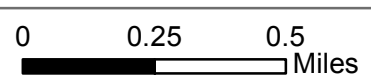
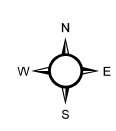
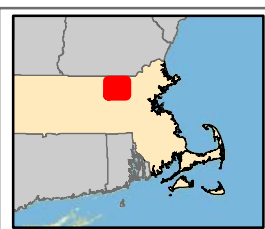
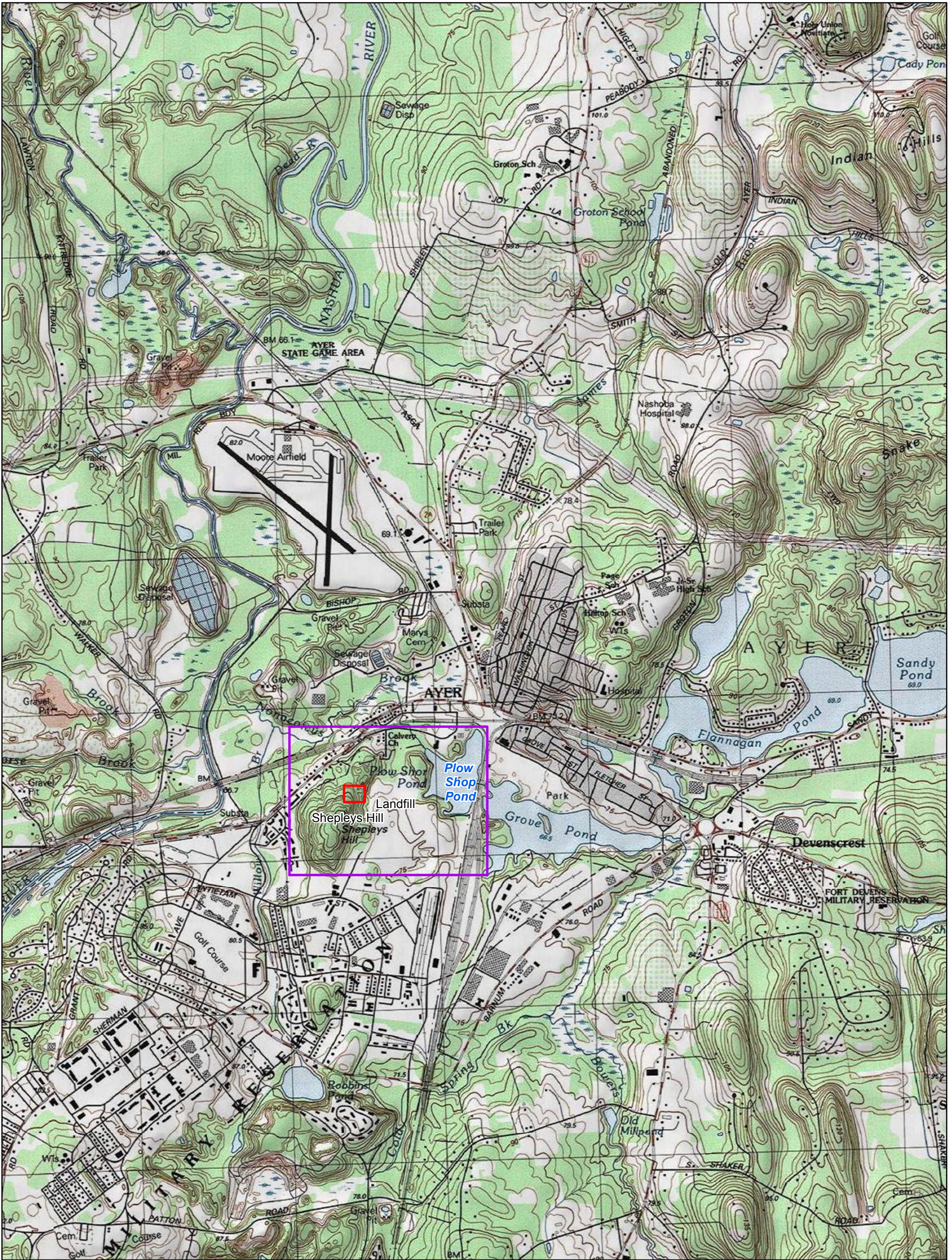
Magalhaes, M. C. F., 2002, Arsenic. An environmental problem limited by solubility. *Pure Appl. Chem.* **74**(10):1843-1850.

Robinson, G.R., Jr., 1981, Bedrock geology of the Nashua River area, Massachusetts – New Hampshire, *USGS Open-File Report 81-593*, 171 p.

Ryan, P. C., Kim, J., Chow, D., Sullivan, C., and Bright, K., 2009. Connection between Ordovician mantle metasomatism and arsenic in Vermont groundwater. GSA Abstracts with Programs 41(3):8, NE GSA Section, 44th Annual Meeting, 22-24 March 2009.

Weeks, E. P., 1979, Barometric pressure fluctuations in wells tapping deep unconfined aquifers, *Water Resources Research*, **15**, 1167 – 1176.

FIGURES

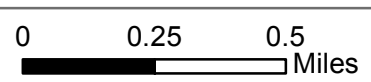
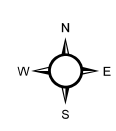
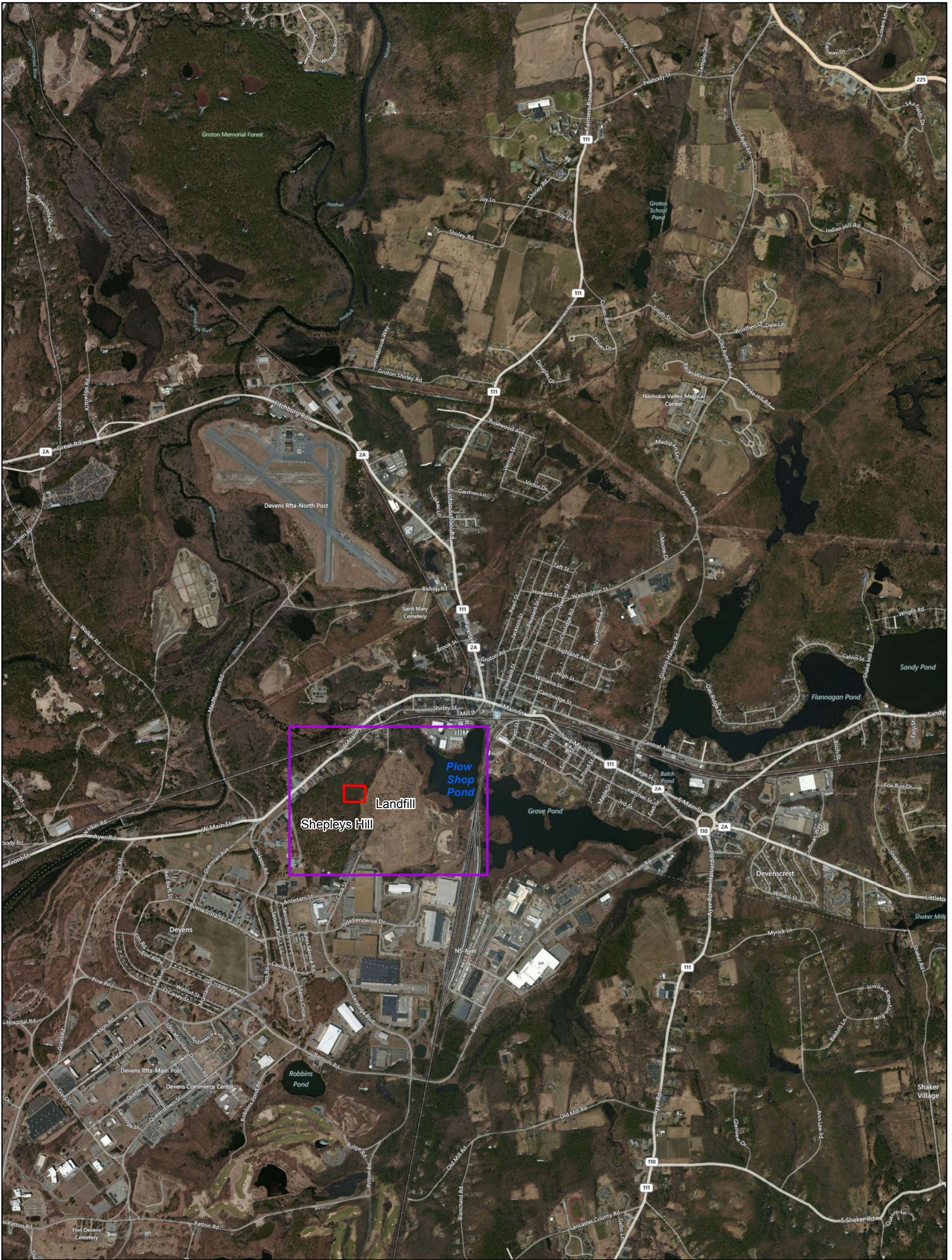


- Shepley's Hill Area
- Site

Figure 1.0-1(a)
 Sub-regional scale topographic map of Shepley's Hill and environs

Shepley's Hill
 Bedrock Investigation 2009
 Devens, MA





- Shepley's Hill Area
- Site

Figure 1.0-1(b)
Sub-regional aerial photograph
of Shepley's Hill and environs
 Shepley's Hill
 Bedrock Investigation 2009
 Devens, MA

Photo Source: Bing Maps
 Map Tracker ID=6725
 Created by the US EPA Region 1
 GIS Center on 2/08/2011



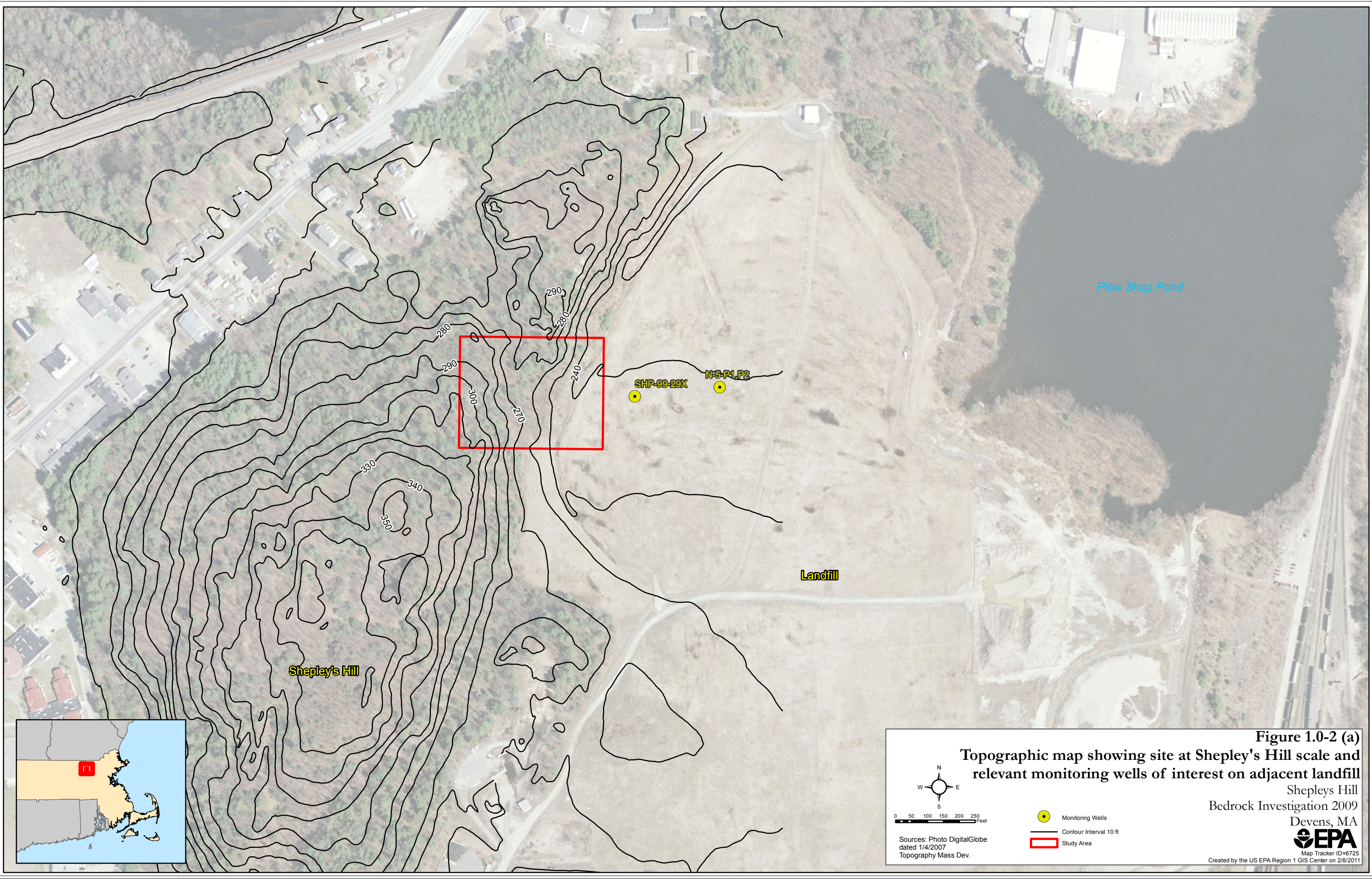
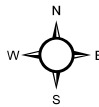


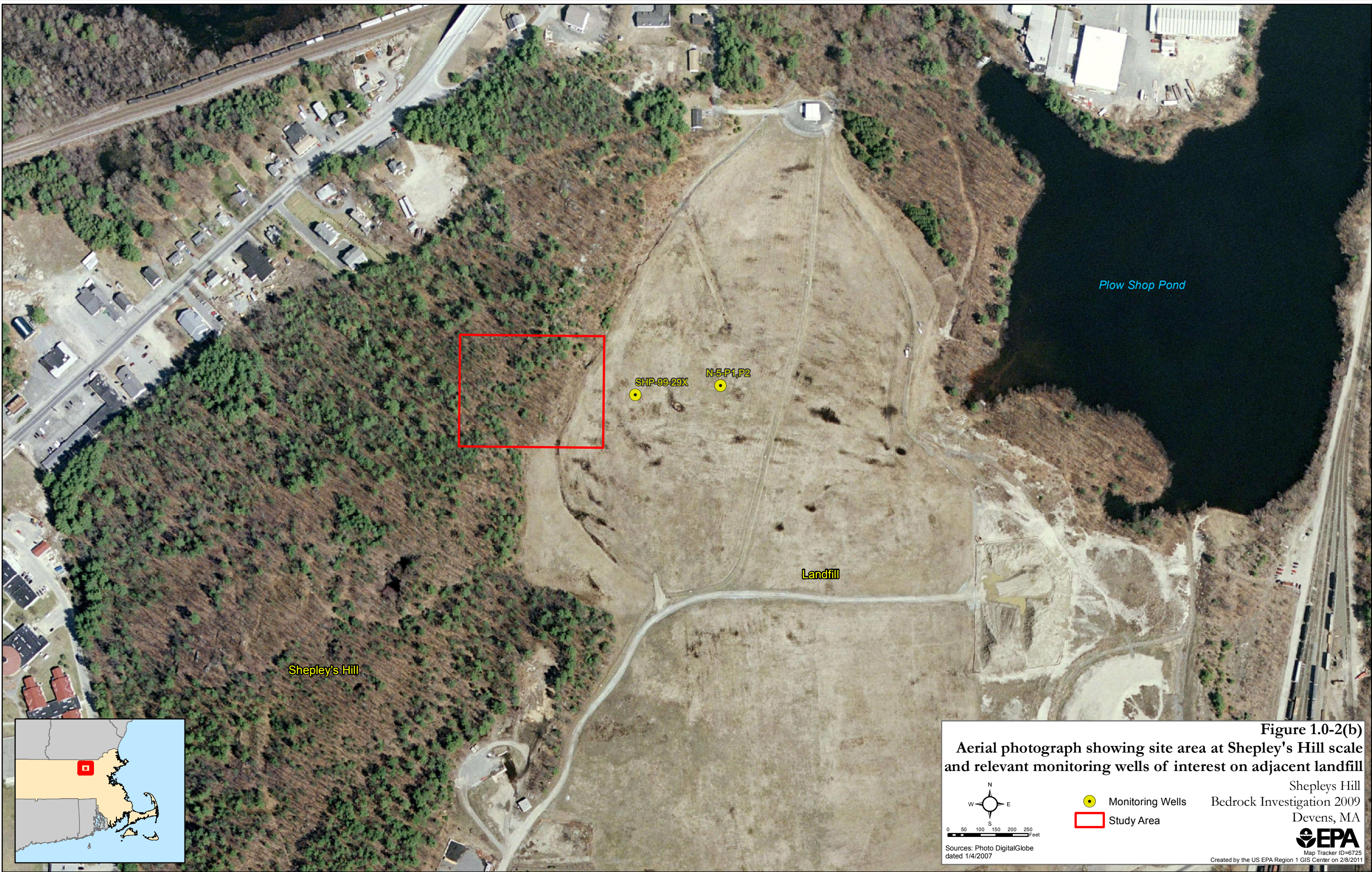
Figure 1.0-2 (a)
Topographic map showing site at Shepley's Hill scale and relevant monitoring wells of interest on adjacent landfill

Shepley's Hill
 Bedrock Investigation 2009
 Devens, MA



Map Tracker ID=6725
 Created by the US EPA Region 1 GIS Center on 2/8/2011


 0 50 100 150 200 250 Feet
 Sources: Photo DigitalGlobe dated 1/4/2007 Topography Mass Dev.
 Monitoring Wells
 Contour Interval 10 ft
 Study Area



Shepley's Hill

Landfill

Plow Shop Pond

SHP-99-29X

N-5-P1,P2



Figure 1.0-2(b)
Aerial photograph showing site area at Shepley's Hill scale and relevant monitoring wells of interest on adjacent landfill

Shepley's Hill
Bedrock Investigation 2009
Devens, MA

 Monitoring Wells
 Study Area


0 50 100 150 200 250 Feet

Sources: Photo DigitalGlobe dated 1/4/2007


Map Tracker ID=6725
Created by the US EPA Region 1 GIS Center on 2/8/2011

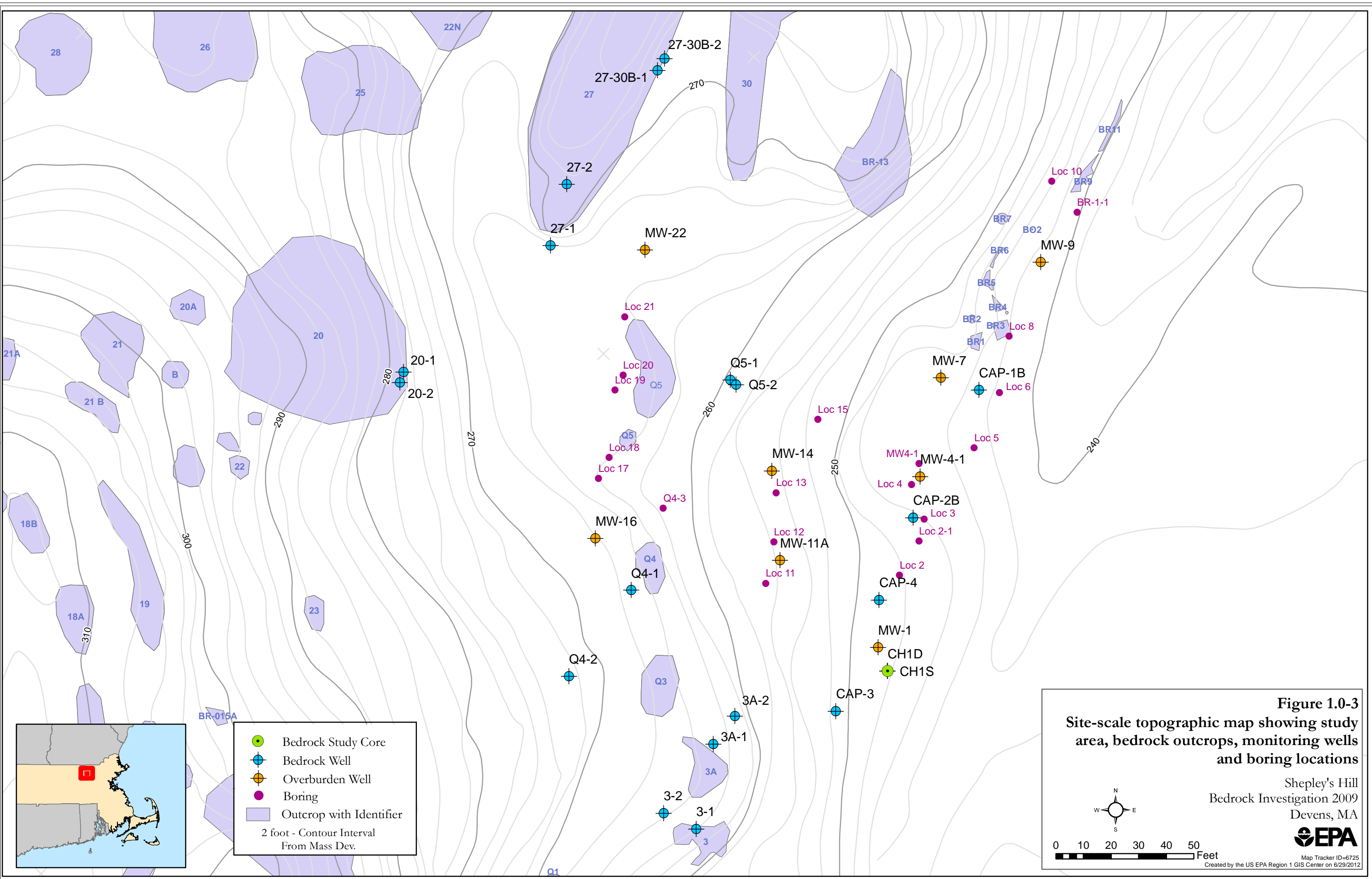
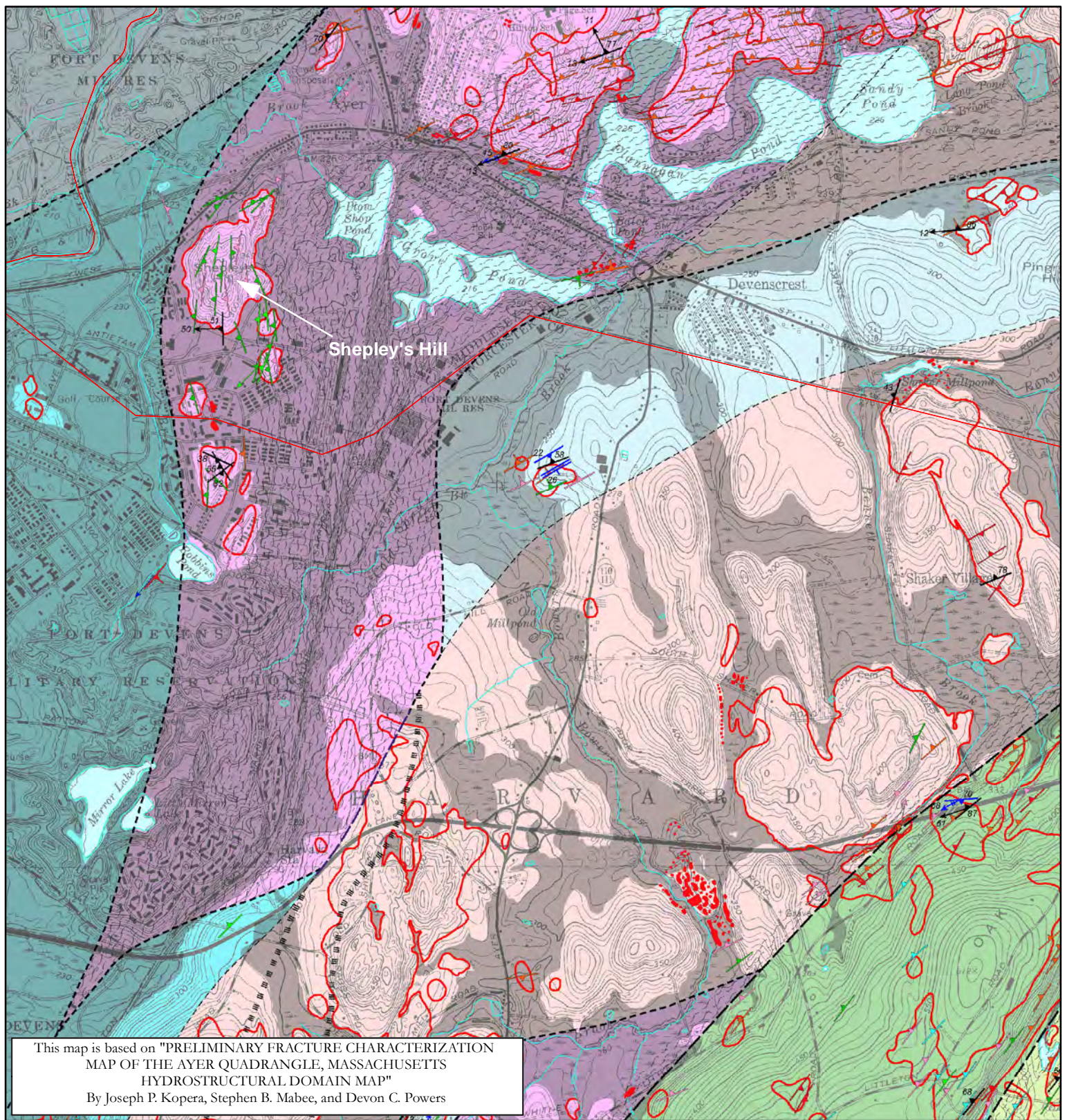


Figure 1.0-3
Site-scale topographic map showing study area, bedrock outcrops, monitoring wells and boring locations

Shepley's Hill
 Bedrock Investigation 2009
 Devens, MA

EPA
 Map Tracker ID=6725
 Created by the US EPA Region 1 GIS Center on 6/29/2012



EXPLANATION OF MAP SYMBOLS

- | | | | |
|-----------------------|---|--|---|
| — | Contact, approximately located (within approximately 50 meters) | | Strike and dip of dominant schistosity. Generally parallel to bedding in stratified rocks of Merrimack Belt |
| - - - - | Contact, location inferred | | Strike and dip of local secondary schistosity and/or cleavage (S2) |
| ***** | Gradational contact in Ayer granites | LINEAR FEATURES | |
| - - - - (schistosity) | Denotes occurrence of actinolite in Berwick formation (after Robison et al., 1978) | | Bearing and plunge of mineral lineation |
| | Bedrock outcrop | | Bearing and plunge of intersection of dominant and local secondary schistosity (S2) |
| | Area where bedrock is shallow (<3 meters below surface) and/or outcrop is extensive | MINOR FOLDS | |
| - - - - | Fault, approximately located (within approximately 50 meters) | | Bearing and plunge of minor fold axis. Such folds are locally second generation (F2) in stratified rocks of Merrimack Belt |
| - - - - - | Fault, inferred | | Strike and dip of axial surface of minor fold. Generally parallel to local secondary schistosity (S2) in stratified rocks of Merrimack Belt |
| | Zone of sheared rocks
Density of pattern reflects relative intensity of shearing | PERMISSIBLE SURFACE MATERIALS | |
| | Permeable Surface Materials - Overlay shading shows areas where permeable and conductive overburden is observed at the surface and may lie above the bedrock. | Moderately to steeply dipping well-layered quartzites, phyllites, and schists of the Merrimack Group | |
| | Ayer and Chelmsford granites and foliated granitoid gneisses of the Devens gneiss complex | | |
| | Gneisses and schists of the Nashoba Formation | | |

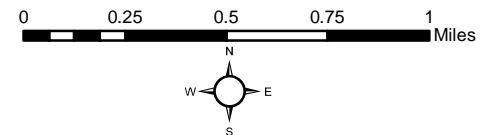


Figure 4.2-1
Sub-regional scale bedrock geologic map of Shepley's Hill and environs

Shepley's Hill
Bedrock Investigation 2009
Devens, MA





— Sheeting Fractures

Figure 5.1.1
Photograph of outcrop showing
exposed joint surface on sheeting
fractures, looking NNE

Shepley's Hill
Bedrock Investigation 2009
Devens, MA



Map Tracker ID=6725
Created by the US EPA Region 1 GIS Center on 4/21/2011

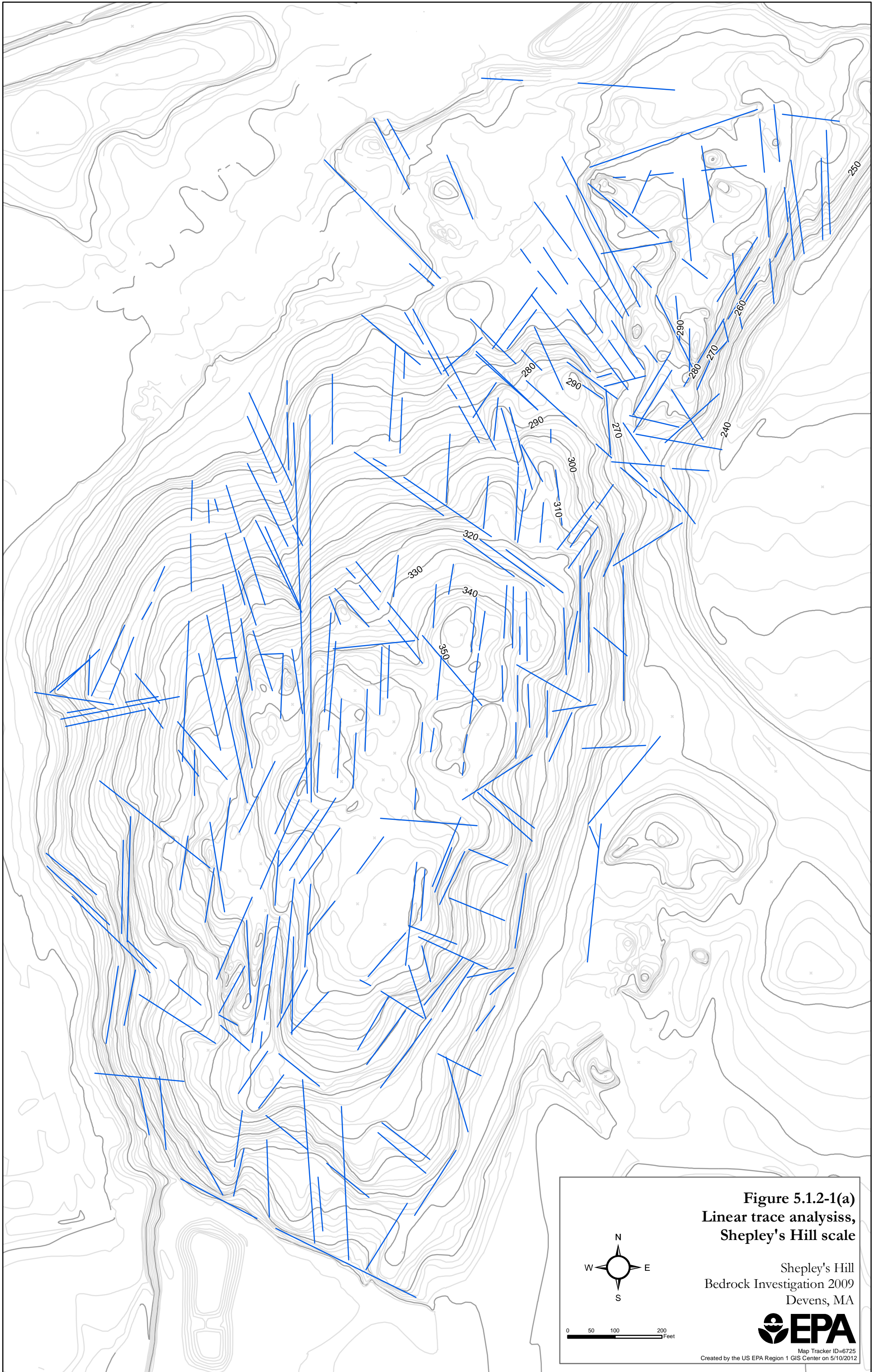
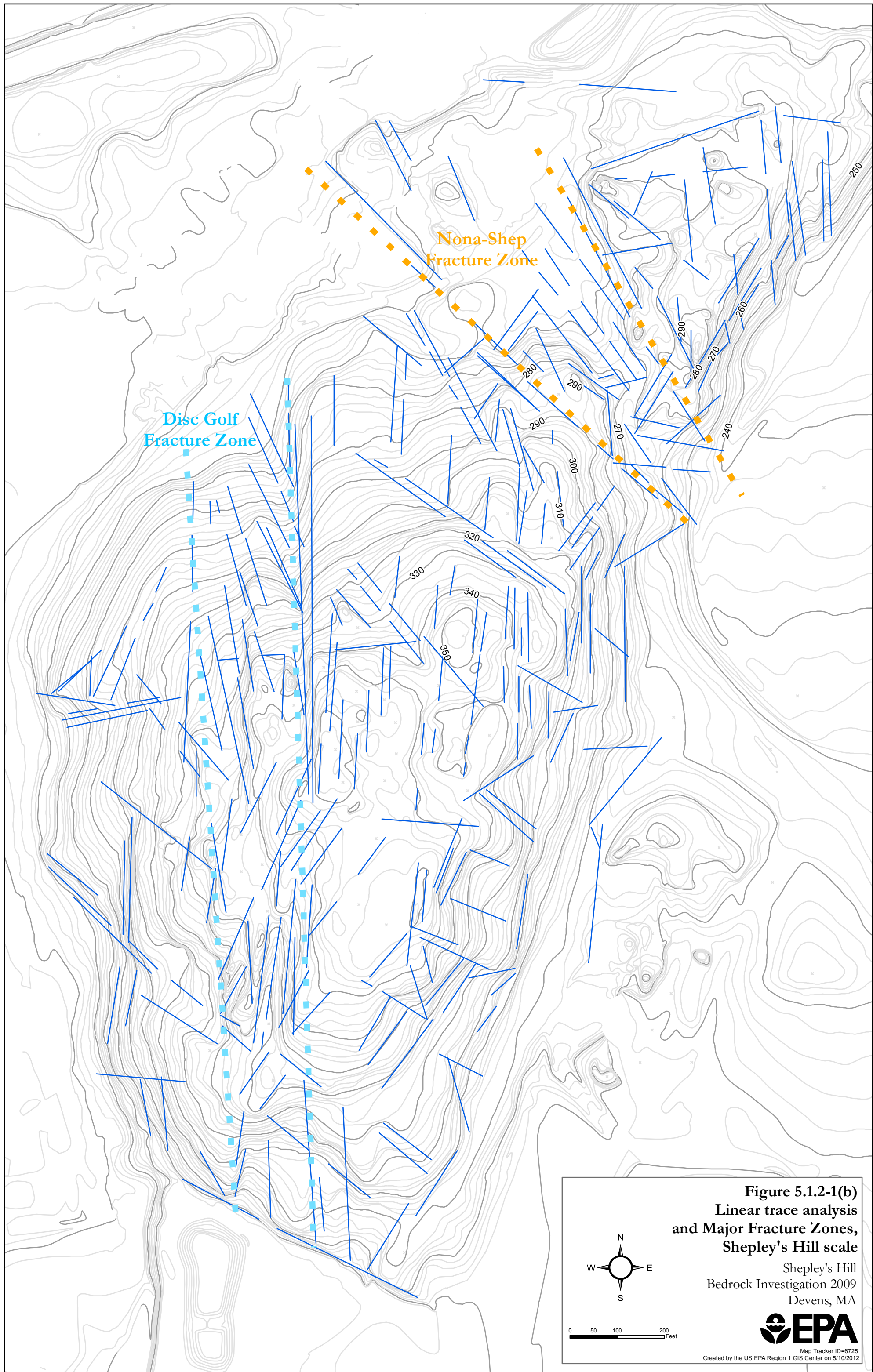


Figure 5.1.2-1(a)
Linear trace analysis,
Shepley's Hill scale

Shepley's Hill
Bedrock Investigation 2009
Devens, MA



Map Tracker ID=6725
Created by the US EPA Region 1 GIS Center on 5/10/2012

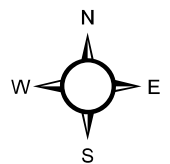


Nona-Shep
Fracture Zone

Disc Golf
Fracture Zone

Figure 5.1.2-1(b)
Linear trace analysis
and Major Fracture Zones,
Shepley's Hill scale

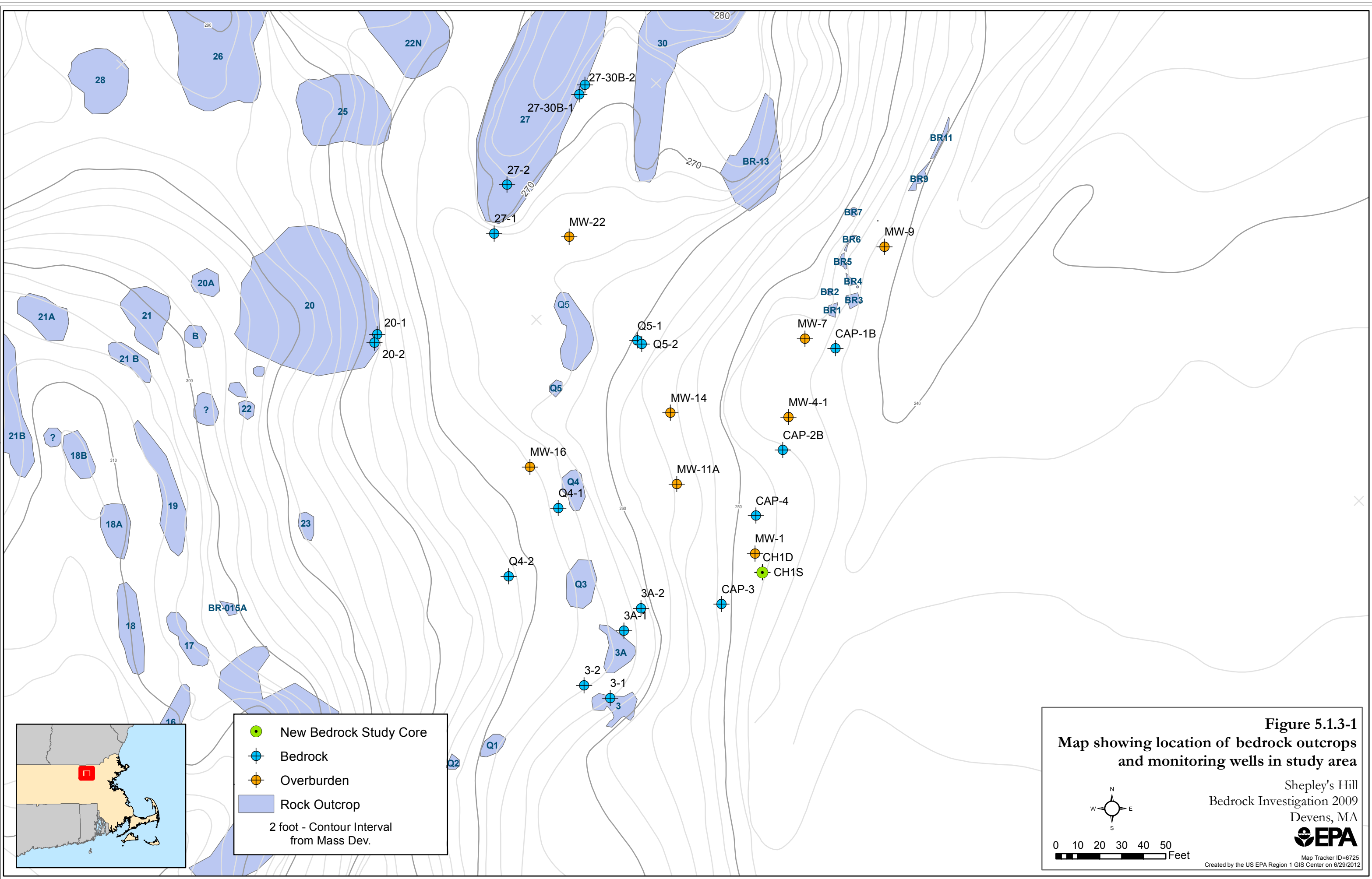
Shepley's Hill
Bedrock Investigation 2009
Devens, MA



0 50 100 200
Feet



Map Tracker ID=6725
Created by the US EPA Region 1 GIS Center on 5/10/2012



- New Bedrock Study Core
- ⊕ Bedrock
- ⊕ Overburden
- Rock Outcrop

2 foot - Contour Interval
from Mass Dev.

Figure 5.1.3-1
**Map showing location of bedrock outcrops
 and monitoring wells in study area**

Shepley's Hill
 Bedrock Investigation 2009
 Devens, MA

0 10 20 30 40 50 Feet

EPA
 Map Tracker ID=6725
 Created by the US EPA Region 1 GIS Center on 6/29/2012

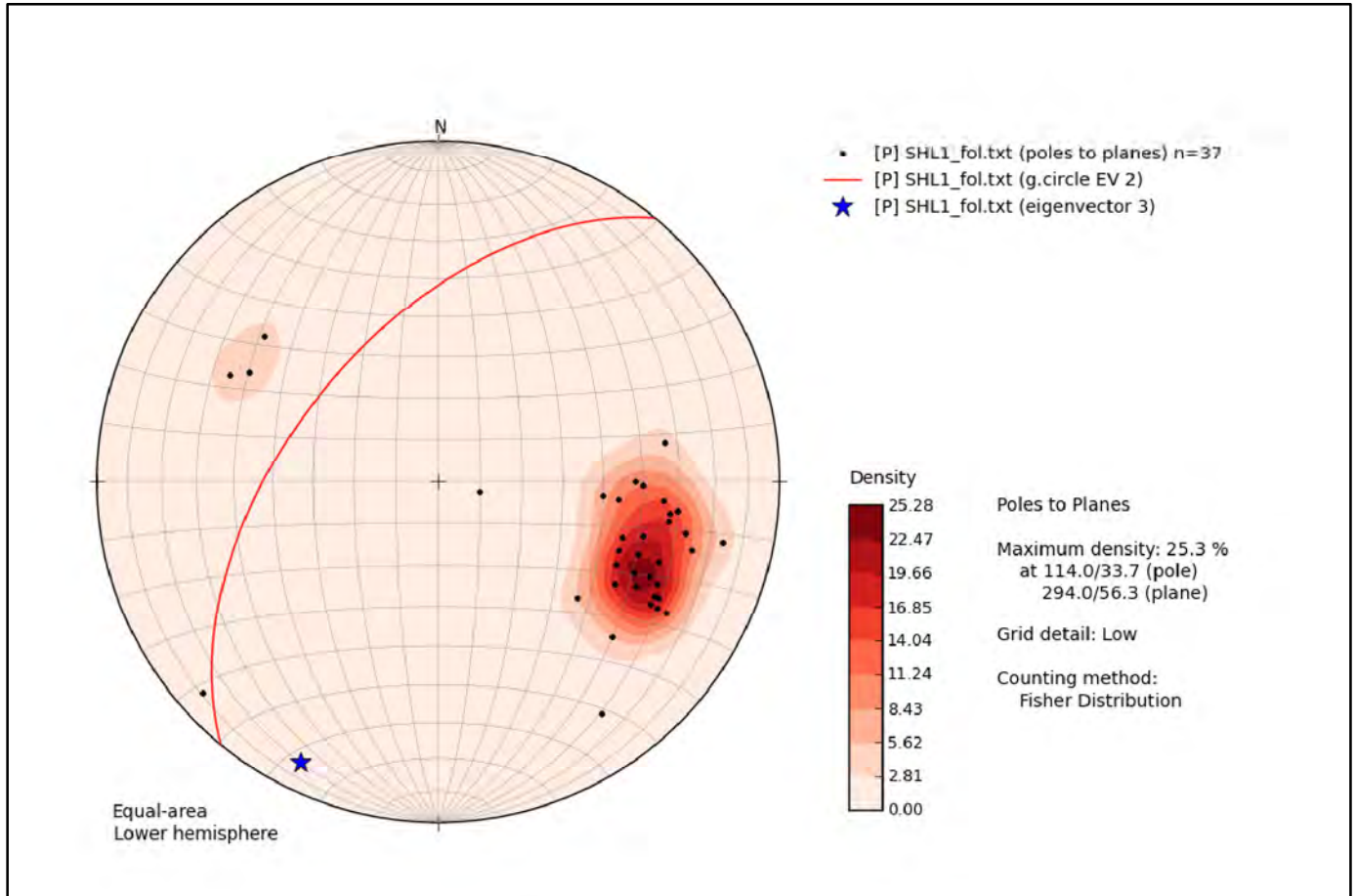


Figure 5.1.3-2
Lower-hemisphere stereonet of
site-scale foliation orientations

Shepley's Hill
Bedrock Investigation 2009
Devens, MA



Map Tracker ID=6725
Created by the US EPA Region 1 GIS Center on 4/21/2011

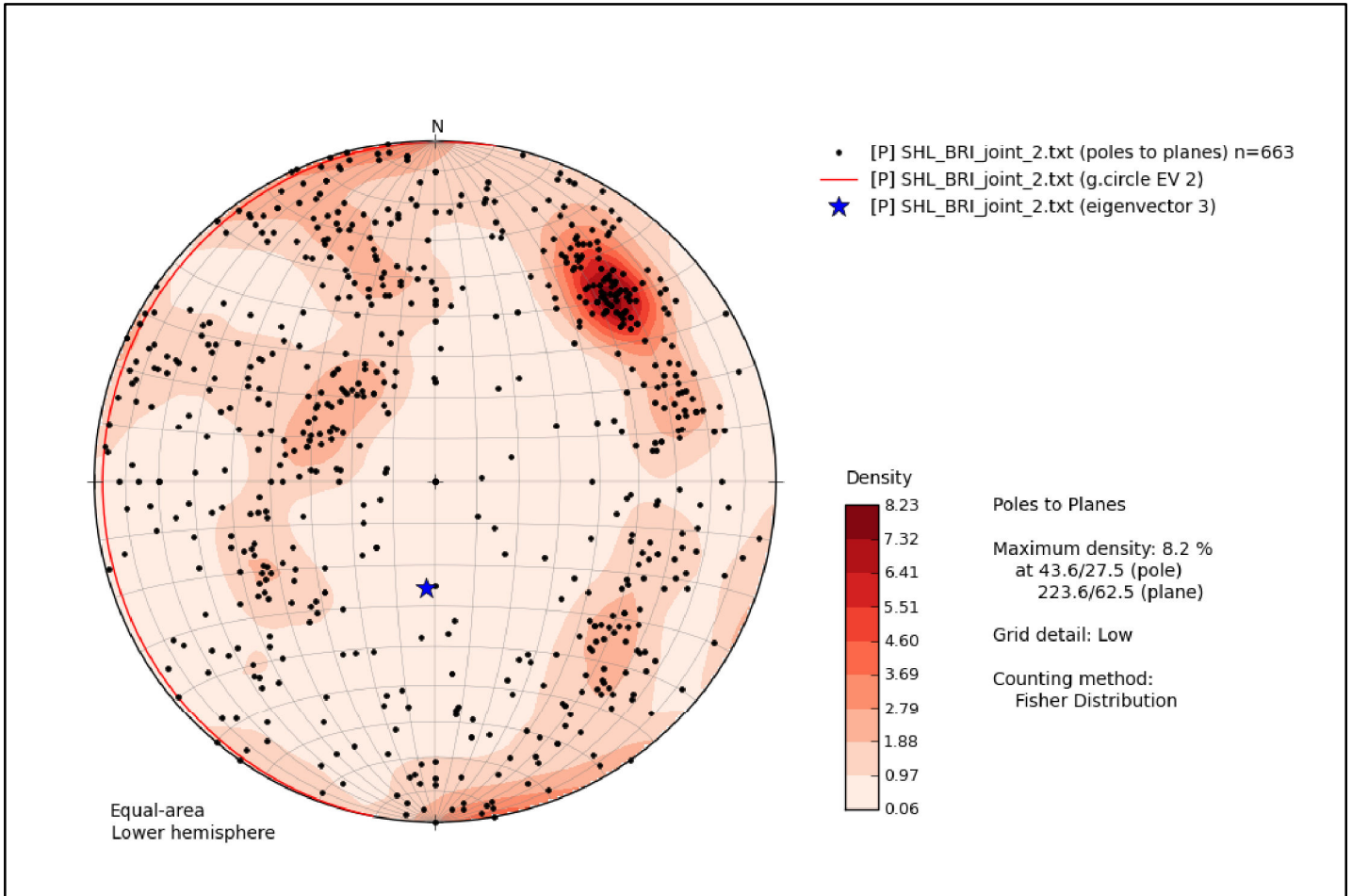


Figure 5.1.3-3
Lower-hemisphere stereonet of
site-scale fracture and joint orientations

Shepley's Hill
 Bedrock Investigation 2009
 Devens, MA



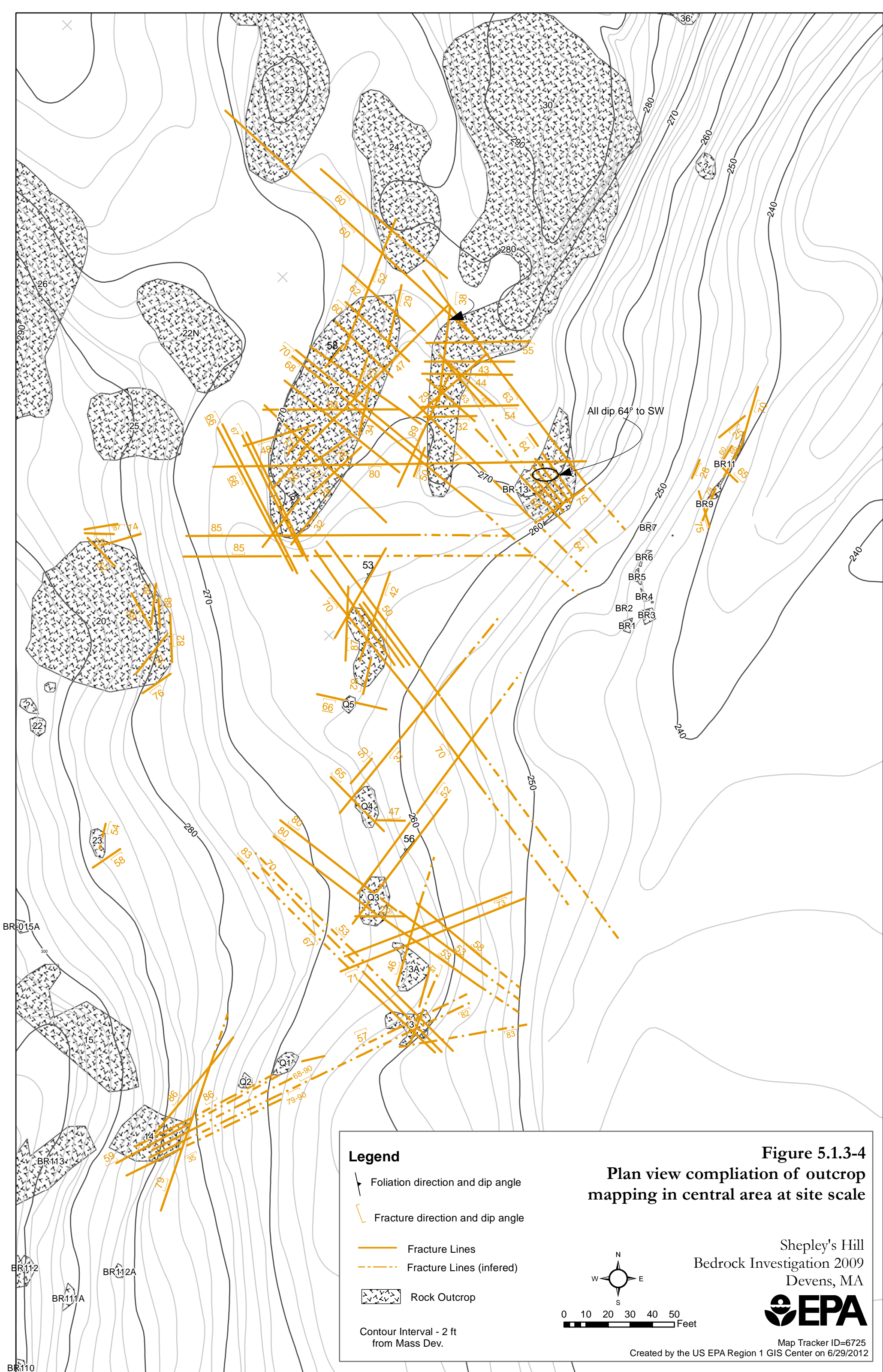


Figure 5.1.3-4
Plan view compilation of outcrop
mapping in central area at site scale

Shepley's Hill
 Bedrock Investigation 2009
 Devens, MA



Map Tracker ID=6725
 Created by the US EPA Region 1 GIS Center on 6/29/2012

Legend

- Foliation direction and dip angle
- Fracture direction and dip angle
- Fracture Lines
- Fracture Lines (inferred)
- Rock Outcrop

Contour Interval - 2 ft
 from Mass Dev.

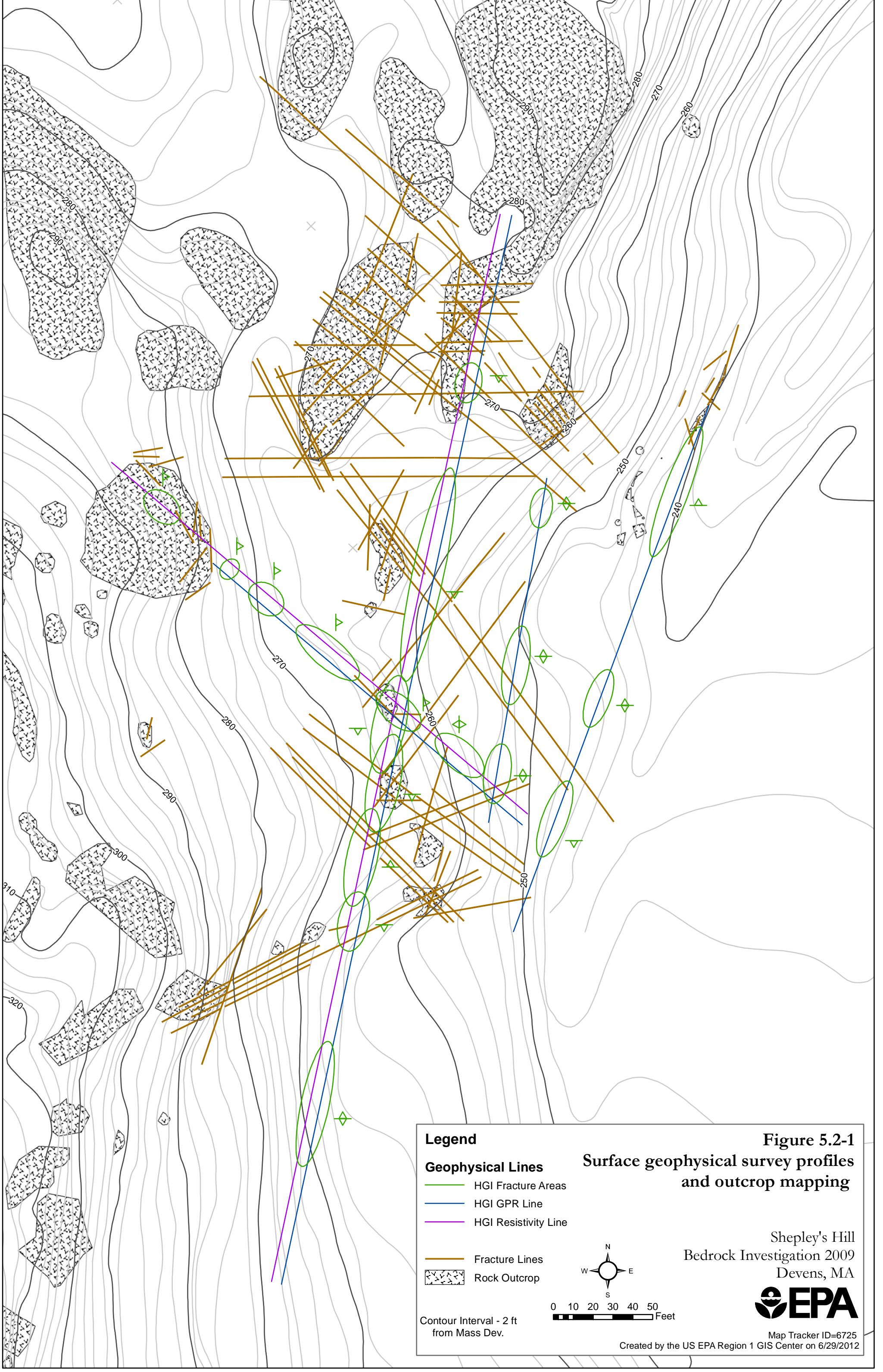


Figure 5.2-1
Surface geophysical survey profiles and outcrop mapping

Shepley's Hill
 Bedrock Investigation 2009
 Devens, MA

Legend

Geophysical Lines

- HGI Fracture Areas
- HGI GPR Line
- HGI Resistivity Line

- Fracture Lines
- Rock Outcrop

Contour Interval - 2 ft
 from Mass Dev.

0 10 20 30 40 50
 Feet

Map Tracker ID=6725
 Created by the US EPA Region 1 GIS Center on 6/29/2012

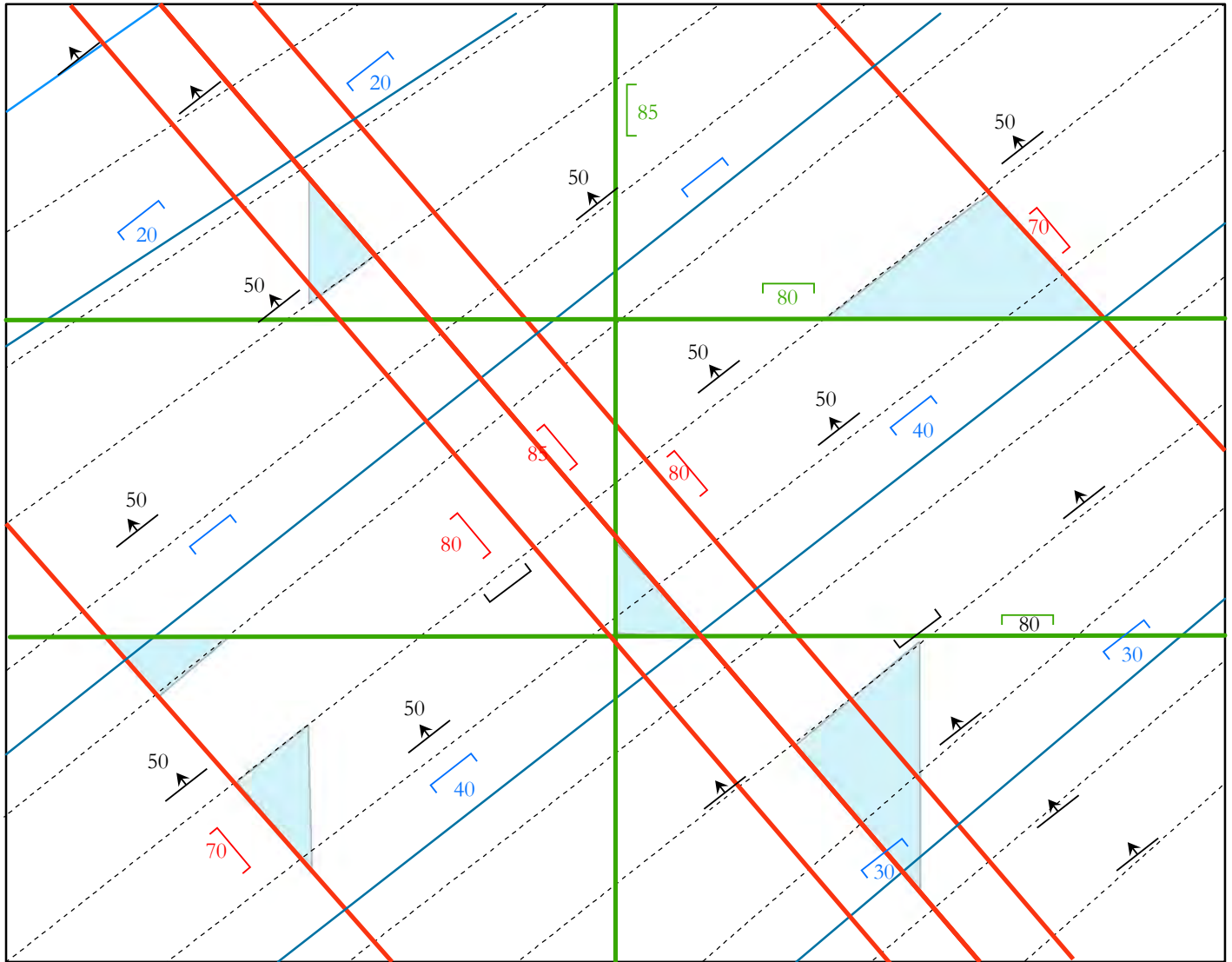


Figure 5.3.1-1

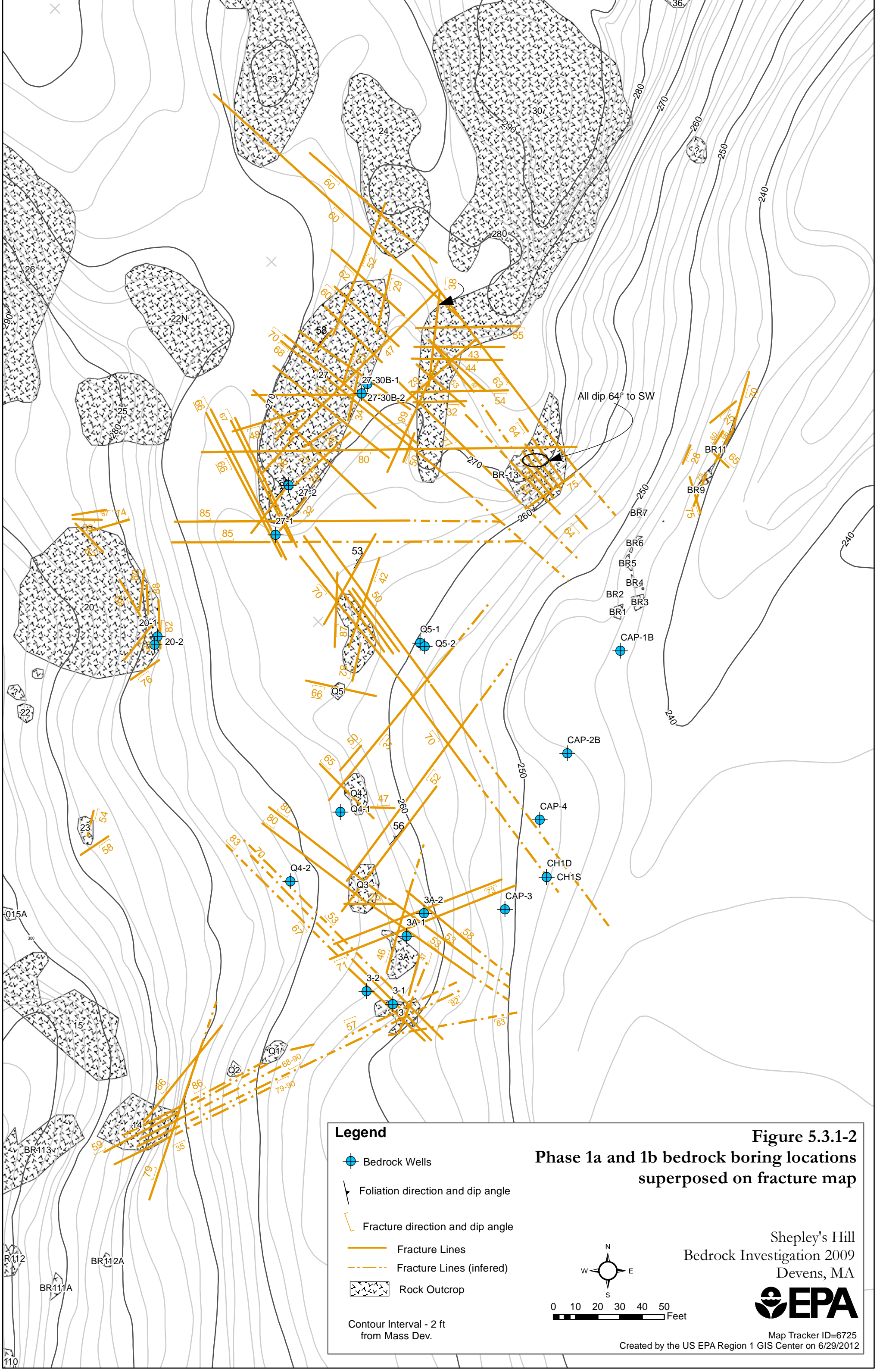
Schematic diagram showing general fracture relationships



- Fracuture N-S or E-W Strike
- Fracuture/joint NW-SE Strike
- Sheeting Fracture NE-SW Strike, dips at shallow to moderate angles to SE
- 50 Foliation; Strikes NE-SW, Dips 50° NW
- 70 Fracture orientaion, dip in direction of tick marks
- Topographic pinnacles and depressions

Shepley's Hill
Bedrock Investigation 2009
Devens, MA





Legend

- Bedrock Wells
- Foliation direction and dip angle
- Fracture direction and dip angle
- Fracture Lines
- Fracture Lines (inferred)
- Rock Outcrop

Contour Interval - 2 ft
from Mass Dev.

Figure 5.3.1-2
Phase 1a and 1b bedrock boring locations
superposed on fracture map

N
W — O — E
S

0 10 20 30 40 50
Feet

Shepley's Hill
 Bedrock Investigation 2009
 Devens, MA



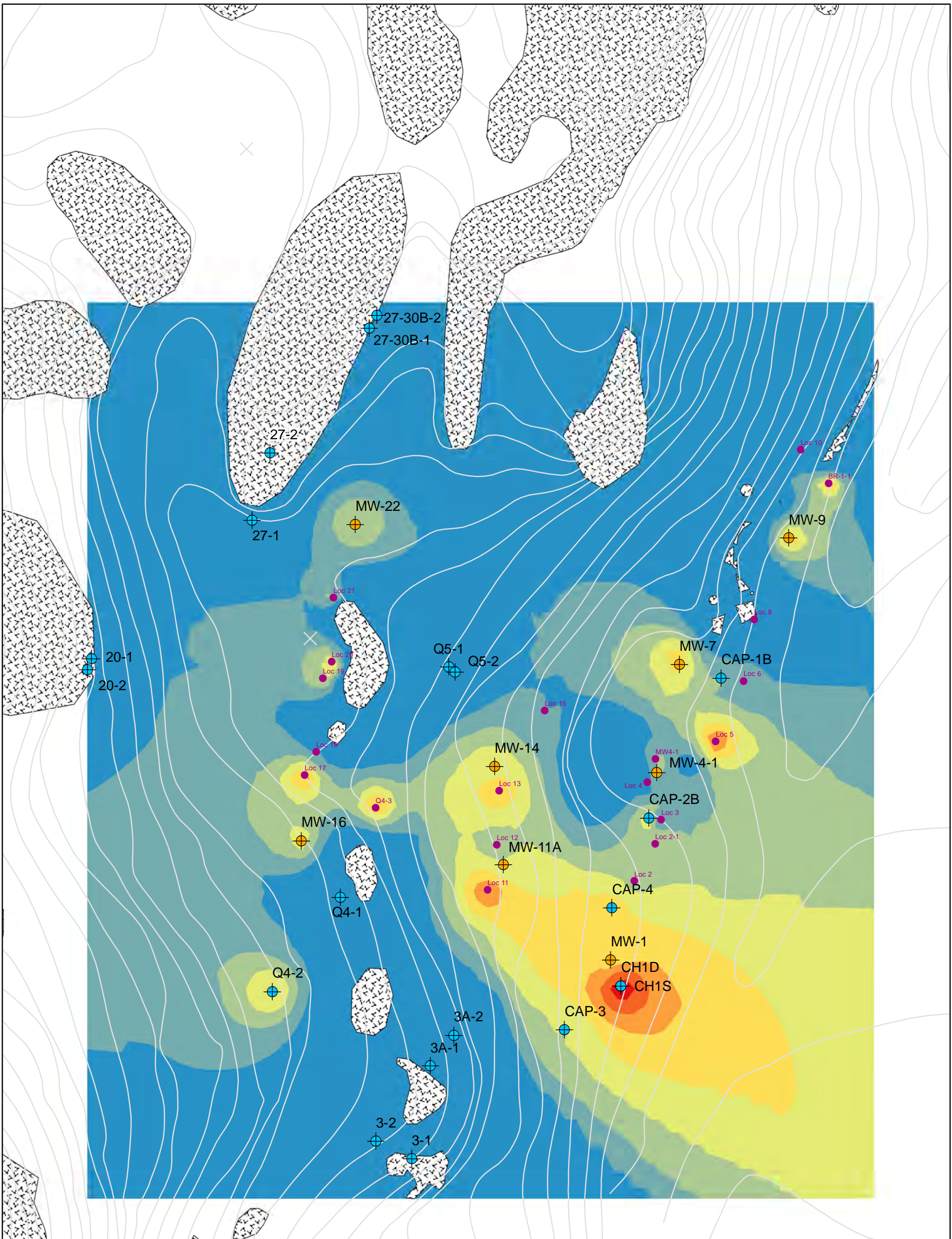


Figure 5.4-1
Contour map of overburden
thickness at site-scale

Legend

 0 - 2	 Bedrock Well
 2 - 4	 Overburden Well
 4 - 6	 Adjusted Wells
 6 - 8	 Borings
 8 - 10	 Rock Outcrop
 10 - 12	Contour Interval - 2 ft from Mass Dev.
 12 - 14	
 14 - 16	


 Shepley's Hill
 Bedrock Investigation 2009
 Devens, MA

Map Tracker ID=6725
 Created by the US EPA Region 1 GIS Center on 6/29/2012

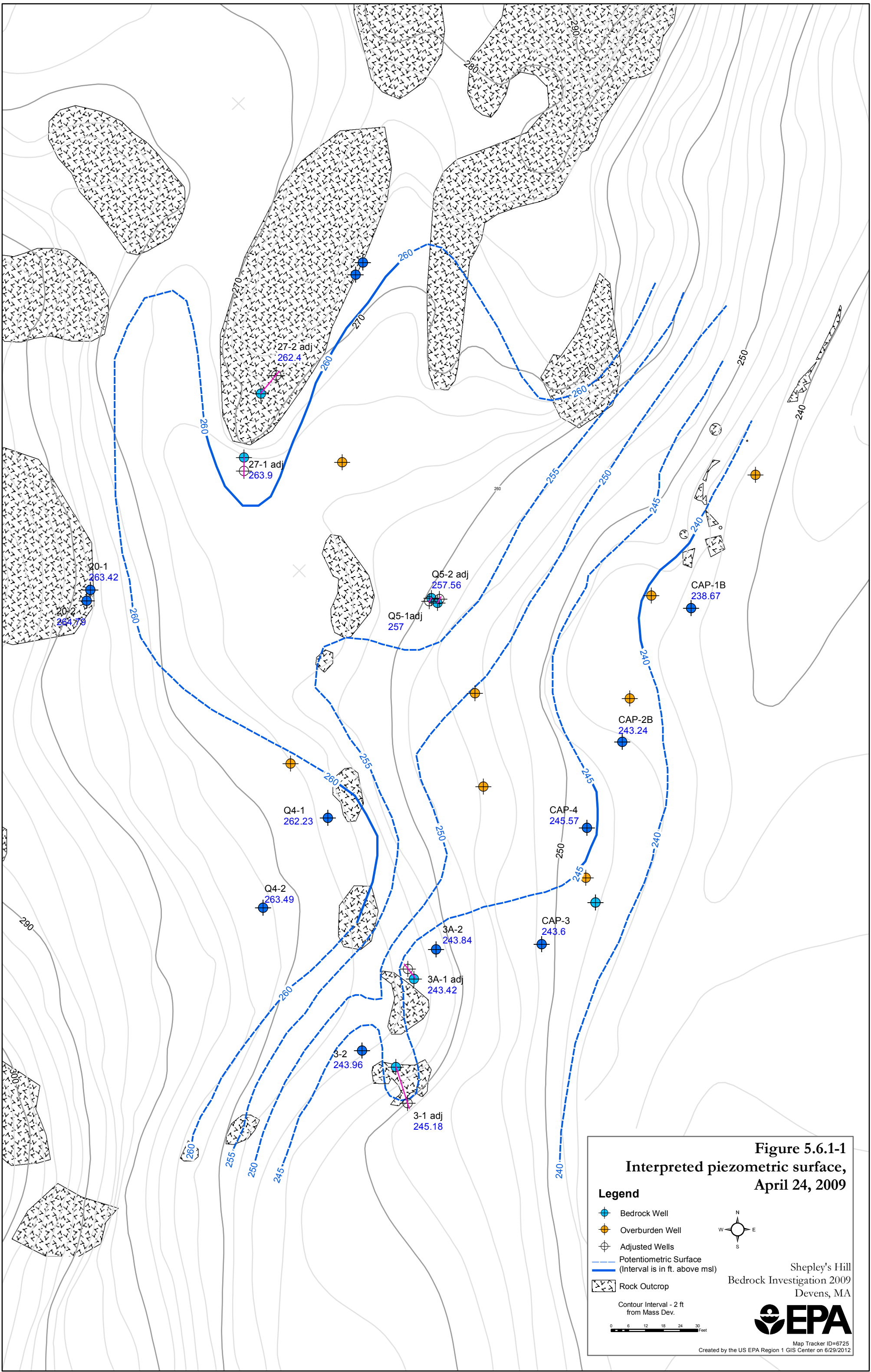
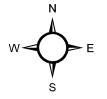


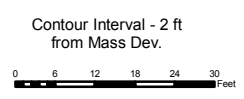
Figure 5.6.1-1
Interpreted piezometric surface,
April 24, 2009

Legend

-  Bedrock Well
-  Overburden Well
-  Adjusted Wells
-  Potentiometric Surface (Interval is in ft. above msl)
-  Rock Outcrop



Shepley's Hill
 Bedrock Investigation 2009
 Devens, MA



Map Tracker ID=6725
 Created by the US EPA Region 1 GIS Center on 6/29/2012

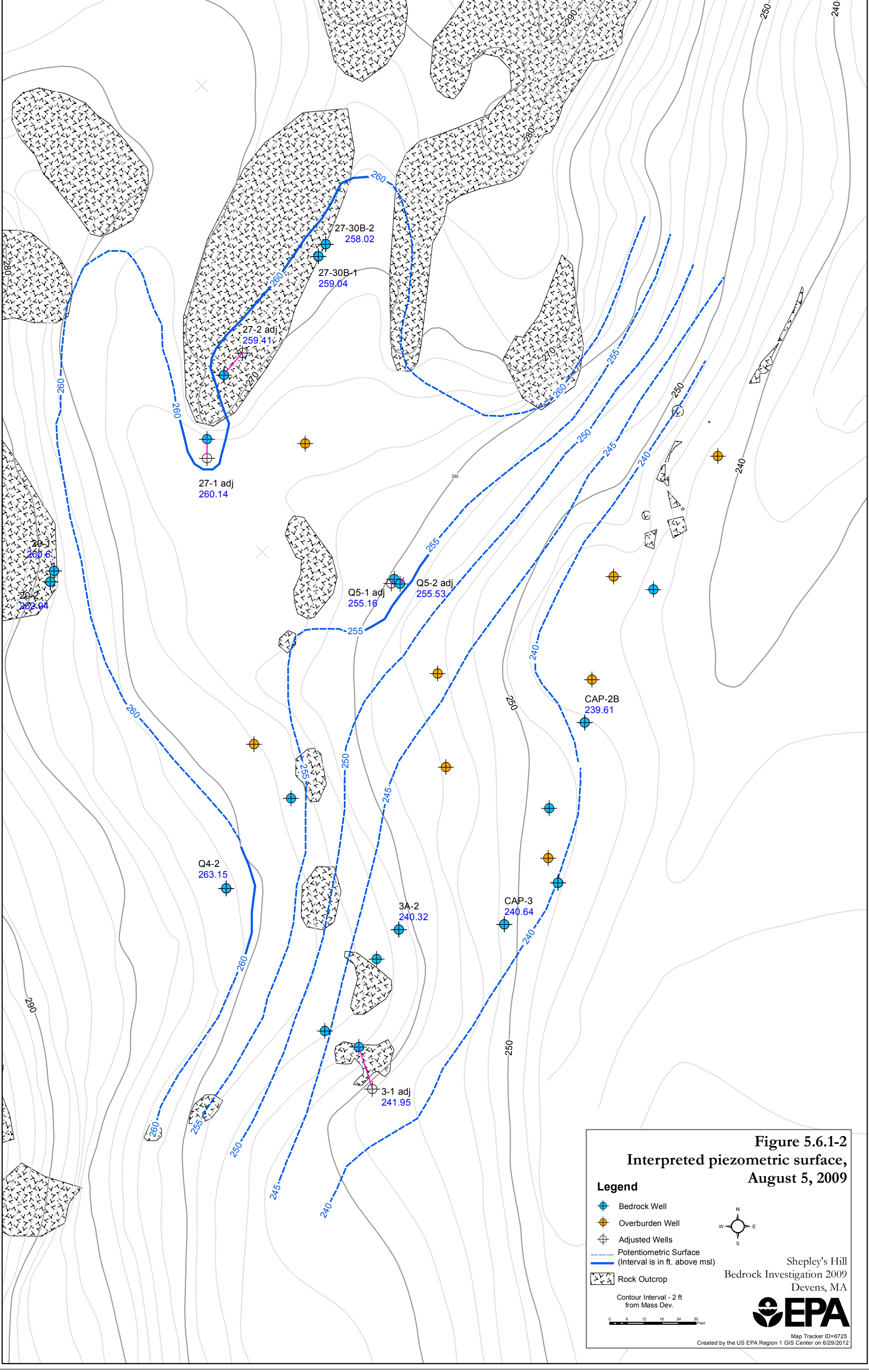


Figure 5.6.1-2
Interpreted piezometric surface,
August 5, 2009

Legend

-  Bedrock Well
-  Overburden Well
-  Adjusted Wells
-  Potentiometric Surface (Interval is in ft. above msl)
-  Rock Outcrop



Shepley's Hill
 Bedrock Investigation 2009
 Devens, MA



Contour Interval - 2 ft
 from Mass Dev.

0 6 12 18 24 30 Feet

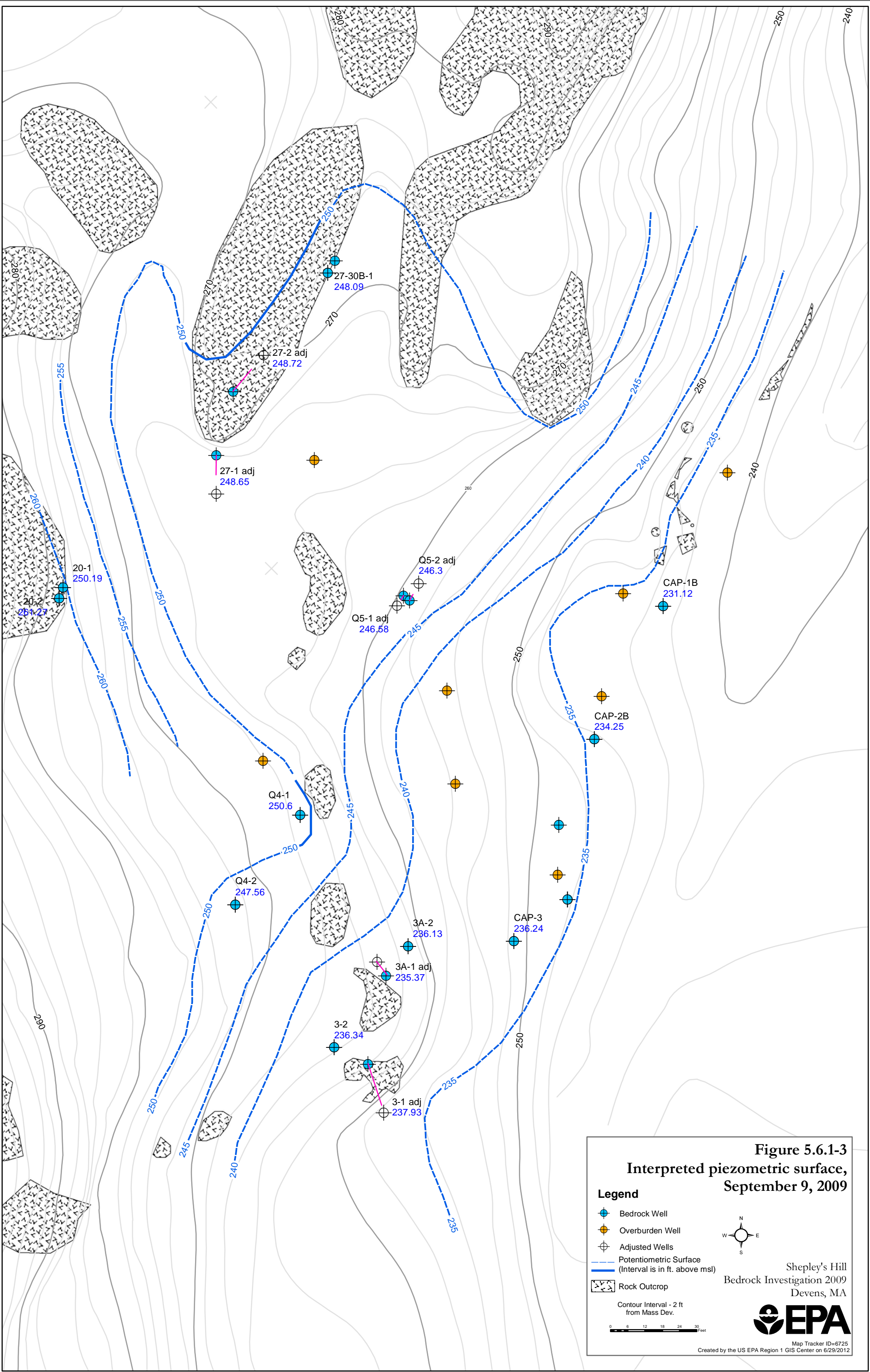
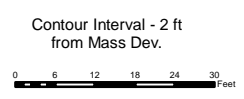


Figure 5.6.1-3
Interpreted piezometric surface,
September 9, 2009

- Legend**
- Bedrock Well
 - Overburden Well
 - Adjusted Wells
 - Potentiometric Surface (Interval is in ft. above msl)
 - Rock Outcrop



Shepley's Hill
 Bedrock Investigation 2009
 Devens, MA



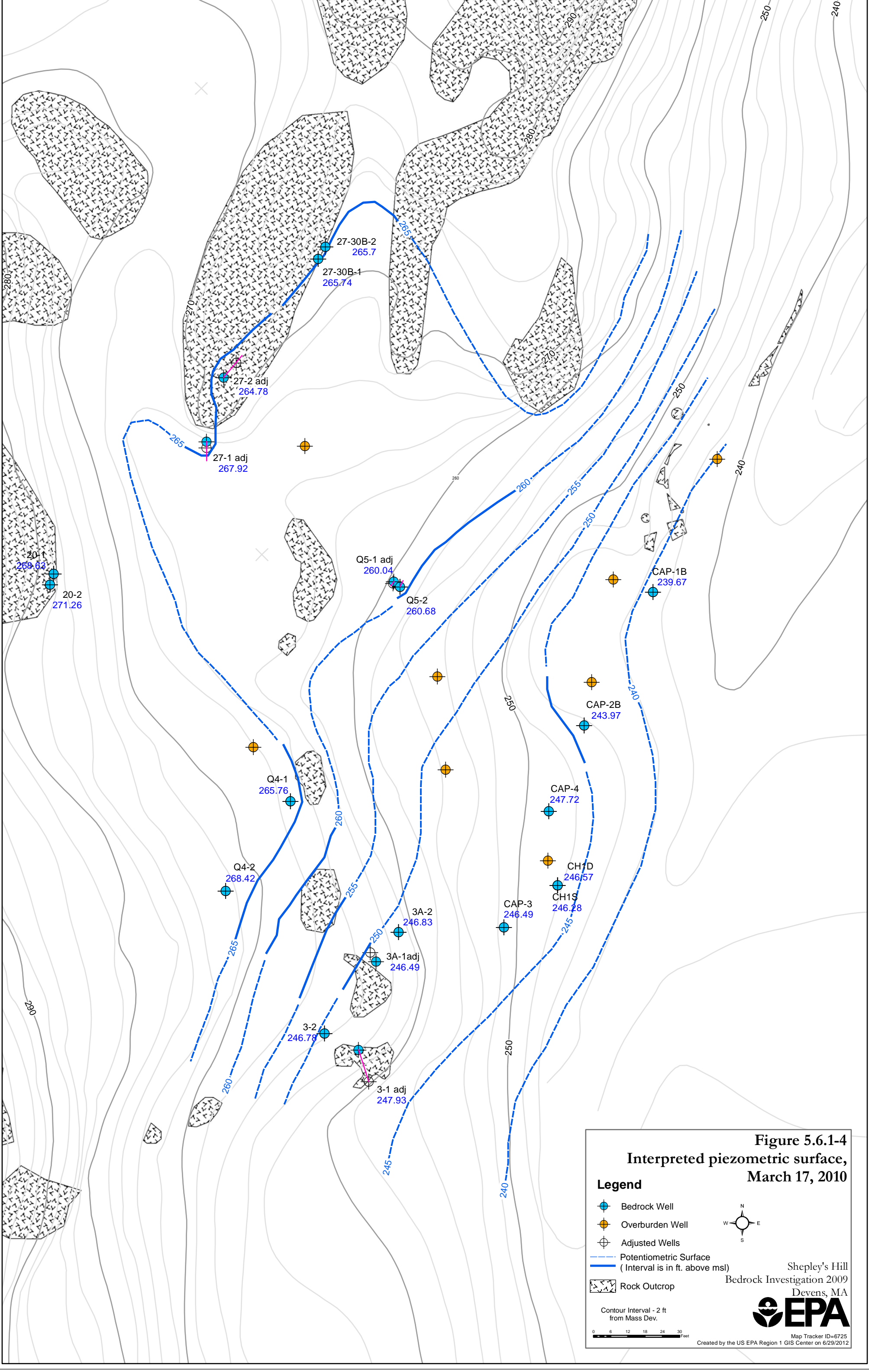


Figure 5.6.1-4
Interpreted piezometric surface,
March 17, 2010

Legend

-  Bedrock Well
-  Overburden Well
-  Adjusted Wells
-  Potentiometric Surface
-  Piezometric Surface (Interval is in ft. above msl)
-  Rock Outcrop



Contour Interval - 2 ft
 from Mass Dev.



Shepley's Hill
 Bedrock Investigation 2009
 Devens, MA



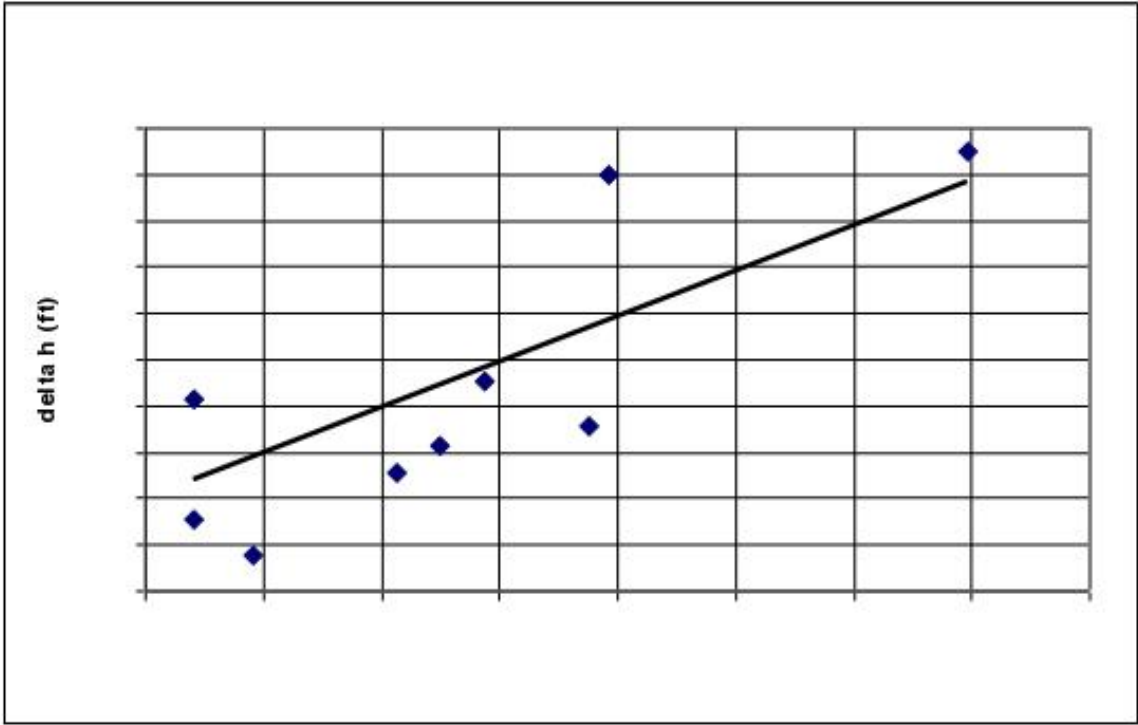


Figure 5.6.5-1(a): Correlation of water-level change and precipitation at 20-1.

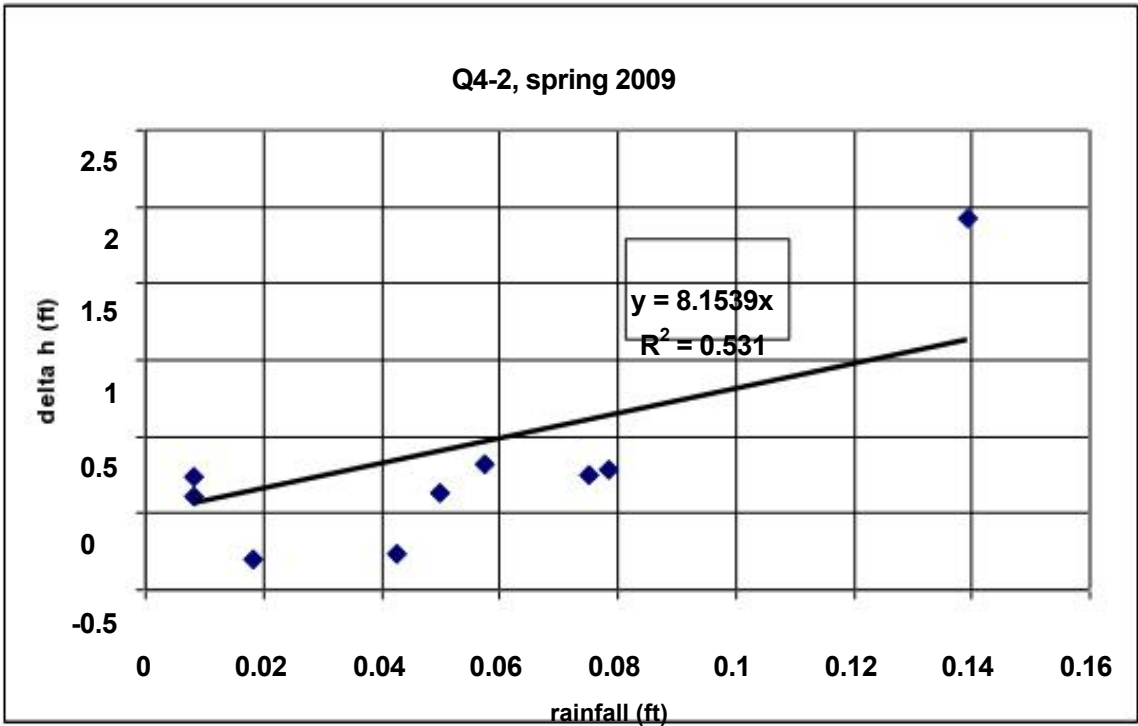


Figure 5.6.5-1(b): Correlation of water-level change and precipitation at Q4-2.

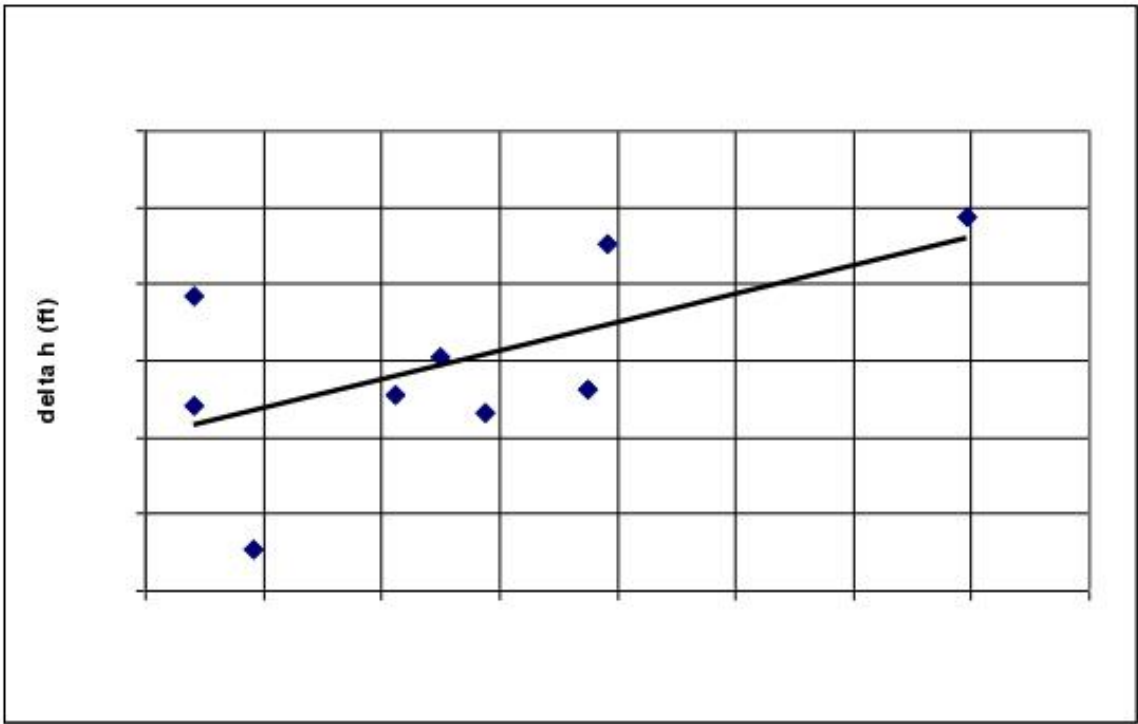


Figure 5.6.5-1(c): Correlation of water-level change and precipitation at 3-1.

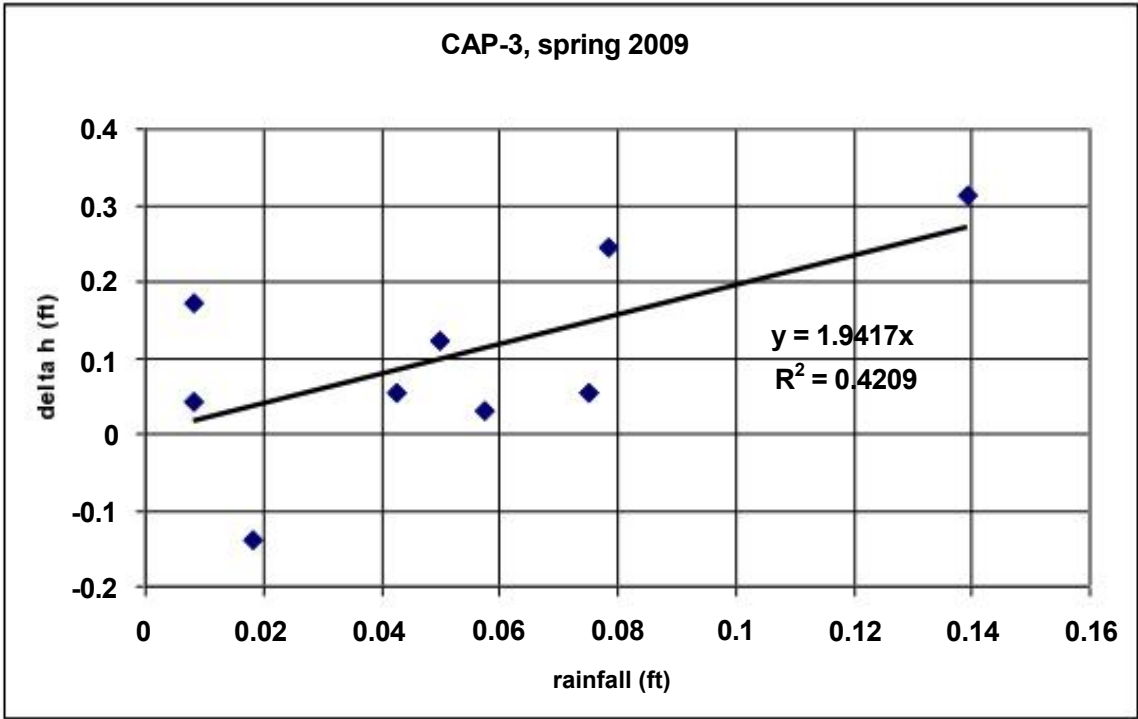


Figure 5.6.5-1(d): Correlation of water-level change and precipitation at CAP-3.

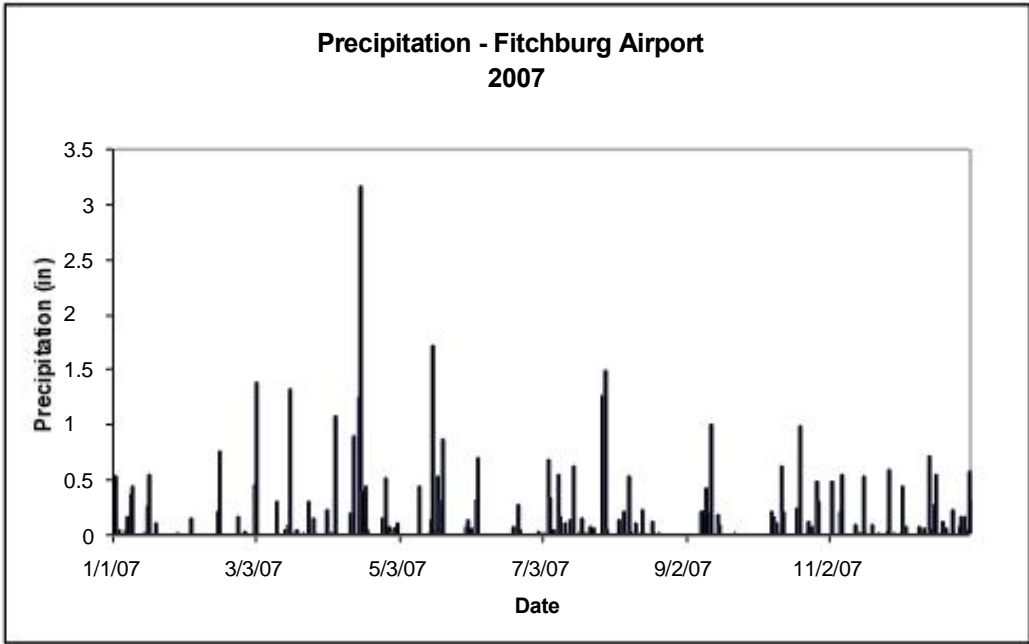
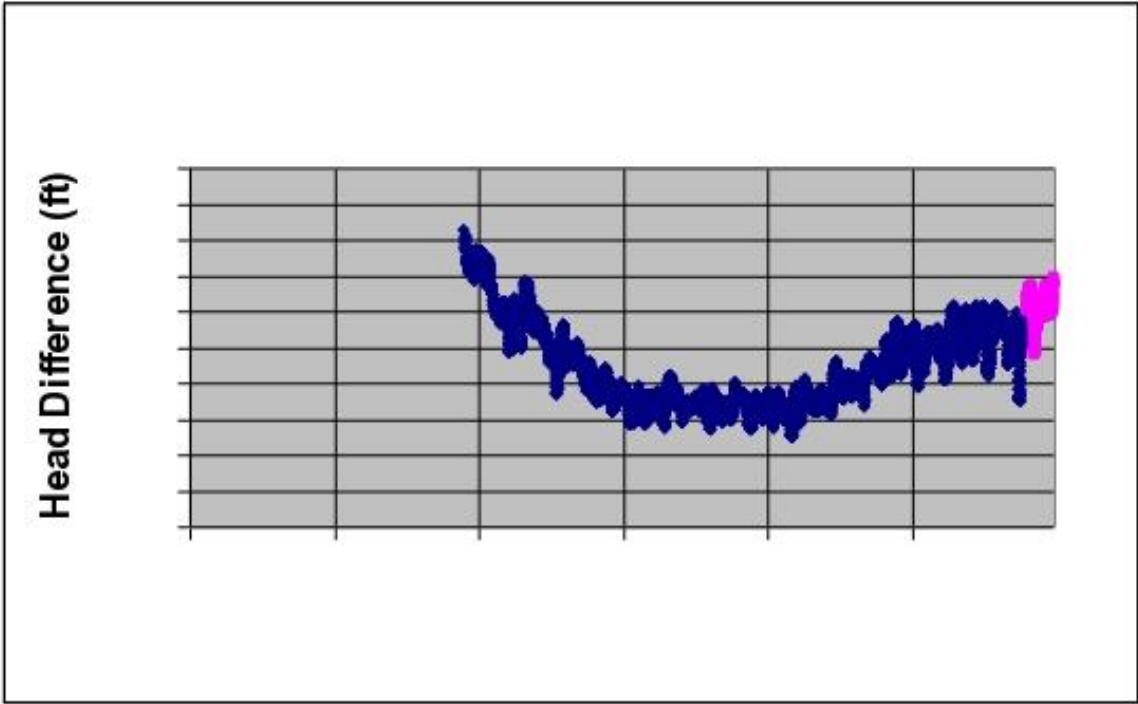


Figure 5.6.6-1(a): Head difference at the N5 piezometer pair (deep minus shallow); 2007. Positive values indicate upward flow; negative values indicate downward flow.

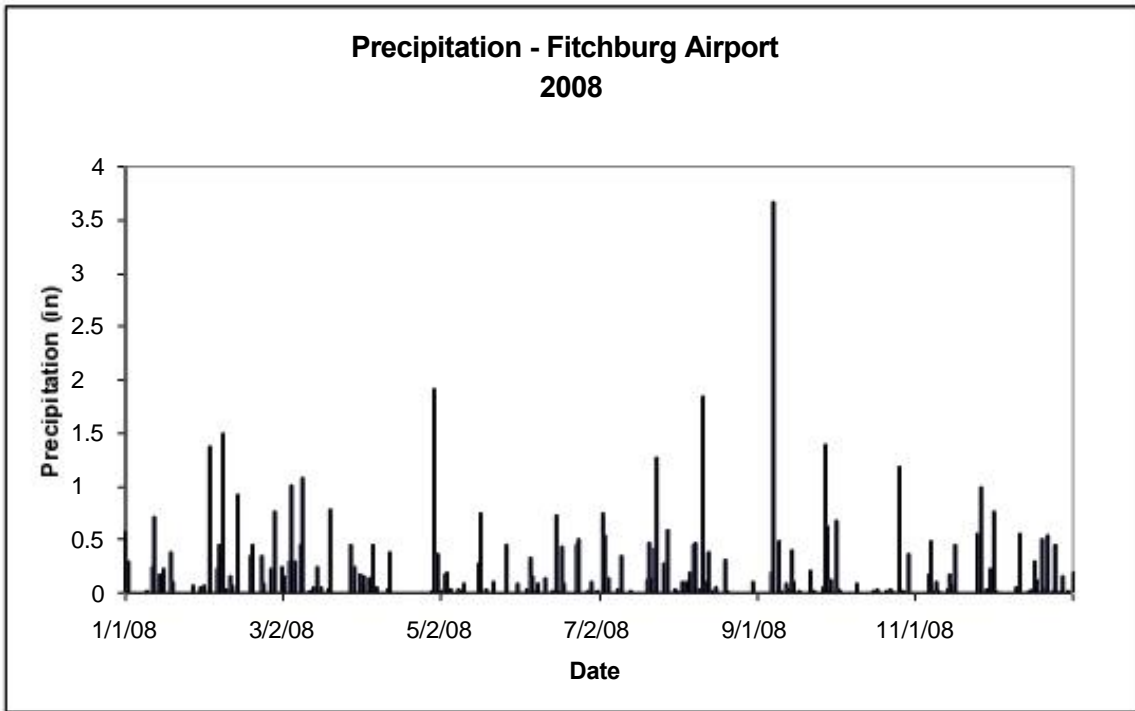
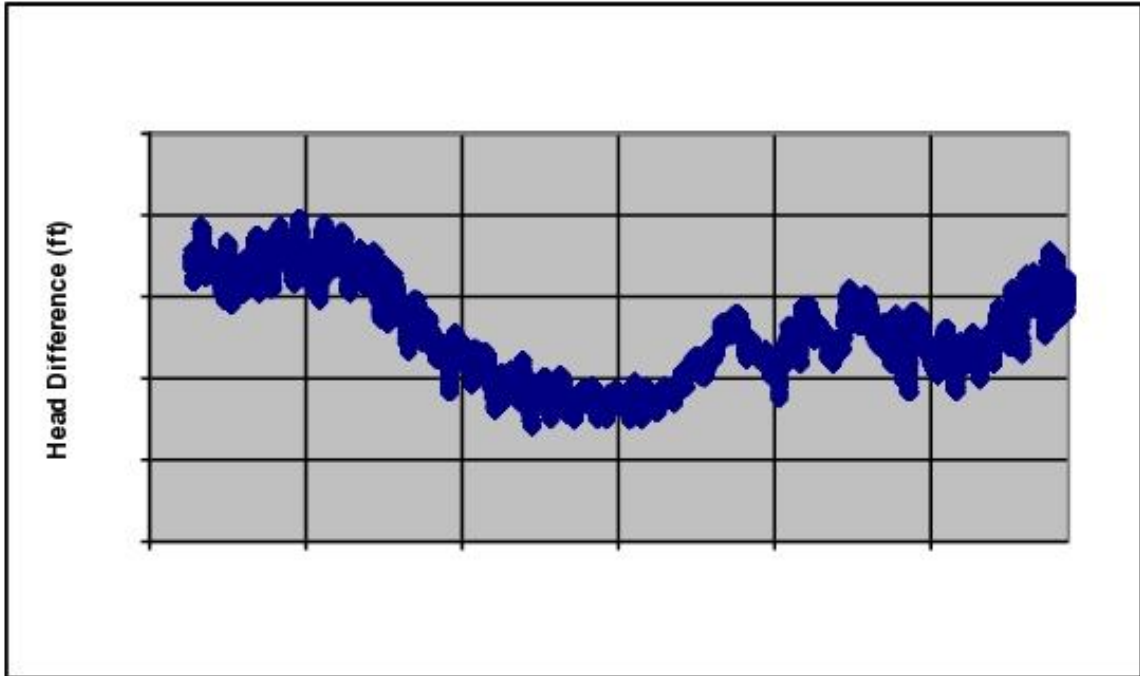


Figure 5.6.6-1(b): Head difference at the N5 piezometer pair (deep minus shallow); 2008. Positive values indicate upward flow; negative values indicate downward flow.

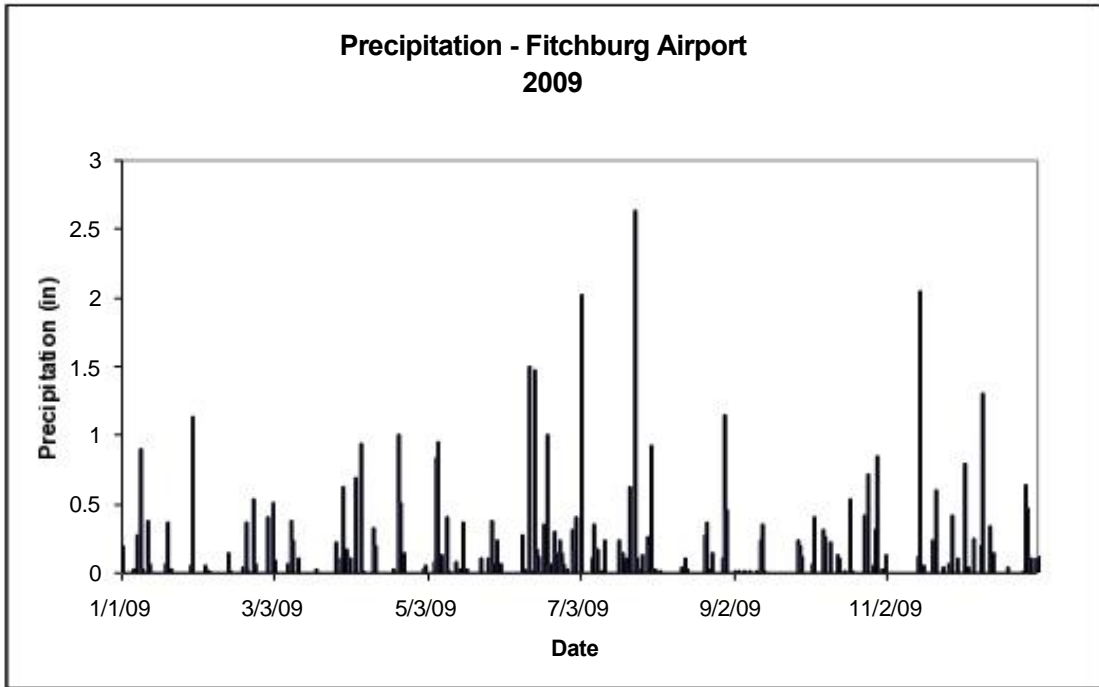
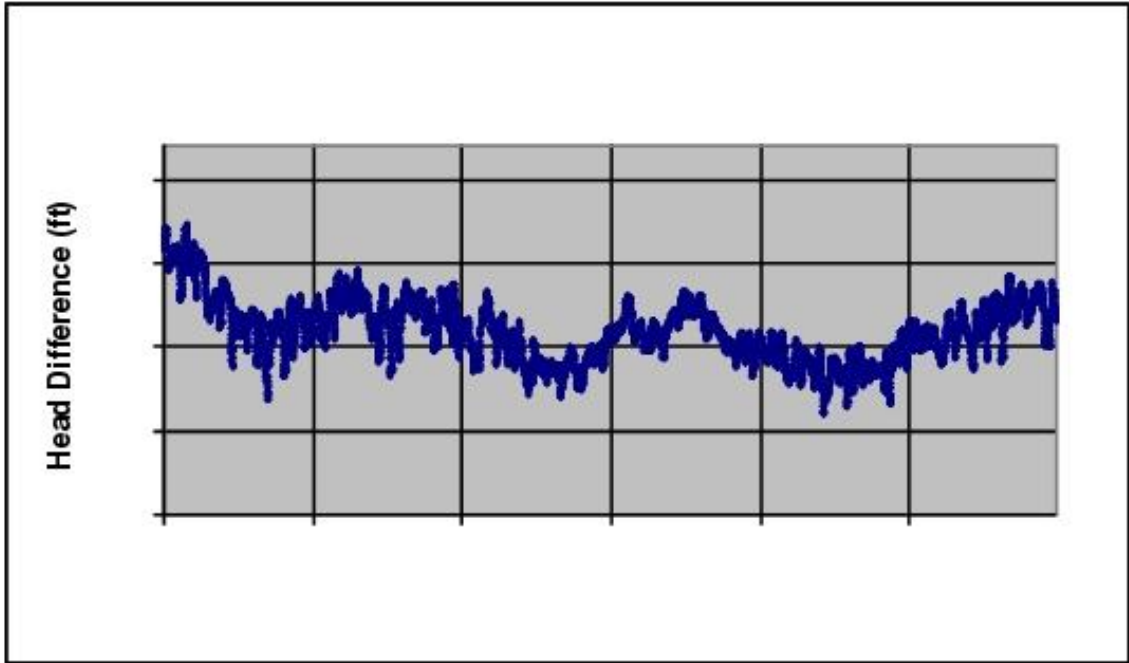


Figure 5.6.6-1(c): Head difference at the N5 piezometer pair (deep minus shallow); 2009. Positive values indicate upward flow; negative values indicate downward flow.

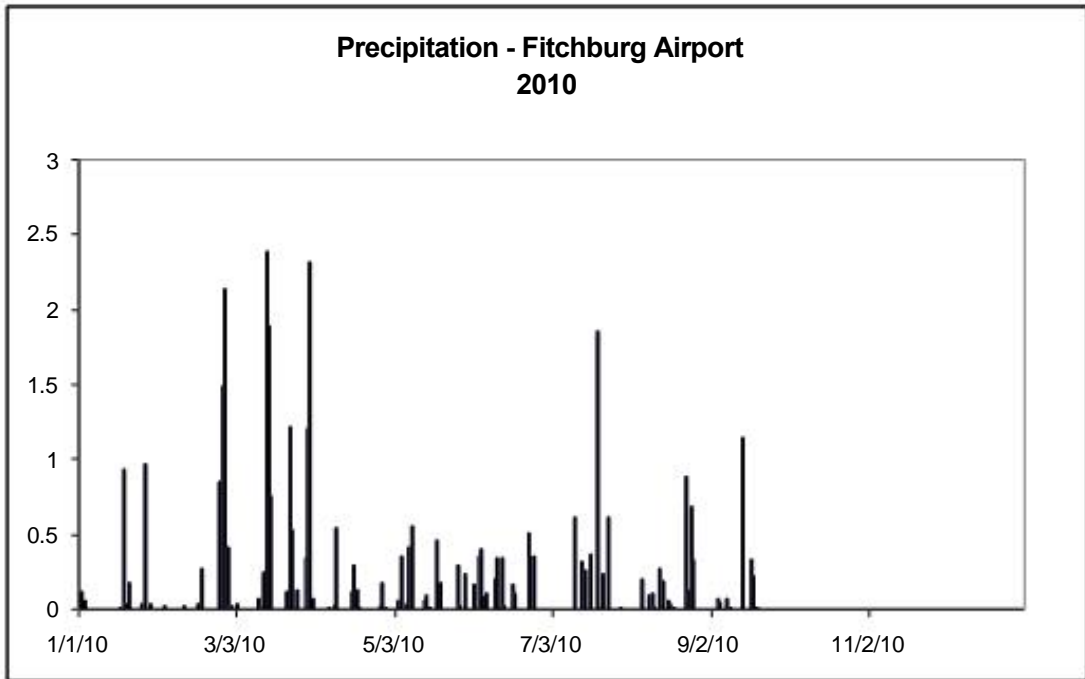
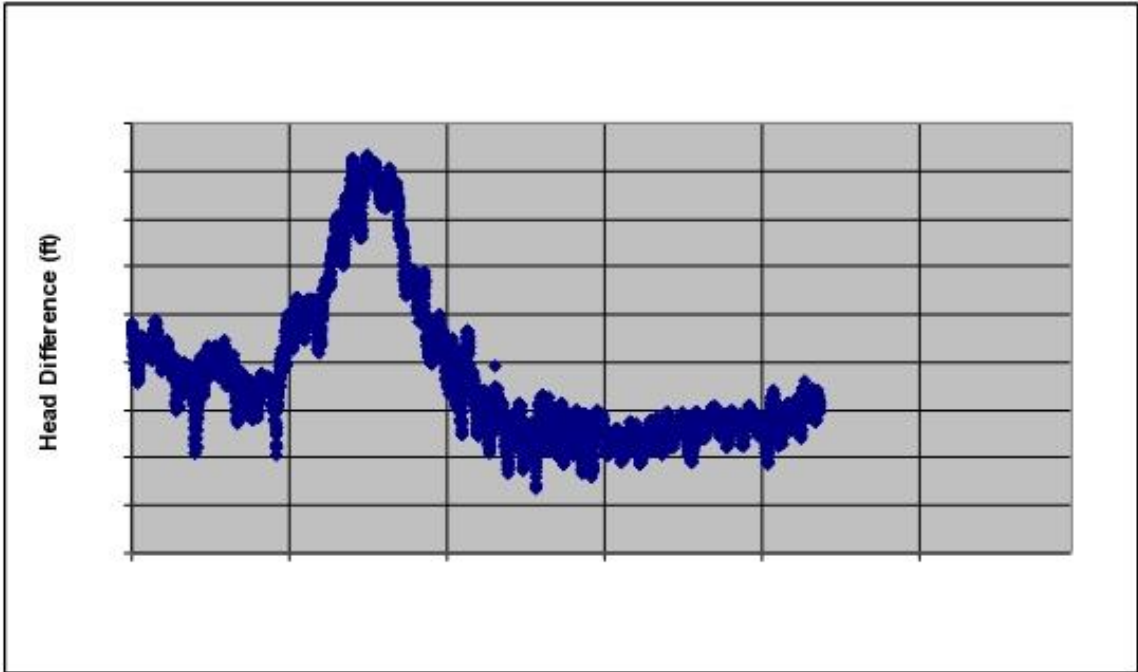


Figure 5.6.6-1(d): Head difference at the N5 piezometer pair (deep minus shallow); 2010. Positive values indicate upward flow; negative values indicate downward flow.

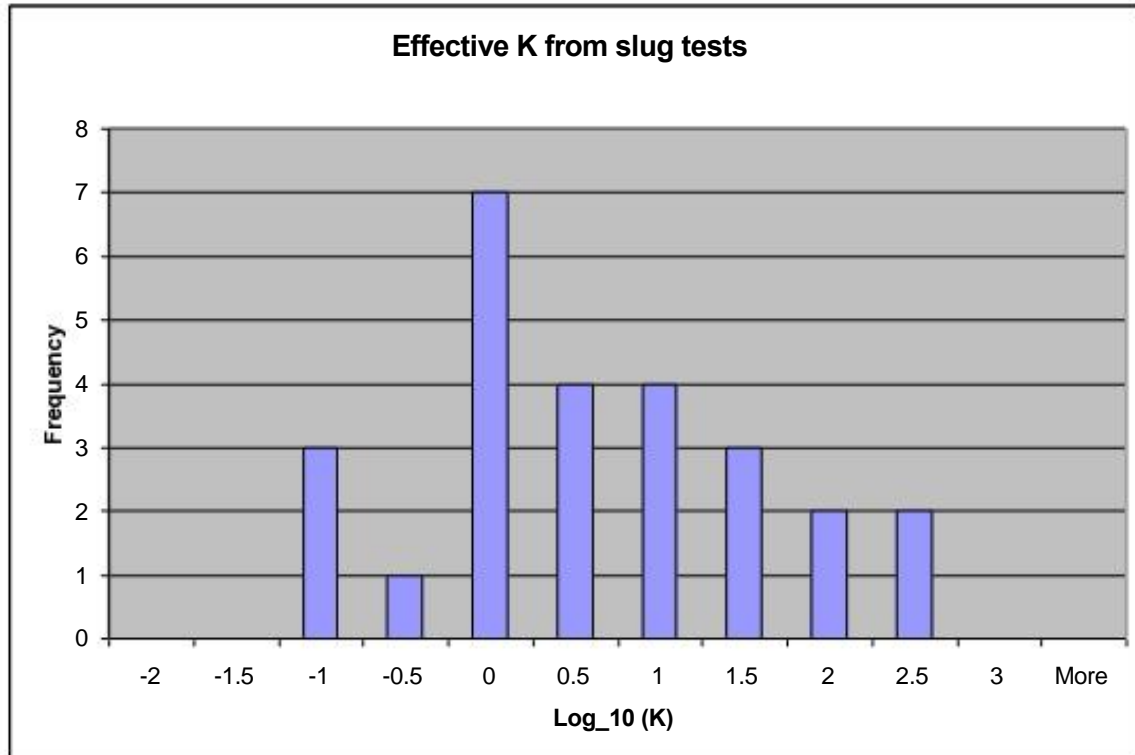


Figure 5.7-1: Histogram of $\log_{10}(K)$; K in ft/d. Values displayed include results from both falling-head and rising-head slug tests on 16 open bedrock borings. One boring was tested at two different times. Distribution is approximately log-normal. Geometric mean is 2.0 ft/d (i.e., the central tendency of the logarithm is 0.3).



Figure 5.10.3-1. Large open fracture at approximately 39 ft. bgs. Note wide bands (several cm thick) of iron oxidation adjacent to fracture surface.



Figure 5.10.3-2. Close-up of fracture in Figure 5.10.3-1 showing bleached zone surrounding iron-oxidation band; bleaching is inferred to be relict hydrothermal alteration.



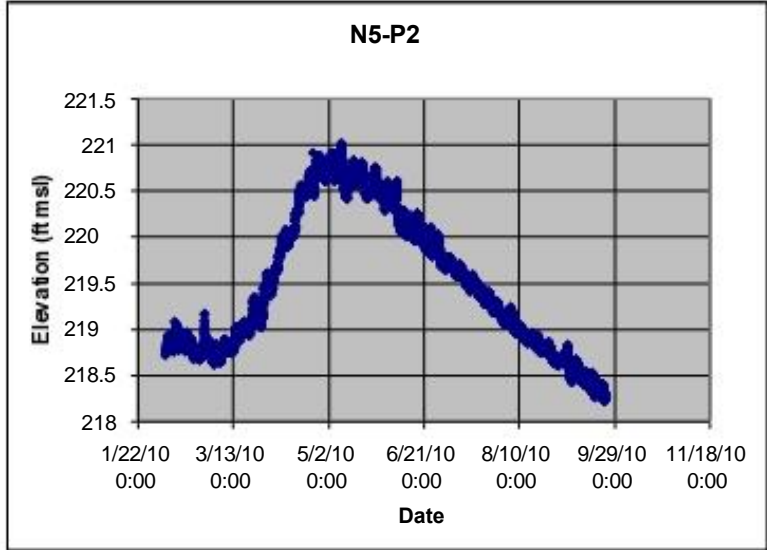
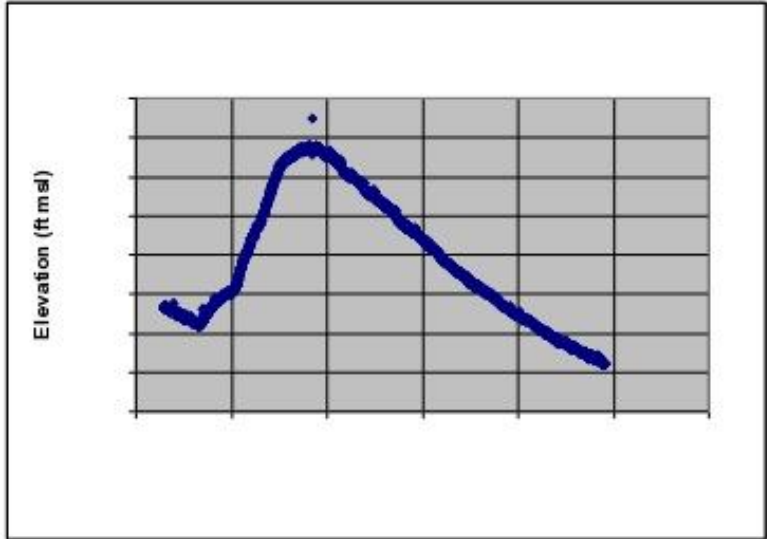
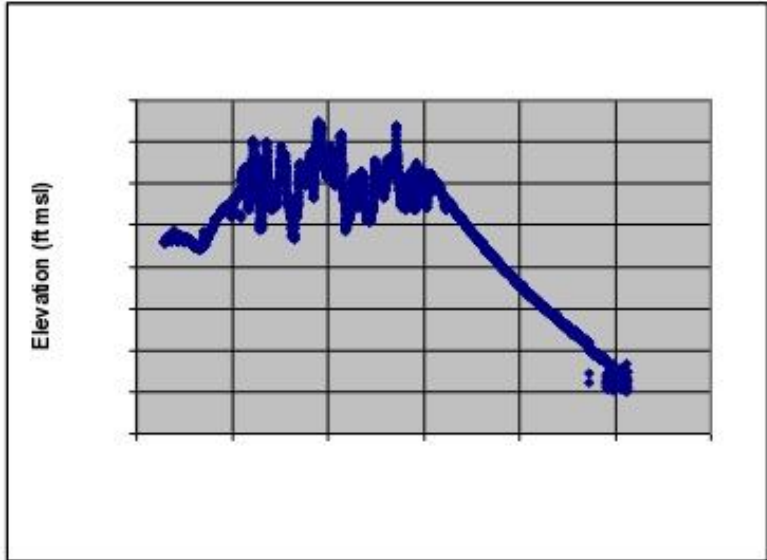
Figure 5.10.3-3(a). Vertically oriented calcite-filled vein with sulfide minerals (tentatively identified as pyrite and arsenopyrite). Depth interval = 108.25-108.4 ft.

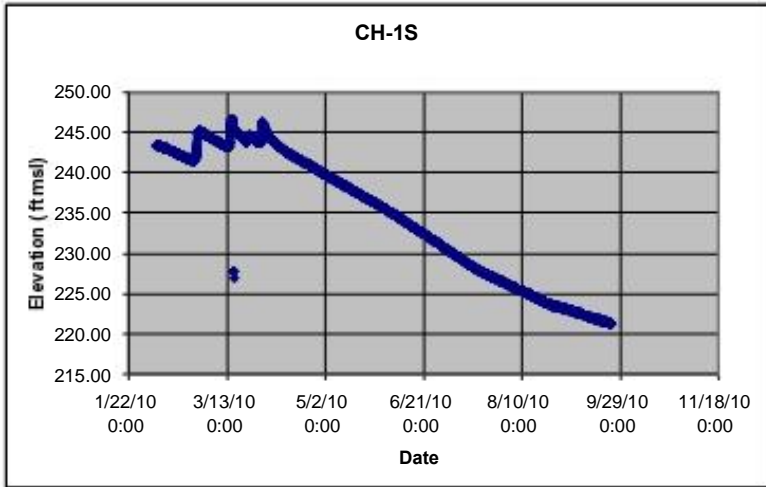
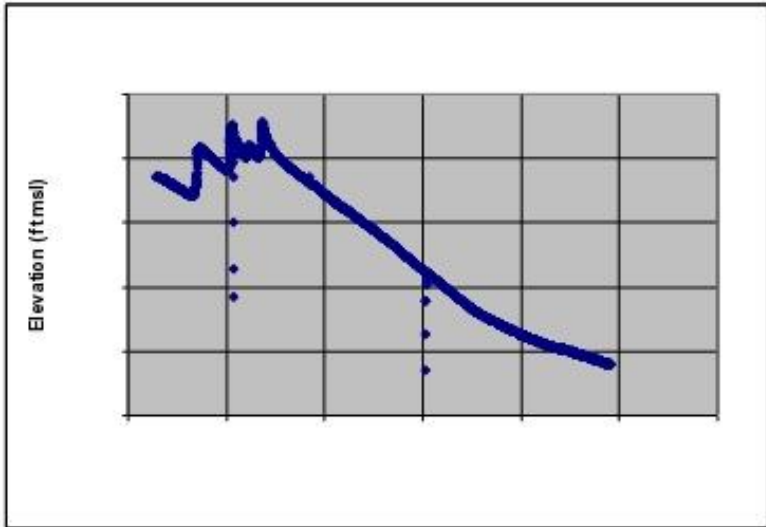
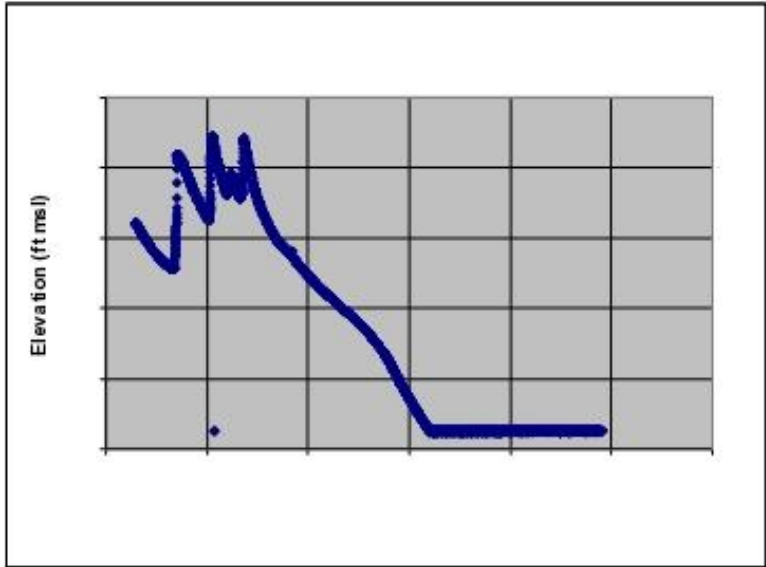


Figure 5.10.3-3(b). Quartz vein with silver-colored sulfide mineral (possibly arsenopyrite). Depth interval ~133 ft.



Figure 5.10.3-3(c). Large quartz vein with pyrite at approximately 98 ft bgs.





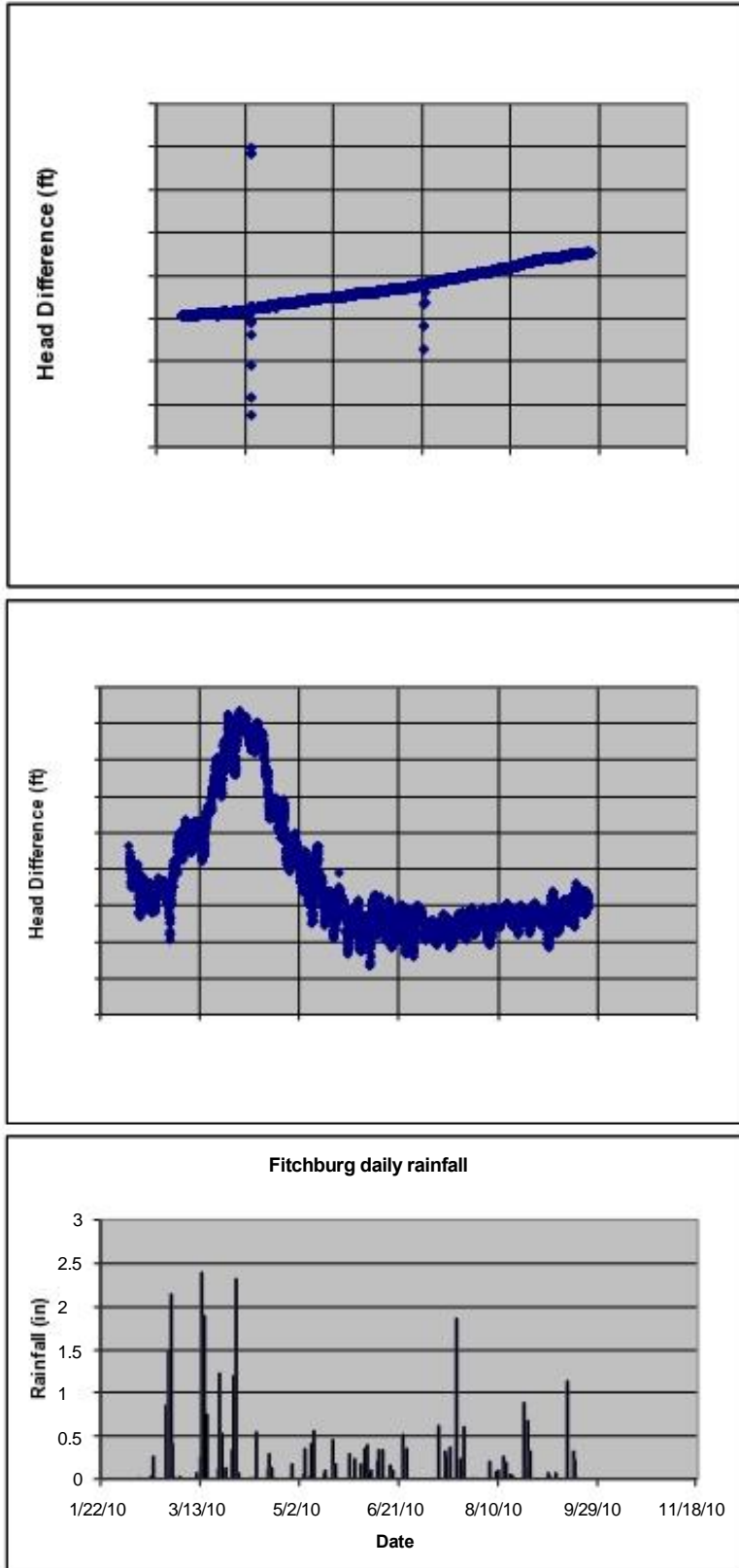


Figure 5.11-1: Water levels in screened wells, 5 February 2010 to 24 September 2010.

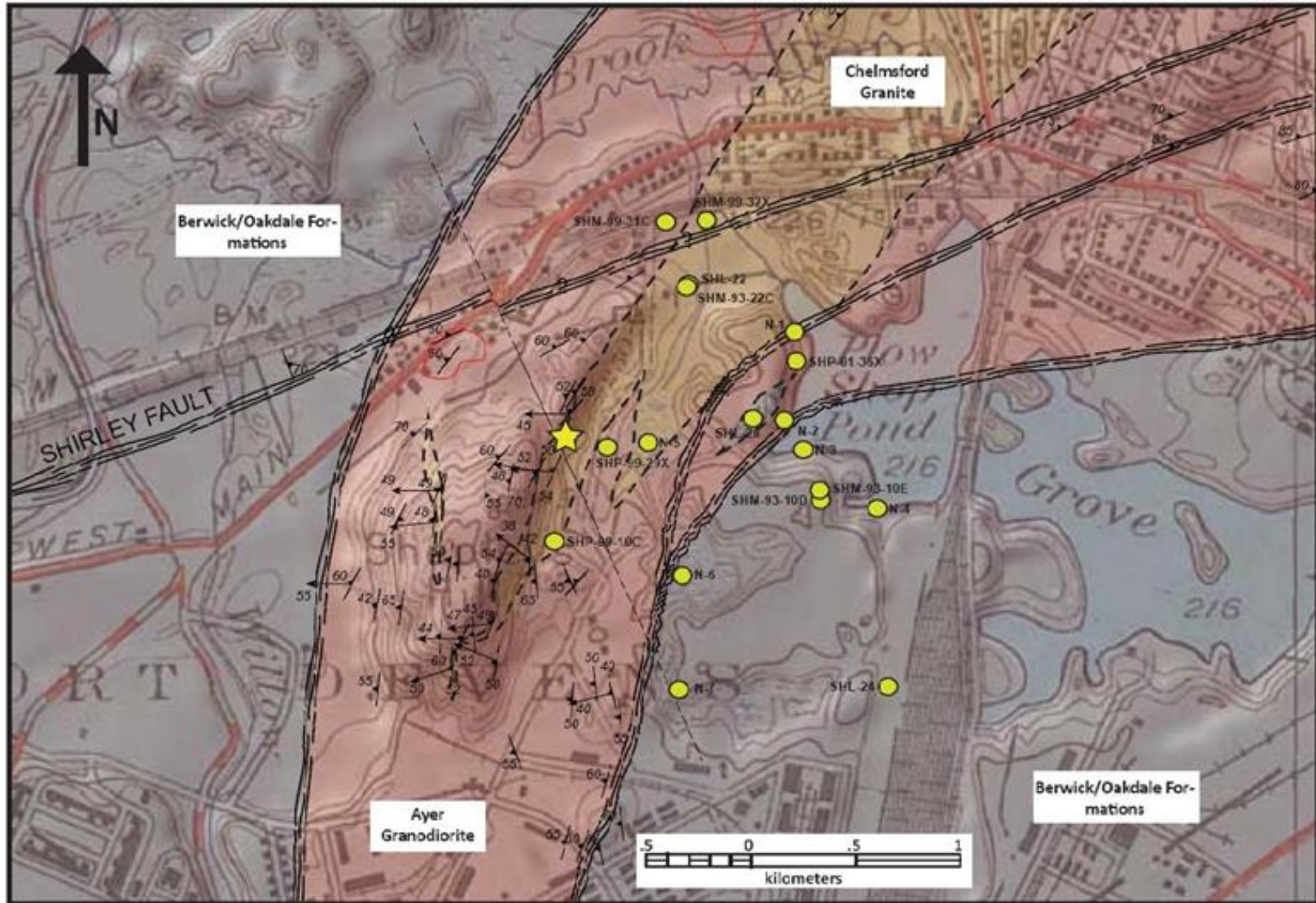


Figure 6.0-1. Locations of bedrock core samples examined. Filled yellow circles indicate borings for which core was archived from previous investigations. Yellow star indicates location of corehole CH-1, drilled for the present investigation. Figure from Koteas, et al., 2010.



Figure 6.1.2-1. Core from N5 showing alteration (Fe oxidation) along a fracture surface.

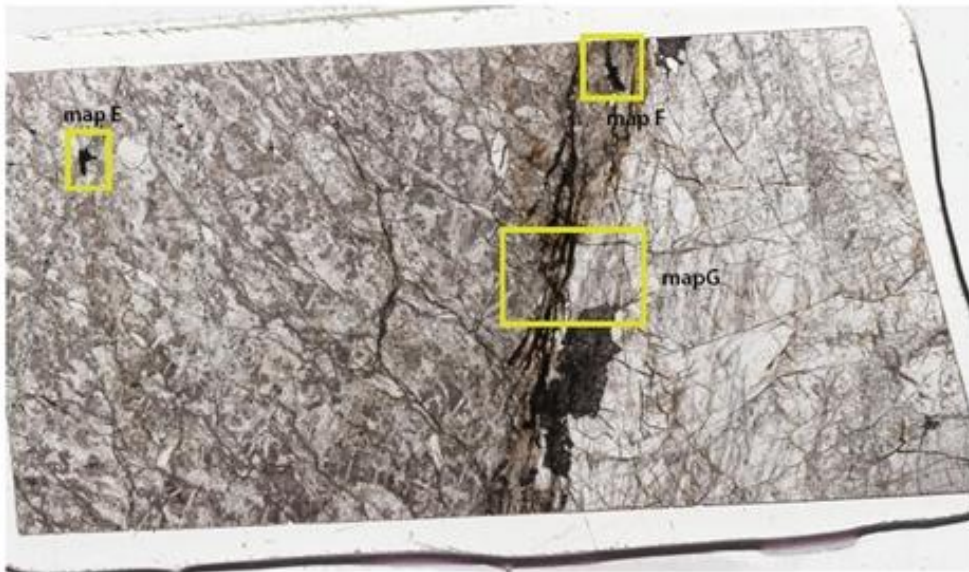


Figure 6.1.2-2. Thin section of sample from SHP-99-29X. Rectangles mark target areas for quantitative analysis by EM.

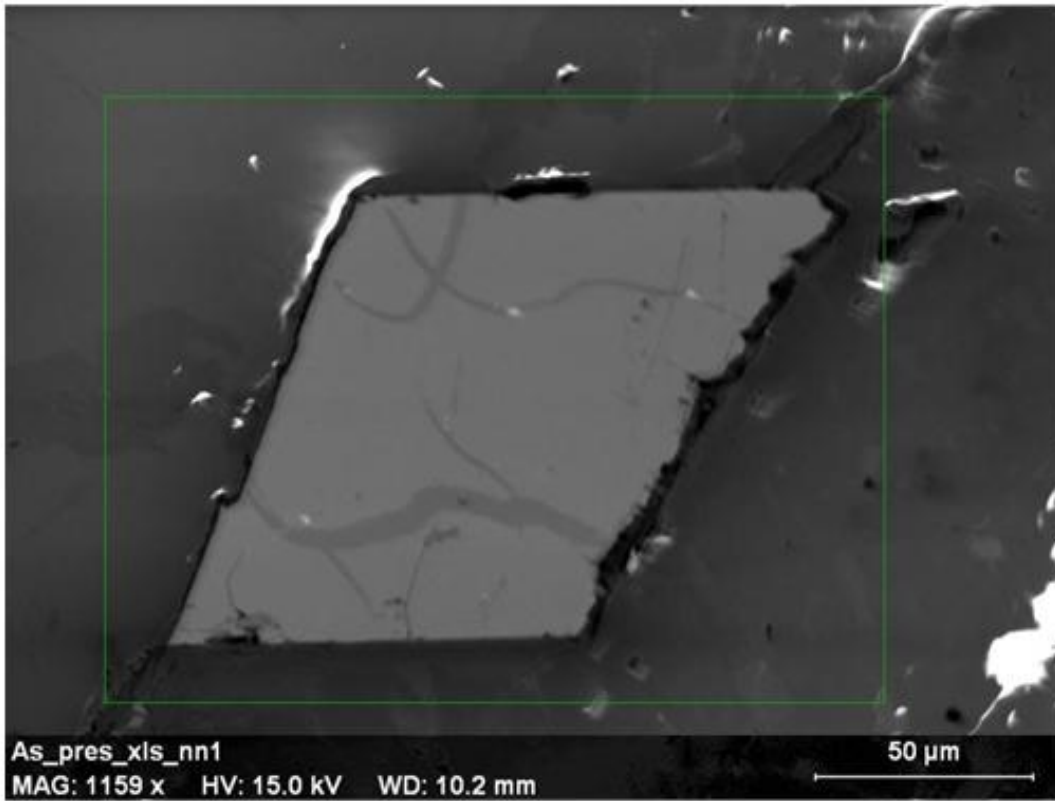


Figure 6.1.2-3(a). Backscattered electron image of arsenopyrite crystal in silicate matrix, from SHP-99-29X core.

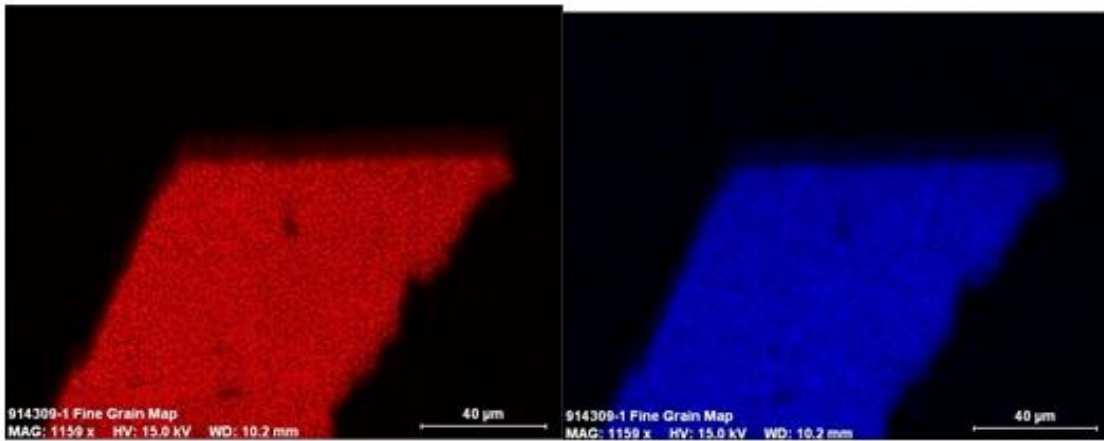


Figure 6.1.2-3(b). Arsenic (red) and sulfur (blue) single-element maps of crystal shown in Figure 6.1.2-3(a).

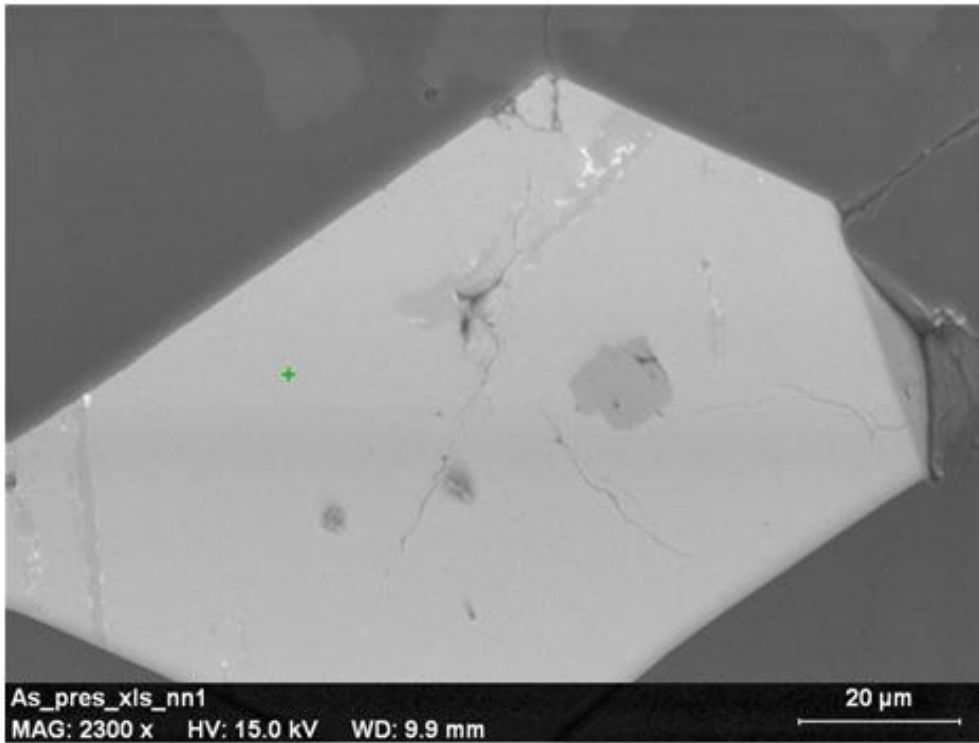


Figure 6.1.2-4(a). SEM image of an arsenopyrite crystal from SHP-99-29X core.

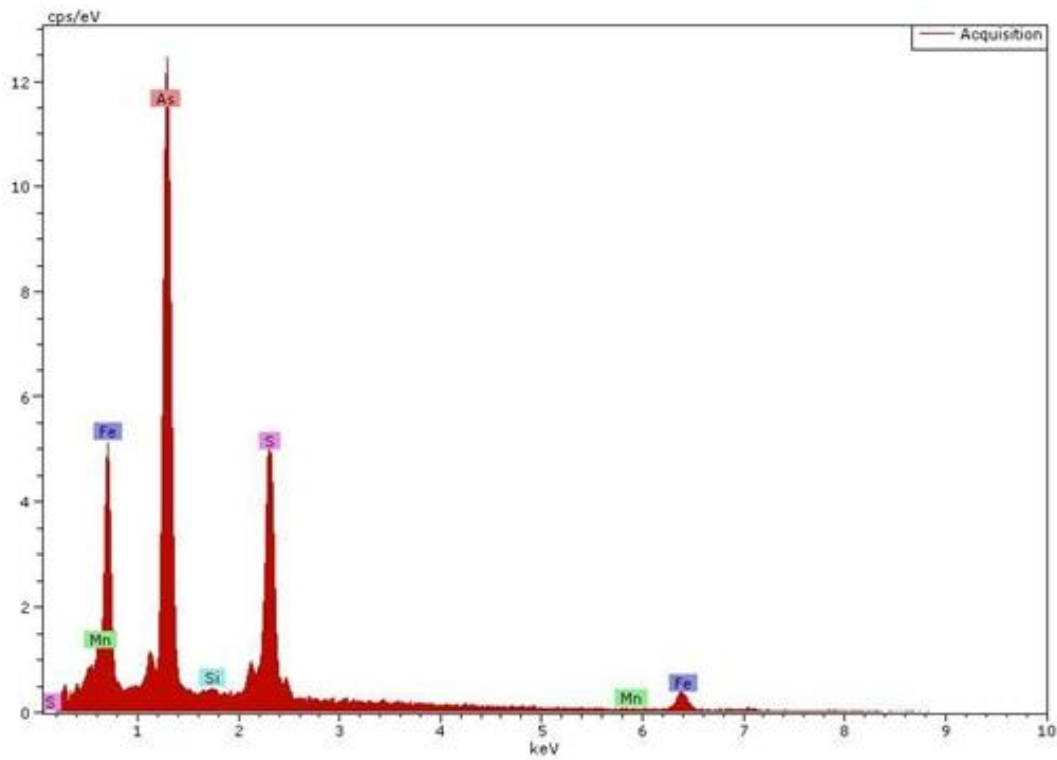


Figure 6.1.2-4(b). Element scan at point marked in Figure 4a. Most prominent peaks (left to right) correspond to Fe, As, and S.

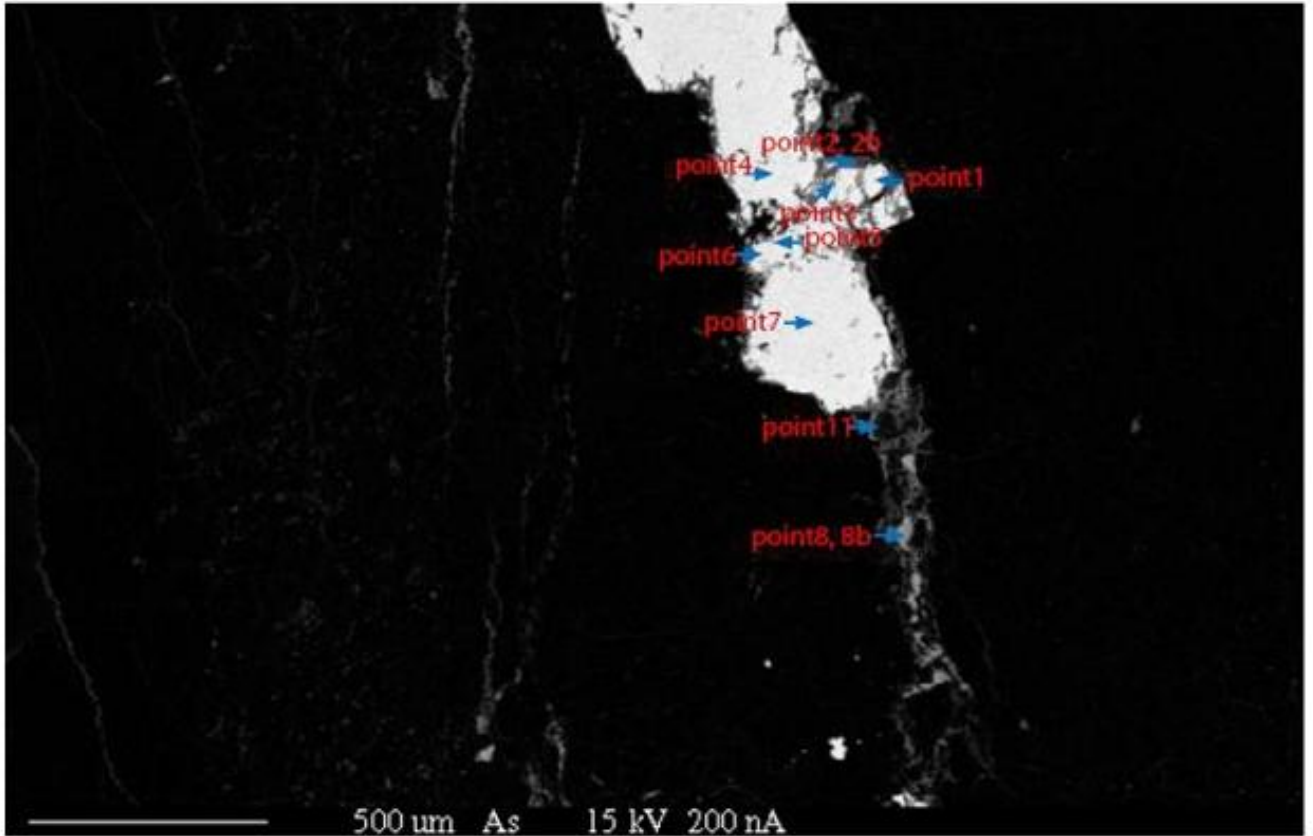


Figure 6.1.2-5. EM image of a sulfide crystal in a sample from SHP-99-29X; quantitative analysis (data presented in text, from Map Label F in Fig. 6-2) was performed at the points indicated. Results are consistent with an identification of arsenopyrite.

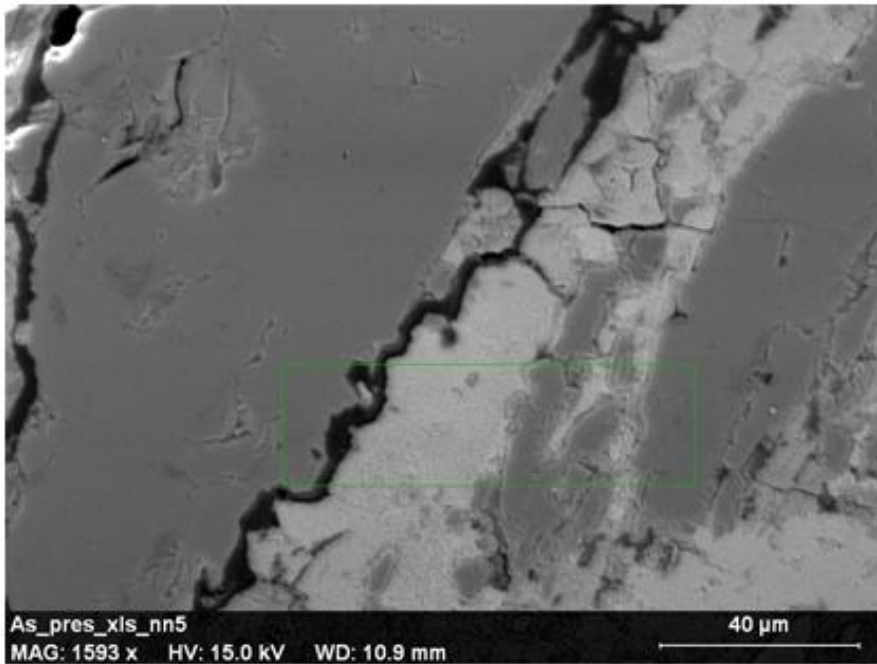


Figure 6.1.2-6(a). Vein filling (backscattered electron image) from SHP-99-29X.



Figure 6.1.2-6(b). As element map of area outlined in Figure 6a.

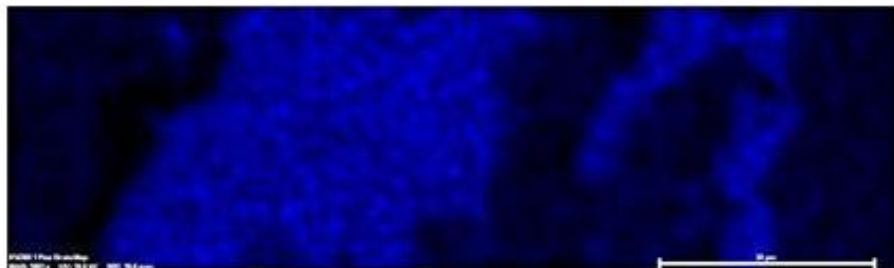


Figure 6.1.2-6(c). S element map of area outlined in Figure 6a.

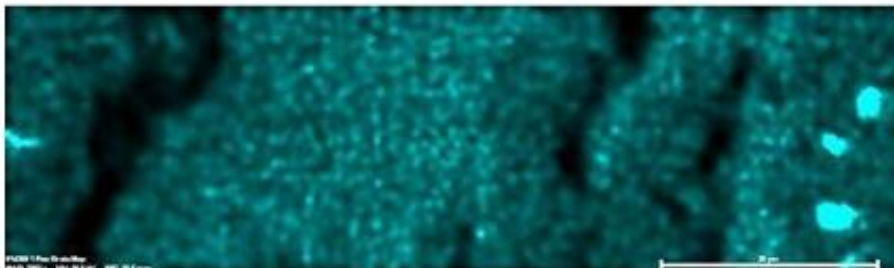


Figure 6.1.2-6(d). Na element map of area outlined in Figure 6a.

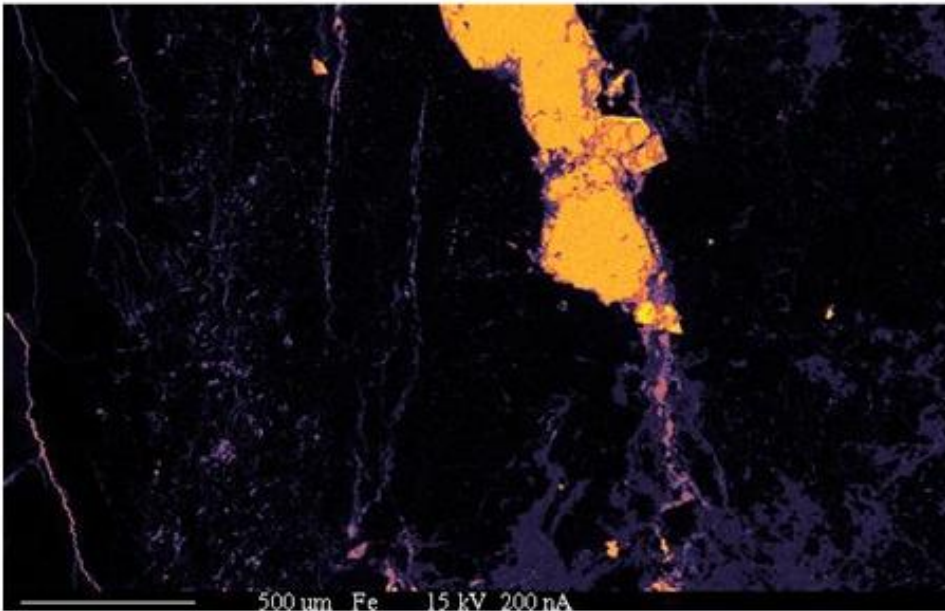


Figure 6.1.3-1(a). Element map of Fe for the area shown in Figure 6-5 (arsenopyrite from SHP-99-29X). Note Fe in microcrack below the arsenopyrite crystal.

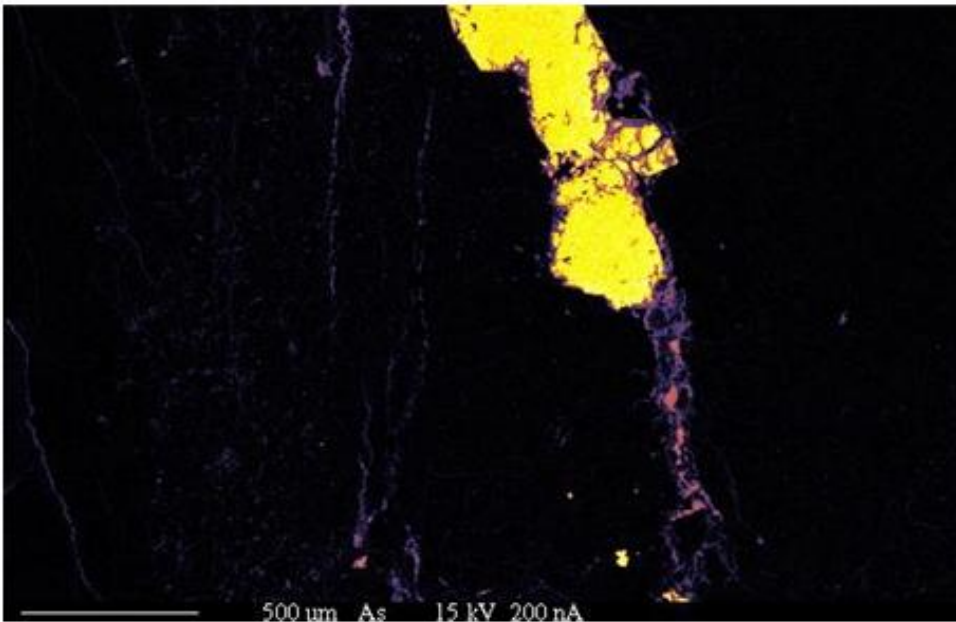


Figure 6.1.3-1(b). Element map of As for the area shown in Figure 6-5 (arsenopyrite from SHP-99-29X). Note As, in association with Fe, in microcrack below the arsenopyrite crystal.

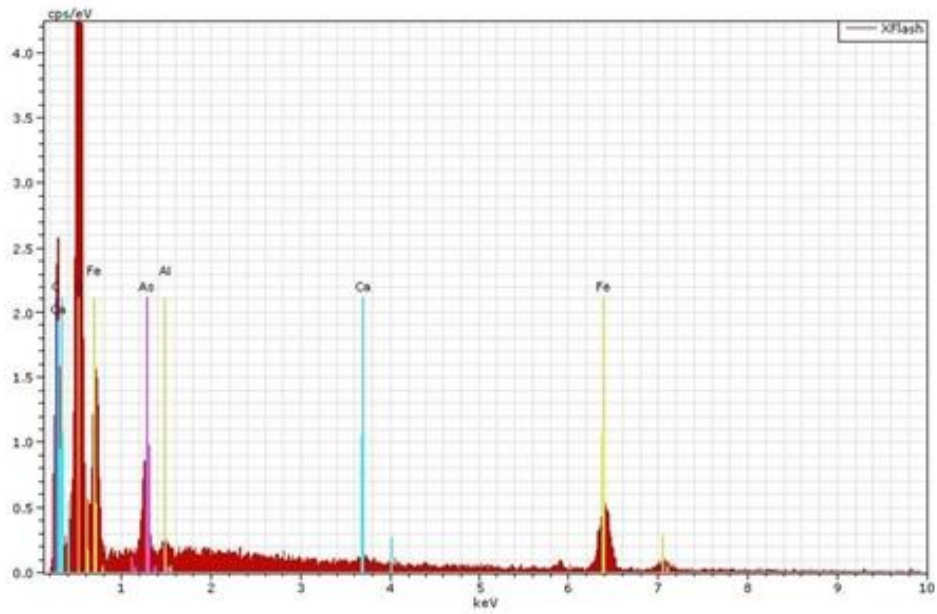
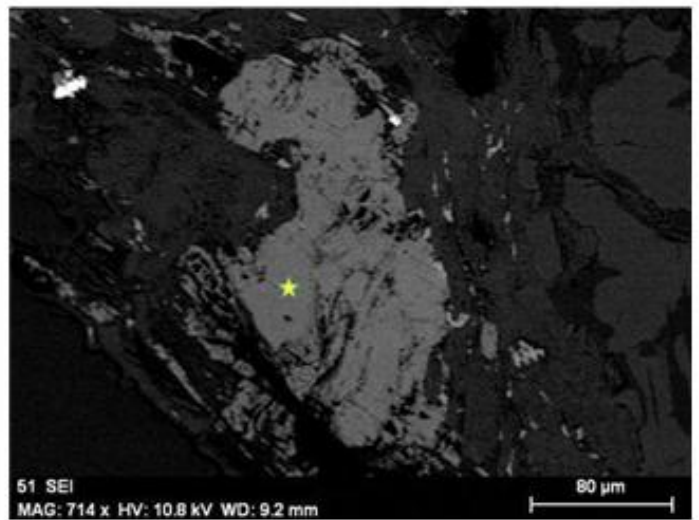


Figure 6.2.3-1. Deep corehole sample from 24.8-25.1 ft depth; bright area composed primarily of Fe-oxide with As (EDS scan at point marked by yellow star in photomicrograph).

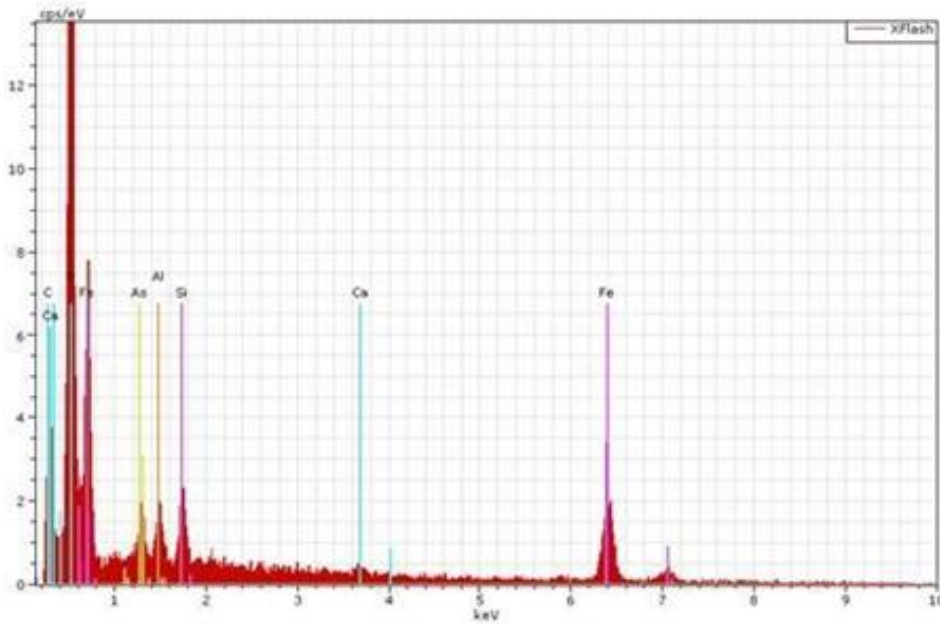
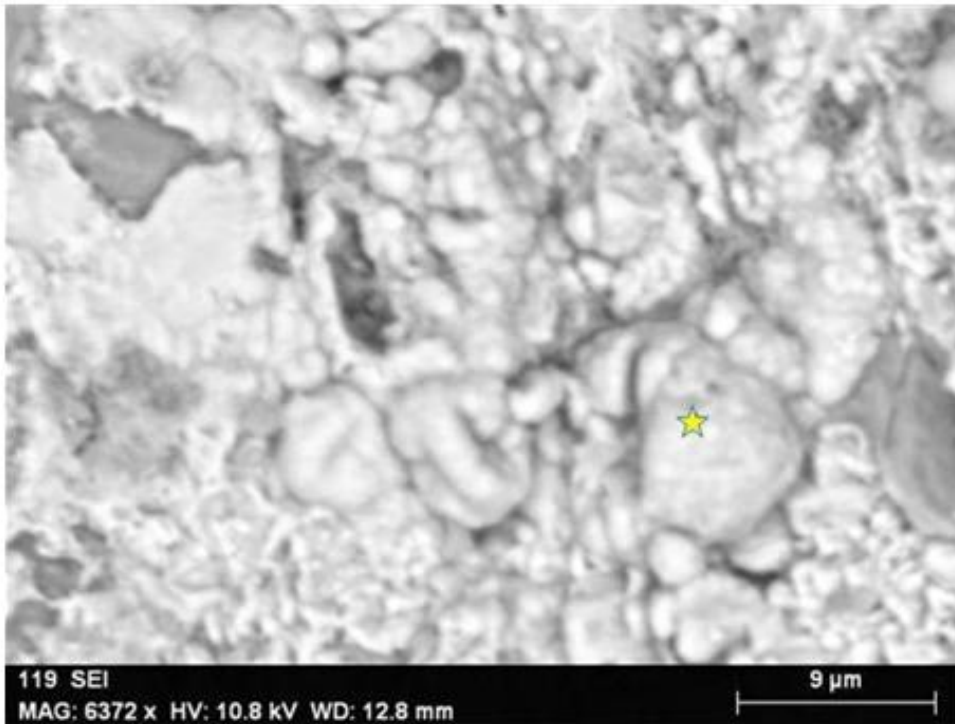


Figure 6.2.3-2. Deep corehole 88.9 ft depth sample: As-bearing “rubby” coating on fracture surface (EDS scan at point in photomicrograph). Coating contains Fe, As, Al, Si, and Ca.

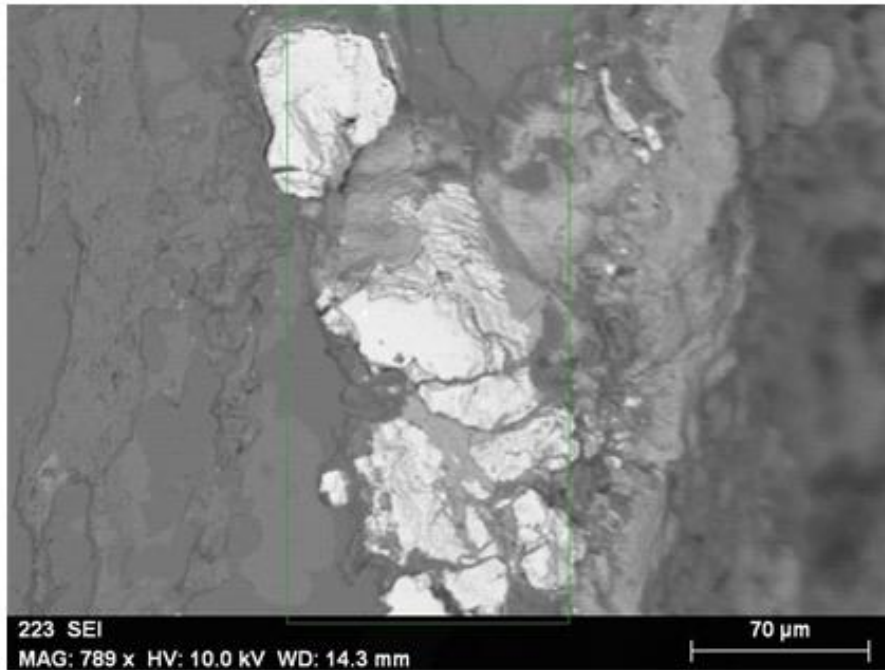


Figure 6.2.3-3(a). 97.9 ft depth: Arsenopyrite fracture mapping area BSE

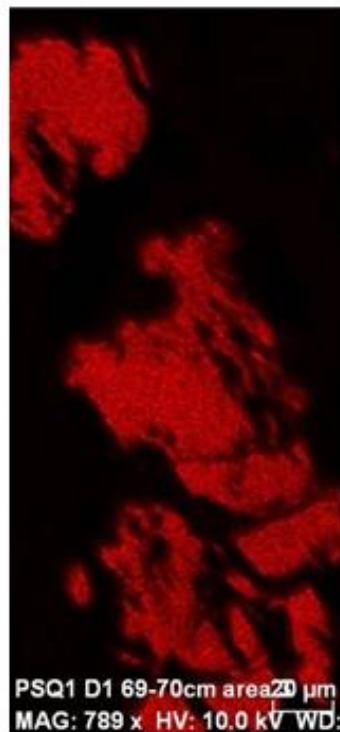


Figure 6.2.3-3(b). 97.9 ft depth: Arsenopyrite fracture mapping area; As (blue), S (red)

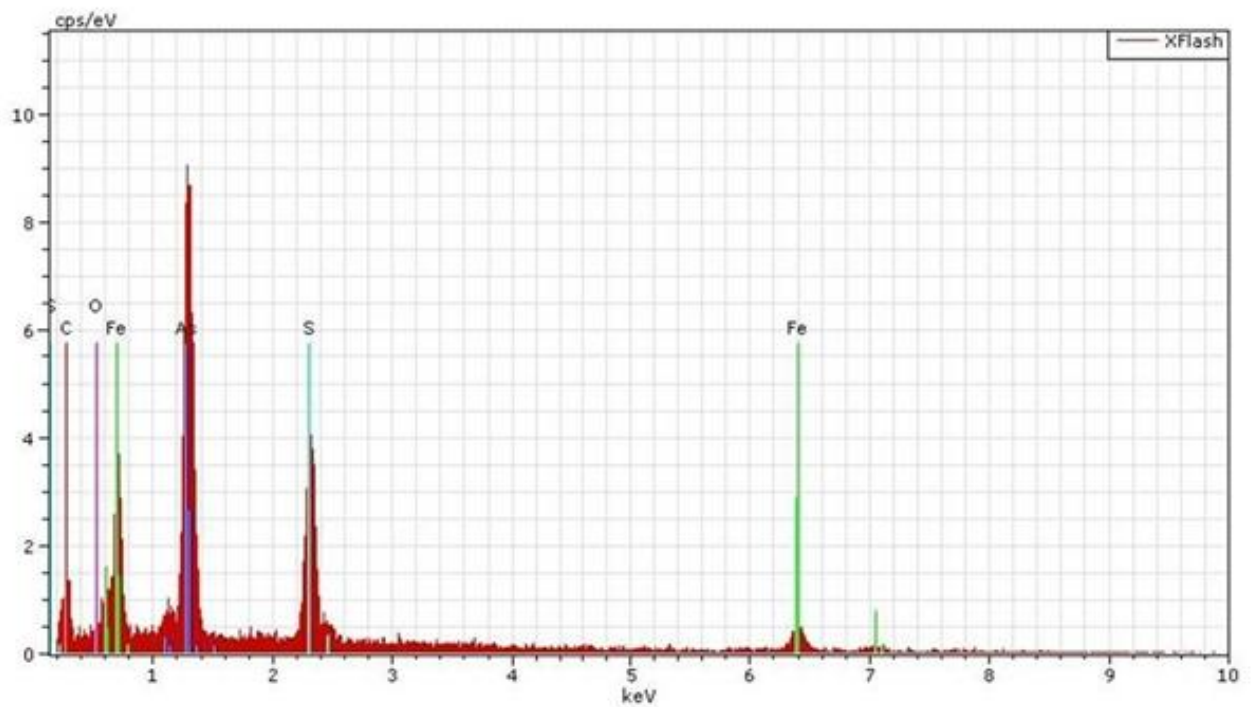
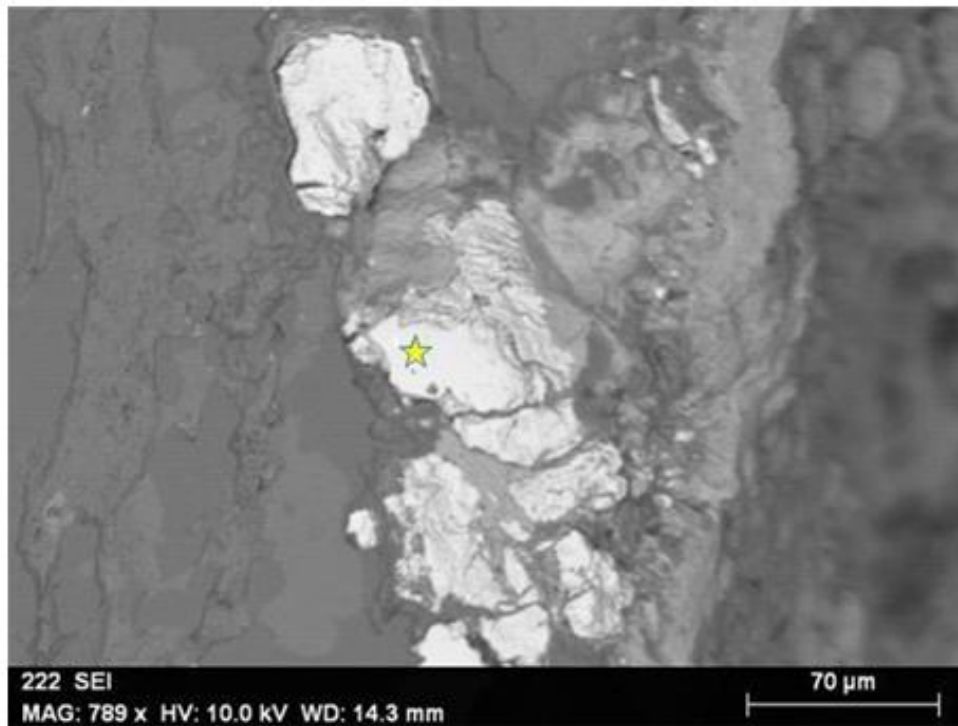


Figure 6.2.3-4. 97.9 ft depth: Arsenopyrite (EDS scan at point in photomicrograph); identification is based on presence of Fe, As, and S.

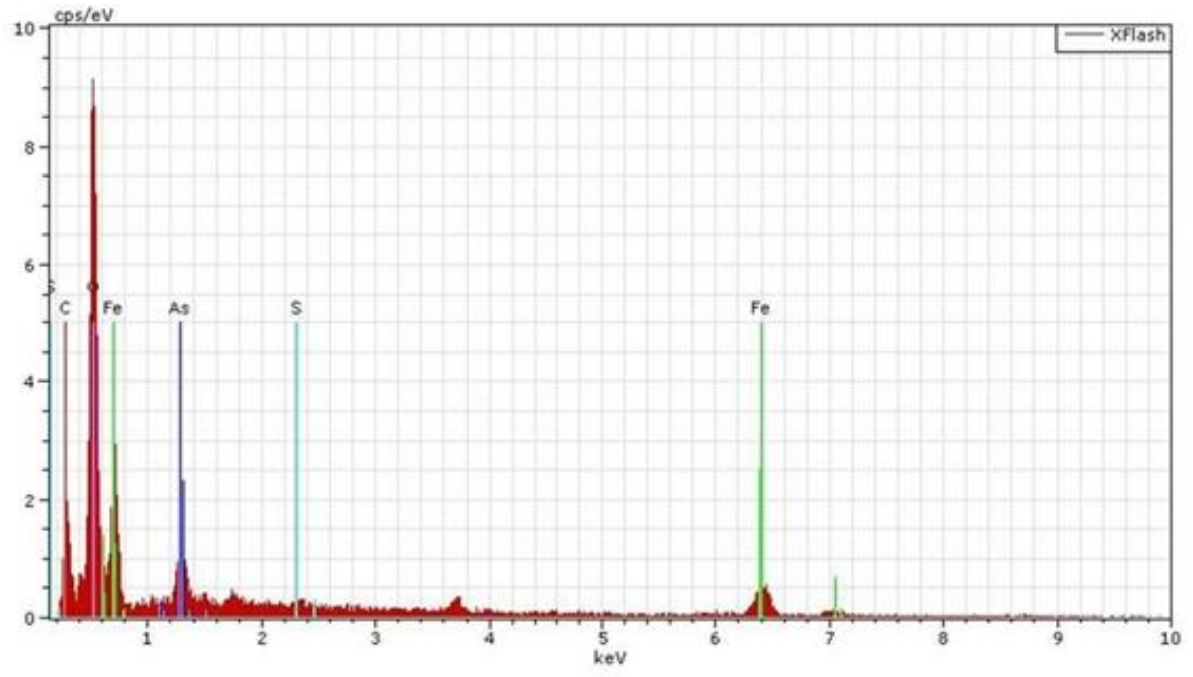
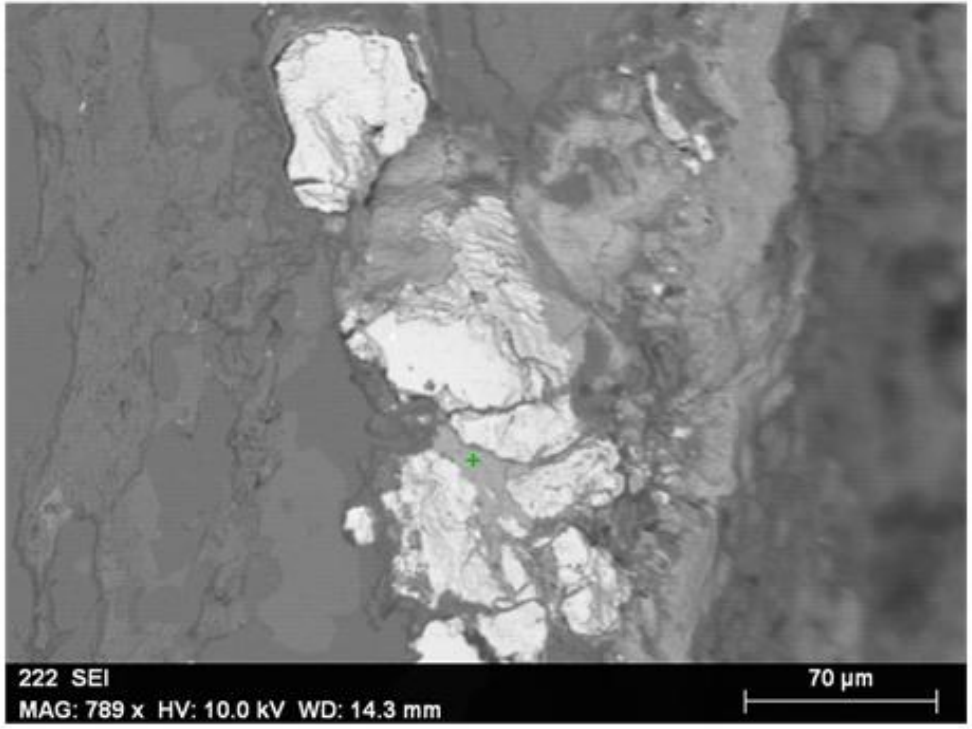


Figure 6.2.3-5. Deep corehole 97.9 ft depth: coating adjacent to arsenopyrite (EDS scan at point in photomicrograph), inferred to be As-bearing Fe-oxide based on absence of S.

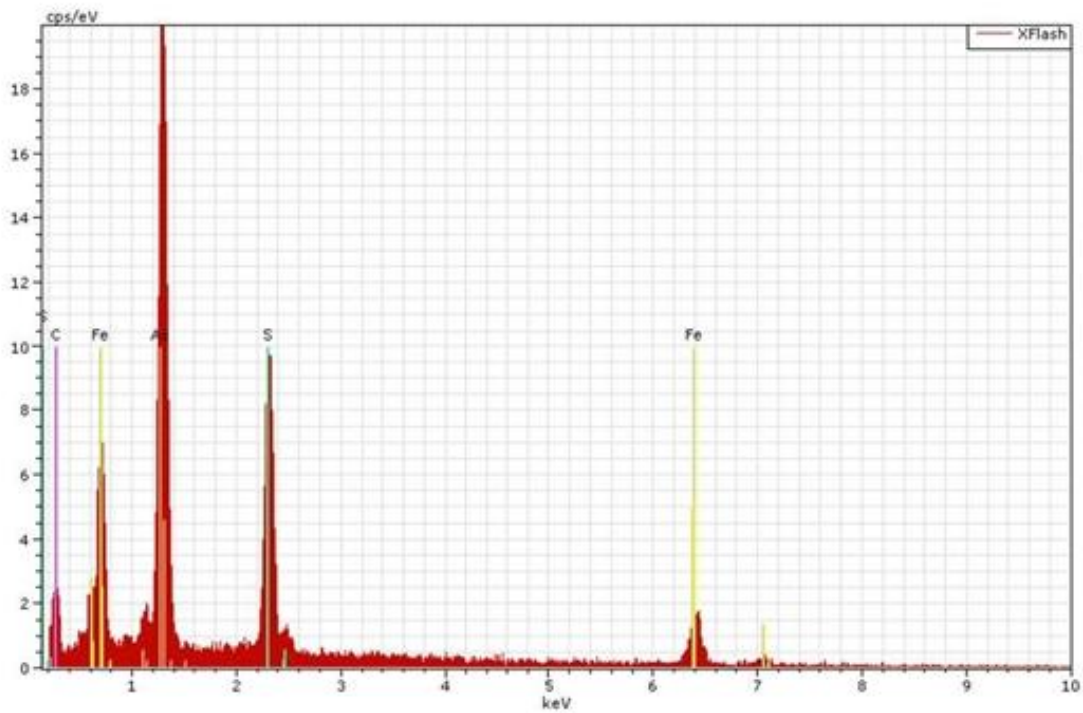
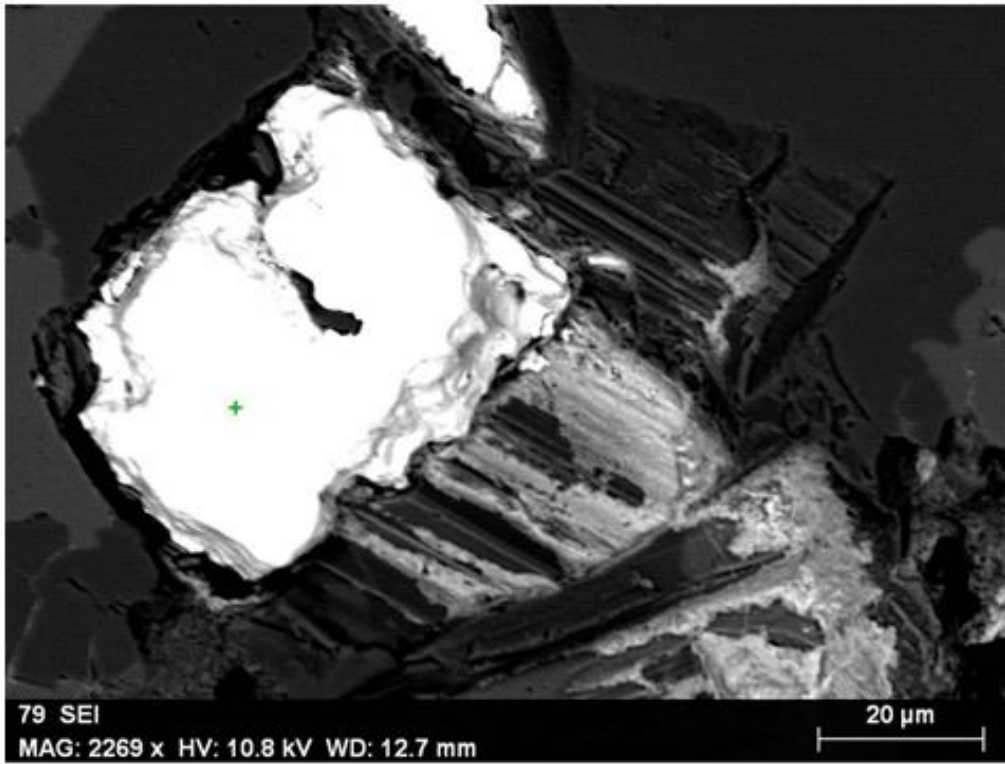


Figure 6.2.3-6. Deep corehole 97.9 ft depth: Arsenopyrite grain (bright area) with corroded margins (EDS scan at point in photomicrograph).

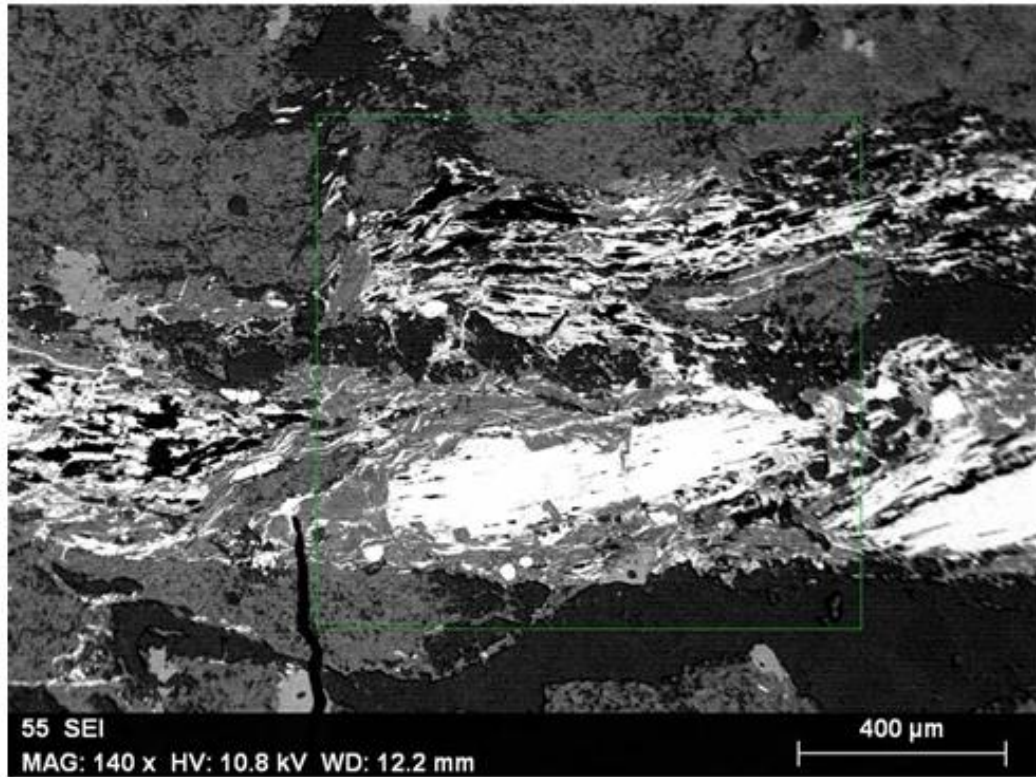


Figure 6.2.3-7(a). Deep corehole 125.7 ft depth: BSE image of mapping area

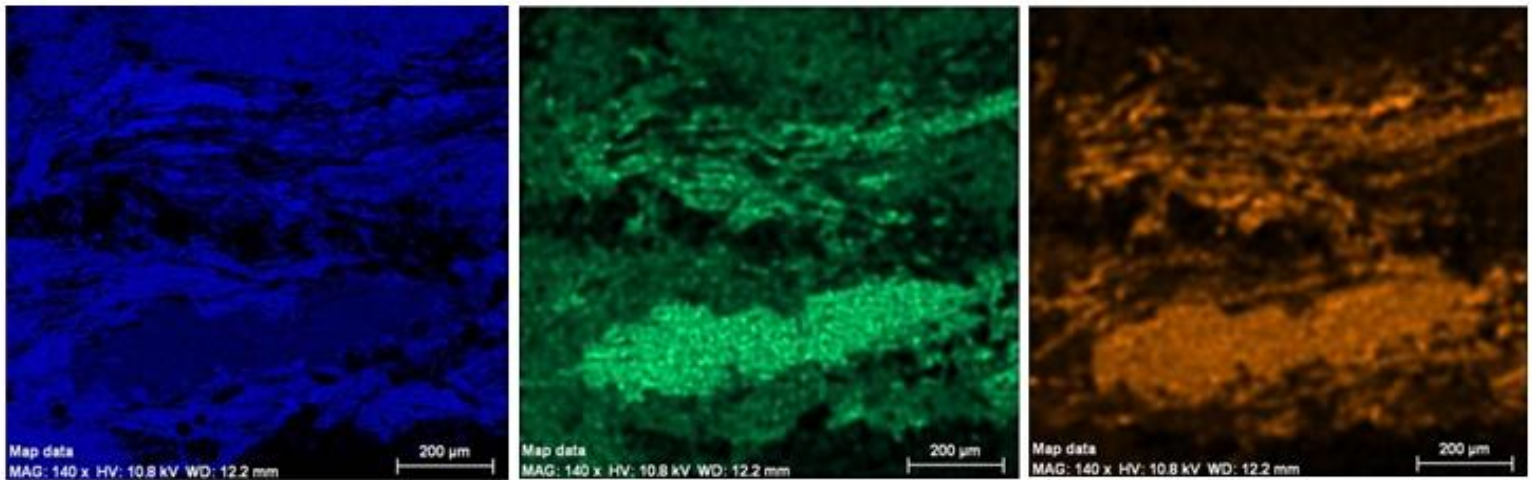
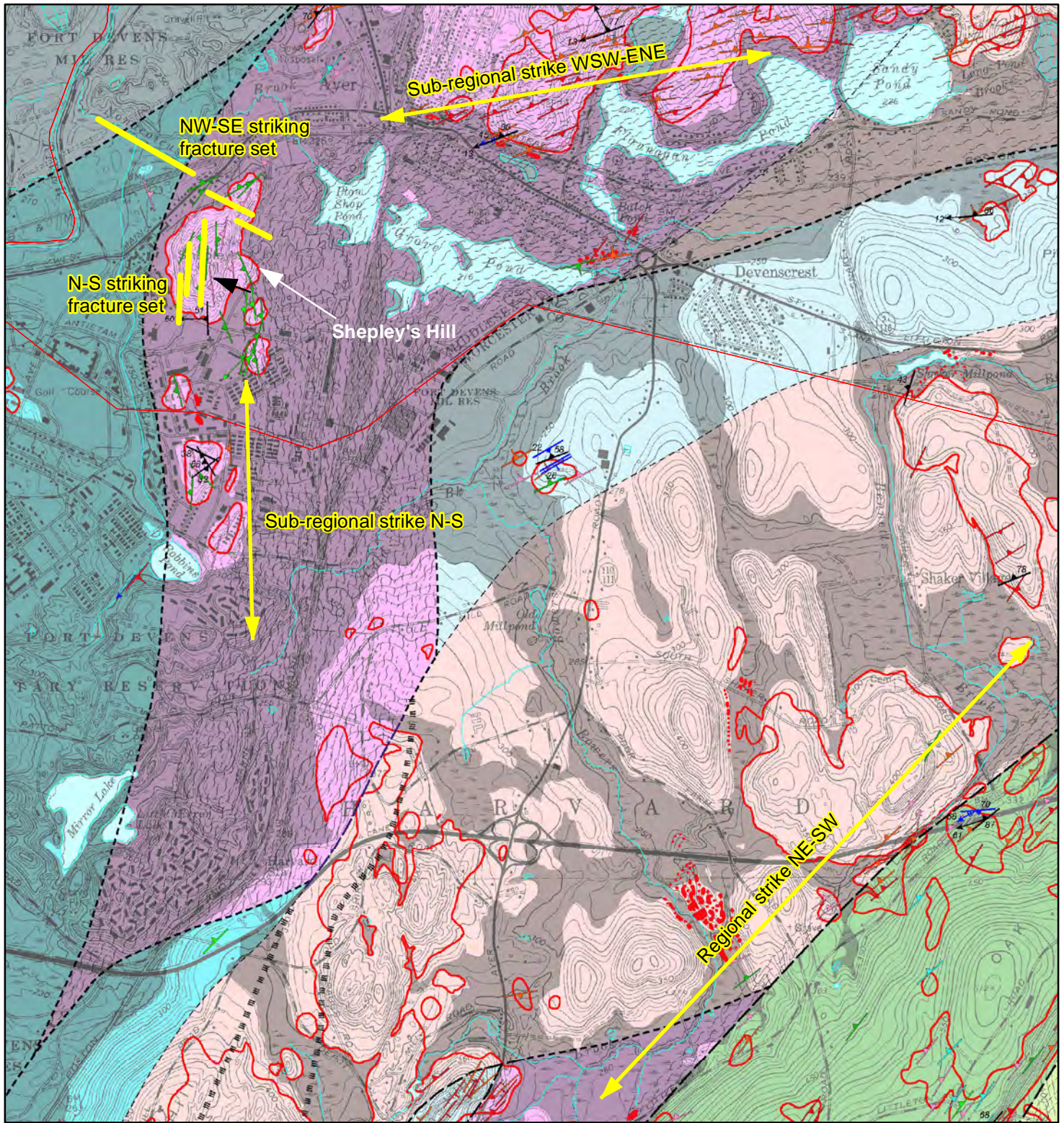


Figure 6.2.3-7(b). Deep corehole 125.7 ft depth: mapping area; Al (blue); As (green); Fe (orange). These images suggest that As is present with Feoxide and aluminosilicate minerals (possibly biotite?).



0 0.25 0.5 0.75 1 Miles



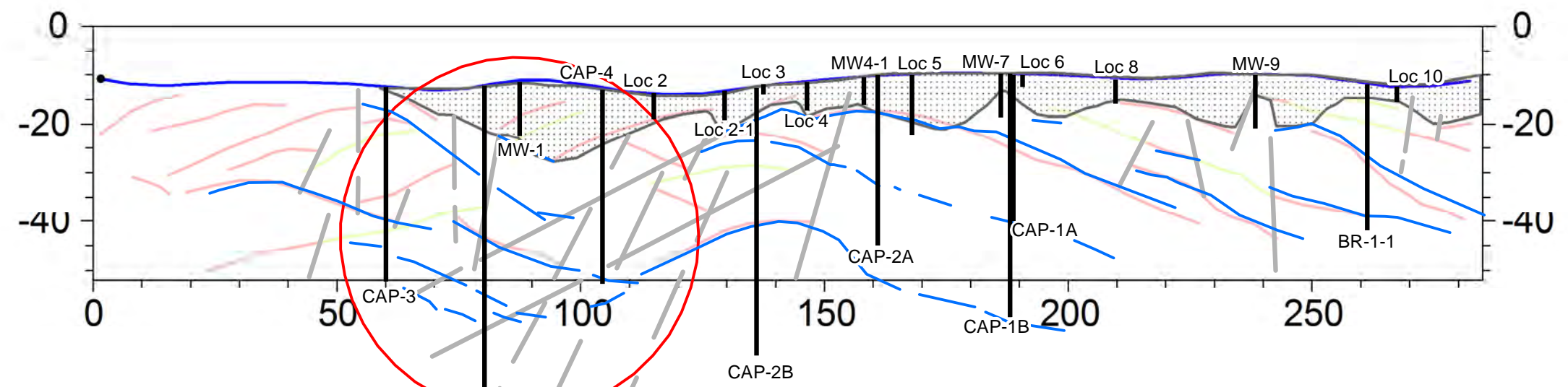
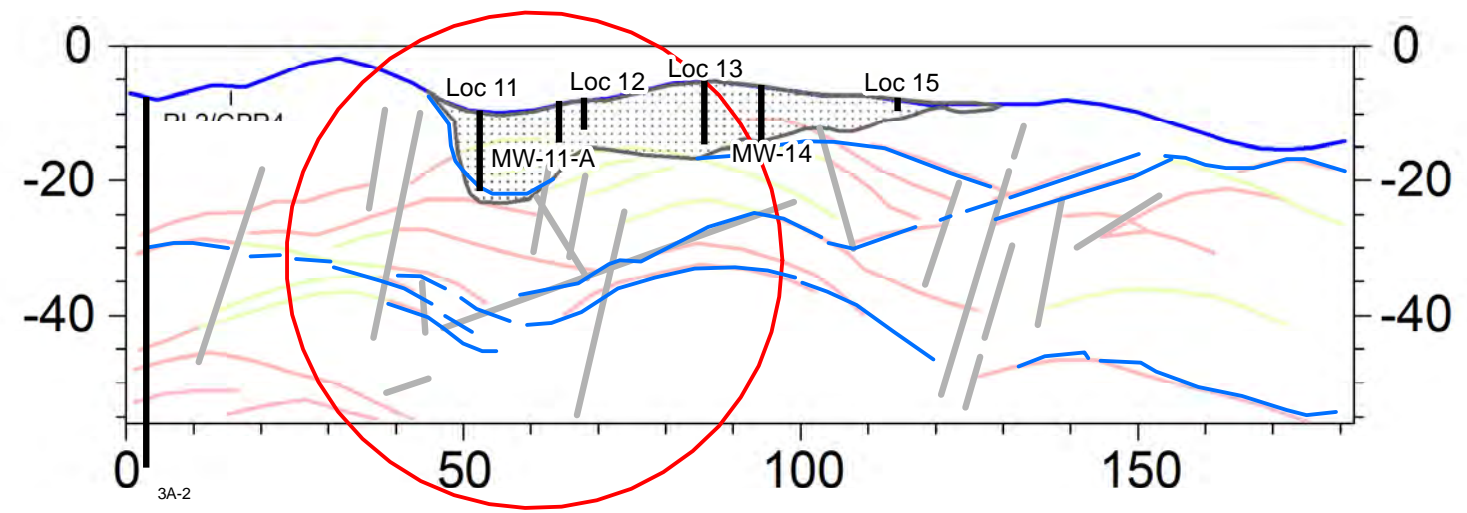
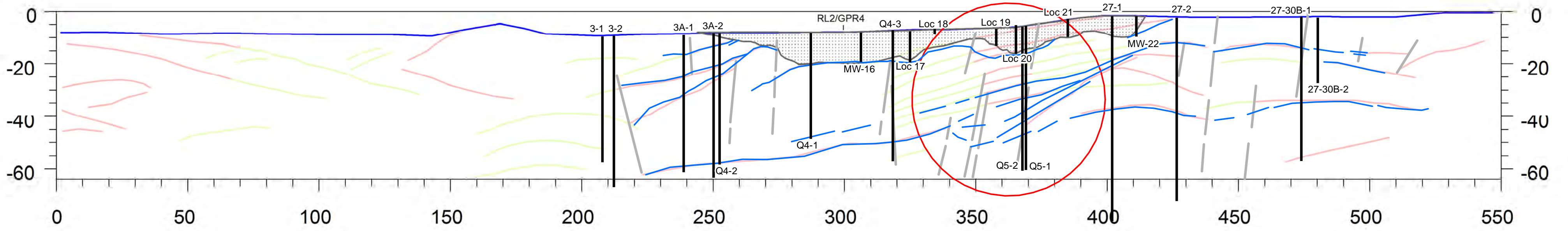
Figure 7.1.1
Sub-regional geology
and fracture features

Shepley's Hill
 Bedrock Investigation 2009
 Devens, MA



Map Tracker ID=6725
 Created by the US EPA Region 1 GIS Center on 4/21/2011

This map is based on "PRELIMINARY FRACTURE CHARACTERIZATION
 MAP OF THE AYER QUADRANGLE, MASSACHUSETTS
 HYDROSTRUCTURAL DOMAIN MAP"
 By Joseph P. Kopera, Stephen B. Mabee, and Devon C. Powers



Legend

- MW
| Existing Borings / Wells
- GPR Reflectors, Larger Aperture Fractures
- GPR Reflectors, Fractures
- Laterally Extensive Sheeting Fractures
- Steeply Dipping Fractures
- ▨ Overburden
- Core of Nona-Shep Fracture Zone

Figure 7.3-1
North-south interpretive geologic
cross sections at site scale

Shepley's Hill
Bedrock Investigation 2009
Devens, MA



Map Tracker ID=6725
Created by the US EPA Region 1 GIS Center on 3/14/2011

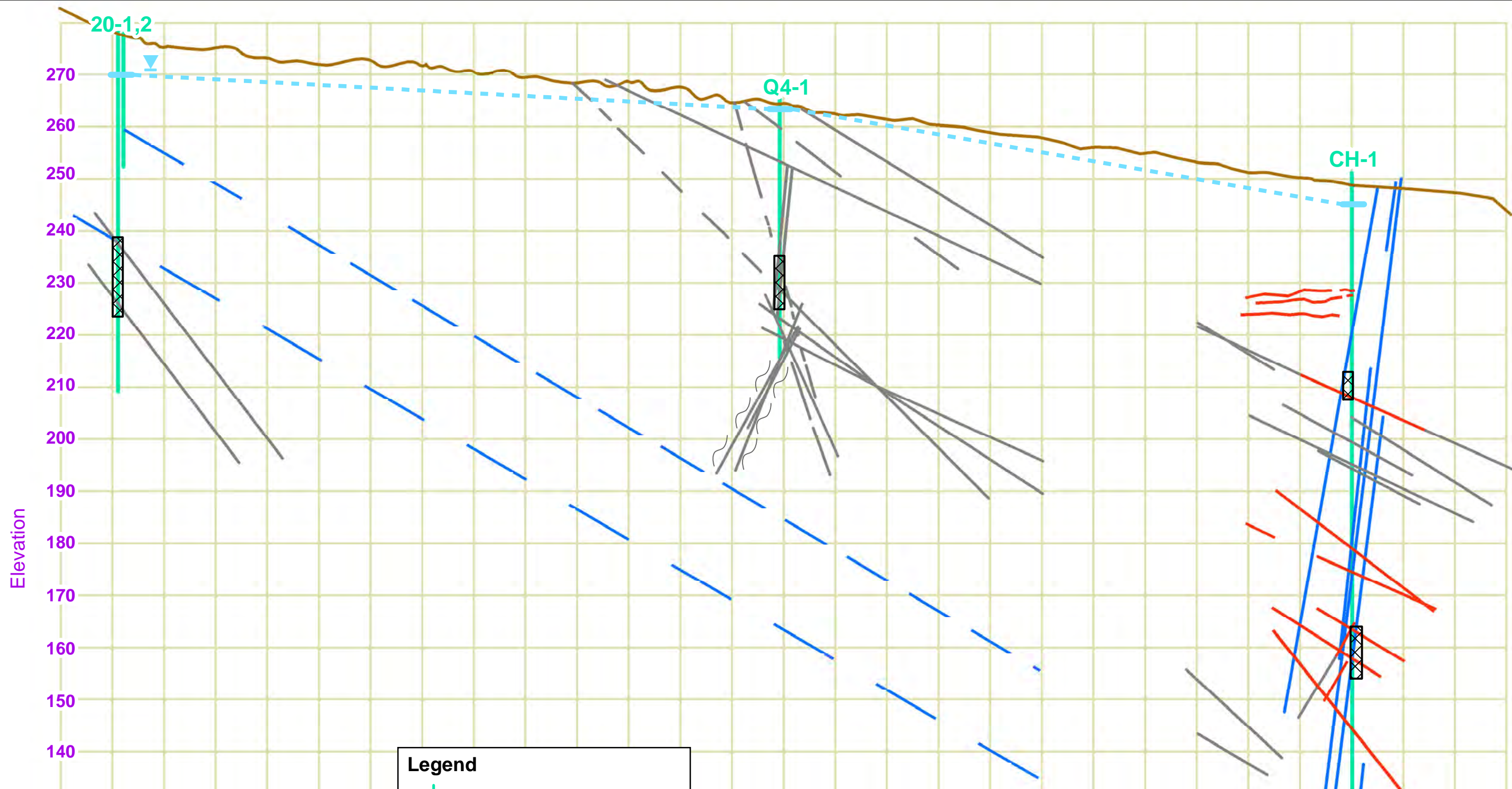


Figure 7.3-2
East-west interpretive geologic
cross section
 Shepley's Hill
 Bedrock Investigation 2009
 Devens, MA



Legend

- Monitoring Well
- Screened Interval
- Steeply Dipping Fractures
- Highly Oxidized Fractures
- Sheeting Fractures
- Foliating Parallel Fractures

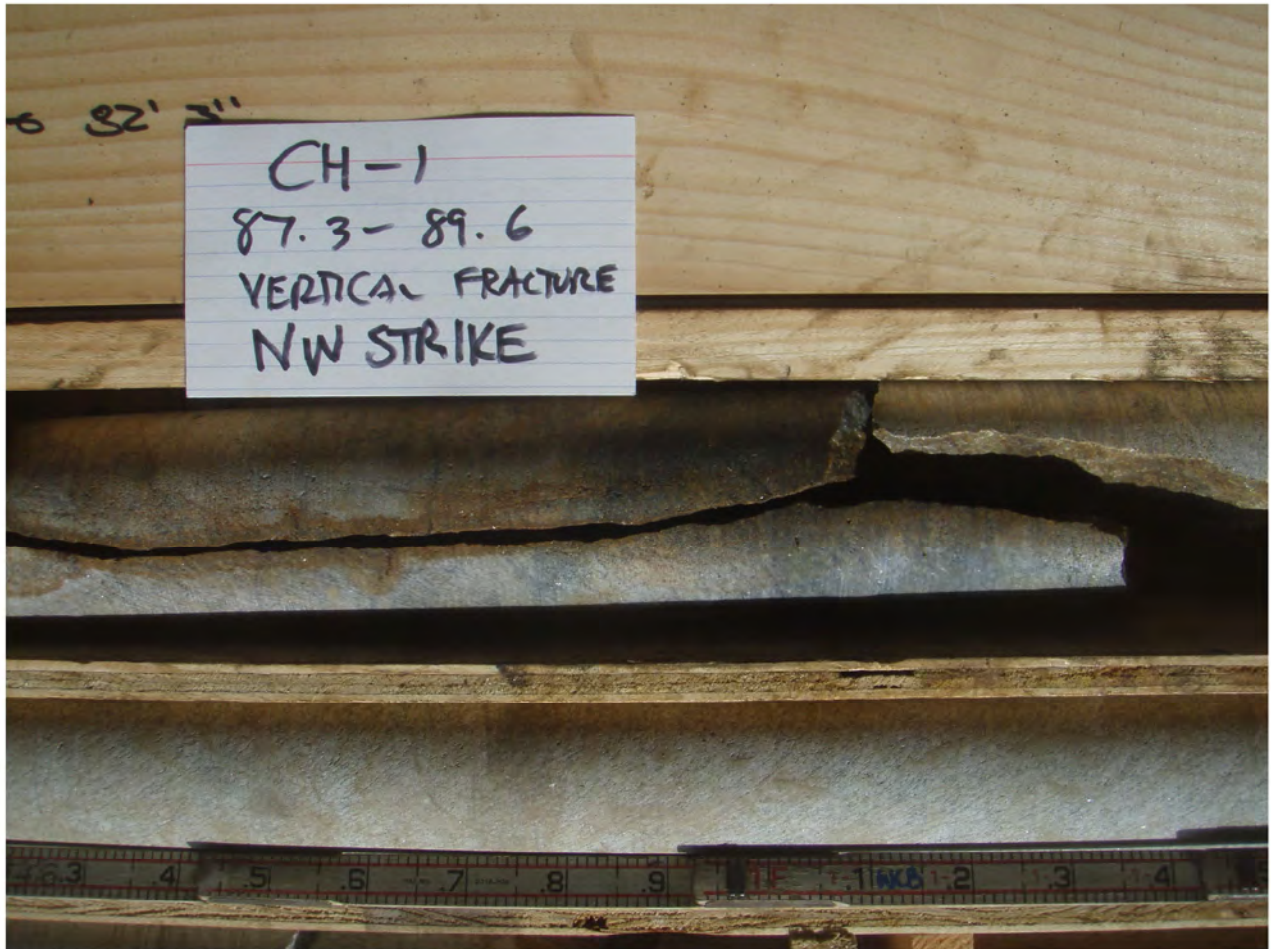


Figure 7.3-3
Photograph of northwest-striking
subvertical fracture intersected
by CH-1, 87.3-89.6 ft bgs

Shepley's Hill
Bedrock Investigation 2009
Devens, MA



Map Tracker ID=6725
Created by the US EPA Region 1 GIS Center on 4/21/2011

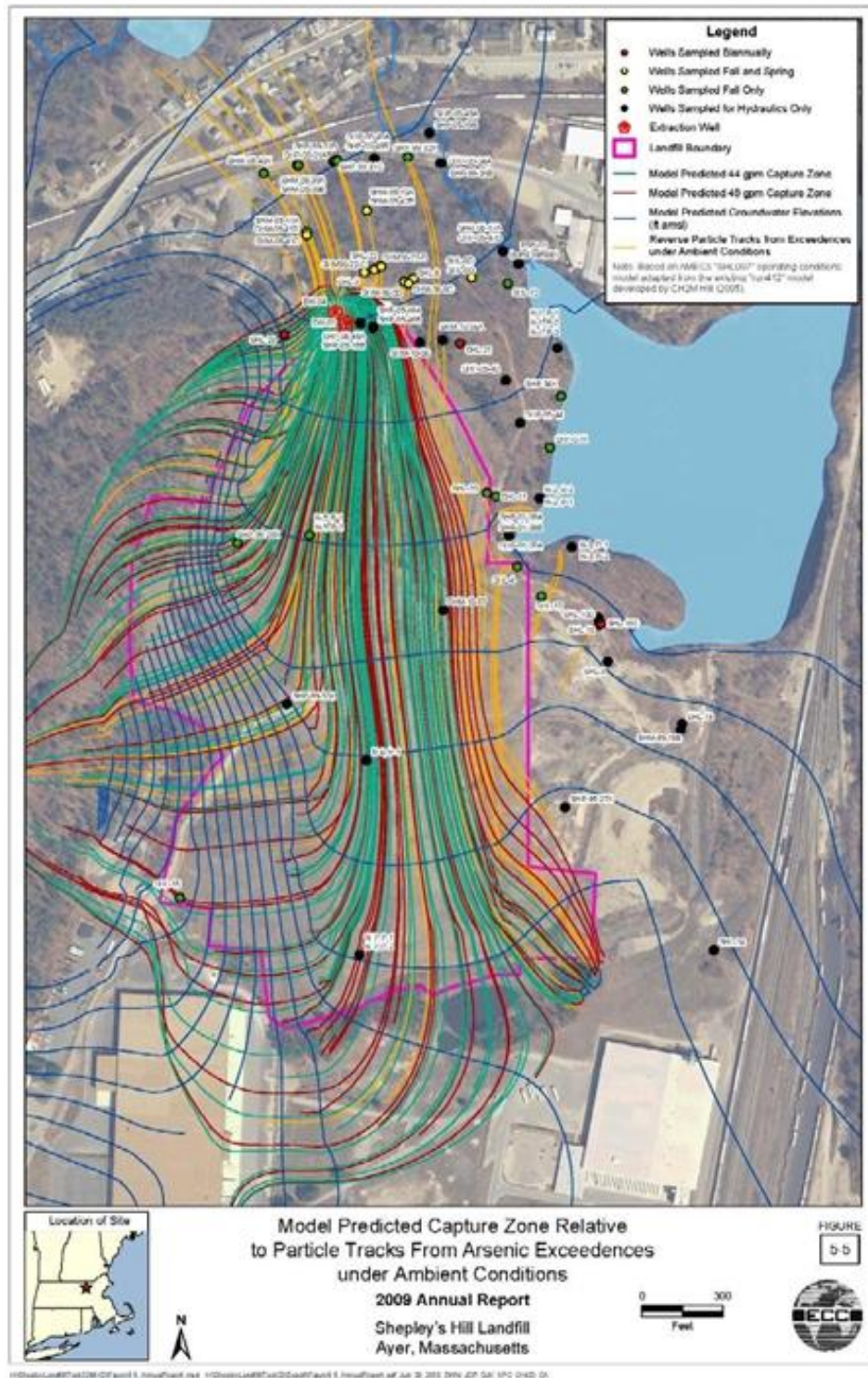


Figure 8.0-1: Modeled particle tracks under ambient conditions and with groundwater extraction at 44 and 49 gpm (combined) at EW-01 and EW-04. From ECC (2009).

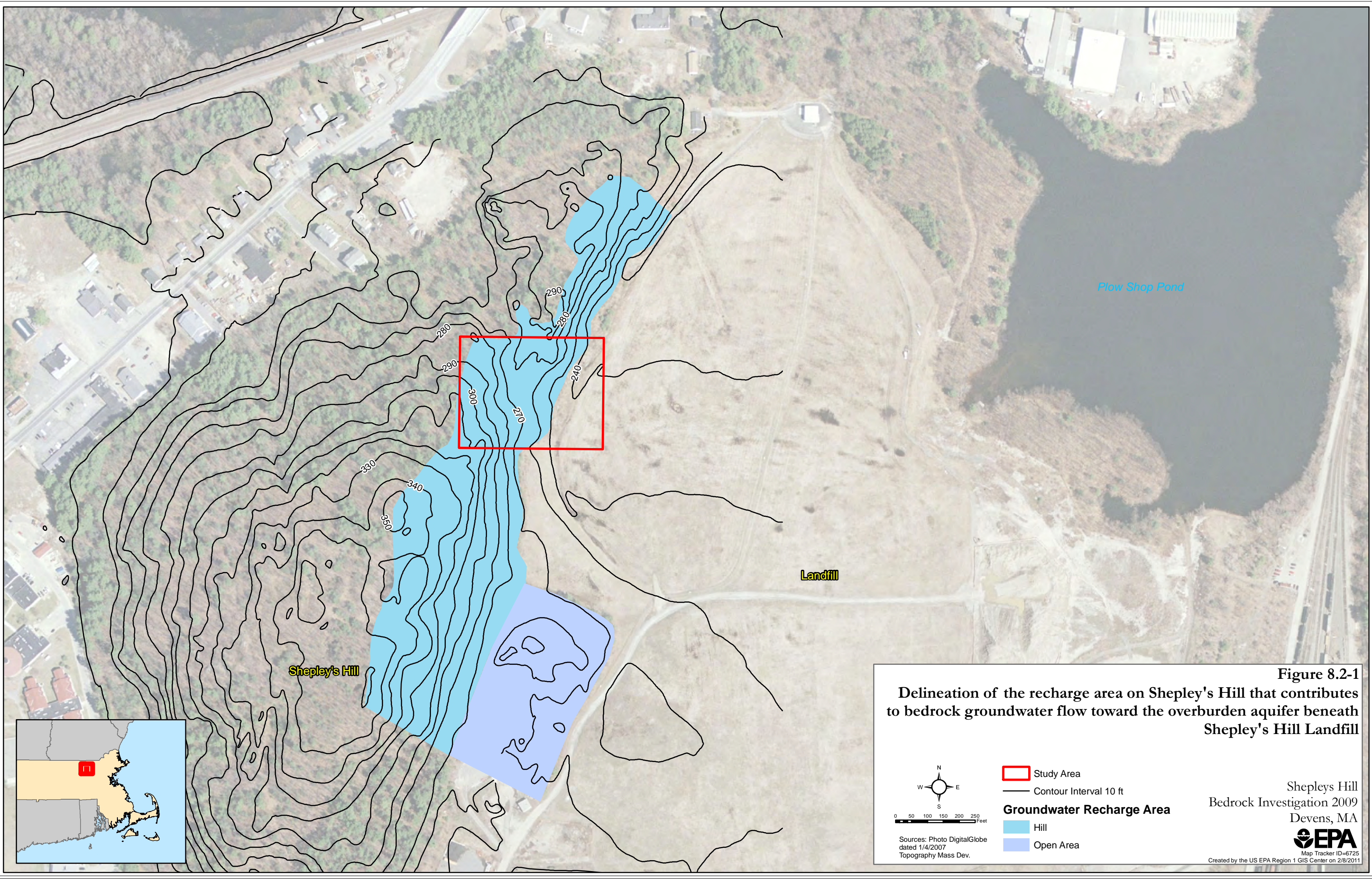
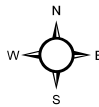
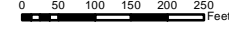


Figure 8.2-1
Delineation of the recharge area on Shepley's Hill that contributes to bedrock groundwater flow toward the overburden aquifer beneath Shepley's Hill Landfill

Sources: Photo DigitalGlobe dated 1/4/2007
 Topography Mass Dev.

Study Area
 Study Area
 Contour Interval 10 ft

Groundwater Recharge Area
 Hill
 Open Area

Shepleys Hill
 Bedrock Investigation 2009
 Devens, MA

 Map Tracker ID=6725
 Created by the US EPA Region 1 GIS Center on 2/8/2011

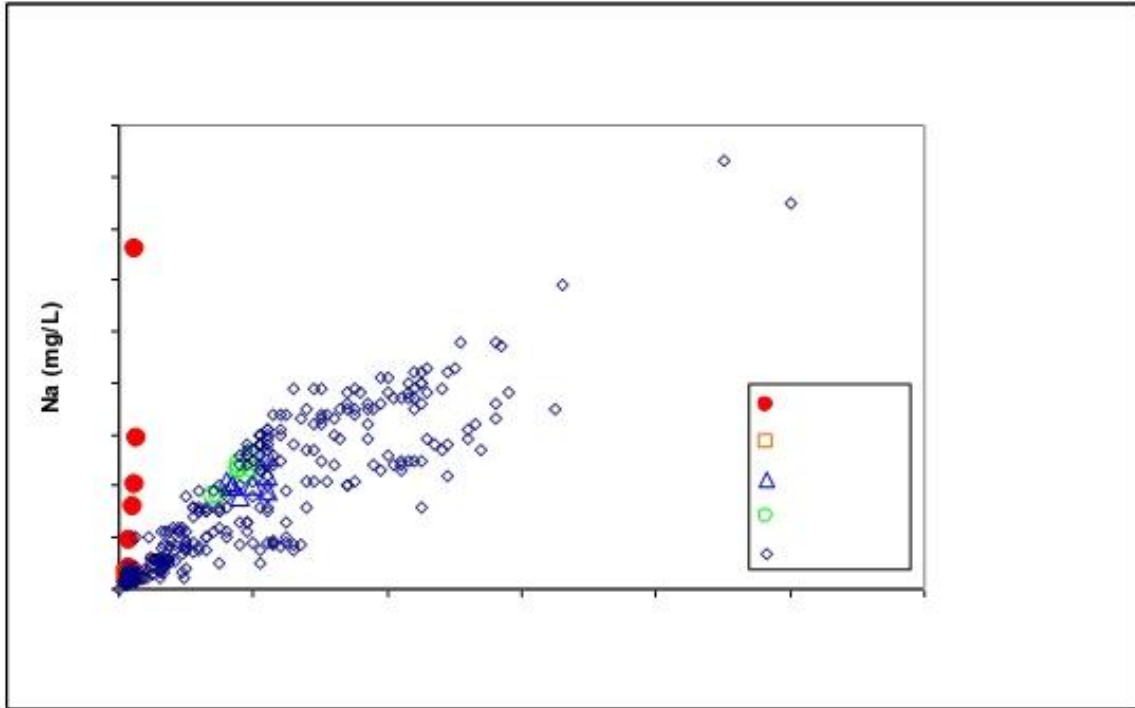


Figure 9.3-1. Sodium and chloride in groundwater from the new bedrock wells. Sodium values in bedrock groundwater are comparable to those reported from the Long-Term Monitoring Program, while chloride is at the low end of the range.

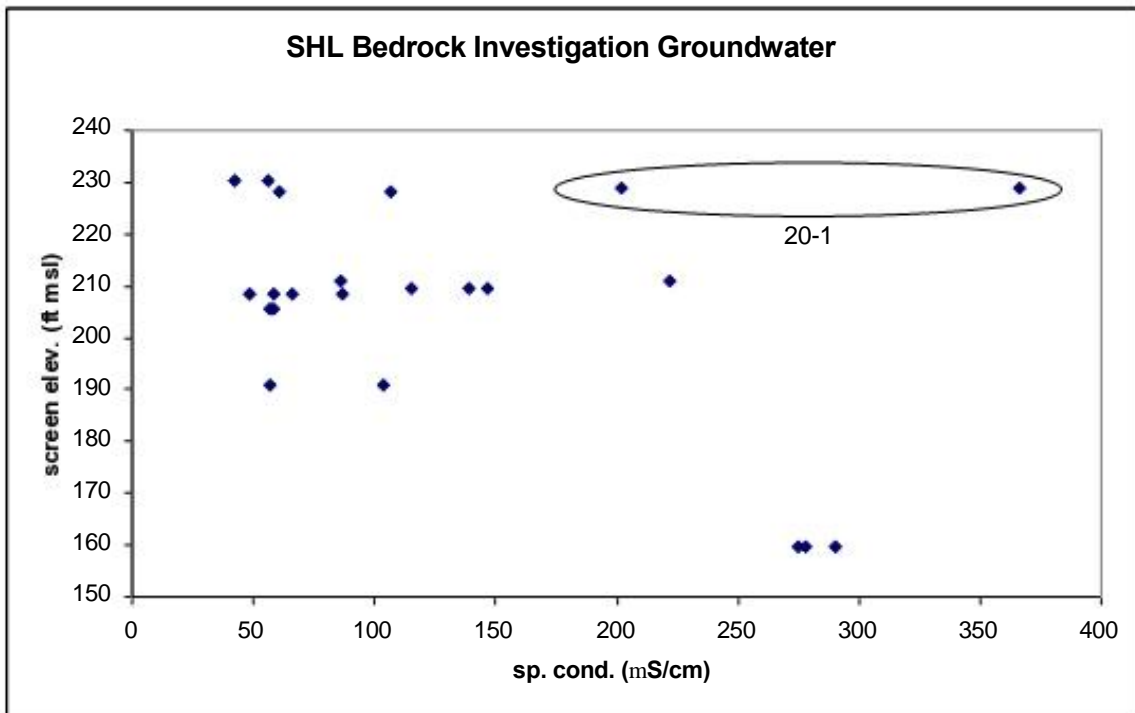


Figure 9.3-2(a). Specific conductivity in bedrock groundwater as a function of screen elevation. Note that bedrock well 20-1 is anomalously high, with an average specific conductivity comparable to the deepest screen (CH-1D).

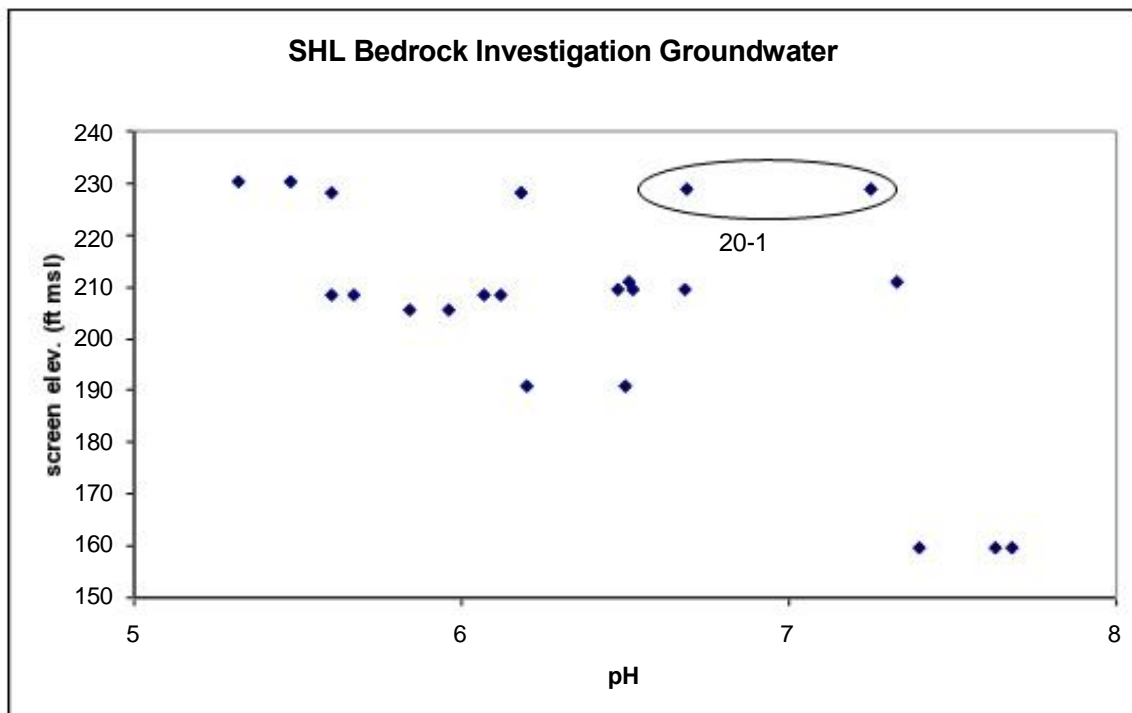


Figure 9.3-2(b). pH in bedrock groundwater as a function of screen elevation. Note that the average pH in bedrock well 20-1 is somewhat elevated in comparison to groundwater from other wells of similar depth.

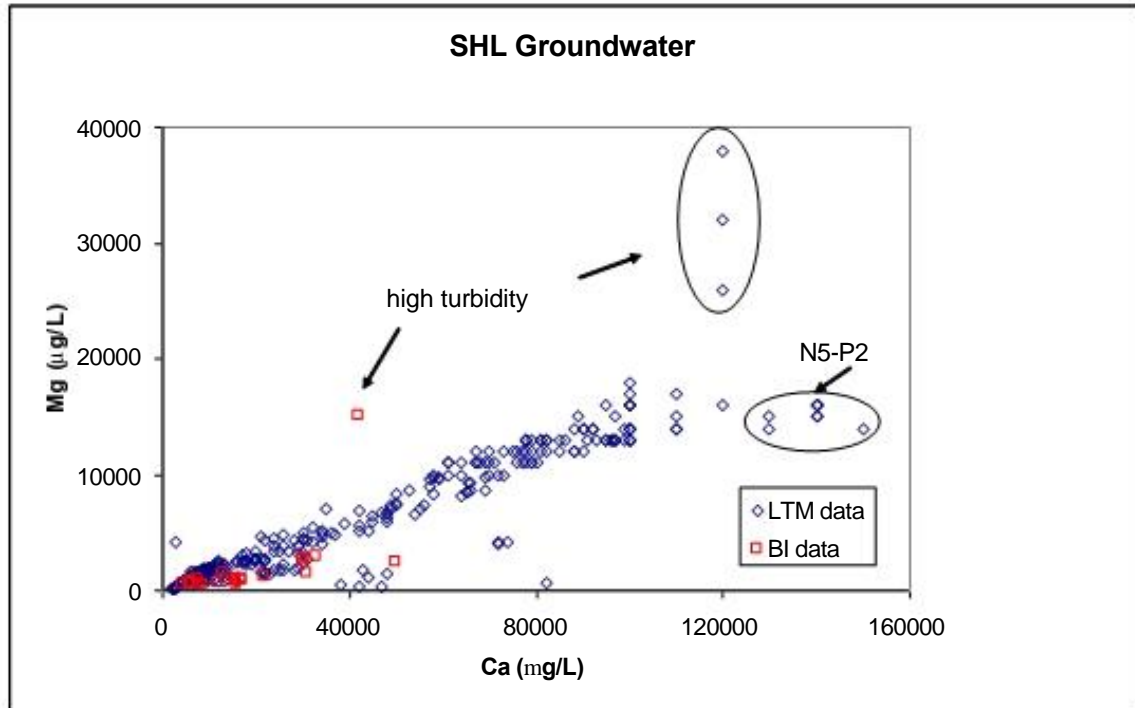


Figure 9.3-3. Calcium and magnesium in bedrock wells. Both Ca and Mg are low in comparison to results from the Long-Term Monitoring Program and may reflect different geochemical controls on solubility in the new bedrock wells in comparison to reactions involving Ca and Mg in overburden groundwater.

TABLES

Table 5.3.2-1: Shallow Bedrock Borehole Characteristics

Borehole	Length from gs (ft)	Diameter (in)	Angle down from horiz (degrees)	Azimuth (degrees)	OB thickness (ft)	Well installed?	Notes
CAP-1B	54.9	3.5	90		7		
CAP-2B	58.7	3.5	90		8	Y	
CAP-3	40.91	3.5	90		6		
CAP-4	13.8	3.5	90		9		collapsed
3-1	48.9	4	58	342	0		
3-2	59.2	4	90		0	Y	
3A-1	52.2	4	80	327	0		
3A-2	54.9	4	90		0		
20-1	68.7	4	90		0	Y	
20-2	25.2	4	90		0		
27-1	79	3.5	60	180	0	Y	
27-2	71.6	3.5	59	40	0	Y	
Q5-1	54.7	3.5	75	213	0	Y	
Q5-2	55.5	3.5	65	28	0		
Q4-1	50.8	4	90		7.5	Y	
Q4-2	53	3.5	90		8.5		
27_30B-1	59	3.5	90		0	Y	
27_30B-2	22.25	3.5	90		0		

Table 5.7-1: Hydraulic Conductivity Inferred from Slug Tests in Open Bedrock Borings

Borehole	Date	Saturated L (ft)	K (ft/day)		K (cm/s)		Average (ft/day)
			Falling	Rising	Falling	Rising	
3-2	9/4/2008	26.12	2.70E+00	3.52E+00	9.53E-04	1.24E-03	3.11E+00
3A-2	9/4/2008	25.11	7.99E+01	1.20E+02	2.82E-02	4.23E-02	9.99E+01
3A-2	7/30/2009	26.93	7.55E+01	1.13E+02	2.66E-02	4.00E-02	9.44E+01
Q4-1	9/10/2009	37.49	1.21E+00	1.33E+00	4.28E-04	4.70E-04	1.27E+00
3-1	7/30/2009	20.46	5.64E+00	6.79E+00	1.99E-03	2.40E-03	6.21E+00
27-2	7/30/2009	55.54	9.17E+00	1.04E+01	3.24E-03	3.68E-03	9.80E+00
27-1	7/30/2009	68.71	1.07E+00	7.85E-01	3.77E-04	2.77E-04	9.27E-01
20-1	8/4/2009	50.42	6.89E-02	6.43E-02	2.43E-05	2.27E-05	6.66E-02
27-30B-1	8/4/2009	44.47	2.95E+01	2.95E+01	1.04E-02	1.04E-02	2.95E+01
Q5-1	8/4/2009	48.27	8.35E-01	7.06E-01	2.94E-04	2.49E-04	7.70E-01
Q5-2	8/4/2009	52.85	3.60E-01	9.78E-02	1.27E-04	3.45E-05	2.29E-01
Q4-2	8/4/2009	40.46	8.81E-01	7.38E-01	3.11E-04	2.60E-04	8.10E-01
CAP-2B	8/4/2009	48.76	1.49E-01	5.95E-01	5.27E-05	2.10E-04	3.72E-01
3A-1	10/23/2009	21.84	4.69E+00	1.63E+00	1.65E-03	5.75E-04	3.16E+00
20-2	10/23/2009	7.28					
27-30B-2	10/23/2009	1.08					
CAP-1B	10/23/2009	44.83	5.84E-01	5.90E-01	2.06E-04	2.08E-04	5.87E-01
CAP-4	10/23/2009	3.42					
CAP-3	10/23/2009	25.67	1.68E+01	1.42E+01	5.94E-03	5.02E-03	1.55E+01

Table 5.9-1 Screen Intervals for Shallow Bedrock Monitoring Wells

Location	Angle from vertical	Screen interval (ft bgs) [1]	Target
3-2	90°	60 - 55	chip log shows oxidized zone ~60 ft bgs; caliper breakout ~56 ft bgs; HPFM flow entering ~50 - 54 ft bgs
Q4-1	90°	42 - 32	caliper breakout ~34.5 ft bgs; HPFM increase above 34.5 ft bgs; ATV shows low-angle fractures ~34 ft bgs and ~37 ft bgs
20-1	90°	55.7 - 40.7	fast hydraulic response seen in transducer records; HPFM flow enters in ~50 - 54 ft bgs interval; discrete fractures ~39.5 ft bgs and ~42 ft bgs; high on hill
27-1	60°	66.2 - 61.2	angled into “valley” feature; change in resistivity and HPFM ~60 ft bgs
27-2	59°	70.4 - 60.4	HPFM indicates strong downflow in deep interval
27-30B-1	90°	46.3 - 36.3	“gusher” when drilling ~42 ft bgs; caliper breakout ~42 ft bgs; HPFM increase and fluid resistivity change ~37.5 ft bgs
Q5-1	75°	54.3 - 49.3	angled into “valley” feature; caliper breakout ~48 ft bgs;
CAP-2B	90°	59 - 54	ATV shows prominent fractures ~23 and ~31 ft bgs; boring collapse prevented installation of shallow paired well

[1] measured along boring for angled holes

Table 5.9-2: Development of Shallow Bedrock Wells

Well	Date Drilled	Date of Well Installation	Date Developed	Pump	Volume (gal)	Number of Well Volumes	Comments
3-2	2/11/2008	9/24/2009	9/24/2009	footvalve	3.5	1.5	fairly clear; well displaced ~1.5 ft
Q4-1	2/11/2008	9/25/2009	9/28/2009	submersible	15	7.7	clear
20-1	2/11/2008	9/24/2009	10/14/2009	footvalve	7.5	3.1	fairly clear
27-1	9/18/2008	9/23/2009	9/24/2009	footvalve	20	5.5	fairly clear; well displaced ~0.75 ft
27-2	9/18/2008	9/23/2009	9/28/2009	submersible	15	4.2	fairly clear
27-30B-1	9/18/2008	9/24/2009	9/28/2009	submersible	14	7.4	very clear; purged dry
Q5-1	9/18/2008	9/24/2009	9/24/2009	footvalve	30	8.5	silty; slow recharge
CAP-2B	9/18/2008	9/24/3009	10/13/2009	peristaltic	15	5.7	clear

Table 7.3-1: Site-Scale Fracture Network Summary

Feature Type	Feature Class	Strike Orientation	Strike Length (ft)	Dip and Direction	Dip Length (ft)	Spacing (ft)	Comment
Sheeting Fractures	Major	NE-SW to N-S	≥ 200	10 ^o - 50 ^o east	≥ 100	≤ 20 -30	More heavily oxidized in uppermost 50 ft of bedrock; oxidized to greater depths near intersections with major steep features
Nona-Shep Fracture zone	Major	NW-SE to NNW-SSE	>100	60 ^o To near vertical; dips to SW	>100	≤ 10 to ≥ 20	Trace of Nona-Shep Fault Zone steps to south within study area; Fracture-spacing is ≤ 10 ft within 50 of fault axis and ≥ 20 feet outside of axial zone.
N-S Joints	Major	N-S	≥ 50	Sub-vertical	≥ 50	≤ 50	Potential for major N-S fracture system beneath landfill cap adjacent to study area
E-W fractures	Major	E-W	~50	60 ^o To near vertical; dips to S	~50	≤ 20	cross-connect individual NW-SE striking fractures of Nona-Shep fracture Zone; less significant away from Nona-Shep zone
Sub-horizontal fractures	Minor	Various	20-30	flat	20-30	≤ 70	occur in tightly-spaced groups proximal to steeply dipping fractures; connects sheeting fractures and steeply-dipping fractures
Foliation-parallel joints	Minor	NE-SW to NNE-SSW	≤ 20	50 ^o - 60 ^o west	≤ 20	>50	Limited oxidation where associated with intersecting steep fractures.
Steeply dipping; NE-SW striking	Minor	NE-SW to NNE-SSW	<50	> 60 ^o west	<50	>50	Conjugate to NW-SE striking structures

Table 9.2-1. Bedrock Borehole Water Chemistry

Wells	Screen Elev.	Sample Date	uS/cm Sp. Cond.	pH	mV ORP	mg/L DO	NTU turb.	mg/L Br	mg/L Cl	mg/L F	mg/L Nitrate	mg/L Nitrite	mg/L Sulfate	mg/L o-Phosphate	mg/L total P
CAP-2B	190.9721	11/5/2009	57	6.5	172.6	2.09	3.6	0.1	1.7	0.15	0.2	1.1	8.6	0.03	11
	190.9721	3/16/2010	104	6.2	251.7	5.21	2.57	0.1	1.6	0.17	5.8	0.1	9.9	0.5	
CH-1S	211.0062	11/5/2009	222	7.33	71.8	4.74	834.2	0.1	2.6	0.61	0.2	1.4	25	0.03	257
	211.0062	3/16/2010	86	6.51	282.2	9.93	62.4	0.1	1.6	0.15	5.3	0.1	8.2	0.5	
Q5-1	208.3229	11/5/2009	87	6.12	289.4	1.97	6.6	0.1	1.2	0.12	0.2	0.91	8.2	0.03	14
	208.3229	3/16/2010	66	6.07	349.1	6.38	0.44	0.1	1.6	0.1	4.9	0.1	8.5	0.5	
CH1-D	159.5062	11/5/2009	290	7.68	199.4	0.55	14.4	0.1	2.7	0.72	0.2	1.9	9.9	0.03	43
	159.5062	3/16/2010	278	7.4	163.6	-3.4	1.28	0.1	2.8	0.77	12	0.1	9.4	0.5	
	159.5062	6/22/2010	275	7.63	99.9	2.35	0.6	0.1	2.4	0.8	0.1	0.1	7.5	1	
Q4-1	228.129	11/5/2009	107	6.18	202.1	8.28	0.1	0.1	1.6	0.11	0.1	0.1	9.2	0.1	5.7
	228.129	3/16/2010	61	5.6	132.7	11.26	2.51	0.1	1.6	0.1	5.1	0.1	8.5	0.5	
3-2	209.4892	11/5/2009	139	6.68	210.6	13.45	7.4	0.1	1.6	0.21	0.1	0.1	8.9	0.1	15
	209.4892	3/16/2010	147	6.52	88.6	5.57	12.7	0.1	1.7	0.24	8.2	0.1	8.5	0.5	
	209.4892	6/24/2010	115	6.48	140.2	6.12	2.53	0.1	1.6	0.2	0.1	0.1	7.6	1	
27-1	205.7036	11/5/2009	57	5.84	218.5	10.8	17.9	0.1	1.2	0.1	0.1	0.1	8.4	0.1	64
	205.7036	3/16/2010	58	5.96	343.2	8.74	0.73	0.1	1.4	0.1	4.7	0.1	8.9	0.5	
20-1	228.9681	11/5/2009	366	7.25	214	17.13	4.77	0.1	2.1	0.33	0.1	0.1	35	0.1	9
	228.9681	3/16/2010	202	6.69	76.4	7.17	4.5	0.1	1.6	0.17	8.5	0.1	18	0.5	
27-2	208.4634	11/5/2009	58	5.67	232.8	8.5	5.31	0.1	1.3	0.1	0.1	0.1	9.9	0.1	12
	208.4634	3/16/2010	48	5.6	130	9.48	10.5	0.1	1.5	0.1	4	0.1	8.6	0.5	
27-30B-1	230.4214	11/5/2009	56	5.48	245.6	7.73	2.85	0.1	1.4	0.11	0.1	0.1	9.1	0.1	5
	230.4214	3/16/2010	42	5.32	150.2	9.26	0.42	0.5	1.5	0.1	3.9	0.1	8.6	0.5	

Bold = ND

Table 9.2-1. Bedrock Borehole Water Chemistry

Wells	Screen Elev.	Sample Date	mg/L alk	ug/L Al	ug/L As	ug/L Ba	ug/L Ca	ug/L Cr	ug/L Co	ug/L Cu	ug/L Fe	ug/L Pb	ug/L Mg	ug/L Mn	ug/L Ni	ug/L K	ug/L Na	ug/L V	ug/L Zn
CAP-2B	190.972	11/5/2009	36	170	10	10	16000	10	10	20	90	10	910	27	10	480	3400	20	100
	190.972	3/16/2010	38	170	20	20	16000	20	20	40	67	20	560	45	20			20	100
CH-1S	211.006	11/5/2009	81	97000	27	150	42000	11	63	48	31000	51	15000	1800	31	4700	66000	20	130
	211.006	3/16/2010	31	5000	20	26	13000	20	20	40	1900	20	1400	99	20			20	100
Q5-1	208.323	11/5/2009	27	510	10	10	12000	10	10	20	270	10	710	89	10	550	2900	20	100
	208.323	3/16/2010	16	110	20	20	8600	20	20	40	40	20	450	20	20			20	100
CH1-D	159.506	11/5/2009	130	610	370	31	30000	10	10	20	350	10	2600	120	10	2200	29000	20	100
	159.506	3/16/2010	130	110	290	26	30000	20	20	40	40	20	2700	21	20			20	100
	159.506	6/22/2010	130	110	400	22	33000	20	20	20	40	20	2900	20	20	3800	20000	20	20
Q4-1	228.129	11/5/2009	36	65	10	10	16000	10	10	20	38	10	810	20	10	430	3200	20	100
	228.129	3/16/2010	16	160	20	20	8100	20	20	40	80	20	420	20	20			20	100
3-2	209.489	11/5/2009	52	720	63	10	17000	10	10	20	440	10	890	29	10	820	9500	20	100
	209.489	3/16/2010	60	810	91	20	22000	20	20	40	1100	20	1100	65	20			20	100
	209.489	6/24/2010	44	110	67	20	17000	20	20	20	88	20	770	20	20	560	4100	20	20
27-1	205.704	11/5/2009	13.5	1300	10	19	7600	10	10	20	1200	10	990	36	10	640	2000	20	100
	205.704	3/16/2010	10	110	20	20	6400	20	20	40	40	20	710	20	20			20	100
20-1	228.968	11/5/2009	130	130	10	47	50000	10	10	20	280	10	2400	2000	10	4300	16000	20	100
	228.968	3/16/2010	81	110	20	21	31000	20	20	40	94	20	1500	1500	20			20	100
27-2	208.463	11/5/2009	10.5	340	10	10	6100	10	10	20	250	10	640	26	10	370	3000	20	100
	208.463	3/16/2010	8	710	20	20	5800	20	20	40	570	20	630	25	20			20	100
27-30B-1	230.421	11/5/2009	15	190	10	10	6100	10	10	20	72	10	600	20	10	330	2400	20	100
	230.421	3/16/2010	4.3	110	20	20	4200	20	20	40	40	20	480	20	20			20	100

